MECHANISTIC ANALYSIS OF COCRYSTAL DISSOLUTION: IMPACT OF PHYSICOCHEMICAL PROPERTIES, pH, SURFACTANT, AND BUFFER

by

Fengjuan Cao

A dissertation submitted in partial fulfillment
of the requirements for the degree of
Doctor of Philosophy
(Pharmaceutical Sciences)
in the University of Michigan
2016

Doctoral Committee:

Research Professor Gregory E. Amidon, Co-Chair
Professor Nair Rodriguez-Hornedo, Co-Chair
Professor Zhan Chen
Professor Duxin Sun

ACKNOWLEDGEMENTS

I would like to acknowledge all the support and help that I have received during my time in graduate school. First, I would like to express my sincerest appreciation to my advisors, Dr. Gregory E. Amidon and Dr. Nair Rodriguez-Hornedo for their guidance and continuous support through my graduate study. I am so grateful to be co-advised by them and have received invaluable advice from them. Their knowledge, patience and encouragement have kept me moving my research project forward. Their constant challenges have made me think critically and independently. Without their guidance and training, I would not become the scientist I am now. I would also like to thank the rest of my committee, Dr. Zhan Chen and Dr. Duxin Sun for their time, suggestions and comments on my dissertation research. I would like to especially thank Dr. Gordon Amidon for his passion and insightful comments on my research.

I would like to thank all the past and present members in both labs of Dr. Gregory E. Amidon and Dr. Nair Rodriguez-Hornedo. It has been a wonderful experience working with Paola Borba, Katie Cavanagh, Yitian Chen, Dr. Brian Krieg, Dr. Gislaine Kuminek, Dr. Maya Lipert, Dr. Deanna Mudie, Alanny Bahia de Oliveira da Rocha, Dr. Lily Roy, Patrick Sinko and Nicholas Waltz. All the excitements and great discussions in lab have made my graduate school journey enjoyable. Special thanks to Dr. Brian Krieg, Dr. Maya Lipert, Dr. Deanna Mudie, and Dr. Lily Roy for getting me started in the lab and working on my research project.

This research has been made possible by financial support from the National Institute of General Medical Sciences of the National Institutes of Health (R01GM107146) and the University

of Michigan, College of Pharmacy including the Fred W. Lyons fellowship, Arbour Henry scholarship, Everett Hiestand scholarship and Sheu, Chingju Wang fellowship.

Lastly, I would like to thank my parents, my brother and sister for their endless support and encouragement. Especially my mom, who is always there to offer advice and encouragement when I feel overwhelmed and discouraged.

TABLE OF CONTENTS

LIST OF TABLES

LIST OF FIGURES

ABSTRACT

Cocrystals have gained tremendous interest in pharmaceutical development due to their potential to increase bioavailability. Dissolution could be a major determinant for oral bioavailability, however, its mechanism for these cocrystalline materials has not been well recognized. Lacking knowledge of the dissolution mechanism can lead to misinterpretation of *in vitro* and *in vivo* behavior. The purpose of this dissertation is to provide a mechanistic understanding of the dissolution behavior of cocrystals to rationalize the selection process and improve *in vivo* predictions.

Cocrystals usually contain components with different physicochemical properties, such as ionization, diffusivity, and micellar solubilization and each of these properties can impact their rates of dissolution. The main focus of this dissertation is to develop mass transport analyses to evaluate the roles of these properties on dissolution under varying solution conditions. The different diffusivities between the cocrystal components led to the development of two different analyses, the surface saturation and interfacial equilibrium models to describe the dissolution process of cocrystals. Better agreement with the experimental data makes the surface saturation model the preferred choice for flux predictions.

This dissertation has demonstrated that the dissolution of cocrystals with ionizable components is dictated by the pH at the dissolving solid surface. This interfacial pH is influenced by both the cocrystal properties and solution composition. Depending on solution conditions, both carbamazepine and ketoconazole cocrystals can exhibit higher, equal, or lower dissolution rates

compared to their parent drugs. The carbamazepine cocrystals studied here maintain both dissolution advantage and thermodynamic stability because of their diffusivity advantage. The pH dependence of ketoconazole dissolution is mitigated through cocrystallization with acidic coformers. Similar to pharmaceutical salts, cocrystals also exhibit common coformer effect in which the dissolution rates decrease with increasing coformer solution concentration. By incorporating the independently determined values of physicochemical properties of cocrystal components and solution composition into the mass transport analyses, the flux of cocrystals as a function of bulk pH, surfactant, coformer and buffer concentration can be accurately predicted. These mass transport analyses provide the fundamental knowledge of cocrystal dissolution and the opportunity to predict and rationalize the design of cocrystals for optimal oral absorption.

CHAPTER 1

INTRODUCTION

Solubility is one of the important physicochemical properties that needs to be evaluated during the drug discovery and development process, since it is a significant factor that affects the dissolution rate and consequently, the oral absorption of the drug[1]. This is particularly important for drugs that fall into the Biopharmaceutics Classification System (BCS) class II compounds, where solubility is likely the limiting factor for oral absorption due to the low solubility and high permeability properties of the drugs[1, 2]. Despite the importance of solubility, the number of poorly water soluble drugs is increasing due to the need of larger and more lipophilic molecules for the newly discovered drug targets[1, 3]. Currently, the number of poorly water soluble drugs accounts for 40% of the marketed drugs and 75% of the drugs that are under development[1]. As a result, the enhancement of aqueous solubility has remained a challenge for the successful development of drug products in the pharmaceutical industry[1, 3]. Many strategies have been employed to overcome this challenge and these include both formulation and solid state approaches[1, 4]. Formulation strategies include but are not limited to the use of cosolvents, surfactants, complexation agents and lipid systems[1]. While formulation approaches rely mainly on the use of excipients for improving solubility, solid state approaches focus on the solid structure modifications of the active pharmaceutical ingredients (APIs) and these include amorphous forms, polymorphs, solvates, hydrates, formation of salts and cocrystals[4]. Each of these solid forms displays unique physicochemical properties that can influence the performance of the pharmaceutical materials[5].

Among the solid state approaches, cocrystals are an emerging class of engineered solid forms in pharmaceutical research and development, which have generated tremendous interest due to their potential advantages over other solid forms[3, 4, 6]. Polymorphism offers limited number of crystalline structures since there is only a few number of different crystal forms that can be identified for a given API [7]. Cocrystal engineering provides opportunities to produce a large diversity of crystal forms due to the abundance of coformers available for formation[3, 4, 8]. Unlike salt formation which is limited to only ionizable compounds, cocrystallization is possible for nonionizable compounds. Cocrystals have high crystal lattice energy and thus offer better stability for formulations compared to amorphous and solvated drugs[1, 7]. More importantly, cocrystals offer large solubility range and versatility in fine-tuning the solubility of the parent drugs[9-12].

Cocrystal engineering can generate a variety of crystal forms with physicochemical properties that are distinct from the APIs and these properties include but are not limited to crystallinity, melting point, physical and chemical stability, mechanical properties, solubility, dissolution and bioavailability[4]. Among these properties, solubility and dissolution are of particular interest due to their importance in the oral absorption of drugs[1, 2]. Cocrystals have the potential to improve aqueous solubility of pharmaceutical compounds that can translate into higher dissolution rate and thus better bioavailability[3]. Consequently, a thorough understanding of the solubility and dissolution mechanisms of cocrystals is necessary to interpret their *in vivo* performance.

Cocrystal solubility is dependent on not only its own properties, but also the solution conditions such as pH, solubilizing agents and coformer concentration[10, 12, 13]. Depending on the solution conditions, the same cocrystal can exhibit higher, equal or lower solubility compared to the parent drug. This solubility phenomenon results in transition points that are important for

evaluating the thermodynamic stability of cocrystals. At the transition point, the solubility of the drug and cocrystal are equal, but below or above, cocrystal can have higher solubility. These transition points can be defined as the eutectic point, pH_{max}, S^* and critical stabilization concentration (CSC)[10, 12, 14-16]. The solubility product behavior of cocrystal in which the solubility of the cocrystal decreases with increasing coformer concentration can lead to a transition point also known as the eutectic point[15]. The existence of pH_{max} is due to the different solubility pH dependence between the drug and cocrystal[14, 17]. The preferential solubilization of the drug over the coformer by solubilizing agent can lead to a transition point that is characterized by a solubilizing agent concentration (CSC) and a solubility value (S^*)[10, 16]. The existence of these transition points makes the thermodynamic stability of cocrystals controllable through varying solution conditions. Knowledge of these transition points can be useful for fine tuning the solubility advantages of cocrystals to modulate their dissolution rates.

Dissolution studies of cocrystals have been evaluated in different media[3, 8, 18-21], however, a fundamental understanding of the dissolution mechanism is still lacking to explain the different behavior. Properties of both cocrystal and solution have been shown to be important parameters for determining the solubility of cocrystals, but their roles on dissolution remain to be established. Cocrystals usually contain components with different physicochemical properties, such as ionization, diffusivity and micellar solubilization. It has been shown that the pH at the dissolving surface of ionizable compounds during dissolution could be different from the bulk solution pH[22-24]. Knowing that the cocrystal components can be ionizable, it is important to evaluate how these properties could affect the pH microenvironment within the diffusion layer because of the pH dependent solubility of the cocrystals. Diffusion coefficient is another parameter that influences dissolution and for most cocrystals, the components can have different diffusivities because of the

difference in molecular size and hydrophobicity. Being able to identify the roles of the different properties of cocrystal components can help to establish the dissolution mechanism of cocrystals.

One of the prerequisites for successful oral formulation development is to select the solid form with optimal physicochemical properties that can lead to desired bioperformance and the selection process is based on the thorough understanding of these properties. The two important properties that influence bioavailability are solubility and dissolution. Since the solubility mechanisms of cocrystals have been established, the focus of this dissertation is dissolution. This chapter provides the fundamental principles and concepts that are essential for understanding the dissolution behavior of cocrystals. A statement of research objectives is also included in this chapter to give an overview of this dissertation.

Cocrystal Design and Synthesis

Cocrystals are crystalline materials that contain two or more different molecular components in the same crystal lattice with well-defined stoichiometric ratios and these components are usually APIs and coformers that are both solids at room temperature[7, 25, 26]. The design of cocrystals is based on the principles of crystal engineering and concepts of supramolecular chemistry, in which the components are selected based on favorable intermolecular interactions[27, 28]. The supramolecular synthons responsible for the formation of cocrystals include non-covalent interactions, such as hydrogen bonds, π-π interactions and Vander Waals forces[7, 26]. Among these interactions, hydrogen bonding is the most important and common interaction[7, 26]. Supramolecular synthons can be classified into two categories, homosynthons, which are interactions between identical functional moieties, whereas heterosynthons are interactions between different functional moieties[29, 30]. Heterosynthons are important interactions

for cocrystal design because they are energetically favored over homosynthons[28]. The common hydrogen bond synthons of cocrystals are shown in Figure 1.1[26].

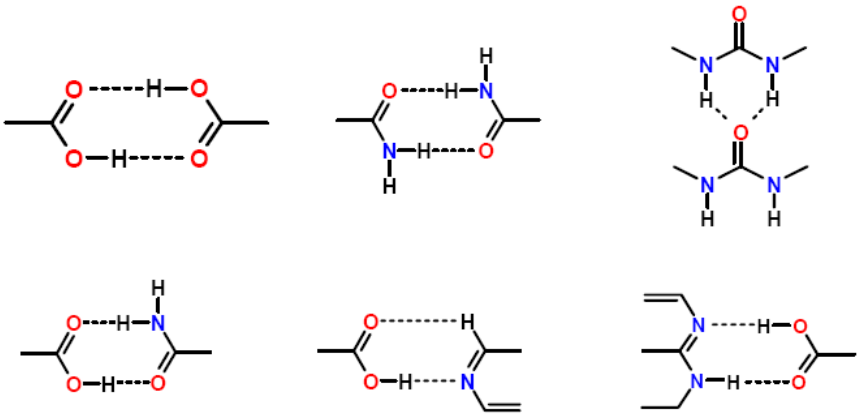

Figure 1.1. Common supramolecular synthons formed between carboxylic acids and amide groups[26].

Various techniques have been developed to synthesize cocrystals, which include, but are not limited to solution crystallization, mechanical grinding and melt crystallization[3]. Among these techniques, reaction crystallization method (RCM) offers several advantages over other methods[31]. RCM is not only suitable for high throughput screening of cocrystals, but also good for large scale synthesis[31]. The mechanism of RCM is based on generating supersaturation in solution with respect to only one solid phase, which is the cocrystal[31]. Because of the solubility product behavior, supersaturation of incongruently saturated cocrystals can be generated in solution by increasing concentration of one component in excess to the stoichiometric ratio[13, 31]. The synthesis of cocrystals can be guided by solubility phase diagrams similar to the one shown in Figure 1.2[32]. The diagram indicates the regions of thermodynamic stability of the cocrystal and its components, which is very important for identifying the solution conditions that favor the formation of cocrystals[31, 32]. Among the four regions shown in Figure 1.2, solution concentrations in both region

II and IV are supersaturated with respect to the cocrystal. However, only pure cocrystal can form in region IV because region II is also supersaturated with respect to drug.

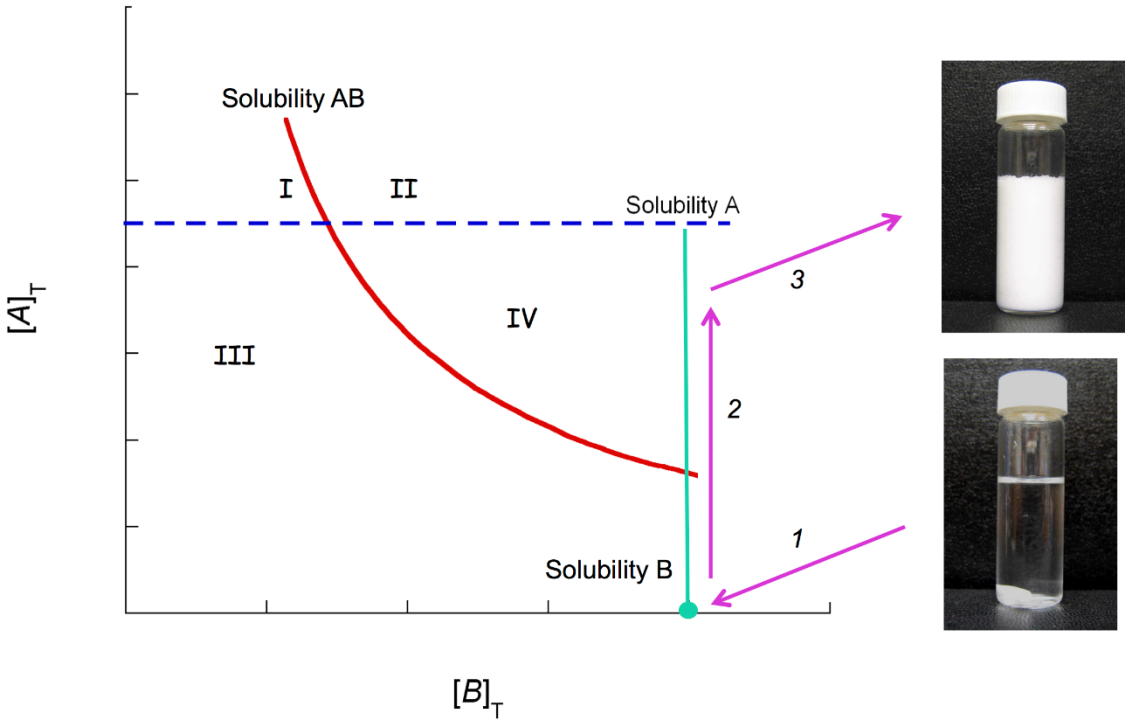

Figure 1.2. Schematic phase solubility diagram indicating thermodynamic stability regions and formation pathway of cocrystal. Lines represent solubility of drug A, coformer B, and cocrystal AB. Cocrystal solubility decreases with coformer concentration $[B]_T$. Subscript T represents total concentrations. Arrows represent a path along which cocrystal is the only phase that can crystallize. Region I: solution is supersaturated with respect to drug, and cocrystal can convert to drug. Region II: solution is supersaturated with respect to both drug and cocrystal, and both can crystallize. Region III: solution is below saturation of drug, cocrystal, and coformer. Region IV: solution is supersaturated with respect to cocrystal, and cocrystal can crystallize[32].

Cocrystal solubility

Solubility is determined by two important parameters, lattice and solvation energy. Lattice energy refers to the intermolecular forces of the solute and solvation energy is the interaction between the solute and solvent molecules in solution[1]. The solubility mechanism involves the breaking of intermolecular bonds of the solid form and then follows by the formation of solvent-

solute bonds[1, 9]. Therefore, the strategies for enhancing solubility are to reduce the intermolecular forces of the solute and/or maximize the solvation energy[1]. It is important to know the primary barrier for solubility in order to determine what strategy to use for enhancing solubility[1]. Studies have shown that the main barrier for cocrystal aqueous solubility is the solvation energy because of the hydrophobic nature of the drug[9]. Consequently, the aqueous solubility of cocrystals can be modulated through solution interactions, such as ionization, complexation and micellar solubilization[9]. The common solution phase interactions of cocrystals are illustrated in Figure 1.3 [9].

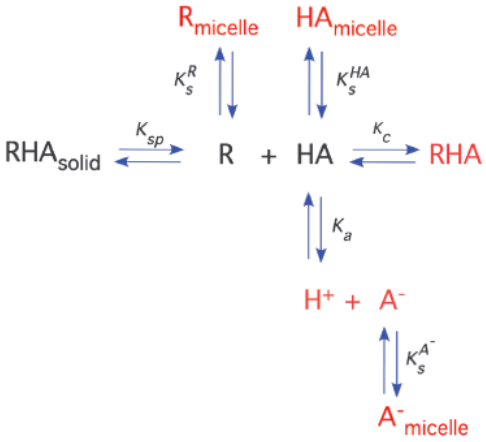

Figure 1.3. Cocrystal solution phase interactions and associated equilibria for a 1:1 cocrystal RHA with a non-ionizable drug (R) and an ionizable coformer (HA) in micellar solution[9].

Ionization

The solubility pH dependence of a poorly water soluble drug can be modified via cocrystallization with coformers of different ionization properties, such as acidic, basic, amphoteric and zwitterionic[12]. Mathematical models have been developed to predict the solubility pH dependence of cocrystals based on the chemical equilibria of both components in solution[12]. Consider a 1:1 cocrystal with R as the non-ionizable drug and HA as the acidic coformer, the

chemical equilibria in solution include cocrystal dissociation and coformer ionization, which can be described as follows:

$$RHA_{solid} \leftrightharpoons R_{aq} + HA_{aq} \quad (1.1)$$

$$K_{sp} = [R]_{aq}[HA]_{aq} \quad (1.2)$$

$$HA_{aq} \leftrightharpoons H^+ + A^-_{aq} \quad (1.3)$$

$$K_a = \frac{[H^+][A^-]_{aq}}{[HA]_{aq}} \quad (1.4)$$

where K_{sp} is the solubility product, K_a is the ionization constant of the coformer and subscript aq denotes the aqueous phase[12]. By applying mass balance for each component in solution, the total drug and coformer concentrations can be expressed as[12]:

$$[R]_T = [R]_{aq} \quad (1.5)$$

$$[A]_T = [HA]_{aq} + [A^-]_{aq} \quad (1.6)$$

By combining the mass balance equations with the equilibrium constants, the total drug concentration can be expressed as[12]:

$$[R]_T = \frac{K_{sp}}{[A]_T}\left(1 + \frac{K_a}{[H^+]}\right) \quad (1.7)$$

When cocrystal is in equilibrium with solution under stoichiometric conditions, the cocrystal solubility is equal to the total drug concentration, as well as the total coformer concentration[12]:

$$S_{cocrystal} = [R]_T = [A]_T \quad (1.8)$$

By combining equations 1.7 and 1.8, the stoichiometric solubility of a 1:1 cocrystal with nonionizable drug and monoacidic coformer can be expressed as follow[12]:

$$S_{cocrystal} = \sqrt{K_{sp}\left(1 + \frac{K_a}{[H^+]}\right)} \quad (1.9)$$

Solubility equations for cocrystals of varying ionization properties and stoichiometries can be derived in a similar manner[12]. The development of these mathematical models can give *a priori* predictions of the solubility pH dependence of pharmaceutical cocrystals. The ability of cocrystals in modulating the pH dependent solubility of the parent drugs is demonstrated in Figure 1.4. Depending on the ionization properties of the coformers, the solubility behavior of cocrystals as a function of pH can be very different from that of the parent drug. For example, a non-ionizable drug exhibits no pH dependent solubility as shown in Figure 1.4, (a) and (b). However, the cocrystal of this drug with diacidic coformer leads to increase in solubility as a function of pH, whereas the cocrystal with amphoteric coformer results in a U-shaped solubility curve. The solubility behavior is also predicted for cocrystals of a basic drug (Figure 1.4, c) and a zwitterionic drug (Figure 1.4, d) with acidic coformers.

(a) (b)

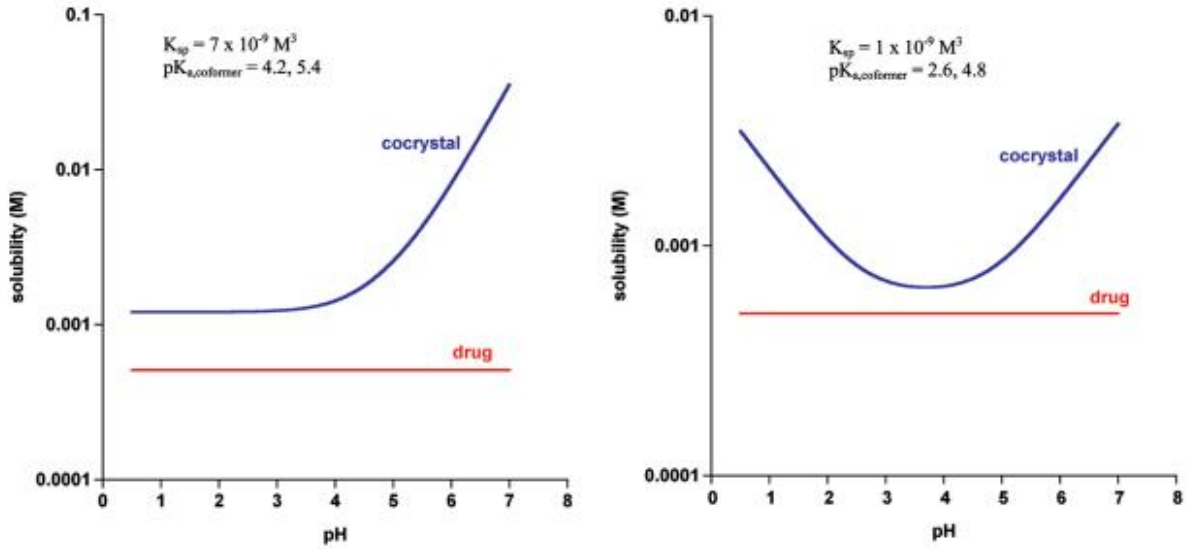

(c) (d)

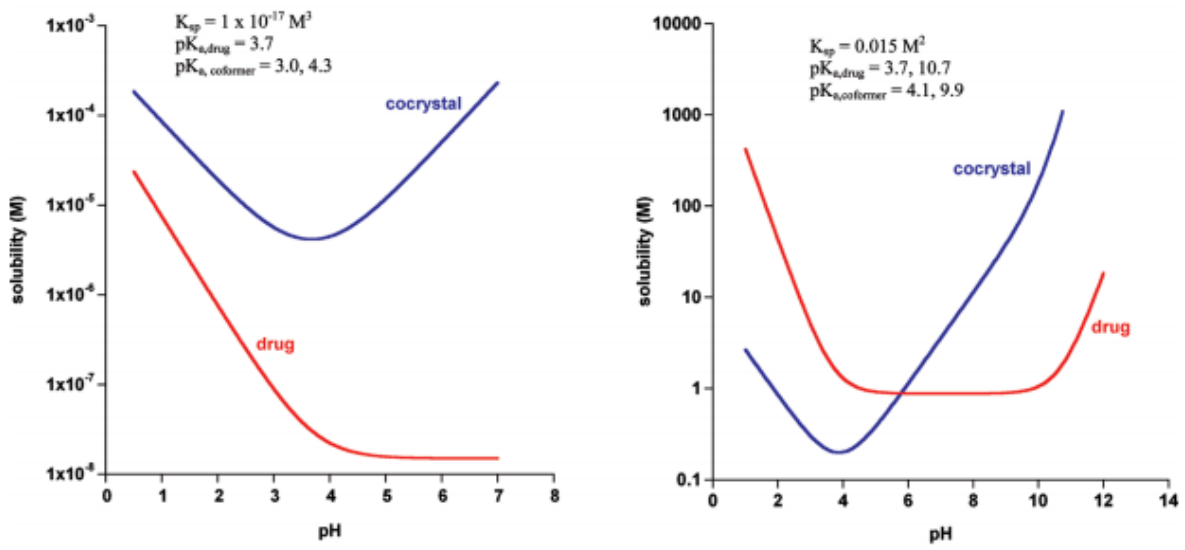

Figure 1.4. Theoretical solubility-pH profiles for (a) 2:1 R_2H_2A cocrystal, (b) 2:1 R_2HAB cocrystal, (c) 2:1 B_2H_2A cocrystal and (d) 1:1 $^{-}ABH^{+}H_2X$ cocrystal calculated using previously developed equations[12]. Drug and coformer pK_a values and cocrystal K_{sp} are included in each graph.

Transition point: pH_{max}

A transition point, pH_{max} can exist if the solubility curve of the drug intersects with that of the cocrystal at a given pH value. This transition point is an important parameter for determining the stability region of cocrystals. An example demonstrating this transition point is shown in Figure 1.5 for a dibasic drug, ketoconazole and its cocrystals with diacidic coformers[33]. At pH_{max}, the solubility of the drug is the same as the cocrystals. Below pH_{max}, the drug has higher solubility, but above it, the cocrystal solubility is higher. By changing the solution pH, the thermodynamically stable cocrystal (below pH_{max}) can become unstable in solution (above pH_{max}).

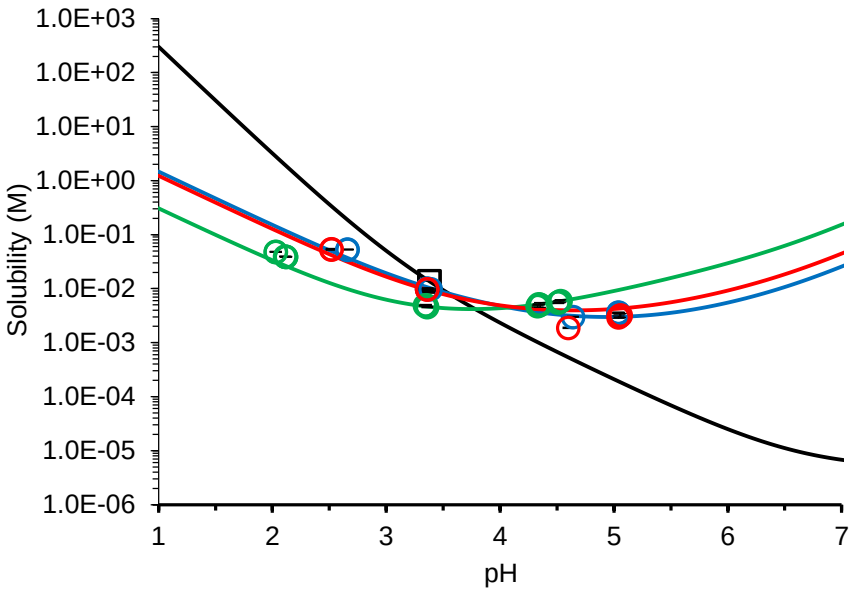

Figure 1.5. Solubility pH dependence of ketoconazole (—), ketoconazole-adipic acid (—), ketoconazole-succinic acid (—) and ketoconazole-fumaric acid (—). The transition point, pH_{max}, is at the intersection between the drug and cocrystal solubility curves. Solid lines represent the theoretical predictions and the symbols are the experimental data[33].

Micellar solubilization

Surfactants are common excipients used in pharmaceutical formulation development to enhance the solubility of poorly water soluble drugs[34]. Studies have shown that the behavior of cocrystals in surfactant solution is different from that of the single components[10, 35, 36]. A schematic representation of micellar solubilization of cocrystal is demonstrated in Figure 1.6. The solubilization process involves several equilibria between the cocrystal solid phase and its components in the aqueous and micellar pseudophases[35]. As shown in Figure 1.6, surfactant can solubilize the cocrystal components to different extents because of the different hydrophobicity between the components. The hydrophobic drug is preferentially solubilized in the micelles, while the hydrophilic coformer is mostly in the aqueous phase. Because of the differential solubilization between the cocrystal components, the solubility dependence on surfactant concentration of the cocrystal is different from the drug. The solubility of hydrophobic drug usually exhibits linear

dependence on surfactant concentration, while the cocrystal solubility exhibits nonlinear dependence. The linear dependent solubility of a nonionizable drug in surfactant solution can be described as

$$S_{drug} = S_0(1 + K_s^R[M]) \tag{1.10}$$

and the nonlinear dependent solubility of 1:1 cocrystal RHA with nonionizable drug and acidic coformer in surfactant solution is described as

$$S_{cocrystal} = \sqrt{K_{sp}(1 + K_s^R[M])\left(1 + K_s^{HA}[M] + \frac{K_a}{[H^+]}\right)} \tag{1.11}$$

where S_0 is the intrinsic solubility of the drug, K_s^R and K_s^{HA} are the solubilization constants of the drug and coformer respectively, and M is the micellar surfactant concentration, which is equal to the total surfactant concentration minus the critical micellar concentration (CMC) [35].

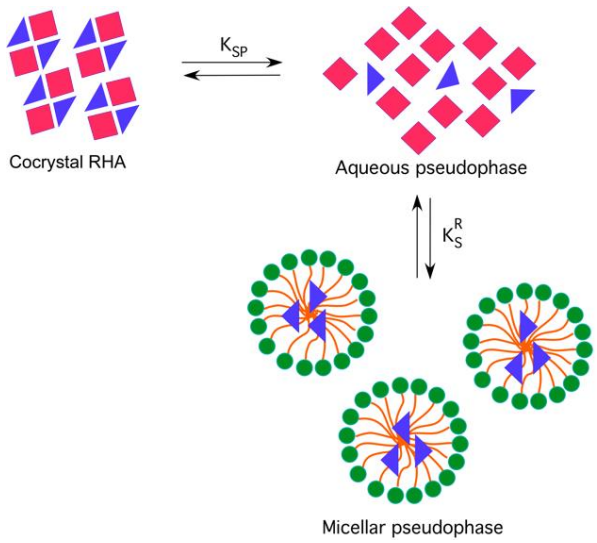

Figure 1.6. Schematic illustration of the equilibria between the cocrystal phase and its components in the aqueous and micellar pseudophases. This scheme represents micellar solubilization of one cocrystal component (for instance drug), leading to excess coformer in the aqueous pseudophase and in this way stabilizing the cocrystal phase[35].

Transition point: CSC

Solubilizing agents such as surfactants, polymers and lipids can induce transition point for cocrystals with higher solubility than the parent drug under the assumption that these agents preferentially solubilize the drug over the coformer. This transition point is characterized by a solubilizing agent concentration (i.e. CSC) required to achieve equivalent solubility between the drug and cocrystal, and a solubility value (S^*)[10, 16]. Similar to pH_{max}, CSC marks the stability region for cocrystals in solution containing solubilizing agents. Below the CSC, cocrystal is the thermodynamically unstable phase relative to the less soluble drug[10]. Above the CSC, cocrystal becomes thermodynamically stable because it is less soluble than the drug[10].

Surfactants can impart stability to the otherwise unstable cocrystals and the effectiveness of stabilization is dependent on the relative magnitude of the micellar solubilization constants between the components[10, 35]. As demonstrated in Figure 1.7, the greater the difference in micellar solubilization between the drug and coformer, the lower the surfactant concentration required to achieve the CSC value[10, 35]. The existence of CSC is due to the preferential solubilization, so it will disappear if the solubilization of the drug is the same as the coformer as shown in Figure 1.7[10, 35].

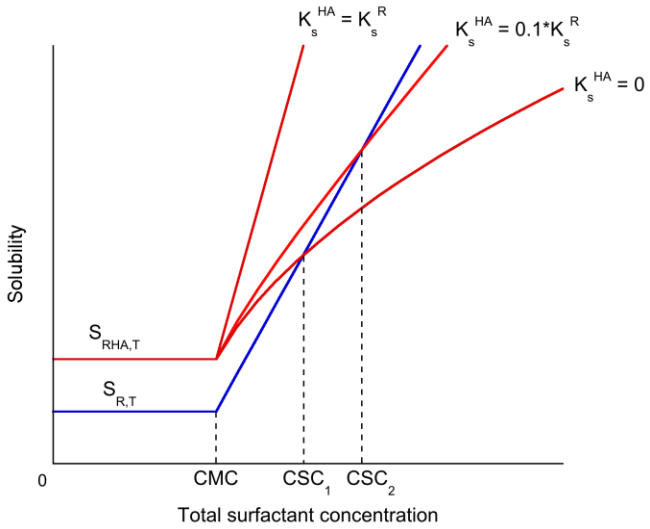

Figure 1.7. Schematic representation of the cocrystal (RHA) and drug (R) solubility with respect to the total surfactant concentration. K_s^R and K_s^{HA} are the solubilization constants for R and HA, respectively. CMC is the critical micellar concentration and CSC is the critical stabilization concentration[35].

Eutectic point measurement

Dissolution is the common method used in evaluating the solubility of cocrystals [3, 8, 21, 37]. However, this method usually fails to capture the true dissolution concentration time profile because cocrystals are supersaturating drug delivery systems and may lead to drug crystallization during dissolution[9]. Because of the solution mediated phase transformation, the thermodynamic solubility of cocrystals can be underestimated using the kinetic measurements. To address this problem, the eutectic point measurement has been developed to determine the thermodynamic equilibrium solubility of cocrystals[15]. At the eutectic point, the solid phases of both drug and cocrystal are in equilibrium with solution, and the solution concentrations of drug and coformer are dependent on the solution conditions, such as temperature, pH, solvent and additives[15]. The eutectic point can be established by following the flowchart illustrated in Figure 1.8. By measuring the solution concentrations of the cocrystal components ($[drug]_{eu}$ and $[coformer]_{eu}$) at the eutectic point, the thermodynamic solubility of the cocrystal can be determined[15].

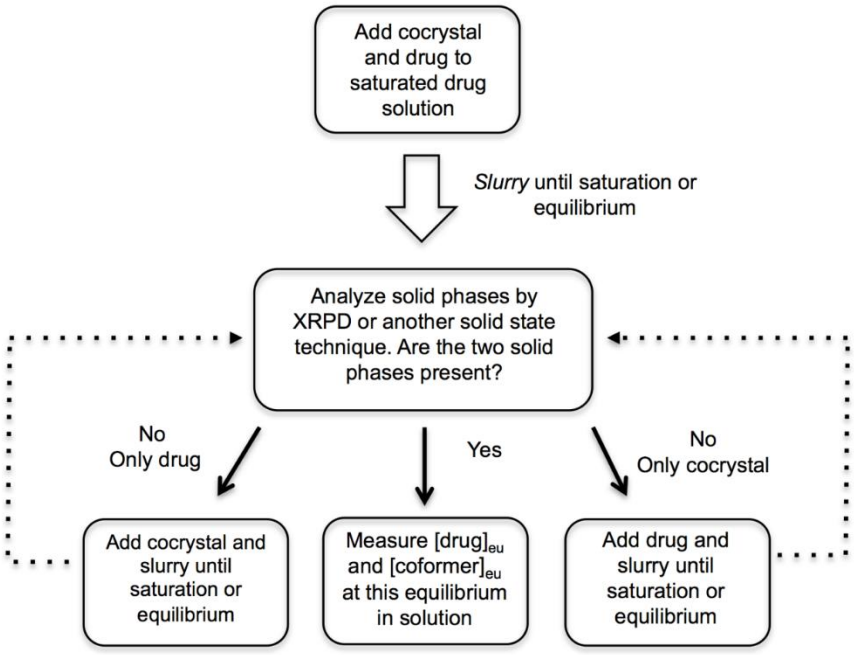

Figure 1.8. Flowchart of representative methods used to determine the equilibrium solution concentrations of cocrystal components at the eutectic point. In this case, the solid phases at equilibrium are cocrystal and solid drug[15, 32].

Cocrystal dissolution and bioavailability

There are numerous examples in the literature trying to demonstrate the advantage of cocrystals over the parent drugs by comparing the solubility, dissolution and bioavailability data[3]. However, cocrystals do not always exhibit better performance than the parent compounds and the *in vitro* dissolution data does not always correlate well with the *in vivo* data[8, 18, 21, 38]. Experimental designs and interpretation of the results can be improved by understanding the solubility and dissolution mechanisms of cocrystals. This section includes a few examples of cocrystal dissolution and bioavailability studies from the literature.

Carbamazepine

Carbamazepine (CBZ) is a BCS II antiepileptic drug that is known to have four different anhydrous polymorphs, as well as hydrates and solvates[39, 40]. It has limited bioavailability because of its poor water solubility, so it usually requires higher doses to achieve the desired pharmacological effect[41]. Cocrystallization offers advantage for improving aqueous solubility of CBZ over salt formation due to its neutral property. Many cocrystals have been discovered for CBZ and some have been demonstrated to have improved solubility[15, 38, 42]. CBZ cocrystals are excellent examples for which the solubility pH dependence of neutral compounds can be tailored through cocrystallization with different coformers. Among these cocrystals, CBZ saccharin (CBZ-SAC) has been studied intensively and its performance has been compared with the marketed product, Tegretol[41]. The dissolution studies of CBZ-SAC were performed in stimulated gastric fluid at 37°C with different particle sizes and the results showed that the dissolution rate increased with smaller particle sizes[41]. It was concluded that the smaller particle size of CBZ-SAC can prevent the conversion of cocrystal to the more stable drug form in solution; however, such statement was not conclusive because only one dissolution medium was studied and the solid phase analyses were performed only on particle size of 500 μm or greater[41]. The pharmacokinetic studies performed in dogs showed no statistical difference in pharmacokinetic parameters between the cocrystal and Tegretol, which is shown in Figure 1.9[41]. This comparable result is likely due to the transformation of cocrystal back to the parent drug, which could potentially cause by the increased solubility of the cocrystal at higher pH environment in the intestine[43]. In addition, the cocrystal capsule is formulated differently from the marketed product. To improve *in vivo* performance, the formulations of poorly water soluble drugs usually contain additives that can solubilize the drug. CBZ-SAC may have better *in vivo* performance if it is formulated the same as the marketed

product. In conclusion, this study has demonstrated the need to understand the effect of particle size and solution environment on cocrystal solubility and dissolution.

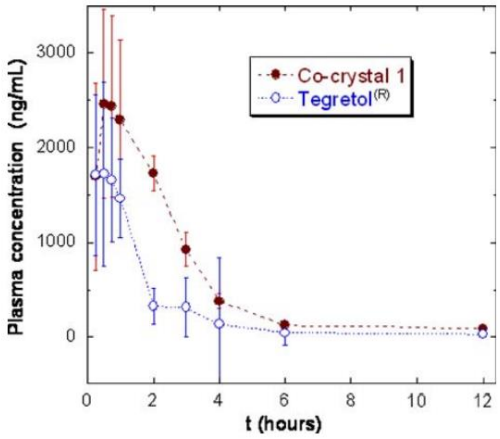

Figure 1.9. Average plasma time curves of CBZ concentrations from a cross-over experiment in fasted beagle dogs (n = 4) given oral doses of 200 mg of the active drug as Tegretol tablets and CBZ-SAC[41].

Indomethacin

Indomethacin (IND) is a nonsteroidal drug with anti-inflammatory, antipyretic and analgesic properties, which belongs to the BCS class II compounds[44]. The two polymorphic forms of IND are α and γ, with the γ form being thermodynamically stable at room temperature[44]. IND is a weakly acidic drug with a pK_a value of 4.5 and its γ form has a solubility of 2.5-4 µg/ml in water. This low solubility could be the potential cause for low and erratic bioavailability[44]. To improve the solubility and dissolution of IND, it was cocrystallized with SAC. The powder dissolution study indicated that the dissolution of the cocrystal was higher in pH 7.4 phosphate buffer compared to the γ form[44]. The conversion of the cocrystal to the γ form was noticed during dissolution, but in-depth understanding of the dissolution behavior is lacking[44].

The dissolution and bioavailability of IND-SAC were evaluated and compared to the marketed product Indomee[18]. *In vitro* dissolution studies were performed in both pH 7.4 phosphate

buffer and 0.1 M HCl with 0.5% Tween 80 at pH 1.2[18]. The results indicated that IND-SAC exhibited higher dissolution rate in both dissolution media compared to IND, but displayed comparable dissolution rate as the marketed product[18]. This study demonstrated the pH effect on the dissolution of IND-SAC, in which the dissolution rate increased at high pH due to the acidity of IND and SAC[11, 18]. Bioavailability of IND, IND-SAC and marketed product were evaluated in beagle dogs. The cocrystal was prepared in hard gelatin capsules containing only lactose, whereas the marketed product contained more additives[18]. As shown in Figure 1.10, the AUC and C_{max} of IND-SAC were higher than IND, but similar to the marketed product[18]. Again, this similar bioavailability between the cocrystal and the marketed product is potentially due to the additives used in the marketed product to optimize the formulation[18].

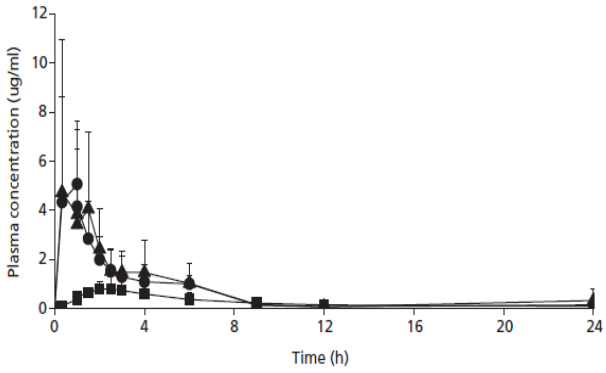

Figure 1.10. Plasma concentration vs. time profiles for IND after oral administration of various formulations in beagle dogs: (●) IND–SAC cocrystal (ground); (■) 1:1 Physical mixture of IND (γ) and SAC; (▲) Indomee®. Error bars show standard deviation[18].

Meloxicam

Meloxicam is a BCS class II non-steroidal anti-inflammatory and antipyretic drug[45]. It has a solubility of 0.012 mg/mL in water and its solubility is pH dependent due to its ionization property[45]. Meloxicam has five polymorphic forms and it can exist in four different tautomeric forms depending on the solution environment[45]. The cation form is the dominate species under

acidic conditions; the zwitterion or enol form exists in neutral conditions; and the anion form presences in basic conditions[45]. Meloxicam has an acidic pK_a of 4.18 and a basic pK_a of 1.09[46]. Because of its low solubility, the therapeutic onset time of meloxicam is long. Several cocrystals with different carboxylic acids as coformers have been discovered to improve the solubility and thus decrease the onset time of meloxicam[45].

As one of the cocrystals, the kinetic solubility and bioavailability of meloxicam-aspirin cocrystal were evaluated[47]. The cocrystal did not exhibit any solubility advantage in water at room temperature compared to the parent drug[47]. However, the cocrystal showed a 44 fold solubility enhancement in pH 7.4 phosphate buffer at 37°C compared to the parent drug[47]. The oral bioavailability of the cocrystal was 69%, whereas the parent drug was only 16%[47].

A more recent study evaluated the correlation between the *in vitro* dissolution data and *in vivo* performance of meloxicam cocrystals[8]. The *in vitro* dissolution of meloxicam and its 12 cocrystals were performed in pH 6.5 phosphate buffer solutions at 37°C and the pharmacokinetic studies were performed using Sprague-Dawley rats, in which the rats were dosed with cocrystals suspended in 5% polyethylene glycol 400 (PEG 400) and 95% methylcellulose solutions[8]. All the cocrystals exhibited faster dissolution rates at early time points, but eventually equilibrated to similar dissolution rate as meloxicam due to conversion[8]. The pharmacokinetic study showed similar behavior as the dissolution[8]. The correlation between the *in vitro* dissolution rates and *in vivo* absorption rates of the cocrystals was determined using linear regression analysis with a R^2 of 0.7067, which is shown Figure 1.11[8]. However, such correlation is not very accurate due to the following reasons. First, phosphate buffer is not a very good representation of the physiological conditions. The gastric intestinal (GI) tract contains bile salts, which are natural surfactants that can improve bioavailability by increasing dissolution rate[48]. Second, the dissolution studies were

performed using pure cocrystals, whereas the pharmacokinetic studies used cocrystal suspensions in PEG 400 and methylcellulose solutions. These polymers may have an impact on the solubility of the cocrystals. To have better IVIV correlation, the dissolution studies should be conducted in physiological relevant conditions.

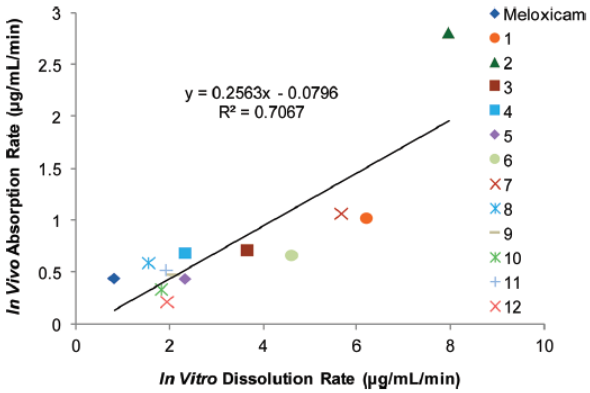

Figure 1.11. Correlation between *in vitro* dissolution rates and *in vivo* absorption rates of meloxicam and its cocrystals[8].

Lamotrigine

Lamotrigine is a BCS class II anticonvulsant drug, which exhibits poor water solubility (0.17 mg/mL at 25°C) and dissolution rate[49]. Despite the fact that lamotrigine is a weak base with a pK_a of 5.7, its aqueous solubility is still very low in 0.1 M HCl (4.1 mg/mL)[49]. Novel crystal forms of lamotrigine have been discovered to improve the solubility, which include three cocrystals, one cocrystal hydrate, three salt forms, two solvates and one hydrated form[49]. Some of these crystal forms were selected to determine their dissolution rates and pharmacokinetic behavior[49]. As shown in Figure 1.12, Lamotrigine methylparaben form II cocrystal exhibited lower maximal concentration during dissolution in water compared to the parent drug; however, it was able to achieve higher maximal concentration during dissolution in 0.1 M HCl solution[49]. This different dissolution behavior is most likely due to the pH effect on dissolution. However, the

authors stated that the dissolution profiles in acidic conditions were not affected by pH because there was no significant change in the final pH of the solution[49]. Although the pH in the bulk solution did not change, the pH at the dissolving surface can be different and this interfacial pH is the determining factor for the dissolution behavior.

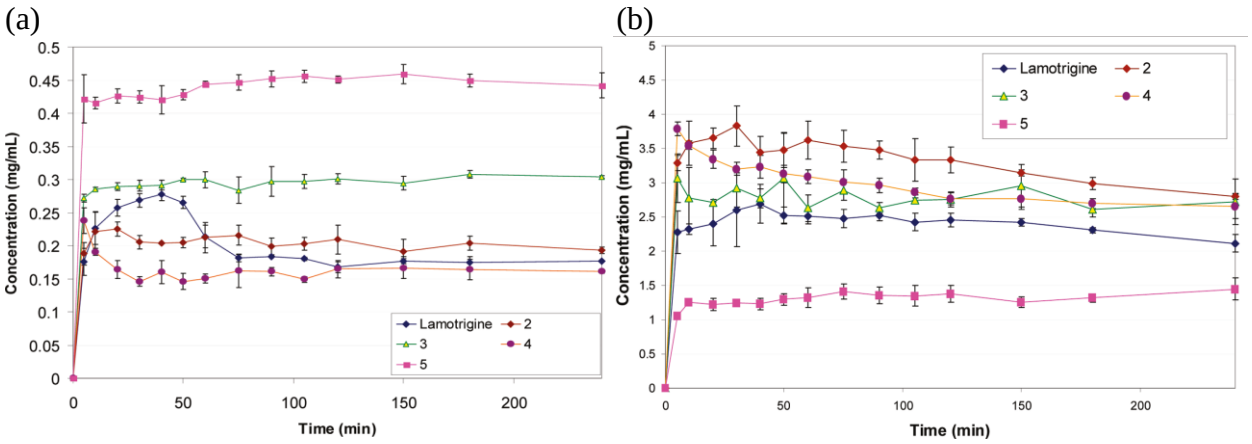

Figure 1.12. Dissolution profiles in water (a) and 0.1 M HCl (b) of lamotrigine and its crystal forms. 2: lamotrigine methylparaben cocrystal form II; 3: lamotrigine nicotinamide cocrystal; 4: lamotrigine nicotinamide cocrystal monohydrate; 5: lamotrigine saccharin salt[49].

The mechanism of dissolution

Dissolution is defined as the "the mixing of two phases with the formation of one new homogeneous phase", and this process involves five major steps: 1) the wetting of drug particle surface by water; 2) the breakdown of solid state bonds; 3) the solvation of drug molecules with water; 4) the diffusion of drug molecules away from the dissolving surface into the well-stirred bulk solution and 5) the convection within the well-stirred bulk solution[50]. In most cases, the first three steps happen instantaneously and thus, diffusion is usually the rate limiting step that determines the dissolution rate[51].

Dissolution is the prerequisite of drug absorption for almost all drugs that are given orally and the purpose of *in vitro* dissolution studies is to provide a fast and inexpensive way to predict

in vivo performance of drugs[50, 52]. Thus, it is essential to understand the mechanism of dissolution and the development of mechanistic models for the dissolution process can be very beneficial[50]. The first diffusion controlled dissolution experiment was conducted by Noyes and Whitney in 1897 and based on their observations, they proposed the dissolution mechanism to be the diffusion from the thin film of saturated solution that surrounded the dissolving substances[50, 51, 53]. In 1904, Nernst and Brunner modified the Noyes and Whitney model and postulated the existence of a diffusion layer adhering to the dissolving surface[50, 51, 54, 55]. Based on the concept of diffusion layer and Fick's first law, they derived the Nernst-Brunner equation[54, 55],

$$\frac{dM}{dt} = \frac{DS}{h}(C_s - C_t) \tag{1.12}$$

where *dM/dt* is the rate of dissolution, *D* is the diffusion coefficient of the drug, *S* is the surface area of the drug, *h* is the thickness of the diffusion layer, C_s and C_t are the solubility of the drug and the concentration of the drug in the bulk solution at time t, respectively[50]. Based on this equation, the rate of dissolution is influenced by diffusion, surface area, solubility and thickness of the unstirred boundary layer.

Rotating disk dissolution

Intrinsic dissolution rate (IDR) is a useful tool to characterize drugs and it has been used to determine the relationship between dissolution rate and crystalline form, as well as to study the effect of surfactants and pH on the dissolution of poorly soluble drugs[56]. IDR has recently been suggested to use for BCS classification because its correlation with *in vivo* dissolution rate is better compared to solublity[56]. IDR is defined as the dissolution rate of pure drug substance when extrinsic factors, such as surface area, agitation, pH, ionic strength and temperature of the dissolution medium, are held constant[56, 57]. IDR can be measured by dissolution methods such as

the fixed disk system and rotating disk system[57]. Rotating disk system is the commonly used method and it is also known as the "Wood's apparatus"[57]. One advantage of using this apparatus is that the hydrodynamic boundary layer has been well defined. According to Levich model[58], the thickness of the diffusion boundary layer for rotating disk is defined as:

$$h = 1.612D^{1/3}v^{1/6}\omega^{-1/2} \quad (1.13)$$

where v is the kinematic viscosity of the medium and ω is the angular velocity in radians per unit time[58].

The rate of dissolution can be expressed in terms of flux, which is defined as the amount of material flowing through a unit cross section of a barrier in a unit time[52]. According to Fick's first law, flux is described as follow:

$$J = -D\frac{dC}{dx} \quad (1.14)$$

where J is the flux and $\frac{dC}{dx}$ is the concentration gradient within the diffusion layer[52]. Combining equations 1.12, 1.13 & 1.14, the equation describing the flux of drug substance across the diffusion layer for rotating disk system can be derived as[22]

$$J = 0.62D^{2/3}v^{-1/6}\omega^{1/2}C_s \quad (1.15)$$

This equation is based on the assumption that dissolution is conducted under sink conditions, where C_t is equal to zero[22].

Mass transport analyses of carboxylic acids

Rotating disk dissolution apparatus has been used to examine the effect of pH on the dissolution kinetics of three carboxylic acids, benzoic acid, 2-naphthoic acid and indomethacin

under unbuffered conditions[22]. Mass transport model has been developed to describe the dissolution process with simultaneous diffusion and chemical reactions within the hydrodynamic boundary layer adjacent to the dissolving surface[22]. The chemical reactions happening at the dissolving surface during dissolution can alter the pH microenvironment and cause the pH at the interface to be different from that of the bulk solution[22]. The development of the mass transport model allows the prediction of this interfacial pH and the flux that depends on this pH.

The dissolution pH dependence of the three carboxylic acids confirms that the pH at the dissolving solid surface is different from the bulk solution[22]. These carboxylic acids liberate hydrogen ions that can lower the pH at the dissolving solid surface compared to the bulk solution. The ionization of these acids also results in a buffer effect at the interface such that the interfacial pH remains relatively constant regardless of bulk pH changes as shown in Figure 1.13 (a)[22]. Interfacial pH dictates the dissolution behavior of these acids. As shown in Figure 1.13 (b), the flux values of all three acids increase with bulk pH, but they all reach constant values at the buffering regions where there are minimal changes in interfacial pH[22]. Knowledge of interfacial pH is essential for understanding the dissolution behavior of ionizable compounds. The difficulty in accessing interfacial pH experimentally emphasizes the importance of performing mass transport analyses for ionizable compounds. The mass transport models for predicting interfacial pH and flux consider the properties of the dissolving compounds, such as solubility, pK_a values, and diffusion coefficients, and as well as the composition of the dissolution media, such as buffer species, bulk pH, et al[22-24].

(a) (b)

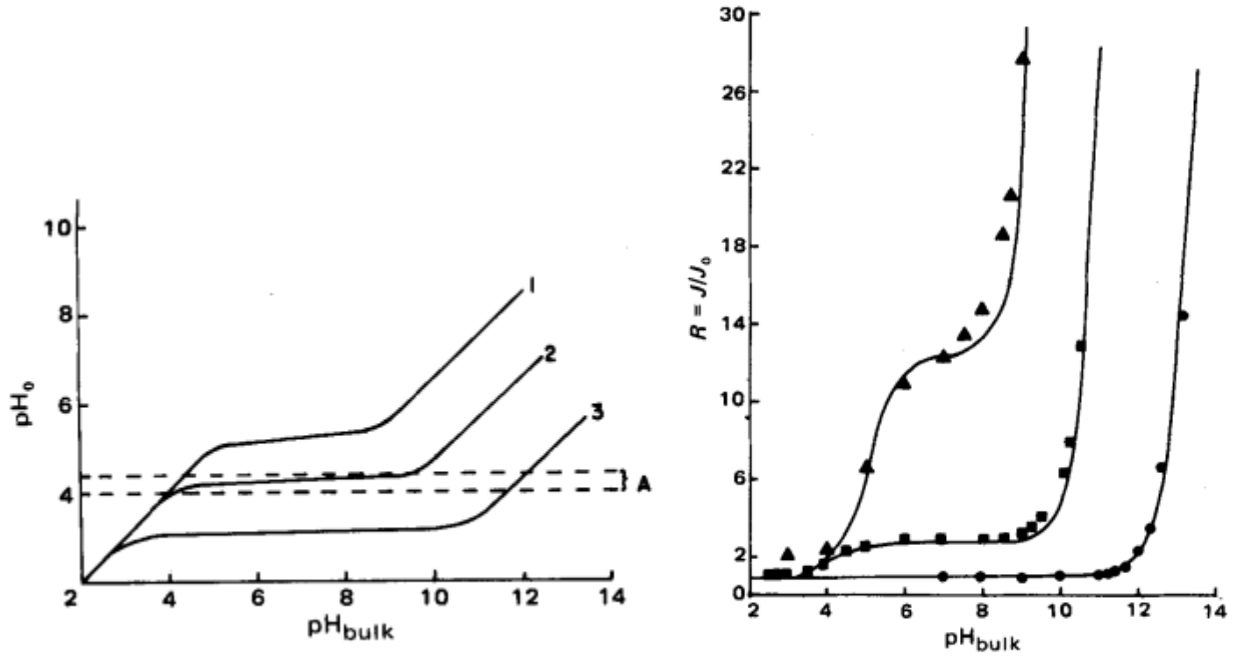

Figure 1.13. (a) Interfacial pH as a function of bulk pH for 1: indomethacin, 2: 2-naphthoic acid and 3: benzoic acid. (b) Flux ratios as a function of bulk pH for indomethacin (▲), 2-naphthoic acid (■) and benzoic acid (●)[22].

Statement of dissertation research

Although the dissolution rates of cocrystals have been widely studied[3, 8, 18-21], not many have considered the mechanism of the dissolution process[59-61]. Due to the lack of knowledge in this area, the purpose of this dissertation research is to provide a mechanistic understanding of the dissolution behavior of cocrystals under the influence of different solution conditions, such as pH and the presence of surfactant, coformer and buffer. The main objective of this research is to develop mass transport models that incorporate the important physicochemical properties of the cocrystals to explain their dissolution behavior under different solution conditions. These mass transport analyses can not only guide the development process of cocrystals, but also provide useful insights for predicting their *in vivo* performance.

Chapter 2 of this thesis studies the dissolution behavior of two carbamazepine cocrystals under the influence of pH and micellar solubilization. The purpose of this chapter is to provide a mechanistic understanding of the dissolution behavior of cocrystals through mass transport analyses. It has been shown that the pH at the dissolving surface of ionizable drug is different from the bulk solution[22-24]. This interfacial pH is important for determining the dissolution rate and can be predicted by developing mass transport models[22-24]. In this chapter, mass transport models are developed by applying Fick's law of diffusion to dissolution with simultaneous chemical reactions in the hydrodynamic boundary layer adjacent to the dissolving cocrystal surface to predict the interfacial pH and flux of the cocrystals. The predictive powers of these models are evaluated by comparing the theoretical predictions of cocrystal flux with the experimental data as a function of pH and surfactant concentration. This chapter also discusses the important roles of cocrystal physicochemical properties, such as solubility, diffusivity, ionization, micellar solubilization in determining the interfacial pH and rates of dissolution.

Chapter 3 provides a mechanistic analysis and comparison of the dissolution behavior of carbamazepine to its two cocrystals under the combination effect of pH and surfactant. In this chapter, a simple mathematical equation is derived based on the mass transport analyses of both drug and cocrystal to describe the dissolution advantage of cocrystal, which is defined as the flux of the cocrystal over that of the drug. The dissolution advantage is dependent on both the solubility and diffusion coefficient advantages of the cocrystal. If the diffusion coefficient of the drug is the same as that of the cocrystal, the cocrystal dissolution advantage is equal to the solubility advantage. This chapter evaluates the cocrystal dissolution advantage under the conditions where the diffusivity of the drug is different from that of the cocrystal. Having a diffusivity advantage can be beneficial because it requires lower or even no solubility advantage to maintain higher

cocrystal dissolution rate. The developed mass transport models can be used to evaluate the dissolution conditions where the cocrystals can display both dissolution advantage and thermodynamic stability.

Chapter 4 evaluates the influence of excess coformer on the dissolution rates of cocrystals. Similar to pharmaceutical salts, cocrystals also exhibit solubility product behavior. This behavior leads to the suppression of salt dissociation in the presence of excess counter ion, which is known as the common ion effect. The solubility of cocrystal has also been shown to decrease in the presence of excess coformer. Using salts as an analogy, the influence of excess coformer on the solubility and dissolution rates of cocrystals is defined as the common coformer effect. Excess coformer can potentially be accumulated in the intestinal lumen if the permeation of the drug is faster than the coformer. The excess coformer in the intestine can affect the dissolution rate if the cocrystal has not completely dissolved. Evaluating the common coformer effect on the dissolution of cocrystals can provide insights on how the differential permeations between the cocrystal components could impact the oral absorption. Another important purpose of this chapter is to validate the surface saturation model developed in Chapter 2 to describe the dissolution mechanism of cocrystals. By varying the coformer concentration in the bulk solution, the surface concentration of coformer can be the same as or higher than the drug concentration.

Chapter 5 investigates and compares the pH effect on the dissolution of a dibasic drug, ketoconazole to its three cocrystals with diacidic coformers. Because of its basicity, the oral absorption of ketoconazole can be impaired for patients with elevated stomach pH. However, *in vivo* performance can be improved under acidic conditions. One of the objectives of this chapter is to examine the potential of cocrystallizing ketoconazole with acidic coformers in enhancing bioavailability. This is achieved by evaluating and comparing the dissolution pH dependence of

ketoconazole to its cocrystals. In this chapter, the mass transport models are expanded to include cocrystals with components of diverse ionization properties, specifically for cocrystals with dibasic drugs and diacidic coformers. The mass transport analyses result in a cubic equation and an eighth order polynomial equation for predicting the interfacial pH for the dissolution of the diabasic drug and its cocrystals with diacidic coformers, respectively. Based on the interfacial pH predictions, the dissolution pH dependence of both ketoconazole and its cocrystals are predicted and compared to the experimental data. The mechanistic understanding of cocrystal dissoluiton provides useful information for the selection process and formulation development.

Chapter 6 studies the effect of buffer on the dissolution rate of a 1:1 cocrystal, carbamazepine-salicylic acid. This chapter extends the mass transport model developed in Chapter 2 to include the chemical reactions between the acidic coformer and the basic buffer species within the hydrodynamic boundary layer. In the presence of monoprotic buffer, a seventh order polynomial equation is required to predict the interfacial pH for the dissolution of 1:1 cocrystals with nonionizable drug and monoacidic coformer. The impact of buffer on the dissolution of cocrystals is evaluated using the mass transport model as a function of bulk pH and buffer concentration. The predictive power of this mass transport model is evaluated by comparing the theoretical flux predictions with the experimental data obtained in different acetate and phosphate buffer concentrations. A constant surfactant concentration (150 mM sodium lauryl sulfate) is used in all dissolution studies to prevent or minimize the cocrystal conversion.

The last chapter of this thesis concludes with the significant findings and future directions of this research. Chapter 2 of this thesis is published in *Molecular Pharmaceutics* 2016, 13(3), 1030-46. A manuscript of Chapter 5 is currently being prepared for publication.

References

1. Williams, H. D.; Trevaskis, N. L.; Charman, S. A.; Shanker, R. M.; Charman, W. N.; Pouton, C. W.; Porter, C. J. H. Strategies to Address Low Drug Solubility in Discovery and Development. *Pharmacological Review* **2013,** *65*, 315-499.

2. Amidon, G. L.; Lennernas, H.; Shah, V. P.; Crison, J. R. A Theoretical Basis for a Biopharmaceutic Drug Classification: The Correlation of *in Vitro* Drug Product Dissolution and *in Vivo* Bioavailability. *Pharmaceutical Research* **1995,** *12*, (3), 413-420.

3. Thakuria, R.; Delori, A.; Jones, W.; Lipert, M. P.; Roy, L.; Rodriguez-Hornedo, N. Pharmaceutical Cocrystals and Poorly Soluble Drugs. *International Journal of Pharmaceutics* **2013,** *453*, (1), 101-125.

4. Schultheiss, N.; Newman, A. Pharmaceutical Cocrystals and Their Physicochemical Properties. *Crystal Growth & Design* **2009,** *9*, (6), 2950-2967.

5. Byrn, S. R.; Pfeiffer, R. R. a. S. J. G., *Solid-State Chemistry of Drugs*. Ssci Inc: 1999.

6. Duggirala, N. K.; Perry, M. L.; Almarsson, O.; Zaworotko, M. J. Pharmaceutical cocrystals: along the path to improved medicines. *Chem Commun* **2016,** *52*, (4), 640-655.

7. Yadav, A. V.; Shete, A. S.; Dabke, A. P.; Kulkarni, P. V. a. S., S.S. Co-Crystals: A Novel Approach to Modify Physicochemical Properties of Active Pharmaceutical Ingredients. *Indian Journal of Pharmaceutical Sciences* **2009,** *71*, (4), 359-370.

8. Weyna, D. R.; Cheney, M. L.; Shan, N.; Hanna, M.; Zaworotko, M. J.; Sava, V.; Song, S.; Sanchez-Ramos, J. R. Improving Solubility and Pharmacokinetics of Meloxicam via Multiple-Component Crystal Formation. *Molecular Pharmaceutics* **2012,** *9*, 2094-2102.

9. Roy, L.; Lipert, M. P.; Rodriguez-Hornedo, N., Co-crystal Solubility and Thermodynamic Stability. In *Rsc Drug Discov*, Royal Society of Chemistry: 2012; pp 247-279.

10. Huang, N.; Rodriguez-Hornedo, N. Engineering Cocrystal Solubility, Stability, and pHmax by Micellar Solubilization. *Journal of Pharmaceutical Sciences* **2011,** *100*, (12), 5219-5234.

11. Alhalaweh, A.; Roy, L.; Rodriguez-Hornedo, N.; Velaga, S. P. pH-Dependent Solubility of Indomethacin-Saccharin and Carbamazepine-Saccharin Cocrystals in Aqueous Media. *Molecular Pharmaceutics* **2012,** *9*, 2605-2612.

12. Bethune, S. J.; Huang, N.; Jayasankar, A.; Rodriguez-Hornedo, N. Understanding and Predicting the Effect of Cocrystal Components and pH on Cocrystal Solubility. *Crystal Growth and Design* **2009,** *9*, (9), 3976-3988.

13. Nehm, S. J.; Rodriguez-Spong, B.; Rodriguez-Hornedo, N. Phase Solubility Diagrams of Cocrystals are Explained by Solubility Product and Solution Complexation. *Crystal Growth & Design* **2006,** *6*, (2), 592-600.

14. Maheshwari, C.; Andre, V.; Reddy, S.; Roy, L.; Duarte, T.; Rodrigez-Hornedo, N. Tailoring aqueous solubility of a highly soluble compound via cocrystallization: effect of coformer ionization, pH(max) and solute-solvent interactions. *Crystengcomm* **2012,** *14*, (14), 4801-4811.

15. Good, D. J. a. R.-H., N. Solubility Advantage of pHarmaceutical Cocrystals. *Crystal Growth & Design* **2009,** *9*, (5), 2252-2264.

16. Lipert, M. P.; Rodriguez-Hornedo, N. Cocrystal Transition Points: Role of Cocrystal Solubility, Drug Solubility, and Solubilizing Agents. *Molecular Pharmaceutics* **2015,** *12*, (10), 3535-3546.

17. Reddy, L. S.; Bethune, S. J.; Kampf, J. W.; Rodriguez-Hornedo, N. Cocrystals and Salts of Gabapentin: pH Dependent Cocrystal Stability and Solubility. *Crystal Growth & Design* **2009,** *9*, (1), 378-385.

18. Jung, M.; Kim, J.; Kim, M.; Alhalaweh, A.; Cho, W.; Hwang, S. a. V., S.P. Bioavailability of Indomethacin-Saccharin Cocrystals. *Journal of Pharmacy and Pharmacology* **2010,** *62*, 1560-1568.

19. Smith, A. J.; Kavuru, P.; Wojtas, L.; Zaworotko, M. J.; Shytle, R. D. Cocrystals of Quercetin with Improved Solubility and Oral Bioavailability. *Molecular Pharmaceutics* **2011,** *8*, (5), 1867-1876.

20. McNamara, D. P.; Childs, S. L.; Giordano, J.; Iarriccio, A.; Cassidy, J.; Shet, M. S.; Mannion, R.; O'Donnell, E.; Park, A. Use of a glutaric acid cocrystal to improve oral bioavailability of a low solubility API. *Pharmaceutical Research* **2006,** *23*, (8), 1888-1897.

21. Cheney, M. L.; Shan, N.; Healey, E. R.; Hanna, M.; Wojtas, L.; Zaworotko, M. J.; Sava, V.; Song, S.; Sanchez-Ramos, J. R. Effects of Crystal Form on Solubility and Pharmacokinetics: A Crystal Enginneering Case Study of Lamotrigine. *Crystal Growth & Design* **2010,** *10*, 394-405.

22. Mooney, K. G.; Mintun, M. A.; Himmelstein, K. J.; Stella, V. J. Dissolution Kinetics of Carboxylic Acids I: Effect of pH under Unbuffered Conditions. *American Pharmaceutical Association* **1981,** *70*, (1), 13-22.

23. Mooney, K. G.; Mintun, M. A.; Himmelstein, K. J.; Stella, V. J. Dissolution Kinetics of Carboxylic Acids II: Effect of Buffers. *American Pharmaceutical Association* **1981,** *70*, (1), 22-32.

24. Aunins, J. G.; Southard, M. Z.; Myers, R. A.; Himmelstein, k. J.; Stella, V. J. Dissolution of Carboxylic Acids III: The effect of Polyionizable Buffers. *Journal of Pharmaceutical Sciences* **1985,** *74*, (12), 1305-1316.

25. Guidance for Industry: Regulatory Classification of Pharmaceutical Co-Crystals. CDER, FDA: 2013.

26. Rodriguez-Hornedo, N.; Nehm, S. J. a. J., A., Cocrystals: Design, Properties, and Formation Mechanisms. In *Encyclopedia of PHarmaceutical Technology*, Francis and Taylor: London, United Kingdom, 2007; pp 615-635.

27. Desiraju, G. R. Supramolecular Synthons in Crystal Engineering - a New Organic-Synthesis. *Angewandte Chemie-International Edition in English* **1995,** *34*, (21), 2311-2327.

28. Vishweshwar, P.; McMahon, J. A.; Bis, J. A. a. Z., M.J. Pharmaceutical Co-Crystals. *Journal of Pharmaceutical Sciences* **2006,** *95*, (3), 499-516.

29. Shattock, T. R.; Arora, K. K.; Vishweshwar, P.; Zaworotko, M. J. Hierarchy of Supramolecular Synthons: Persistent Carboxylic Acid···Pyridine Hydrogen Bonds in Cocrystals That also Contain a Hydroxyl Moiety. *Crystal Growth & Design* **2008,** *8*, (12), 4533-4545.

30. Walsh, R. D. B.; Bradner, M. W.; Fleischman, S.; Morales, L. A.; Moulton, B.; Rodriguez-Hornedo, N.; Zaworotko, M. J. Crystal engineering of the composition of pharmaceutical phases. *Chem Commun* **2003**, (2), 186-187.

31. Rodriguez-Hornedo, N.; Nehm, S. J.; Seefeldt, K. F.; Pagan-Torres, Y. a. F., C.J. Reaction Crystallization of Pharmaceutical Molecular Complexes. *Molecular Pharmaceutics* **2006,** *3*, (3), 362-367.

32. Kuminek, G.; Cao, F.; Rocha, A. B. d. O. d.; Cardoso, S. G.; Rodriguez-Hornedo, N. Cocrystals to Facilitate Delivery of Poorly Soluble Compounds Beyond-Rule-of-5. *Advanced Drug Delivery Reviews* **2016,** *Manuscript under review.*

33. Chen, Y.; Rodriguez-Hornedo, N., Solubility, pH_{max} and Dissolution of Ketoconazole Cocrystals in Aqueous Media. In *AAPS Poster Presentation (M1208)*, Orlando, Florida, 2015.

34. Strickley, R. G. Solubilizing Excipients in Oral and Injectable Formulaitons. *Pharmaceutical Research* **2004,** *21*, (2), 201-230.

35. Huang, N.; Rodriguez-Hornedo, N. Effect of Micellar Solubilization on Cocrystal Solubility and Stability. *Crystal Growth & Design* **2010,** *10*, 2050-2053.

36. Huang, N.; Rodriguez-Hornedo, N. Engineering Cocrystal Thermodynamic Stability and Eutectic Points by Micellar Solubilization and Ionization. *CrystEngComm* **2011,** *13*, 5409-5422.

37. Martin, F. A.; Pop, M. M.; Borodi, G.; Filip, X.; Kacso, I. Ketoconazole Salt and Co-crystals with Enhanced Aqueous Solubility. *Crystal Growth & Design* **2013,** *13*, (10), 4295-4304.

38. Fleischman, S. G.; Kuduva, S. S.; McMahon, J. A.; Moulton, B.; Walsh, R. D. B.; Rodriguez-Hornedo, N. a. Z., M.J. Crystal Engineering of the Composition of Pharmaceutical Phases: Multiple-Component Crystalline Solids Involving Carbamazepine. *Crystal Growth & Design* **2003,** *3*, (6), 909-919.

39. Harris, R. K.; Ghi, P. Y.; Puschmann, H.; Apperley, D. C.; Griesser, U. J.; Hammond, R. B. Structural Studies of the Polymorphs of Carbamazepine, Its Dihydrate, and Two Solvates. *Organic Process Research & Development* **2005,** *9*, 902-910.

40. Kovacevic, I.; Parojcic, J. H., I.; Tubic-Grozdanis, M. a. L., P. Justification of Biowaiver for Carbamazepine, a Low Soluble High Permeable Compound, in Solid Dosage Forms Based on IVIVC and Gastrointestinal Simulation. *Molecular Pharmaceutics* **2009,** *6*, (1), 40-47.

41. Hickey, M. B.; Peterson, M. L.; Scoppettuolo, L. A.; Morrisette, S. L.; Vetter, A. G., H.; Remenar, J. F.; Zhang, Z.; Tawa, M. D.; Haley, S.; Zaworotko, M. J. a. A., O. Performance Comparison of a Co-crystal of Carbamazepine with Marketed Product. *European Journal of Pharmaceutics and Biopharmaceutics* **2007,** *67*, 112-119.

42. Childs, S. L.; Rodriguez-Hornedo, N.; Reddy, L. S.; Jayasankar, A.; Maheshwari, C.; McCausland, L.; Shipplett, R. a. S., B.C. Screening Strategies Based on Solubility and Solution Composition Generate Pharmaceutically Acceptable Cocrystals of Carbazepine. *CrystEngComm* **2008,** *10*, 856-864.

43. Bethune, S. J., Thermodynamic and Kinetic Parameters that Explain Crystallization and Solubility of Pharmaceutical Cocrystals. University of Michigan: Ann Arbor, 2009.

44. Basavoju, S.; Bostrom, D. a. V., S.P. Indomethacin-Saccharin Cocrystal: Design, Synthesis and Preliminary Pharmaceutical Characterization. *Pharmaceutical Research* **2008,** *25*, (3), 530-541.

45. Cheney, M. L.; Weyna, D. R.; Shan, N.; Hanna, M.; Wojtas, L. a. Z., M.J. Supramolecular Architectures of Meloxicam Carboxylic Acid Cocrystals, a Crystal Engineering Case Study. *Crystal Growth & Design* **2010,** *10*, 4401-4413.

46. Luger, P.; Daneck, K.; Engel, W.; Trummlitz, G. a. W., K. Structure and Physicochemical Properties of Meloxicam, A New NSAID. *European Journal of Pharmaceutical Sciences* **1996,** *4*, 175-187.

47. Cheney, M. L.; Weyna, D. R.; Shan, N.; Hanna, M.; Wojtas, L. a. Z., M.J. Coformer Selection in Pharmaceutical Cocrystal Development: a Case Study of a Meloxicam Aspirin Cocrystal that Exhibits Enhanced Solubility and Pharmacokinetics. *Journal of Pharmaceutical Sciences* **2011,** *100*, (6), 2172-2181.

48. Bakatselou, V.; Oppenheim, R. C. a. D., J.B. Solubilization and Wetting Effects of Bile Salts on the Dissolution of Steroids. *Pharmaceutical Research* **1991,** *8*, (12), 1461-1468.

49. Cheney, M. L.; Shan, N.; Healey, E. R.; Hanna, M.; Wojtas, L.; Zaworotko, M. J.; Sava, V.; Song, S. a. S.-R., J.R. Effects of Crystal Form on Solubility and Pharmacokinetics: A Crystal Enginneering Case Study of Lamotrigine. *Crystal Growth & Design* **2010,** *10*, 394-405.

50. Siepmann, J. a. S., F. Mathematical Modeling of Drug Dissolution. *International Journal of Pharmaceutics* **2013,** *453*, (1), 12-24.

51. Sugano, K.; Okazaki, A.; Sugimoto, S.; Tavornvipas, S.; Omura, A. a. M., T. Solubility and Dissolution Profile Assessment in Drug Discovery. *Drug Metab. Pharmacokinet.* **2007,** *22*, (4), 225-254.

52. Martin, A. a. B., P., *Physical Pharmacy: Physcial Chemical Principles in the Pharmaceutical Sciences*. Lippincott Williums & Wilkins: Maryland, 1993.

53. Noyes, A. A. a. W., W.R. The Rate of Solution of Solid Substances in Their Own Soluitons. *Journal of American Chemical Society* **19**, (1897), 930-934.

54. Nernst, W. Theorie der Reaktionsgeschwindigkeit in heterogenen systemen. *Zeitschrift für Physikalische Chemie* **1904,** *47*, 52-55.

55. Brunner, E. Reaktionsgeschwindigkeit in Heterogenen Systemen. *Zeitschrift für Physikalische Chemie* **1904,** *47*, 56-102.

56. Zakeri-Milani, P.; Barzegar-Jalali, M.; Azimi, M. a. V., H. Biopharmaceutical Classification of Drugs Using Intrinsic Dissolution Rate and Rat Intesinal Permeability. *European Journal of Pharmaceutics and Biopharmaceutics* **2009,** *73*, 102-106.

57. Issa, M. G. a. F., H.G. Intrinsic Dissolution as a Tool for Evaluating Drug Solubility in Accordance with the Biopharmaceutics Classification System. *Dissolution Technologies* **2011,** *18*, (2), 6-13.

58. Levich, V. G., *Physico-chemical Hydrodynamics*. Prentice-Hall: Englewood Cliffs, N.J., 1962.

59. Li, M.; Qiao, N.; Wang, K. Influence of Sodium Lauryl Sulfate and Tween 80 on Carbamazepine-Nicotinamide Cocrystal Solubility and Dissoluiton Behaviour. *Pharmaceutics* **2013,** *5*, (4), 508-524.

60. Qiao, N.; Wang, K.; Schlindwein, W.; Davies, A.; Li, M. In Situ Monitoring of Carbamazepine-Nicotinamide Cocrystal Intrinsic Dissolution Behaviour. *European Journal of Pharmaceutics and Biopharmaceutics* **2013,** *83*, (3), 415-426.

61. Lee, H. G.; Zhang, G. G. Z.; Flanagan, D. R. Cocrystal Intrinsic Dissolution Behavior Using a Rotating Disk. *Journal of Pharmaceutical Sciences* **2011,** *100*, (5), 1736-1744.

CHAPTER 2

MECHANISTIC ANALYSIS OF COCRYSTAL DISSOLUTION AS A FUNCTION OF pH AND MICELLAR SOLUBILIZATION*

Abstract

The purpose of this work is to provide a mechanistic understanding of the dissolution behavior of cocrystals under the influence of ionization and micellar solubilization. Mass transport models were developed by applying Fick's Law of diffusion to dissolution with simultaneous chemical reactions in the hydrodynamic boundary layer adjacent to the dissolving cocrystal surface to predict the pH at the dissolving solid-liquid interface (i.e. interfacial pH) and the flux of cocrystals. To evaluate the predictive power of these models, dissolution studies of carbamazepine-saccharin (CBZ-SAC) and carbamazepine-salicylic acid (CBZ-SLC) cocrystals were performed at varied pH and surfactant concentrations above the critical stabilization concentration (CSC), where the cocrystals were thermodynamically stable. The findings in this work demonstrate the pH dependent dissolution behavior of cocrystals with ionizable components is dependent on interfacial pH. This mass transport analysis demonstrates the importance of pH, cocrystal solubility, diffusivity, and micellar solubilization on the dissolution rates of cocrystals.

* This Chapter is published in *Molecular Pharmaceutics*, 2016, 13 (3), 1030-1046, http://pubs.acs.org/doi/full/10.1021/acs.molpharmaceut.5b00862.

Introduction

The enhancement of aqueous solubility has remained a challenge for the successful development of new drug products in the pharmaceutical industry as the number of poorly water soluble drugs is increasing. Many strategies have been employed to overcome this challenge by modifying the solid structure of the drug and these include amorphous forms, polymorphism, solvates, hydrates, salts and cocrystals[1, 2]. Among these approaches, cocrystalline solids have generated tremendous interest due to their potential advantages over other solid forms, such as their diversity in formation and large solubility range[2-4]. Due to their potential of increasing the bioavailability of drugs, many studies have been carried out to understand the solubility and dissolution behavior of cocrystals[3, 5-9]. The solubility behavior of cocrystals has been studied[10-13] and detailed mechanisms of how solution interactions such as ionization and micellar solubilization affect the solubility of cocrystals have been identified by Rodriguez and coworkers[14-17]. Although there are many dissolution studies of cocrystals in the literature[3, 5-9], only a few have considered the mechanism of dissolution[12, 18, 19]. A detailed mechanistic understanding of how physicochemical properties of cocrystal components affect the dissolution behavior still remains to be explored. It is essential to understand the dissolution mechanism of cocrystals because such knowledge can provide a better understanding of the oral absorption of drugs from the cocrystalline solids.

An important consideration for cocrystals is the possibility that solution mediated phase transformation (eg: precipitation of less soluble drug) can occur during dissolution for cocrystals with higher solubility than their parent drugs. This phenomenon has been observed in a number of studies in the literature[12, 19-21]. Rapid conversion back to the parent compound makes the measurement of cocrystal dissolution challenging. Dissolution experiments have been carried out

at low temperature to decrease the dissolution rates of highly soluble cocrystals to capture the intrinsic dissolution rates; however, phase transformation was still observed[20]. It has also been shown that surfactants can thermodynamically stabilize cocrystals due to differences in micellar solubilization between the drug and coformer[17, 22, 23]. The critical stabilization concentration (CSC) has been defined as the surfactant concentration required to achieve equivalent solubility of the cocrystal and parent drug[17]. Cocrystals are thermodynamically unstable below the CSC and crystallization of pure drug can occur, but thermodynamically stable at or above the CSC[17]. Therefore, solid phase transformation can be prevented by performing cocrystal dissolution at or above the CSC.

Cocrystal usually contains a hydrophobic drug and a hydrophilic coformer that have very different physicochemical properties such as ionization, hydrophobicity, and diffusivity. These properties can have very significant effects on the dissolution rates of cocrystals. The ionizable components can undergo simultaneous chemical reactions at the dissolving surface with the chemical species coming from the bulk solution during dissolution. Consequently, the pH at the dissolving surface is not necessarily equivalent to the bulk solution[24]. The first and most important step for determining the dissolution rate of cocrystal with ionizable components is to model the pH at the dissolving surface. Interfacial pH is affected by the degree of ionization of the component at the interface, which is determined by the concentration and pK_a value of the ionizable component[24]. For single component dissolution, the concentration at the dissolving surface is dictated by the solubility of that component. Diffusivity can also influence the concentrations of the components at the dissolving surface for multi-component dissolution with different component diffusion coefficients. The faster diffusing component can lead to a decrease in concentration of that component at the dissolving surface[25]. The dissolution of cocrystal is a

multi-component system with different component diffusivities. Therefore, the concentration of the faster diffusing cocrystal component will have a dependence on the difference in diffusivities between the cocrystal components. The larger the difference between the diffusivities, the lower the concentration of the faster diffusing component will be at the surface.

The purpose of this work is to provide a mechanistically realistic physical mass transport analysis of the dissolution behavior of cocrystals under the combined influence of ionization and micellar solubilization. Mass transport models were developed by applying Fick's Law of diffusion to dissolution with simultaneous chemical reactions in the hydrodynamic boundary layer adjacent to the dissolving cocrystal surface[24]. To evaluate the predictive power of these models, the constant surface area dissolution rates of two model cocrystals with 1:1 stoichiometric ratio, carbamazepine-saccharin (CBZ-SAC) and carbamazepine-salicylic acid (CBZ-SLC) were determined using a rotating disk dissolution apparatus. Carbamazepine is non-ionizable, saccharin and salicylic acid are monoprotic weak acids with reported pK_a values of 1.6 and 3.0, respectively[13, 17].

Materials and methods

Materials

Anhydrous carbamazepine (CBZ), salicylic acid (SLC) and sodium lauryl sulfate (SLS) were purchased from Sigma Chemical Company (St. Louis, MO) and used as received. Carbamazepine dihydrate (CBZD) was prepared by slurrying anhydrous CBZ in deionized water for 24 hours and solid was obtained through vacuum filtration. Saccharin (SAC) was purchased from Acros Organics (Pittsburgh, PA) and used as received. Isopropanol, acetonitrile, methanol and hydrochloric acid were purchased from Fisher Scientific (Pittsburgh, PA). Sodium hydroxide

pellets were purchased from J.T. Baker (Philipsburg, NJ). Water used in this study was filtered through a double deionized purification system (Milli Q Plus Water System) from Millipore Co. (Bedford, MA).

Cocrystal synthesis

Cocrystals were prepared by reaction crystallization method[26] at room temperature. CBZ-SAC was prepared by adding 1:1 molar ratio of CBZ and SAC in isopropanol solution. CBZ-SLC was prepared by adding 1:1 molar ratio of CBZ and SLC in acetonitrile solution containing 0.1 M SLC. Solid phases were characterized by X-ray powder diffraction (XRPD) and differential scanning calorimetry (DSC).

Cocrystal solubility measurements

Cocrystal solubility was measured by determining the eutectic concentrations of the drug and coformer as a function of SLS concentration at pH 1 and 25°C. A detailed discussion of the eutectic point measurement was reported elsewhere[27]. Cocrystals (~100 to 150 mg) and CBZD (~50 to 100 mg) were suspended in 3 mL of aqueous SLS solution and stirred for 4 days. Samples were collected at 24 hour intervals and centrifuged using Corning Costar Spin-X plastic centrifuge tubes with filters to separate the excess solid from solution. Solution concentrations were measured using HPLC and solid phases were analyzed by XRPD. Cocrystal stoichiometric solubility was determined from the measured eutectic concentrations of the cocrystal components using the method previously developed[27].

Cocrystal dissolution measurements

The constant surface area dissolution rates of cocrystals were determined using a rotating disk apparatus. Cocrystal powder (~150 mg) was compressed in a stainless steel rotating disk die

with a tablet radius of 0.50 cm at approximately 85 MPa for 2 minutes using a hydraulic press. The die containing the compact was mounted onto a stainless steel shaft attached to an overhead, variable speed motor. The disk was exposed to 150 mL of the dissolution medium in a water jacketed beaker with temperature controlled at 25°C and a rotation speed of 200 rpm was used. Dissolution medium was prepared on the day of the experiment by dissolving SLS in water and solution pH was adjusted using HCl or NaOH. The pH of dissolution media did not change during the experiments at pH 1-3 for both cocrystals. Although the pH decreased for dissolution at pH 4 and above, the final pH was still within the buffering region. This means that the change in bulk pH during dissolution would not have significant impact on the interfacial pH. Sink conditions were maintained throughout the experiments by ensuring the concentrations at the last time point of the dissolution were less than 10% of the cocrystal solubility. Solution concentrations were measured using HPLC and solid phases after dissolution were analyzed by XRPD.

HPLC

Waters HPLC equipped with a photodiode array detector was used for all analysis. The mobile phase was composed of 55% methanol and 45% water with 0.1% trifluoroacetic acid and the flow rate of 1 mL/min was used. Separation was achieved using Waters, Atlantis, T3 column (5.0 µm, 100 Å) with dimensions of 4.6 x 250 mm. The sample injection volume was 20 µL. The wavelengths for the analytes were as follows: 284 nm for CBZ, 250 nm for SAC and 303 nm for SLC.

XRPD

XRPD diffractograms of solid phases were collected with a benchtop Rigaku Miniflex X-ray diffractometer using Cu-Kα radiation (λ = 1.54 Å), a tube voltage of 30 kV, and a tube current of 15 mA. Data was collected from 5 to 40° at a continuous scan rate of 2.5°/min.

DSC

Crystalline samples were analyzed by DSC using a TA instrument 2910 MDSC system equipped with a refrigerated cooling unit. All experiments were performed by heating the samples at a rate of 10 °C/min under a dry nitrogen atmosphere. Temperature and enthalpy of the instrument were calibrated using high purity indium standard.

Theoretical

The following mass transport analysis utilizes the classic film theory that postulates the presence of a diffusion boundary layer (i.e. stagnant layer) adjacent to the dissolving surface[28]. The dissolution process is determined by the concentration gradient across the diffusion boundary layer and influenced by the simultaneous diffusion and chemical reactions occurring at the dissolving surface and in the adjacent boundary layer[24]. For the dissolution of a 1:1 cocrystal in non-reactive media (eg: no ionization or micellar solubilization), the cocrystal would first dissolve according to its solubility product to give equal molar concentrations of the drug and coformer. Both components would then diffuse across the boundary layer into the bulk solution based on their diffusion coefficients and concentration gradients. Cocrystalline solids have well defined stoichiometry so they will dissolve according to their stoichiometric ratios assuming that there is no precipitation.

At steady state, the dissolution rate of the drug must be the same as the coformer for a 1:1 cocrystal if there is no solid phase transformation during dissolution (eg: drug precipitation). As mentioned above, diffusion across the boundary layer is influenced by component diffusion coefficients and for most cocrystals, the drug molecule is larger than the coformer, so the diffusion coefficient of the drug is usually less than the coformer. The difference in diffusivities between the cocrystal components may be magnified if the dissolution is performed in surfactant solution where the drug may be highly solubilized by micelles, but the coformer is only slightly solubilized. Micellar solubilization typically reduces the diffusion rate of the drug significantly compared to the coformer due to the much lower diffusion coefficient of the drug loaded micelles. With slower diffusion, the transport rate of the drug would be less than the coformer. To maintain stoichiometric dissolution of both components of the cocrystal, the difference in diffusivities can influence the concentrations of the components at the dissolving surface under steady state conditions.

The mass transport process of cocrystals may be analyzed in two ways described here as the interfacial equilibrium and the surface saturation models. Both of these models were developed based on the classic film theory of dissolution[28] and the solubility product behavior of cocrystals. The major difference between the two models is related to the boundary conditions at the solid-liquid interface. For the interfacial equilibrium model, the solubility product of the cocrystal is assumed to apply at the dissolving surface at all times $t \geq 0$. For the surface saturation model, the concentration of the slower diffusing component, typically the drug, is maintained equal to the stoichiometric solubility of the cocrystal while the concentration of the faster diffusing component, typically the coformer, is depleted due to its more rapid diffusion. Due to the depletion of the coformer at the dissolving surface, the solubility product of the cocrystal is not maintained for the

surface saturation model. It is appropriate to point out that the application of rotating disk hydrodynamics and the associated hydrodynamic boundary layer are simplifying assumptions where simultaneous chemical reactions and micelle solubilization occur. However, useful predictions may be obtained that provide insight into the mechanisms and rate limiting processes impacting dissolution. More detailed descriptions of the two models are provided in the following sections.

Both models are based on the following assumptions: chemical reactions and solute solubilization within the diffusion layer occur instantaneously, free solute and micelle are in equilibrium throughout the diffusion layer, the ionized form of the coformer is not solubilized by surfactant, the solubilization constant of the coformer does not change with surfactant concentration, aqueous diffusivity of the ionized and non-ionized forms are the same. For simplification of the interfacial pH prediction, the effective diffusivity of the coformer is assumed to be the same as the aqueous diffusivity because it is not significantly solubilized by the surfactant. In this study, the effect of surfactant concentration on the viscosity of dissolution media was not accounted for the mass transport analysis. Although the viscosity of the dissolution media may approximately double at high surfactant concentration (eg: 300 mM)[29], its impact on the hydrodynamic boundary layer is small as shown in equation 10. The viscosity of dissolution media is not expected to significantly affect the diffusion of free species as they are assumed to be diffusing through the aqueous phase where the surfactant concentration is equal to the critical micellar concentration (CMC) and the viscosity is not substantially different from water[30]. The effect of viscosity on the diffusion coefficient of the micelles incorporates the effect of viscosity changes.

Interfacial equilibrium model

A schematic representation of the dissolution process for a 1:1 cocrystal with non-ionizable components, RA, where R is drug and A is coformer, in non-reactive media, is shown in Figure 2.1. The first step of dissolution is the formation of a saturated solution at the solid-liquid interface, which represents the equilibrium between the solid cocrystal and solution. This leads to the dissociation of RA into its components, R and A, according to the solubility product, K_{sp}, as described by the following equations:

$$(RA)_s \leftrightharpoons R_{aq} + A_{aq} \tag{2.1}$$

$$K_{sp} = [R]_{aq}[A]_{aq} \tag{2.2}$$

where subscript s denotes the solid phase and aq denotes the aqueous phase.

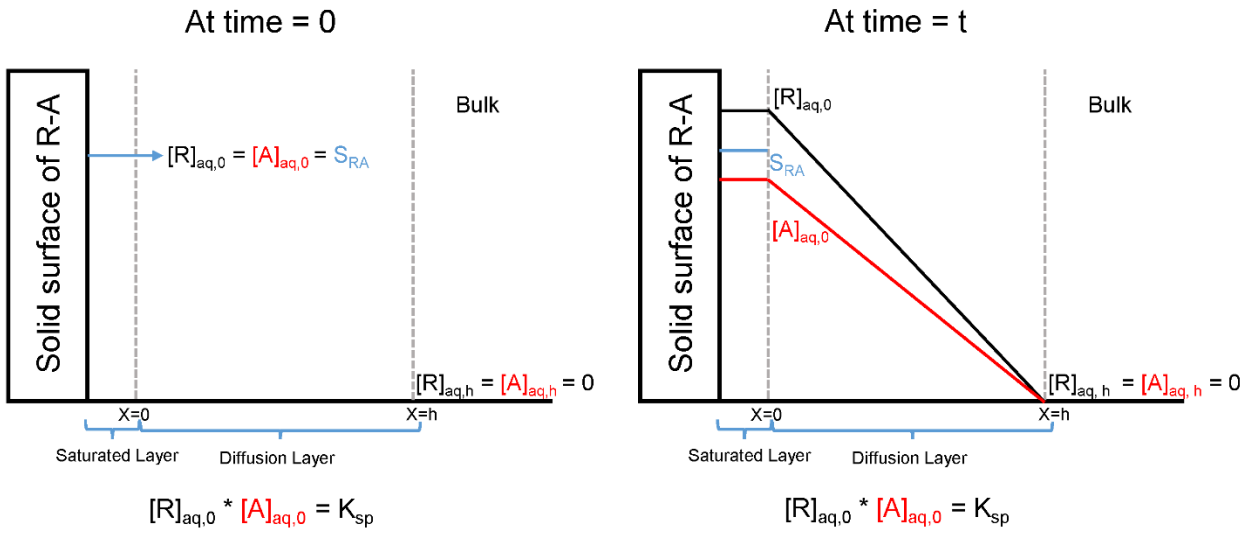

Figure 2.1. Schematic representation of the dissolution process of RA in non-reactive media using the interfacial equilibrium model. $[R]_{aq,0}$ and $[A]_{aq,0}$ represent the concentrations of R and A at the dissolving surface; $[R]_{aq,h}$ and $[A]_{aq,h}$ represent the concentrations of R and A in the bulk assuming sink conditions; S_{RA} is the solubility of the cocrystal and K_{sp} is the solubility product of the cocrystal.

At time = 0, before any component diffusion, the concentration of the drug in the saturated layer should be the same as the coformer for 1:1 cocrystals as shown in Figure 2.1. As diffusion occurs, the chemical equilibrium shown in equation 2.1 is disrupted in the saturated layer because of the decrease in concentration of A due to its more rapid diffusion. To re-establish this equilibrium in the saturated layer, which means keeping K_{sp} constant, the concentrations of R and A would have to vary. A boundary condition assumption at the solid-liquid interface for the interfacial equilibrium model is that the K_{sp} relationship is assumed to apply at all times ($t \geq 0$). Because of the different diffusivities between the cocrystal components, the concentrations of R and A will differ at the dissolving surface for $t > 0$ to maintain stoichiometric dissolution. At steady state, the concentration of R at the solid liquid interface would be higher than the stoichiometric solubility of the cocrystal due to its lower diffusion coefficient, while the concentration of A is consequently smaller to maintain the K_{sp}.

If there is no solid phase transformation or precipitation in the boundary layer or at the solid surface, the dissolution rate of the drug must be the same as the coformer for a 1:1 cocrystal. The dissolution rate of the cocrystal in terms of components can be described by the Nernst-Brunner equation[28, 31] for flux:

$$J_R = \frac{D_R[R]_{aq,0}}{h} = J_A = \frac{D_A[A]_{aq,0}}{h} \tag{2.3}$$

where D is diffusivity, $[R]_{aq,0}$ and $[A]_{aq,0}$ are total concentrations of the drug and coformer at the dissolving surface and h is the thickness of the hydrodynamic boundary layer that reflects the hydrodynamic conditions near the dissolving surface and sink conditions are assumed. Since this model is assumed to maintain K_{sp}, the following relationship is true at all time:

$$[R]_{aq,0} * [A]_{aq,0} = K_{sp} \tag{2.4}$$

The concentration of coformer, $[A]_{aq,0}$ and drug, $[R]_{aq,0}$, at the solid liquid interface can be solved using equations 2.3 and 2.4 as follows:

$$[A]_{aq,0} = (\frac{D_R}{D_A})^{1/2}\sqrt{K_{sp}} \tag{2.5}$$

$$[R]_{aq,0} = \left(\frac{D_A}{D_R}\right)[A]_{aq,0} = \left(\frac{D_A}{D_R}\right)(\frac{D_R}{D_A})^{1/2}\sqrt{K_{sp}} = \left(\frac{D_A}{D_R}\right)^{\frac{1}{2}}\sqrt{K_{sp}} \tag{2.6}$$

The concentrations of both components at the surface are dependent on the solubility and differential diffusivity between the components. A large difference between the component diffusivities increases the concentration difference between the drug and coformer at the solid-liquid interface while maintaining the solubility product.

Surface saturation model

The dissolution process of RA in non-reactive media can also be described using the surface saturation model, illustrated in Figure 2.2. It is assumed that a saturated layer adjacent to the dissolving surface consists of equal molar concentrations of R and A at the saturated solubility of the cocrystal (ie: stoichiometric cocrystal solubility) at time = 0. Before any component diffusion, the concentration product of both components within the saturated layer is equal to the solubility product of the cocrystal. Both components then diffuse across the diffusion layer at equal rates in proportion to their respective diffusion coefficients. As diffusion begins, the concentrations of both components would be depleted, but the depletion of A would be greater because of its greater diffusivity compared to R. In response to the depletion, more solid cocrystal would dissolve to maintain a saturated solution corresponding to the solubility of the cocrystal in the saturated layer. As the slower diffusing component, the rate of R depletion determines the rate

of replenishment. Therefore, the concentration of R at the dissolving surface is maintained at the stoichiometric solubility of the cocrystal:

$$[R]_{aq,0} = \sqrt{K_{sp}} \tag{2.7}$$

while the concentration of A may be lower. By assuming the dissolution rate of the drug is equal to the coformer, the concentration of A at the surface can be solved as follows:

$$J_R = \frac{D_R\sqrt{K_{sp}}}{h} = J_A = \frac{D_A[A]_{aq,0}}{h} \tag{2.8}$$

$$[A]_{aq,0} = \frac{D_R}{D_A}\sqrt{K_{sp}} \tag{2.9}$$

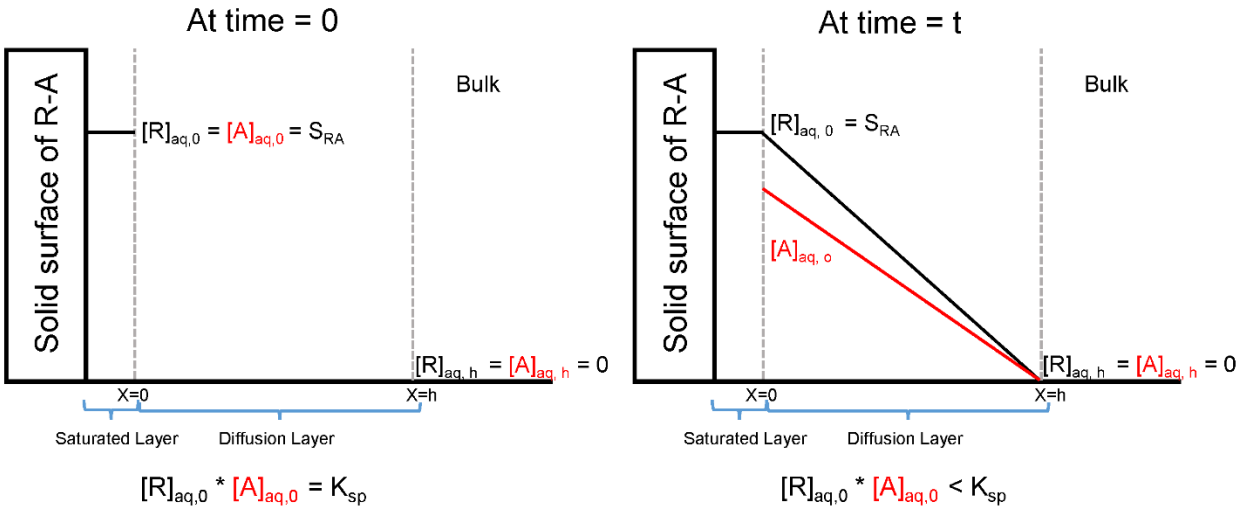

Figure 2.2. Schematic representation of the dissolution process of RA in non-reactive media using the surface saturation model. $[R]_{aq,0}$ and $[A]_{aq,0}$ represent the concentrations of R and A at the dissolving surface; $[R]_{aq,h}$ and $[A]_{aq,h}$ represent the concentrations of R and A in the bulk assuming sink conditions; S_{RA} is the solubility of the cocrystal and K_{sp} is the solubility product of the cocrystal.

The concentration of the drug at the surface is the same as the stoichiometric solubility of the cocrystal, but the coformer concentration is dependent on both the cocrystal solubility and differential diffusivity between the cocrystal components. The greater the difference in diffusivity,

the lower the concentration of coformer is at the surface. Because of the lower coformer concentration, the solubility product no longer applies beyond the interface at $x > 0$.

The assumptions made for both models are based upon the fact that the diffusion coefficients of the cocrystal components are different. Under stoichiometric dissolution for a 1:1 cocrystal, the dissolution rates of both species are observed to be equal with no solid phase transformation. The difference in diffusion coefficients can result in unequal concentrations of the cocrystal components at the dissolving surface and impact the ability of the cocrystal to maintain the solubility product, K_{sp}. The interfacial equilibrium model is assumed to maintain constant K_{sp} at all time at the dissolving surface during dissolution with the result that the drug concentration is higher but a lower coformer concentration. The surface saturation model assumes that the drug concentration remains equal to the stoichiometric solubility of the cocrystal, but with a lower coformer concentration to maintain stoichiometric dissolution and without maintaining K_{sp} constant at the dissolving surface. If the drug and coformer have equal diffusion coefficients, the concentrations of both components at the surface will be the same and the two models will merge into one.

Rotating Disk Dissolution Hydrodynamics

Dissolution experiments may be performed using a variety of experimental systems. For this study, rotating disk dissolution experiments were performed. Two significant advantages of this system include the maintenance of a constant surface area available for dissolution as well as defined hydrodynamics that provide an a priori estimate of the hydrodynamic boundary layer adjacent to the rotating surface. According to Levich[32], the hydrodynamic boundary layer thickness, *h*, is given by:

$$h = 1.612 D^{\frac{1}{3}} v^{\frac{1}{6}} \omega^{-\frac{1}{2}} \quad (2.10)$$

where v is the kinematic viscosity and ω is the angular velocity in radians per unit time.

Both interfacial equilibrium and surface saturation models described above are based on the assumption that the diffusion layer is the same for both the drug and coformer. However, according to equation 2.10, the diffusion layer thickness has a dependence on the diffusion coefficient. The diffusion coefficients of the drug and coformer in water can be different due to their molecular sizes difference. The different hydrophobicity between the drug and coformer can also magnify the difference in diffusivity in surfactant solution. The differential diffusivity can result in a significant difference between the diffusion layer of the two cocrystal components as h is directly proportional to the diffusion coefficient.

An alternative approach for the two models is to redefine the diffusion layer thicknesses for both the drug and coformer as they have different diffusion coefficients and consequently different diffusion layer thicknesses according to equation 2.10. Applying equation 2.10 separately for the diffusion layer of R ($h_R = 1.612 D_R^{1/3} v^{\frac{1}{6}} \omega^{-\frac{1}{2}}$) and A ($h_A = 1.612 D_A^{1/3} v^{\frac{1}{6}} \omega^{-\frac{1}{2}}$) to equation 2.3 and applying equation 2.4, the concentrations of R and A at the dissolving surface for the interfacial equilibrium model are shown to become a function of the diffusion coefficients:

$$[A]_{aq,0} = (\frac{D_R}{D_A})^{1/3} \sqrt{K_{sp}} \quad (2.11)$$

$$[R]_{aq,0} = (\frac{D_A}{D_R})^{1/3} \sqrt{K_{sp}} \quad (2.12)$$

And similarly, applying equation 2.10 separately for R and A to equation 2.8, the concentration of A at the surface for the surface saturation model becomes:

$$[A]_{aq,0} = (\frac{D_R}{D_A})^{2/3}\sqrt{K_{sp}} \quad (2.13)$$

and $[R]_{aq,0}$ is given by equation 2.7.

Dissolution in reactive media

Cocrystals can contain components with different ionization properties (eg: nonionizable drug and ionizable coformer) and these components can undergo chemical reactions at the solid liquid interface and in the boundary layer with the species from the bulk solution. These reactions can alter the pH and concentrations at the dissolving surface. A schematic representation of the dissolution process for a 1:1 cocrystal with R as the non-ionizable drug and HA as the monoprotic acidic coformer is shown in Figure 2.3. As cocrystal is initially exposed to solution, it dissociates into its components, R and HA at the dissolving surface. Both R and HA diffuse across the diffusion layer with a thickness of *h*, however, HA can simultaneously react with incoming base (B^-) from the bulk solution to form A^- and HB.

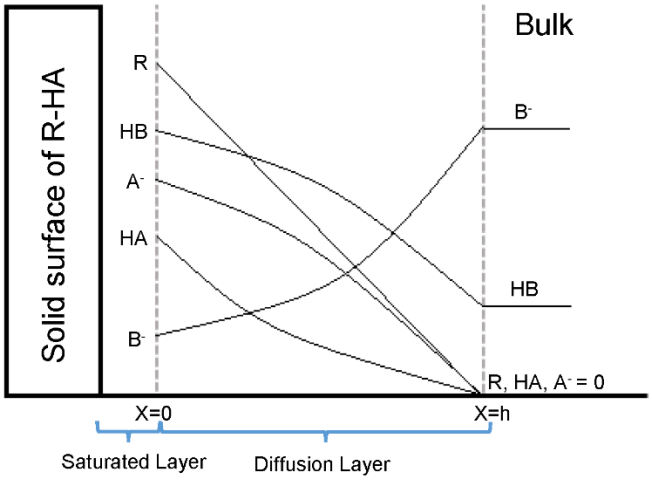

Figure 2.3. Schematic representation of the dissolution process[24] for a 1:1 cocrystal with R as the non-ionizable drug and HA as the monoprotic acidic coformer in the presence of a reactive medium containing base, B^-. A^- and HB are the products of the reaction.

For the dissolution of RHA in a reactive medium containing hydroxide ion and water as the reactive basic species (eg: no additional buffer), the chemical reactions occurring at the surface and within the boundary layer include the self-dissociation of the cocrystal into R, HA and ionization of HA as it is a weakly acidic coformer. The chemical equilibria and the equations for equilibrium constants for the dissolution of RHA are provided in Appendix A.

Dissolution in surfactant solution

Previous studies have shown that surfactants can solubilize the cocrystal components to different extents due to the different hydrophobicity of the drug and coformer[17, 22, 23]. Typically, the drug component is more hydrophobic and it is highly solubilized by surfactants compared to the coformer. The equilibria reflecting the solubilization of drug (R) and the unionized form of coformer (HA) are given in Appendix 2A.

Because of the differential solubilization, the parent drug, which is typically less soluble than the cocrystal in the absence of surfactant, can achieve the same solubility as the cocrystal in solution containing surfactant concentration at the CSC[17, 22, 23]. As surfactant concentration exceeds the CSC, the parent drug becomes more soluble, so drug precipitation during dissolution of the cocrystal can be prevented. The two cocrystals studied here have higher solubility than the parent drug, so dissolution experiments were performed in media containing surfactant concentrations above the CSC to prevent solid phase transformation. Among the surfactants studied in our lab, sodium lauryl sulfate (SLS) solubilizes CBZ to the greatest extent so it was chosen to study in this work.

Mass transport analysis

Detailed derivations of the mass transport analysis for the two models applying the above considerations are provided in Appendix 2A. The different boundary conditions of the cocrystal components from the two models lead to different mass transport analyses. These mass transport analyses allow for predictions of cocrystal flux as a function of bulk pH and surfactant concentration by taking the pH at the surface into consideration. The comparison of the mass transport analyses between the two models are shown in the Results section.

Results

Physicochemical properties

The physicochemical properties of the cocrystal and its components such as solubility products, ionization constants, micellar solubilization constants and diffusion coefficients are required to predict the interfacial pH and flux of the cocrystal components. These values can be obtained independently. The solubility products of the model cocrystals, the ionization constants of their coformers and the diffusion coefficients in water are summarized in Table 2.1 for carbamazepine-saccharin (CBZ-SAC) and carbamazepine-salicylic acid (CBZ-SLC). The solubility product of CBZ-SLC was determined by measuring the eutectic concentrations of the components as a function of surfactant concentration. The solubility product of CBZ-SAC was obtained from the literature[13]. The diffusion coefficients in water were estimated using the approach of Othmer Thaker[33]. According to Othmer Thaker's equation for estimating diffusion in dilute water solutions, the aqueous diffusion coefficient is inversely proportional to the molecular volume of the substance[33]. As a larger molecule, the diffusion coefficient of CBZ in water is smaller than both SAC and SLC.

Table 2.1. Physicochemical properties of model cocrystals and their components.

Cocrystal (R-HA)	K_{sp} (mM^2)	pK_a of HA	Aqueous diffusion coefficient[c] (x 10^{-6} cm^2/sec)	
			$D_{R_{aq}}$	$D_{HA_{aq}}$
CBZ-SAC	1.00[a]	1.6[a]	5.7	7.6
CBZ-SLC	0.40	3.0[b]	5.7	7.7

[a]From reference[13]. [b]From reference[17]. [c]Estimated using Othmer Thaker's equation[33].

The micellar solubilization constants of the drug and coformers are summarized in Table 2.2. The solubilization power of a surfactant can be influenced by the size and shape of the micelles[34, 35]. It was reported in the literature that the size and shape of the micelles may change as surfactant and additive concentrations change[36]. Therefore, it was not surprising to observe that SLS solubilizes CBZ to different extents at different concentrations. The solubilization of coformers in SLS is small compared to the drug, and the K_s values were assumed to be independent of SLS concentration in the range studied. The diffusion of CBZ in SLS solution would be smaller than the coformers because CBZ is significantly solubilized in the micelles compared to both SAC and SLC.

Table 2.2. Micellar solubilization constants of CBZ, SAC and SLC in SLS solution.

Components	K_s in SLS (mM^{-1})					
	22-44 mM	70 mM	100 mM	150 mM	250 mM	400 mM
CBZ	0.58[a]	0.465[b] ± 0.004	0.45[b] ± 0.01	0.43[b] ± 0.01	0.392[b] ± 0.003	0.35[b] ± 0.01
SAC	0.013[a]					
SLC	0.060[a]					

[a]From reference[17]. The K_s values for SAC and SLC are assumed to be constant for SLS concentrations ranging from 22 to 400 mM.

[b]Determined using $S_T = S_{aq}(1 + K_s^R[m])$, where S_T is the total solubility of the drug in SLS solution and S_{aq} is the aqueous solubility in water, which is 0.53 mM[17]. The total drug solubility in SLS solution is the same as the eutectic concentrations of CBZ shown in Figure 4 because both solid drug and cocrystal are in equilibrium with solution at the eutectic point[27].

Solubility study

The concentrations of the cocrystal components at the eutectic point are shown in Figure 2.4 for both cocrystals at pH 1 as a function of SLS concentration. Since all the experiments were performed above the CSC, the eutectic concentrations of the drug were greater than the coformers, meaning the solubility of the cocrystal is less than the drug under these conditions. At the eutectic point, the solid phases of both drug and cocrystal are in equilibrium with solution, and thus the drug eutectic concentration is at its solubility at the same solution conditions[27]. This allows the calculations of solubilization constants for the drug shown in Table 2.2. Using previously developed model[27], the solubility of CBZ-SAC and CBZ-SLC were determined from the eutectic concentrations and plotted in Figure 2.5. The lowest SLS concentration used was 22 mM, which is above the reported CMC of SLS in the literature (6 mM)[17]. The formation of micelles in solution preferentially solubilizes CBZ and results in solubility enhancement as SLS concentration increases. SLS does not solubilize SAC and SLC to the same extent as CBZ because these coformers are more hydrophilic. The differential solubilization between the drug and coformers causes the solubility of the cocrystal to increase nonlinearly as a function of surfactant concentration and the slightly nonlinear nature of the curves in Figure 2.5 may be attributed to this.

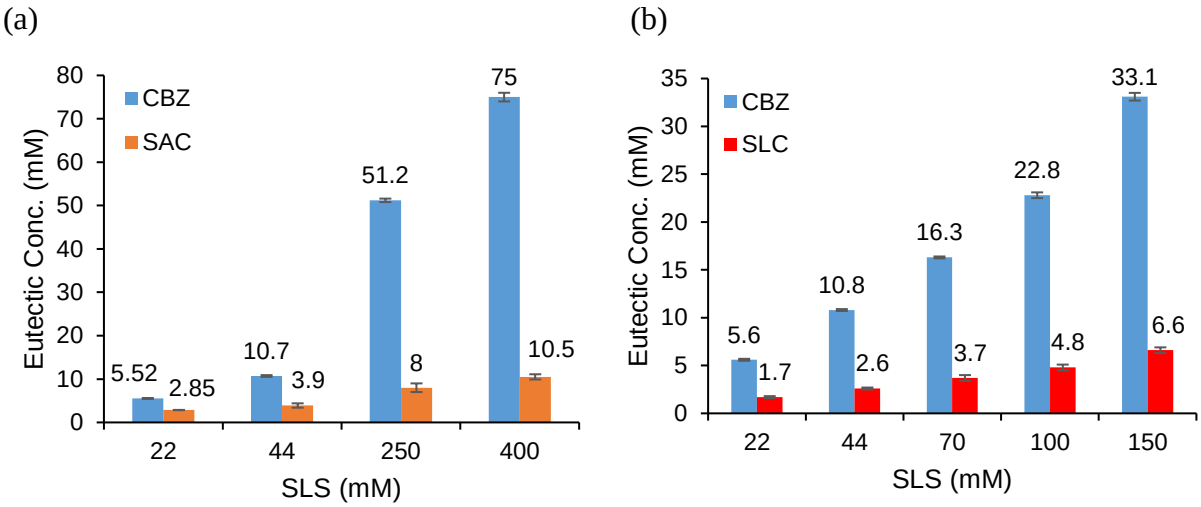

Figure 2.4. Eutectic measurements for CBZ-SAC (a) and CBZ-SLC (b) at pH 1 as a function of SLS concentration.

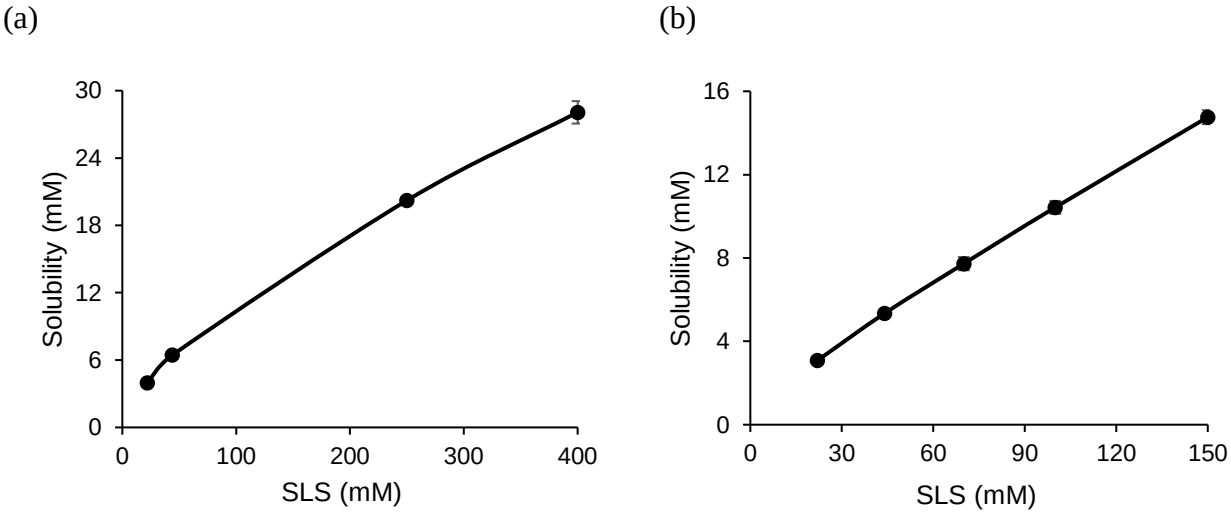

Figure 2.5. Solubility of cocrystals, CBZ-SAC (a) and CBZ-SLC (b) at pH 1 as a function of surfactant concentration. Cocrystal solubility was determined using eutectic concentrations from Figure 2.4 by $S_{cc} = \sqrt{[drug]_{eutectic}[coformer]_{eutectic}}$[27].

Effect of surfactant on dissolution

The dissolution profiles of CBZ-SAC and CBZ-SLC at different SLS concentrations at constant pH (pH = 1) where the coformers are mostly nonionized are shown in Figure 2.6. Since experiments were conducted above the CSC where the cocrystals were thermodynamically stable,

the dissolution behavior of both cocrystals was linear as expected under sink conditions. Similar to solubility, the dissolution rates of both cocrystals increase as SLS concentration increases.

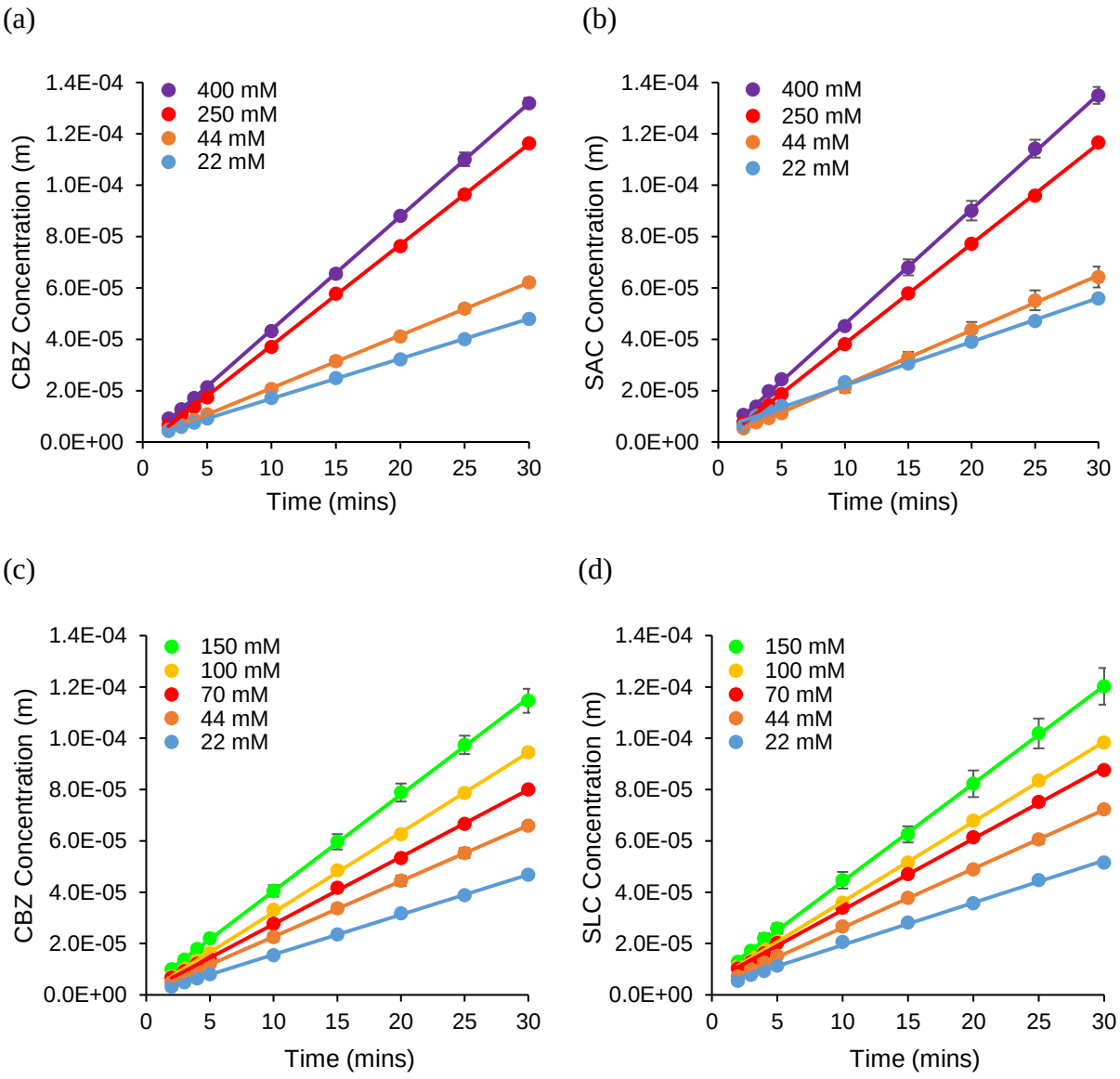

Figure 2.6. Dissolution profiles for CBZ-SAC in terms of CBZ concentrations (a) and SAC concentrations (b); and CBZ-SLC in terms of CBZ concentrations (c) and SLC concentrations (d) at different SLS concentrations at pH1. The solid circles are experimental data points and the solid lines are fitted liner regressions.

The effective diffusion coefficients of CBZ can be estimated from the dissolution rates of the cocrystals at pH 1 as a function of SLS concentration using equation 2A.49 from Appendix

2A. The micellar diffusivity of CBZ can then be estimated from the effective diffusivity according to the following relationship:

$$D_{R_{eff}} = \frac{D_{aq}+K_S D_m[m]}{1+K_S[m]} \quad (2.14)$$

where $D_{R_{eff}}$ is the effective diffusivity of the drug and D_m is the micellar diffusivity[37]. The micellar diffusivities of CBZ for the two cocrystals as a function of SLS concentration are plotted in Figure 2.7. A power regression can be fitted to describe the relationship between micellar diffusivity and SLS concentration. Micellar diffusivity of CBZ decreases as surfactant concentration increases. The same trend was also observed in the literature[38-40]. Detailed analysis of this is beyond the scope of this study. However, this behavior may be due to the formation of larger micelles as surfactant concentration increases[38] and the potential changes in viscosity. Another possible reason could be the increase in electrostatic repulsion as surfactant concentration increases since SLS is negatively charged[39]. The diffusion of the micelle-drug complexes can be reduced by the electronic repulsion between the negatively charged micelles[39]. The CBZ micellar diffusivities determined from the dissolution of CBZ-SLC are somewhat greater than those determined for CBZ-SAC. The reason for these differences is not known but may be due to the different chemical environments surrounding the micelles between the two cocrystals. Both SAC and SLC are able to ionize and form negatively charged ions that can potentially increase the electronic repulsion in solution. CBZ-SAC has a higher K_{sp} value and SAC is more acidic than SLC, so the degree of SAC ionization is higher than SLC at the same pH. The higher SAC ion concentration in solution may cause a greater increase in electronic repulsion for CBZ-SAC than CBZ-SLC. Consequently, the diffusion of micelles may be slower in CBZ-SAC dissolution than in CBZ-SLC dissolution. For this study, the micellar diffusivities shown in Figure 2.7 are used to assess the mass transport

models described here. It is also appropriate to point out that equation 2A.49 from Appendix 2A does not take into account kinetic processes involving surfactant and micelles that may occur at the dissolving surface.

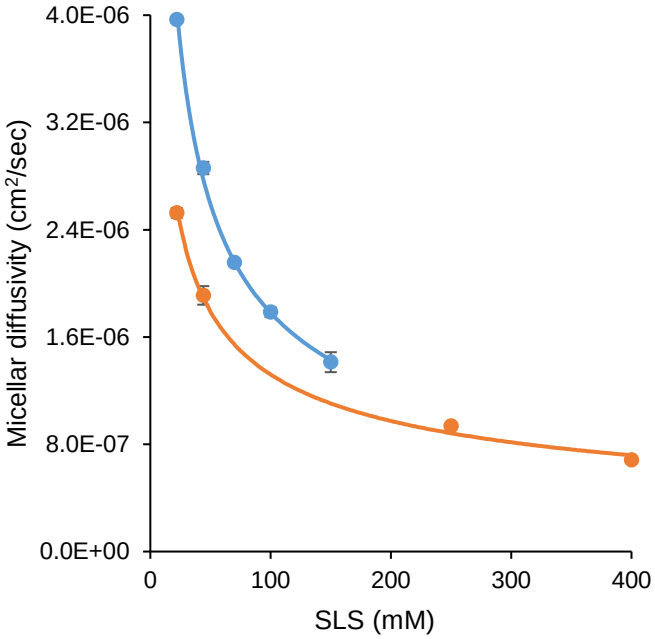

Figure 2.7. Micellar diffusivities of CBZ determined from the dissolution of CBZ-SAC (—) and CBZ-SLC (—) at pH 1 as a function of SLS concentration. The solid circles are experimental data points determined from the dissolution shown in Figure 2.6 using equations 2A.49 from Appendix 2A and 2.14 and solubility shown in Figure 2.5. The solid lines are the fitted power regression. The power regression line for CBZ-SAC is $y = 9.9771E\text{-}06x^{-4.3920E\text{-}01}$ and CBZ-SLC is $y = 2.1553E\text{-}05*x^{-5.4153E\text{-}01}$.

Effect of pH on dissolution

The effect of pH on dissolution of cocrystals was studied at constant surfactant concentration as a function of pH. The dissolution experiments were conducted in 400 mM SLS solution for CBZ-SAC and 150 mM for CBZ-SLC. The dissolution profiles of CBZ-SAC and CBZ-SLC in terms of cocrystal components as a function of pH are shown in Figure 2.8 and 2.9. The linear dissolution behavior of the two cocrystals indicates no solid phase transformation occurred during dissolution as the experiments were performed above the CSC. The dissolution

rates of both cocrystals increase as pH increases and then remain relatively constant in the self-buffering region of the coformers. Since SAC has a lower pK_a than SLC, pH has a greater impact on the dissolution rate of CBZ-SAC compared to CBZ-SLC as reflected in the larger range of dissolution rates in Figure 2.8 compared to Figure 2.9.

(a) (b)

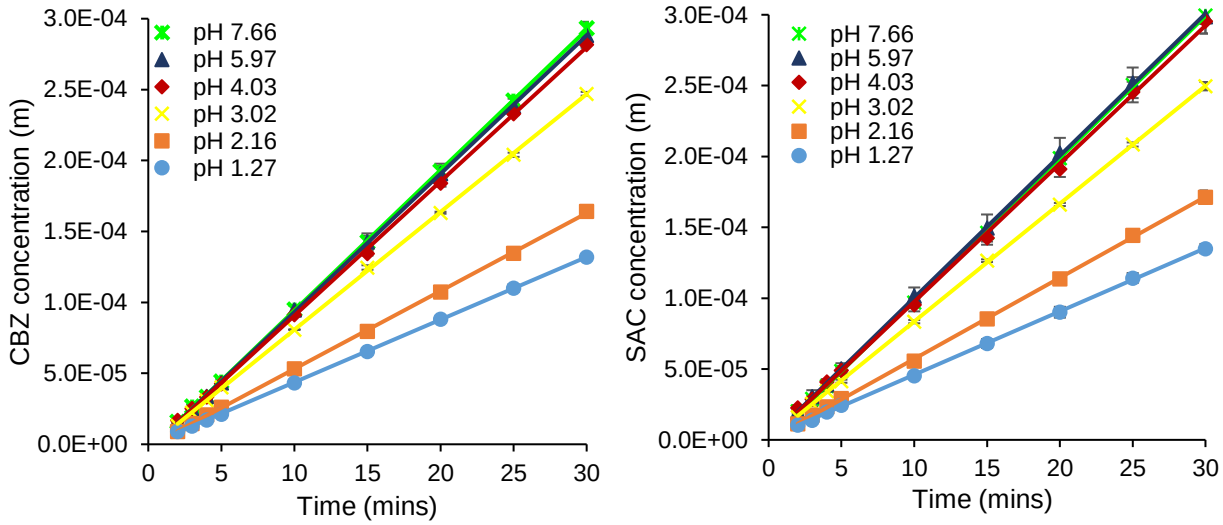

Figure 2.8. Dissolution profiles of CBZ-SAC in terms of CBZ (a) and SAC (b) as a function of bulk pH at 400 mM SLS. The symbols are experimental data points and the solid lines are fitted liner regressions. The pH values represent the initial bulk pH of the dissolution media.

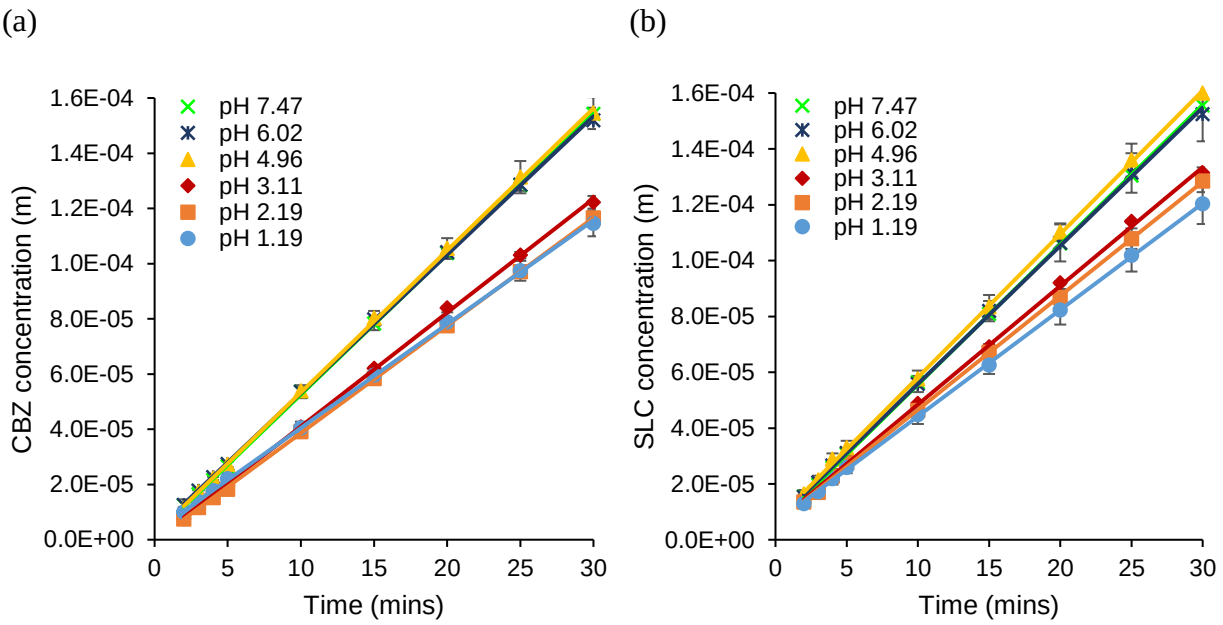

Figure 2.9. Dissolution profiles of CBZ-SLC in terms of CBZ (a) and SLC (b) as a function of bulk pH at 150 mM SLS. The symbols are experimental data points and the solid lines are fitted liner regressions. The pH values represent the initial bulk pH of the dissolution media.

Comparison of flux predictions between the mass transport models

For comparison purposes, only literature reported micellar diffusivities of CBZ in SLS solution were used and no parameters were adjusted to fit the experimental data to the theoretical equations of the two transport models shown in Table 2.3 and Figure 2.10. A micellar diffusivity of 3.6E-7 cm^2/sec at 400 mM SLS was used for CBZ-SAC and for CBZ-SLC, a value of 6.4E-7 cm^2/sec at 150 mM SLS was used[40]. The difference in concentrations of the cocrystal components at the surface predicted using the two models and how this difference could affect the interfacial pH is illustrated in Table 2.3 for the dissolution of CBZ-SAC at 400 mM SLS. The interfacial pH calculated from both models lags behind bulk pH above the pK_a value of SAC (pK_a=1.6) due to the ionization of SAC in the diffusion layer. The interfacial equilibrium model predicts a lower surface pH (approximately 0.3 pH units at pH 6) compared to the surface saturation model. The lower interfacial pH calculated from the interfacial equilibrium model is due to the greater SAC

concentration predicted at the dissolving surface to maintain the K_{sp} of CBZ-SAC. As shown in Table 2.3, the concentrations of both CBZ and SAC at the surface calculated from the interfacial equilibrium model are higher than those calculated from the surface saturation model. Because of the depletion of SAC at the surface of the boundary layer due to faster diffusion, the concentration product of CBZ and SAC from the surface saturation model is less than the K_{sp} of CBZ-SAC. In order to re-establish the equilibrium disrupted by diffusion, both CBZ and SAC concentrations from the interfacial equilibrium model are predicted to increase at the surface to maintain a concentration product equal to the K_{sp} of CBZ-SAC. As seen in Table 2.3 and Figure 2.10, both models result in qualitatively similar predictions. Subtle but potentially important differences in surface concentrations result in different predicted dissolution rates.

Table 2.3. Interfacial pH and concentrations of CBZ and SAC at the surface calculated using the surface saturation and interfacial equilibrium models for the dissolution of CBZ-SAC at 400 mM SLS as a function of bulk pH.

Surface saturation model						
Bulk pH	Interfacial pH[a]	Concentrations at the surface (mM)				$[CBZ]_{aq}$*$[SAC]_{aq}$ (mM^2)
		$[CBZ]_{tot}$[b]	$[CBZ]_{aq}$[c]	$[SAC]_{tot}$[d]	$[SAC]_{aq}$[e]	
1.27	1.27	30.4	0.2	4.2	0.6	0.1
2.16	2.15	36.8	0.3	5.1	0.5	0.1
3.02	2.84	57.4	0.4	8.0	0.3	0.1
4.03	3.10	72.7	0.5	10.1	0.3	0.1
5.97	3.14	75.6	0.5	10.5	0.3	0.1
7.66	3.14	75.6	0.5	10.5	0.3	0.1
Interfacial equilibrium model						
1.27	1.27	81.5	0.6	11.3	1.7	1.0
2.16	2.14	98.3	0.7	13.7	1.4	1.0
3.02	2.70	137.3	1.0	19.1	1.0	1.0
4.03	2.85	155.2	1.1	21.6	0.9	1.0
5.97	2.87	157.9	1.1	22.0	0.9	1.0
7.66	2.87	157.9	1.1	22.0	0.9	1.0

[a]Calculated using equation 2A.45 from Appendix 2A for surface saturation model and equation 2A.57 from Appendix 2A for interfacial equilibrium model with K_{sp}, K_a, K_s and $D_{HA_{aq}}$ values shown in Table 2.1 and 2.2. $D_{HA_{eff}}$ is assumed to be equal to $D_{HA_{aq}}$. The $D_{R_{eff}}$ value for CBZ-SAC (3.9E-7 cm^2/sec) was calculated from equation 2.14 using the D_m value of 3.6E-7 cm^2/sec

from the literature[40]. The diffusion coefficients for H^+ and OH^- are 9.31E-5 and 5.28E-5 cm^2/sec, respectively[41].

[b]Calculated using equation 2A.13 from Appendix 2A with the K_s value from Table 2.2 and calculated $[CBZ]_{aq}$ from surface saturation and interfacial equilibrium models.

[c]Calculated using equations 2A.38 and 2A.51 from Appendix 2A for surface saturation model and interfacial equilibrium model, respectively. K_{sp}, K_a, K_s values are from Table 2.1 and 2.2 and interfacial pH is from a. $D_{R_{eff}}$ is 3.9E-7 cm^2/sec and $D_{HA_{eff}}$ is assumed to be equal to $D_{HA_{aq}}$ shown in Table 2.1.

[d]Calculated using equation 2A.14 from Appendix 2A with the K_s and K_a values from Table 2.1 and 2.2, calculated $[SAC]_{aq}$ from surface saturation and interfacial equilibrium models, and interfacial pH from a.

[e]Calculated using equations 2A.40 and 2A.52 from Appendix 2A for surface saturation model and interfacial equilibrium model, respectively. K_{sp}, K_a, K_s values are from Table 2.1 and 2.2 and interfacial pH is from a. $D_{R_{eff}}$ is 3.9E-7 cm^2/sec and $D_{HA_{eff}}$ is assumed to be $D_{HA_{aq}}$ shown in Table 2.1.

The flux of CBZ-SAC at 400 mM SLS and CBZ-SLC at 150 mM SLS as a function of bulk pH were predicted using both models and the predicted values were compared with the experimental data as shown in Figure 2.10. The predictions from both models follow the same trend as the experimental data. However, the predictions from both models deviate from the experimental data because the effective diffusivities of CBZ used here were estimated from the micellar diffusivities of SLS in the literature determined at conditions different from the study here. The surface saturation model slightly under predicted the flux, while the interfacial equilibrium model over predicted the flux. However, the surface saturation model is able to provide more accurate prediction of cocrystal flux compared to the interfacial equilibrium model. It is difficult to experimentally prove which model more accurately represents the conditions at the dissolving surface as it requires concentration measurements at the dissolving surface. Analysis of the experimental results and theoretical predictions from the surface saturation model indicated somewhat better alignment. Consequently, the surface saturation model is used to perform the mass transport analysis for the two cocrystals studied here.

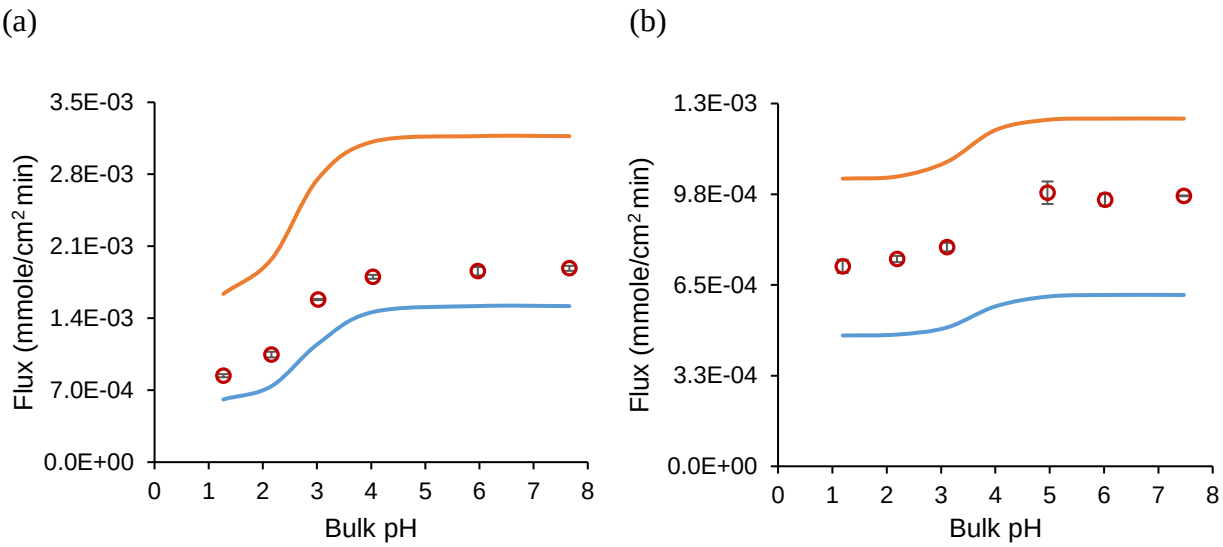

Figure 2.10. Experimental (○) and predicted flux comparison of CBZ-SAC at 400 mM SLS (a) and CBZ-SLC at 150 mM SLS (b) as a function of bulk pH using the surface saturation model (——) and interfacial equilibrium model (——). The flux predictions were calculated using equations 2A.49 and 2A.58 from Appendix 2A based on the interfacial pH predicted from equations 2A.45 and 2A.57 from Appendix 2A for surface saturation and interfacial equilibrium models, respectively. The K_{sp}, K_a, K_s and $D_{HA_{aq}}$ values are shown in Table 2.1 and 2.2. $D_{R_{eff}}$ values for CBZ-SAC is 3.9E-7 cm^2/sec and CBZ-SLC is 7.2E-7 cm^2/sec.

Interfacial pH and CSC predictions from surface saturation model

Interfacial pH can be predicted using equation 2A.45 derived from the surface saturation model shown in Appendix 2A and the physicochemical parameters of the cocrystals and their components (eg: solubility products, ionization constants, solubilization constants and effective diffusivities). The effect of bulk pH and surfactant concentration on interfacial pH for CBZ-SAC and CBZ-SLC is shown in Figure 2.11 utilizing the surface saturation model. At constant surfactant concentration, for bulk pH < pK_a, interfacial pH is approximately equal to bulk pH because the hydrogen ion in the bulk solution suppresses the ionization of the coformers[24]. As bulk pH increases above the pK_a value of the coformer, coformer ionization begins to occur. This, in effect, results in a buffer effect at the interface and the interfacial pH no longer continues to increase linearly with increasing bulk pH[24]. Both cocrystals have the ability to self-buffer the pH

microenvironment in the diffusion layer[24] and this is demonstrated by the plateau region that ranges from bulk pH 4 to 8 in Figure 2.11. CBZ-SAC is able to self-buffer the interfacial pH to around 3.0; while the plateau interfacial pH for CBZ-SLC is around 3.7. The buffering ability is affected by the degree of ionization of the ionizable components at the interface and this is determined by the concentration and pK_a values of the ionizable components. With a higher solubility product and a lower pK_a, CBZ-SAC is able to self-buffer to a lower pH at the interface compared to CBZ-SLC. Surfactant has little or no effect on interfacial pH at bulk pH < pK_a values of the coformers because the interfacial pH is determined by bulk pH. As bulk pH increases above the pK_a of the coformer, the degree of coformer ionization is not affected by SLS significant enough to cause any changes in interfacial pH. For the cocrystals studied here, no significant impact on interfacial pH was predicted or observed as a function of surfactant concentration.

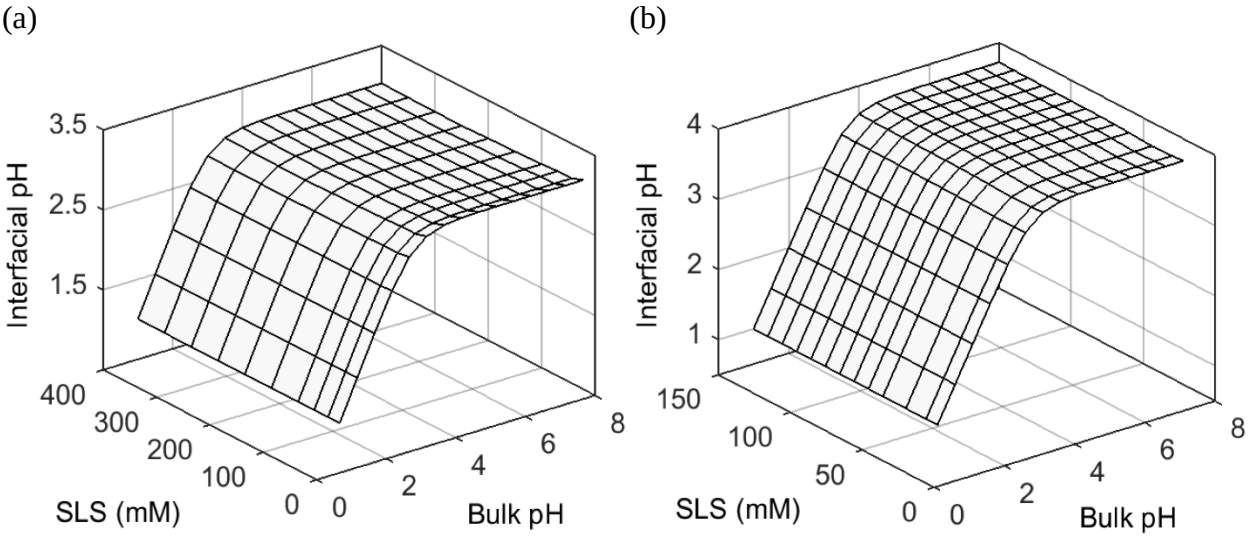

Figure 2.11. Theoretical predictions of interfacial pH for CBZ-SAC (a) and CBZ-SLC (b) as a function of pH and SLS concentration using surface saturation model. Interfacial pH was calculated using equation 2A.45 from Appendix 2A. The K_{sp}, K_a, K_s and $D_{HA_{aq}}$ values are shown in Table 2.1 and 2.2 and $D_{R_{eff}}$ values are from Figure 2.7.

The critical stabilization concentration, CSC has a pH dependence for the cocrystals studied here, so different surfactant concentrations will be required to stabilize the cocrystals at different pH to prevent solid phase transformation. Based on the predicted interfacial pH, the CSC needed at the dissolving cocrystal surface to prevent phase transformation can be estimated using the previously developed model[17]. The surfactant concentrations that are required to stabilize the model cocrystals at different pH are calculated and shown in Table 2.4.

Table 2.4. Estimated SLS concentrations for stabilizing cocrystals during dissolution at different pH using the surface saturation model.

CBZ-SAC			**CBZ-SLC**		
pH		**CSC[b] (mM)**	**pH**		**CSC[b] (mM)**
Bulk	**Interfacial[a]**		**Bulk**	**Interfacial[a]**	
1.0	1.0	12	1.0	1.0	7
2.0	2.0	27	2.0	2.0	7
3.0	2.8	161	3.0	3.0	10
4.0	3.0	306	4.0	3.6	18
5.0	3.0	326	5.0	3.7	21
6.0	3.0	326	6.0	3.7	21
7.0	3.0	326	7.0	3.7	21
8.0	3.0	326	8.0	3.7	21

[a]From Figure 2.11.

[b]Calculated from previously developed model[17].

The CSC of CBZ-SAC is significantly higher than CBZ-SLC since the solubility of CBZ-SAC is higher and thus requires higher surfactant concentration to stabilize the cocrystal during dissolution. Because of the self-buffering ability of the cocrystals, the CSC is essentially the same in the buffering region regardless of the bulk pH.

Surface saturation model flux predictions – pH effect

The flux of the cocrystals were calculated from the dissolution rates and compared to theoretical predictions to evaluate the predictive power of the surface saturation model. The

theoretical flux can be calculated using equation 2A.49 from Appendix 2A and the physicochemical parameters of the cocrystals and their components. The experimental and theoretical flux comparison is shown in Figure 2.12. The experimental data confirmed that the flux of the cocrystal components are equal as expected because the stoichiometry of both cocrystals are 1:1. Also as expected, the flux of CBZ-SAC and CBZ-SLC plateau in the buffering region because there is minimal change in interfacial pH as predicted from the mass transport analysis. By modeling the interfacial pH, the theoretical flux shows excellent agreement with the experimental data using the physicochemical parameters in Table 2.1 and 2.2 and Figure 2.7. Because of the acidity of SAC, the flux of CBZ-SAC is very sensitive to interfacial pH changes and this can lead to the large deviations observed in the buffering region. A 0.2 unit pH change in interfacial pH around 3.0 can lead to a roughly 20% change in the flux of CBZ-SAC. Accurate predictions of interfacial pH are clearly very important for predicting the flux of cocrystals with ionizable components.

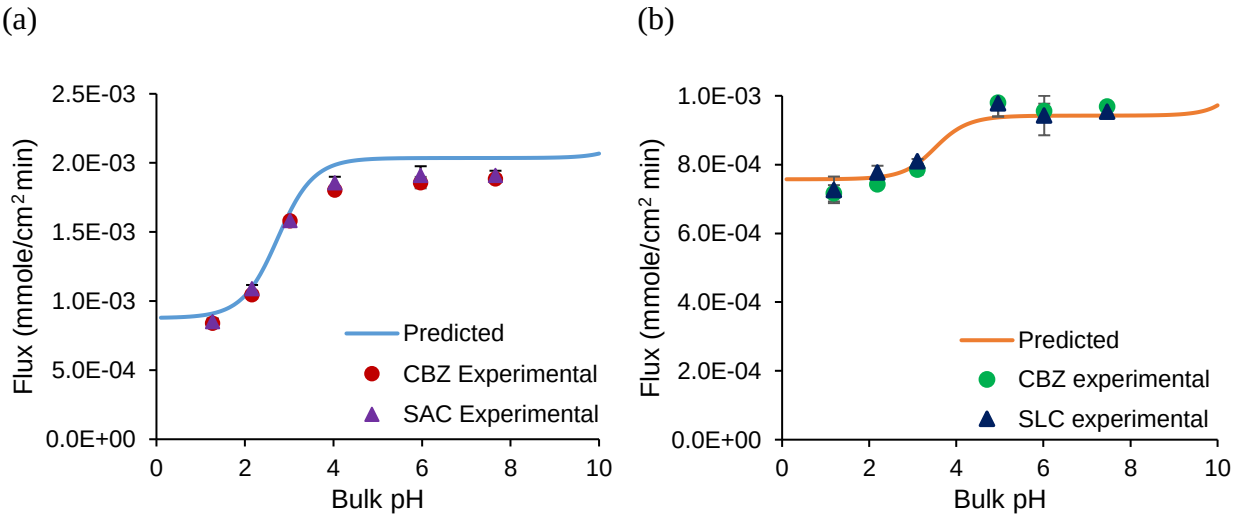

Figure 2.12. Flux of CBZ-SAC at 400 mM SLS (a) and CBZ-SLC at 150 mM SLS (b) as a function of bulk pH. Flux predictions were calculated using equation 2A.49 from Appendix 2A based on the interfacial pH predicted from Figure 2.11. The K_{sp}, K_a, K_s values are shown in Table 2.1 and 2.2 and $D_{R_{eff}}$ values are from Figure 2.7.

Combination effect of pH and surfactant on dissolution

The combination of pH and surfactant effect on the dissolution of cocrystals was studied by performing dissolution experiments at different pH and surfactant concentrations. The dissolution rates were expressed in terms of flux and compared to the predicted values from the surface saturation model. The dependence of flux on pH and surfactant concentration for both cocrystals is shown in the three dimensional plots in Figure 2.13. For both cocrystals, the theoretical values showed excellent agreement with the experimental data. There are fewer experimental data points on the CBZ-SAC plot because much of the area in the plot is not experimentally accessible due to the potential phase transformation during dissolution. At the buffering region (bulk pH 4 to 8), the surfactant concentration required to stabilize CBZ-SAC during dissolution is at least 326 mM (Table 2.4). Due to the potential conversion of CBZ-SAC back to the stable drug form, no dissolution experiments were performed in SLS concentration below 400 mM in the bulk pH range of 4 to 8. The effect of bulk pH on the flux of cocrystal is dictated by the interfacial pH. Any bulk pH changes in the range of 4 to 8 does not have a significant impact on the dissolution of the cocrystal because the cocrystal can self-buffer the pH microenvironment at the dissolving surface to produce essentially the same interfacial pH. Flux increases as surfactant concentration increases; however, the increase is larger at lower surfactant concentration.

(a) (b)

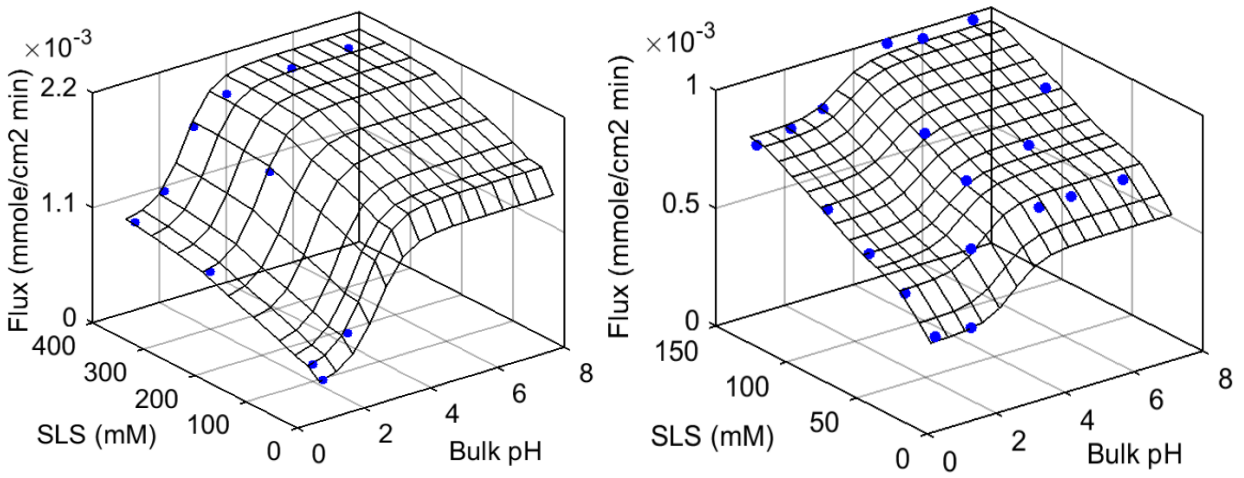

Figure 2.13. Influence of pH and surfactant concentration on flux of CBZ-SAC (a) and CBZ-SLC (b). The wireframe mesh represents the theoretical flux predictions and circles represent the experimentally measured flux of cocrystals in terms of CBZ. Flux predictions were calculated using equation 2A.49 from Appendix 2A based on the interfacial pH predicted from Figure 2.11. The K_{sp}, K_a, K_s values are shown in Table 2.1 and 2.2 and $D_{R_{eff}}$ values are from Figure 2.7.

The effects of surfactant concentration on solubility and micellar diffusivity are opposite. At low surfactant concentrations, the advantage of solubility enhancement on dissolution is greater than the disadvantage of decreased micellar diffusivity, so the increase in flux is greater. As surfactant concentration increases, the disadvantage of reduced micellar diffusivity is slowly approaching the advantage of solubility enhancement and thus the flux increase is smaller. When the opposite effects of surfactant on micellar diffusivity and solubility essentially cancel each other out, the enhancement in flux by surfactant is limited as indicated by the plateau values of CBZ-SAC at surfactant concentrations range from 300 to 400 mM.

Discussion

This work highlights the importance of interfacial pH on determining the flux of cocrystals with ionizable components. Without the knowledge of interfacial pH, one might assume the pH at the dissolving surface is the same as the bulk pH. Assuming this, the flux of both CBZ-SAC

and CBZ-SLC would be expected to increase with increasing bulk pH instead of plateauing at the buffering region. The fifth order equation (equation 2A.45 from Appendix 2A) developed from the mass transport analysis of the surface saturation model gives reasonably accurate predictions of interfacial pH that are otherwise difficult to measure experimentally. This allows the model to capture the plateaued region in the flux of both cocrystals as a function of bulk pH. The surfactant concentrations required to stabilize the cocrystal during dissolution at different bulk pH can also be estimated from the interfacial pH predictions. The use of surfactant can enhance the dissolution of cocrystals, but sometimes the enhancement may not be as large as expected because of the counter balancing effect of surfactant on solubility and micellar diffusion coefficients.

One of the important elements for the mass transport analysis of cocrystal is the concentrations of the cocrystal components at the dissolving surface as they determine the rate of dissolution. The surface concentrations of the components may not follow the cocrystal's stoichiometric ratio because they have different diffusion coefficients. For the cocrystals studied here, the drug has a slower diffusion compared to the coformers. According to the surface saturation model, the slower diffusing component (ie: the drug) is able to maintain a surface concentration at the stoichiometric cocrystal solubility and acts as the determinant for the dissolution of the cocrystal while the faster diffusing component has a lower surface concentration. The mass transport analysis here is only applicable for cocrystals that have the same stoichiometry and ionization property as CBZ-SAC and CBZ-SLC. However, the surface saturation model developed here can be applied to the mass transport analysis for cocrystals with different stoichiometries and ionization properties.

Conclusions

The mechanism of cocrystal dissolution as a function of pH and surfactant concentration has been successfully analyzed through the development and evaluation of a physically realistic mass transport model. This mass transport analysis demonstrated the importance of interfacial pH in determining the flux of cocrystals with ionizable components. The ionizable components have the ability to self-buffer the pH microenvironment at the interface. Evaluation of the physicochemical properties such as solubility product, ionization constant, solubilization constant and diffusion coefficient, are required for accurate prediction of interfacial pH and flux of the cocrystal. The predictive power of the mass transport analysis was evaluated by performing dissolution above the CSC to prevent the conversion of highly soluble cocrystal back to the drug form. The model adequately describes the dissolution behavior of cocrystal as a function of pH and surfactant concentration. Bulk pH itself does not adequately explain the dissolution behavior of cocrystal because the rate of dissolution is affected by the pH at the interface. The effect of surfactant on dissolution of cocrystal is also an important consideration and can diminish as surfactant concentration increases due to the counter balancing effects of surfactant on micellar diffusivity and solubility.

Acknowledgements

Research reported in this publication was partially supported by the National Institute of General Medical Sciences of the National Institutes of Health under award number R01GM107146. The content is solely the responsibility of the authors and does not necessarily represent the official views of the National Institutes of Health. We also gratefully acknowledge partial financial support from the College of Pharmacy, University of Michigan.

References

1. Williams, H. D.; Trevaskis, N. L.; Charman, S. A.; Shanker, R. M.; Charman, W. N.; Pouton, C. W.; Porter, C. J. H. Strategies to Address Low Drug Solubility in Discovery and Development. *Pharmacological Review* **2013,** *65*, 315-499.

2. Schultheiss, N.; Newman, A. Pharmaceutical Cocrystals and Their Physicochemical Properties. *Crystal Growth & Design* **2009,** *9*, (6), 2950-2967.

3. Thakuria, R.; Delori, A.; Jones, W.; Lipert, M. P.; Roy, L.; Rodriguez-Hornedo, N. Pharmaceutical Cocrystals and Poorly Soluble Drugs. *International Journal of Pharmaceutics* **2013,** *453*, (1), 101-125.

4. Yadav, A. V.; Shete, A. S.; Dabke, A. P.; Kulkarni, P. V.; Sakhare, S. S. Co-Crystals: A Novel Approach to Modify Physicochemical Properties of Active Pharmaceutical Ingredients. *Indian Journal of Pharmaceutical Sciences* **2009,** *71*, (4), 359-370.

5. Weyna, D. R.; Cheney, M. L.; Shan, N.; Hanna, M.; Zaworotko, M. J.; Sava, V.; Song, S.; Sanchez-Ramos, J. R. Improving Solubility and Pharmacokinetics of Meloxicam via Multiple-Component Crystal Formation. *Molecular Pharmaceutics* **2012,** *9*, 2094-2102.

6. Jung, M.; Kim, J.; Kim, M.; Alhalaweh, A.; Cho, W.; Hwang, S.; Velaga, S. P. Bioavailability of Indomethacin-Saccharin Cocrystals. *Journal of Pharmacy and Pharmacology* **2010,** *62*, 1560-1568.

7. Smith, A. J.; Kavuru, P.; Wojtas, L.; Zaworotko, M. J.; Shytle, R. D. Cocrystals of Quercetin with Improved Solubility and Oral Bioavailability. *Molecular Pharmaceutics* **2011,** *8*, (5), 1867-1876.

8. McNamara, D. P.; Childs, S. L.; Giordano, J.; Iarriccio, A.; Cassidy, J.; Shet, M. S.; Mannion, R.; O'Donnell, E.; Park, A. Use of a glutaric acid cocrystal to improve oral bioavailability of a low solubility API. *Pharmaceutical Research* **2006,** *23*, (8), 1888-1897.

9. Cheney, M. L.; Shan, N.; Healey, E. R.; Hanna, M.; Wojtas, L.; Zaworotko, M. J.; Sava, V.; Song, S.; Sanchez-Ramos, J. R. Effects of Crystal Form on Solubility and Pharmacokinetics: A Crystal Enginneering Case Study of Lamotrigine. *Crystal Growth & Design* **2010,** *10*, 394-405.

10. Shayanfar, A.; Jouyban, A. Physicochemical Characterization of a New Cocrystal of Ketoconazole. *Powder Technology* **2014,** *262*, 242-248.

11. Keramatnia, F.; Shayanfar, A.; Jouyban, A. Thermodynamic Solubility Profile of Carbamazepine-Cinnamic Acid Cocrystal at Different pH. *Journal of Pharmaceutical Sciences* **2015,** *104*, (8), 2559-65.

12. Li, M.; Qiao, N.; Wang, K. Influence of Sodium Lauryl Sulfate and Tween 80 on Carbamazepine-Nicotinamide Cocrystal Solubility and Dissoluiton Behaviour. *Pharmaceutics* **2013,** *5*, (4), 508-524.

13. Alhalaweh, A.; Roy, L.; Rodriguez-Hornedo, N.; Velaga, S. P. pH-Dependent Solubility of Indomethacin-Saccharin and Carbamazepine-Saccharin Cocrystals in Aqueous Media. *Molecular Pharmaceutics* **2012,** *9*, 2605-2612.

14. Bethune, S. J.; Huang, N.; Jayasankar, A.; Rodriguez-Hornedo, N. Understanding and Predicting the Effect of Cocrystal Components and pH on Cocrystal Solubility. *Crystal Growth and Design* **2009,** *9*, (9), 3976-3988.

15. Roy, L. Engineering Cocrystal and Cocrystalline Salt Solubility by Modulation of Solution Phase Chemistry (Doctoral Dissertation). *University of Michigan* **2013**.

16. Roy, L.; Lipert, M. P.; Rodriguez-Hornedo, N., Co-crystal Solubility and Thermodynamic Stability. In *Rsc Drug Discov*, Royal Society of Chemistry: 2012; pp 247-279.

17. Huang, N.; Rodriguez-Hornedo, N. Engineering Cocrystal Solubility, Stability, and pHmax by Micellar Solubilization. *Journal of Pharmaceutical Sciences* **2011,** *100*, (12), 5219-5234.

18. Lee, H. G.; Zhang, G. G. Z.; Flanagan, D. R. Cocrystal Intrinsic Dissolution Behavior Using a Rotating Disk. *Journal of Pharmaceutical Sciences* **2011,** *100*, (5), 1736-1744.

19. Qiao, N.; Wang, K.; Schlindwein, W.; Davies, A.; Li, M. In Situ Monitoring of Carbamazepine-Nicotinamide Cocrystal Intrinsic Dissolution Behaviour. *European Journal of Pharmaceutics and Biopharmaceutics* **2013,** *83*, (3), 415-426.

20. Childs, S. L.; Chyall, L. J.; Dunlap, J. T.; Smolenskaya, V. N.; Stahly, B. C.; Stahly, G. P. Crystal Engineering Approach to Forming Cocrystals of Amine Hydrochlorides with Organic Acids. Molecular Complexes of Fluoxetine Hydrochloride with Benzoic, Succinic, and Fumaric Aicds. *Journal of American Chemical Society* **2004,** *126*, 13335-13342.

21. Shiraki, K.; Takata, N.; Takano, R.; Hayashi, Y.; Terada, K. Dissolution Improvement and the Mechanism of the Improvement from Cocrystallization of Poorly Water-soluble Compounds. *Pharmaceutical Research* **2008,** *25*, (11), 2581-2592.

22. Huang, N.; Rodriguez-Hornedo, N. Effect of Micellar Solubilization on Cocrystal Solubility and Stability. *Crystal Growth & Design* **2010,** *10*, 2050-2053.

23. Huang, N.; Rodriguez-Hornedo, N. Engineering Cocrystal Thermodynamic Stability and Eutectic Points by Micellar Solubilization and Ionization. *CrystEngComm* **2011,** *13*, 5409-5422.

24. Mooney, K. G.; Mintun, M. A.; Himmelstein, K. J.; Stella, V. J. Dissolution Kinetics of Carboxylic Acids I: Effect of pH under Unbuffered Conditions. *American Pharmaceutical Association* **1981,** *70*, (1), 13-22.

25. Higuchi, W. I.; Mir, N. A.; Desai, S. J. Dissolution Rates of Polyphase Mixtures. *Journal of Pharmaceutical Sciences* **1965,** *54*, (10), 1405-1410.

26. Rodriguez-Hornedo, N.; Nehm, S. J.; Seefeldt, K. F.; Pagan-Torres, Y.; Falkiewicz, C. J. Reaction Crystallization of Pharmaceutical Molecular Complexes. *Molecular Pharmaceutics* **2006,** *3*, (3), 362-367.

27. Good, D. J.; Rodriguez-Hornedo, N. Solubility Advantage of pHarmaceutical Cocrystals. *Crystal Growth & Design* **2009,** *9*, (5), 2252-2264.

28. Nernst, W. Theorie der Reaktionsgeschwindigkeit in heterogenen systemen. *Zeitschrift für Physikalische Chemie* **1904,** *47*, 52-55.

29. Kabir-ud-Din; David, S. L.; Kumar, S. Viscosities of Sodium Dodecyl Sulfate Solutions in Aqueous Ammonium Salts. *Journal of Chemical & Engineering Data* **1997,** *42*, (6), 1224-1226.

30. Poskanzer, A. M.; Goodrich, F. C. Surface Viscosity of Sodium Dodecyl Sulfate Solutions with and without Added Dodecanol. *The Journal of Physical Chemistry* **1975,** *79*, (20), 2122-2126.

31. Brunner, E. Reaktionsgeschwindigkeit in Heterogenen Systemen. *Zeitschrift für Physikalische Chemie* **1904,** *47*, 56-102.

32. Levich, V. G., *Physico-chemical Hydrodynamics*. Prentice-Hall: Englewood Cliffs, N.J., 1962.

33. Othmer, D. F.; Thakar, M. S. Correlating Diffusion Coefficients in Liquids. *Industrial and Engineering Chemistry* **1953,** *45*, (3), 589-593.

34. Rangel-Yagui, C. O.; Junior Pessoa, A.; Tavares, L. C. Micellar Solubilization of Drugs. *Journal of Pharmaceutical Sciences* **2005,** *8*, (2), 147-163.

35. Imae, T.; Abe, A.; Taguchi, Y.; Ikeda, S. Solubilization of a Water-Insoluble Dye in Aqueous Solutions of Dodecyltrimethylammonium Halides, and Its Relation to Micelle Size and Shape. *Journal of Colloid and Interface Science* **1986,** *109*, (2), 567-575.

36. Birdi, K. S., *Handbook of Surface and Colloid Chemistry*. CRC Press; 3rd Ed.: 2008.

37. Amidon, G. E.; Higuchi, W. I.; Ho, N. F. H. Theoretical and Experimental Studies of Transport of Micelle-Solubilized Solutes. *Journal of Pharmaceutical Sciences* **1982,** *71*, (1), 77-84.

38. Rao, V. M.; Lin, M.; Larive, C. K.; Southard, M. Z. A Mechanistic Study of Griseofulvin Dissolution into Surfactant Solutions Under Laminar Flow Conditions. *Journal of Pharmaceutical Sciences* **1997,** *86*, (10), 1132-1137.

39. Sun, W.; Larive, C. K.; Southard, M. Z. A Mechanistic Study of Danazol Dissolution in Ionic Surfactant Solutions. *Journal of Pharmaceutical Sciences* **2003,** *92*, (2), 424-435.

40. Chen, A.; Wu, D.; Johnson, C. S. Determination of the Binding Isotherm and Size of the Bovine Serum Albumin-Sodium Dodecyl Sulfate Coomplex by Diffusion-Ordered 2D NMR. *Journal of Physical Chemistry* **1995,** *99*, (2), 828-834.

41. Cussler, E. L., *Diffusion Mass Transfer in Fluid Systems*. 2nd ed.; Cambridge University Press: New York, 1997.

APPENDIX 2A

The chemical equilibria and the equations for equilibrium constants during the dissolution of 1:1 cocrystal, RHA with R as the nonionizable drug and HA as the weak acidic coformer in the presence of surfactant can be described as follows:

$$(RHA)_{solid} \leftrightharpoons R_{aq} + HA_{aq} \quad (2A.1)$$

$$K_{sp} = [R]_{aq}[HA]_{aq} \quad (2A.2)$$

$$R_{aq} + m \leftrightharpoons R_m \quad (2A.3)$$

$$K_s^R = \frac{[R]_m}{[R]_{aq}[m]} \quad (2A.4)$$

$$HA_{aq} + m \leftrightharpoons HA_m \quad (2A.5)$$

$$K_s^{HA} = \frac{[HA]_m}{[HA]_{aq}[m]} \quad (2A.6)$$

$$H_2O + HA_{aq} \leftrightharpoons H_3O^+ + A_{aq}^- \quad (2A.7)$$

$$K_a = \frac{[H_3O^+][A^-]_{aq}}{[HA]_{aq}} \quad (2A.8)$$

$$H_3O^+ + OH^- \leftrightharpoons 2H_2O \quad (2A.9)$$

$$K_w = [H_3O^+][OH^-] \quad (2A.10)$$

$$HA_{aq} + OH^- \leftrightharpoons H_2O + A_{aq}^- \quad (2A.11)$$

$$K_1 = \frac{[A^-]_{aq}}{[HA]_{aq}[OH^-]} \quad (2A.12)$$

where K_S^R is the solubilization constant of R and K_S^{HA} is the solubilization constant of HA, m is the micellar concentration in the solution and is equal to the total surfactant concentration minus the CMC, K_a is the ionization constant of HA, K_w is the dissociation constant of water, K_1 is the ratio of K_a/K_w. Subscript aq denotes the aqueous phase and m denotes the micellar phase. An assumption in this analysis is that the ionized coformer is not solubilized by surfactant.

The total concentrations of the cocrystal components, $R_{tot,0}$ and $A_{tot,0}$ at the dissolving surface can be described as:

$$R_{tot,0} = R_{aq,0}(1 + K_S^R[m]) \quad (2A.13)$$

$$A_{tot,0} = HA_{aq,0}(1 + \frac{K_a}{H_0^+} + K_S^{HA}[m]) \quad (2A.14)$$

When the cocrystal is in equilibrium with solution at the dissolving surface at time = 0 before any diffusion, the stoichiometric solubility of RHA is as follow:

$$S_{cc} = R_{tot,0} = A_{tot,0} = \sqrt{K_{sp}(1 + K_S^R[m])(1 + \frac{K_a}{H_0^+} + K_S^{HA}[m])} \quad (2A.15)$$

The flux of all the species across the diffusion layer includes both the diffusion and chemical reactions happening during dissolution. At steady state, the diffusion and simultaneous chemical reactions of the individual species within the diffusion layer can be written using Fick's law as follows[24]:

$$\frac{\partial [R]_{aq}}{\partial t} = D_{R_{aq}} \frac{\partial^2 [R]_{aq}}{\partial x^2} + \phi_1 = 0 \quad (2A.16)$$

$$\frac{\partial [R]_m}{\partial t} = D_{R_m} \frac{\partial^2 [R]_m}{\partial x^2} + \phi_2 = 0 \quad (2A.17)$$

$$\frac{\partial [HA]_{aq}}{\partial t} = D_{HA_{aq}} \frac{\partial^2 [HA]_{aq}}{\partial x^2} + \phi_3 = 0 \quad (2A.18)$$

$$\frac{\partial [A^-]_{aq}}{\partial t} = D_{A^-_{aq}} \frac{\partial^2 [A^-]_{aq}}{\partial x^2} + \phi_4 = 0 \quad (2A.19)$$

$$\frac{\partial [HA]_m}{\partial t} = D_{HA_m} \frac{\partial^2 [HA]_m}{\partial x^2} + \phi_5 = 0 \quad (2A.20)$$

$$\frac{\partial [OH^-]}{\partial t} = D_{OH^-} \frac{\partial^2 [OH^-]}{\partial x^2} + \phi_6 = 0 \quad (2A.21)$$

$$\frac{\partial [H^+]}{\partial t} = D_{H^+} \frac{\partial^2 [H^+]}{\partial x^2} + \phi_7 = 0 \quad (2A.22)$$

where $\phi_{1\text{-}7}$ are the reaction rate functions. At equilibrium, the reaction rate of the reactant should be the opposite of the product. Based on the chemical equilibria, the followings can be written:

$$\phi_1 = -\phi_2 \quad (2A.23)$$

$$\phi_3 = -\phi_4 - \phi_5 \quad (2A.24)$$

The reaction rate of A^- can be reflected by the reaction rate of H^+ and OH^-, therefore,

$$\phi_4 = \phi_7 - \phi_6 \quad (2A.25)$$

Based on equation 2A.25, equation 2A.24 can be written as:

$$\phi_3 = \phi_6 - \phi_5 - \phi_7 \quad (2A.26)$$

Based on the equations 2A.23, 2A.24 and 2A.26, the following mass balance equations can be written:

$$D_{R_{aq}} \frac{d^2 [R]_{aq}}{dx^2} = -D_{R_m} \frac{d^2 [R]_m}{dx^2} \quad (2A.27)$$

$$D_{HA_{aq}} \frac{d^2 [HA]_{aq}}{dx^2} = -D_{A^-_{aq}} \frac{d^2 [A^-]_{aq}}{dx^2} - D_{HA_m} \frac{d^2 [HA]_m}{dx^2} \quad (2A.28)$$

$$D_{HA_{aq}} \frac{d^2\,[HA]_{aq}}{dx^2} = D_{OH^-} \frac{d^2\,[OH^-]}{dx^2} - D_{H^+} \frac{d^2[H^+]}{dx^2} - D_{HA_m} \frac{d^2\,[HA]_m}{dx^2} \quad (2A.29)$$

Integrating equations 2A.27 to 2A.29 once gives:

$$D_{R_{aq}} \frac{d[R]_{aq}}{dx} = -D_{R_m} \frac{d\,[R]_m}{dx} + C_1 \quad (2A.30)$$

$$D_{HA_{aq}} \frac{d\,[HA]_{aq}}{dx} = -D_{A^-_{aq}} \frac{d[A^-]_{aq}}{dx} - D_{HA_m} \frac{d\,[HA]_m}{dx} + C_2 \quad (2A.31)$$

$$D_{HA_{aq}} \frac{d\,[HA]_{aq}}{dx} = D_{OH^-} \frac{d\,[OH^-]}{dx} - D_{H^+} \frac{d[H^+]}{dx} - D_{HA_m} \frac{d\,[HA]_m}{dx} + C_3 \quad (2A.32)$$

Since A^-_{aq} is the product of the reaction between HA and OH^-, so its flux can be reflected by both OH^- and H^+:

$$-D_{A^-_{aq}} \frac{d[A^-]_{aq}}{dx} = D_{OH^-} \frac{d\,[OH^-]}{dx} - D_{H^+} \frac{d[H^+]}{dx} \quad (2A.33)$$

With this mass balance relationship, it can be seen that

$$C_2 = C_3 \quad (2A.34)$$

Integrating equations 2A.30 to 2A.32 once gives:

$$D_{R_{aq}}[R]_{aq} = -D_{R_m}[R]_m + C_1 x + C_4 \quad (2A.35)$$

$$D_{HA_{aq}}[HA]_{aq} = -D_{HA_m}[HA]_m - D_{A^-_{aq}}[A^-]_{aq} + C_2 x + C_5 \quad (2A.36)$$

$$D_{HA_{aq}}[HA]_{aq} = D_{OH^-}[OH^-] - D_{H^+}[H^+] - D_{HA_m}[HA]_m + C_3 x + C_6 \quad (2A.37)$$

Interfacial pH and flux of the species can be evaluated by solving these mass balance equations with the boundary conditions obtained from the surface saturation and interfacial equilibrium models.

Surface saturation model

Given that the concentration of the drug is the same as the solubility of the cocrystal at the surface for the surface saturation model, the aqueous concentration of the drug at the surface can be solved using equation 2A.13 and 2A.15:

$$R_{aq,0} = \frac{\sqrt{K_{sp}(1+K_S^R[m])(1+\frac{K_a}{H_0^+}+K_S^{HA}[m])}}{1+K_S^R[m]} \quad (2A.38)$$

Assuming the dissolution of RHA in the presence of surfactant gives equal flux of R and HA:

$$J_{R_{tot}} = \frac{D_{R_{eff}}[R]_{tot,0}}{h} = J_{A_{tot}} = \frac{D_{HA_{eff}}[A]_{tot,0}}{h} \quad (2A.39)$$

where $D_{R_{eff}}$ and $D_{HA_{eff}}$ are the effective diffusion coefficients of the drug and coformer, which are defined in equation 2.14 as the total diffusion of the free and micelle solubilized solute.[37] Given equations 2A.13-2A.15 above and applying the equation for diffusion layer thickness shown in equation 2.10, the aqueous concentration of the coformer at the surface is given by:

$$[HA]_{aq,0} = (\frac{D_{R_{eff}}}{D_{HA_{eff}}})^{2/3} \frac{\sqrt{K_{sp}(1+K_S^R[m])(1+\frac{K_a}{H_0^+}+K_S^{HA}[m])}}{1+\frac{K_a}{H_0^+}+K_S^{HA}[m]} \quad (2A.40)$$

Based on equations 2A.38 and 2A.40, the following boundary conditions for each species can be written for the surface saturation model:

At $x = 0$: at $x = h$:

$[R]_{aq,0} = \frac{\sqrt{K_{sp}(1+K_S^R[m])(1+\frac{K_a}{H_0^+}+K_S^{HA}[m])}}{1+K_S^R[m]}$ $[R]_{aq,h} = 0$ (under sink condition)

$[HA]_{aq,0} = (\frac{D_{R_{eff}}}{D_{HA_{eff}}})^{2/3} \frac{\sqrt{K_{sp}(1+K_S^R[m])(1+\frac{K_a}{H_0^+}+K_S^{HA}[m])}}{1+\frac{K_a}{H_0^+}+K_S^{HA}[m]}$ $[HA]_{aq,h} = 0$ (under sink condition)

$[R]_{m,0} = unknown$ $[R]_{m,h} = 0$ (under sink condition)

$[HA]_{m,0} = unknown$ $[HA]_{m,h} = 0$ (under sink condition)

$[A^-]_{aq,0} = unknown$ $[A^-]_{aq,h} = 0$ (under sink condition)

$[H^+] = [H^+]_0$ $[H^+] = [H^+]_h$

$[OH^-] = [OH^-]_0$ $[OH^-] = [OH^-]_h$

Evaluation of pH at the solid surface

Applying the above boundary conditions to equations 2A.36 and 2A.37, at *x = 0*:

$$D_{HA_{aq}}(\frac{D_{R_{eff}}}{D_{HA_{eff}}})^{2/3} \frac{\sqrt{K_{sp}(1+K_S^R[m])(1+\frac{K_a}{H_0^+}+K_S^{HA}[m])}}{1+\frac{K_a}{H_0^+}+K_S^{HA}[m]} = -D_{HA_m}[HA]_{m,0} - D_{A_{aq}^-}[A^-]_{aq,0} + C_5 \quad (2A.41)$$

$$D_{HA_{aq}}(\frac{D_{R_{eff}}}{D_{HA_{eff}}})^{2/3} \frac{\sqrt{K_{sp}(1+K_S^R[m])(1+\frac{K_a}{H_0^+}+K_S^{HA}[m])}}{1+\frac{K_a}{H_0^+}+K_S^{HA}[m]} = D_{OH^-}[OH^-]_0 - D_{H^+}[H^+]_0 - D_{HA_m}[HA]_{m,0} + C_6 \quad (2A.42)$$

and at *x = h*, since sink conditions are assumed, equations 2A.36 and 2A.37 can be written as:

$$C_2 h + C_5 = 0 \quad (2A.43)$$

$$0 = D_{OH^-}[OH^-]_h - D_{H^+}[H^+]_h + C_3 h + C_6 \quad (2A.44)$$

Combining equations 2A.41 to 2A.44 and algebraically solving for interfacial pH, $[H^+]_0$, yields the following equation:

$$A[H^+]_0{}^5 + B[H^+]_0{}^4 + C[H^+]_0{}^3 + D[H^+]_0{}^2 + E[H^+]_0 + F = 0 \quad (2A.45)$$

where

$A = D_{H^+}^2(1 + K_S^{HA}[m]);$

$B = -2D_{H^+}(D_{H^+}[H^+]_h - D_{OH^-}[OH^-]_h)(1 + K_S^{HA}[m]) + D_{H^+}^2 K_a;$

$C = -2D_{H^+}D_{OH^-}K_w(1 + K_S^{HA}[m]) + (1 + K_S^{HA}[m])(D_{H^+}[H^+]_h - D_{OH^-}[OH^-]_h)^2 - 2D_{H^+}(D_{H^+}[H^+]_h - D_{OH^-}[OH^-]_h)K_a;$

$D = 2D_{OH^-}K_w(D_{H^+}[H^+]_h - D_{OH^-}[OH^-]_h)(1 + K_S^{HA}[m]) - 2D_{H^+}D_{OH^-}K_wK_a + (D_{H^+}[H^+]_h - D_{OH^-}[OH^-]_h)^2 K_a;$

$E = (D_{OH^-}K_w)^2(1 + K_S^{HA}[m]) + 2D_{OH^-}K_w(D_{H^+}[H^+]_h - D_{OH^-}[OH^-]_h)K_a - (D_{A_{aq}^-}^{1/3} D_{R_{eff}}^{2/3} \mathrm{K_a}\sqrt{K_{sp}(1 + K_S^R[m])})^2;$

$F = K_a(D_{OH^-}K_w)^2.$

Evaluation of flux of the cocrystal components

Applying the boundary conditions to equation 2A.35, at *x = 0*:

$$D_{R_{aq}} \frac{\sqrt{K_{sp}(1+K_S^R[m])(1+\frac{K_a}{H_0^+}+K_S^{HA}[m])}}{1+K_S^R[m]} = -D_{R_m}K_S^R[m]\frac{\sqrt{K_{sp}(1+K_S^R[m])(1+\frac{K_a}{H_0^+}+K_S^{HA}[m])}}{1+K_S^R[m]} + C_4 \quad (2A.46)$$

and at $x = h$, assuming sink conditions:

$$0 = C_1 h + C_4 \quad (2A.47)$$

Combining equations 2A.46 and 2A.47 and solving for $-C_1$ for the flux of the cocrystal in terms of drug:

$$J_R = \frac{D_{R_{eff}}}{h_R}\sqrt{K_{sp}(1 + K_S^R[m])(1 + \frac{K_a}{H_0^+} + K_S^{HA}[m])} \quad (2A.48)$$

By substituting equation 2.10 into equation 2A.48, it becomes:

$$J_R = 0.62 D_{R_{eff}}^{2/3} \omega^{1/2} v^{-1/6} \sqrt{K_{sp}(1 + K_S^R[m])(1 + \frac{K_a}{H_0^+} + K_S^{HA}[m])} \quad (2A.49)$$

The flux of the cocrystal in terms of coformer can be also solved in a similar manner by applying the boundary conditions to equation 2A.36:

$$J_{HA} = \frac{D_{HA_{eff}}^{\frac{1}{3}} D_{R_{eff}}^{\frac{2}{3}}}{h_{HA}} \sqrt{K_{sp}(1 + K_S^R[m])(1 + \frac{K_a}{H_0^+} + K_S^{HA}[m])} \quad (2A.50)$$

By substituting equation 2.10 into equation 2A.50, it can be shown to equal equation 2A.49. This is expected since the flux of drug and coformer should be the same for a 1:1 cocrystal even though they have different diffusivities.

Interfacial equilibrium model

Given equations 2A.2, 2A.13, 2A.14, 2A.15, 2A.39 and applying the equation for diffusion layer thickness shown in equation 2.10, the aqueous concentrations of R and HA at the dissolving surface required to maintain constant K_{sp} at all time $t \geq 0$ are as follows:

$$[R]_{aq,0} = (\frac{D_{HA_{eff}}}{D_{R_{eff}}})^{1/3} \frac{\sqrt{K_{sp}(1+K_S^R[m])(1+\frac{K_a}{H_0^+}+K_S^{HA}[m])}}{1+K_S^R[m]} \quad (2A.51)$$

$$[HA]_{aq,0} = (\frac{D_{R_{eff}}}{D_{HA_{eff}}})^{1/3} \frac{\sqrt{K_{sp}(1+K_S^R[m])(1+\frac{K_a}{H_0^+}+K_S^{HA}[m])}}{1+\frac{K_a}{H_0^+}+K_S^{HA}[m]} \quad (2A.52)$$

Based on equations 2A.51 and 2A.52, the following boundary conditions for each species can be written for the interfacial equilibrium model:

At $x = 0$: at $x = h$:

$[R]_{aq,0} = (\frac{D_{HA_{eff}}}{D_{R_{eff}}})^{1/3} \frac{\sqrt{K_{sp}(1+K_S^R[m])(1+\frac{K_a}{H_0^+}+K_S^{HA}[m])}}{1+K_S^R[m]}$ $[R]_{aq,h} = 0$ (under sink condition)

$[HA]_{aq,0} = (\frac{D_{R_{eff}}}{D_{HA_{eff}}})^{1/3} \frac{\sqrt{K_{sp}(1+K_S^R[m])(1+\frac{K_a}{H_0^+}+K_S^{HA}[m])}}{1+\frac{K_a}{H_0^+}+K_S^{HA}[m]}$ $[HA]_{aq,h} = 0$ (under sink condition)

$[R]_{m,0} = unknown$ $[R]_{m,h} = 0$ (under sink condition)

$[HA]_{m,0} = unknown$ $[HA]_{m,h} = 0$ (under sink condition)

$[A^-]_{aq,0} = unknown$ $[A^-]_{aq,h} = 0$ (under sink condition)

$[H^+] = [H^+]_0$ $[H^+] = [H^+]_h$

$[OH^-] = [OH^-]_0$ $[OH^-] = [OH^-]_h$

Evaluation of pH at the solid surface

Applying the above boundary conditions to equations 2A.36 and 2A.37, at *x = 0*:

$$D_{HA_{aq}}(\frac{D_{R_{eff}}}{D_{HA_{eff}}})^{1/3} \frac{\sqrt{K_{sp}(1+K_S^R[m])(1+\frac{K_a}{H_0^+}+K_S^{HA}[m])}}{1+\frac{K_a}{H_0^+}+K_S^{HA}[m]} = -D_{HA_m}[HA]_{m,0} - D_{A_{aq}^-}[A^-]_{aq,0} + C_5 \quad (2A.53)$$

$$D_{HA_{aq}}(\frac{D_{R_{eff}}}{D_{HA_{eff}}})^{1/3} \frac{\sqrt{K_{sp}(1+K_S^R[m])(1+\frac{K_a}{H_0^+}+K_S^{HA}[m])}}{1+\frac{K_a}{H_0^+}+K_S^{HA}[m]} = D_{OH^-}[OH^-]_0 - D_{H^+}[H^+]_0 - D_{HA_m}[HA]_{m,0} + C_6 \quad (2A.54)$$

and at *x = h*:

$$C_2 h + C_5 = 0 \quad (2A.55)$$

$$0 = D_{OH^-}[OH^-]_h - D_{H^+}[H^+]_h + C_3 h + C_6 \quad (2A.56)$$

Combining equations 2A.53 to 2A.56 and algebraically solving for interfacial pH yields the following equation:

$$A[H^+]_0{}^5 + B[H^+]_0{}^4 + C[H^+]_0{}^3 + D[H^+]_0{}^2 + E[H^+]_0 + F = 0 \qquad (2A.57)$$

where,

$A = D_{H^+}^2(1 + K_s^{HA}[m]);$

$B = -2D_{H^+}(D_{H^+}[H^+]_h - D_{OH^-}[OH^-]_h)(1 + K_s^{HA}[m]) + D_{H^+}^2 K_a;$

$C = -2D_{H^+}D_{OH^-}K_w(1 + K_s^{HA}[m]) + (1 + K_s^{HA}[m])(D_{H^+}[H^+]_h - D_{OH^-}[OH^-]_h)^2 - 2D_{H^+}(D_{H^+}[H^+]_h - D_{OH^-}[OH^-]_h)K_a;$

$D = 2D_{OH^-}K_w(D_{H^+}[H^+]_h - D_{OH^-}[OH^-]_h)(1 + K_s^{HA}[m]) - 2D_{H^+}D_{OH^-}K_wK_a + (D_{H^+}[H^+]_h - D_{OH^-}[OH^-]_h)^2 K_a;$

$E = (D_{OH^-}K_w)^2(1 + K_s^{HA}[m]) + 2D_{OH^-}K_w(D_{H^+}[H^+]_h - D_{OH^-}[OH^-]_h)K_a - (D_{A_{aq}^-}^{2/3} D_{R_{eff}}^{1/3} \mathrm{K_a} \sqrt{K_{sp}(1 + K_s^R[m])})^2;$

$F = K_a(D_{OH^-}K_w)^2.$

This equation is very similar to the one obtained from the surface saturation model. The only difference is the coefficient E in the equation because of the different boundary layer conditions.

Evaluation of flux of the cocrystal components

Applying the new boundary conditions to mass balance equations 2A.35 and 2A.36, the flux of the cocrystal in terms of components can be re-evaluated as:

$$J_R = J_{HA} = 0.62(D_{R_{eff}}D_{HA_{eff}})^{1/3}\omega^{1/2}\nu^{-1/6}\sqrt{K_{sp}(1 + K_s^R[m])(1 + \frac{K_a}{H_0^+} + K_s^{HA}[m])} \qquad (2A.58)$$

Unlike the surface saturation model, the flux of the cocrystal is not only dependent on the effective diffusivity of the drug, but also the coformer.

CHAPTER 3

MECHANISTIC BASIS OF COCRYSTAL DISSOLUTION ADVANTAGE

Abstract

The current interest in cocrystal development resides in the advantages that the cocrystal may have in solubility and dissolution compared to the parent drug. The mechanism of cocrystal solubility advantage has been studied in detail, however, limited research has been carried out on the dissolution of cocrystals. The purpose of this work is to provide a mechanistic analysis and comparison of the dissolution behavior of carbamazepine (CBZ) and its two cocrystals, carbamazepine-saccharin (CBZ-SAC) and carbamazepine-salicylic acid (CBZ-SLC) under the influence of pH and micellar solubilization. A simple mathematical equation is derived based on the mass transport analyses of both the drug and cocrystal to describe the dissolution advantage of cocrystal, which is defined as the ratio of the cocrystal flux over the drug flux. The dissolution advantage of cocrystal has a dependence on both the solubility and diffusivity advantages. In this work, the effective diffusivity of CBZ in the presence of surfactant is determined to be different from those of the cocrystals. The higher effective diffusivities of the cocrystals can impart dissolution advantages to cocrystals with lower solubility than the parent drugs while still maintaining thermodynamic stability. Dissolution conditions where cocrystals display both thermodynamic stability and dissolution advantage can be obtained from the mass transport models and this information is useful for both cocrystal selection and formulation development.

Introduction

Cocrystallization is one of the powerful strategies used in pharmaceutical development to improve the aqueous solubility of inherently insoluble drugs[1-6]. Cocrystallization usually involves the formation of cocrystal through hydrogen bonding between the hydrophobic drug and hydrophilic coformer[7, 8]. As a new and different solid form, the physicochemical properties of cocrystal need to be fully evaluated in order to develop a feasible formulation. Among these properties, solubility and dissolution are of particular interests due to their importance in determining the oral absorption of drugs[9]. A thorough understanding of the solubility and dissolution mechanisms of cocrystals not only aids the formulation development, but also provides an improved perspective on the oral absorption of drugs from the cocrystalline solids.

One of the motivations for cocrystal development is the solubility advantages that these cocrystalline materials can generate[1-6]. However, these solubility advantages are not constant and they can vanish under certain solution conditions, such as pH and the presence of solubilizing additive[10-15]. Cocrystals can exhibit higher, equal or lower solubility compared to the parent drugs depending on the solution conditions. Important transition points, such as pH_{max} and critical stabilization concentration (CSC), have been identified to access the solubility behavior of cocrystals[10, 11, 15]. Cocrystal is thermodynamically unstable below the CSC, but it is thermodynamically stable above the CSC[10, 12, 13]. CSC can be achieved using any additives that preferentially solubilize the drug compared to the coformer[10, 12, 13]. Without knowing these important concepts, cocrystals could lose their solubility advantages compared to the parent drugs if the concentrations of solubilizing agents used are above the CSC. Consequently, a thorough understanding of the transition point is essential for fine-tuning the formulations of cocrystals to achieve desired solubility advantages.

Another question of interest for cocrystal development is whether cocrystal could exhibit higher dissolution rate compared to the parent drug. Knowing the dissolution behavior of cocrystals adds another level of confidence in formulation development. The dissolution mechanism of cocrystals under the influence of pH and surfactant has been evaluated through the development of mass transport models[16]. The mass transport analyses indicate that the physicochemical properties of cocrystals and their components, such as solubility products, ionization constants, solubilization constants and diffusion coefficients, are important parameters for determining the rates of cocrystal dissolution[16]. Dissolution rate is directly proportional to the solubility of the cocrystal. This relationship leads to an important question to be addressed in this study, which is whether a cocrystal solubility advantage is necessary to obtain higher cocrystal dissolution rate compared to the parent drug.

Here, a simple mathematical model is presented to determine the dissolution advantages of cocrystals compared to the parent drugs. This model is evaluated using a model drug, carbamazepine (CBZ) and its two cocrystals with 1:1 stoichiometry, carbamazepine saccharin (CBZ-SAC) and carbamazepine salicylic acid (CBZ-SLC). CBZ is non-ionizable and both SAC and SLC are acidic coformers with pK_a values of 1.6 and 3.0[1, 10], respectively. The stable form of CBZ in solution is its dihydrated form. To eliminate the complication of conversion, CBZ dihydrate (CBZD) was used for this study. Constant surface area dissolution of both CBZD and its two cocrystals was determined using rotating disk apparatus. Both CBZ-SAC and CBZ-SLC have higher solubility than CBZD, so dissolution studies were performed in solution containing sodium lauryl sulfate (SLS) concentration at or above the CSC to prevent solid phase transformation during dissolution. Effect of pH and surfactant concentration on the dissolution of CBZD and two CBZ cocrystals was evaluated and compared in this study.

Materials and methods

Materials

Anhydrous carbamazepine (CBZ), salicylic acid (SLC) and sodium lauryl sulfate (SLS) were purchased from Sigma Chemical Company (St. Louis, MO) and used as received. Carbamazepine dihydrate (CBZD) was prepared by slurrying anhydrous CBZ in deionized water for 24 hours and solid was obtained through vacuum filtration. Saccharin (SAC) was purchased from Acros Organics (Pittsburgh, PA) and used as received. Isopropanol, acetonitrile, methanol and hydrochloric acid were purchased from Fisher Scientific (Pittsburgh, PA). Sodium hydroxide pellets were purchased from J.T. Baker (Philipsburg, NJ). Water used in this study was filtered through a double deionized purification system (Milli Q Plus Water System) from Millipore Co. (Bedford, MA).

Cocrystal synthesis

Cocrystals were prepared by reaction crystallization method[17] at room temperature. CBZ-SAC was prepared by adding 1:1 molar ratio of CBZ and SAC in isopropanol solution. CBZ-SLC was prepared by adding 1:1 molar ratio of CBZ and SLC in acetonitrile solution containing 0.1 M SLC. Solid phases were characterized by X-ray powder diffraction (XRPD) and differential scanning calorimetry (DSC).

Cocrystal solubility

Cocrystal solubility was measured by determining the eutectic concentrations of the drug and coformer as a function of SLS concentration at pH 1 and 25°C. A detailed discussion of the eutectic point measurement was reported elsewhere[18]. Cocrystals (100 – 150 mg) and CBZD (50

– 100 mg) were suspended in 3 mL of aqueous SLS solution and stirred for 4 days. Samples were collected at 24 hour intervals and centrifuged using Corning Costar Spin-X plastic centrifuge tubes with filters to separate the excess solid from solution. Solution concentrations were measured using HPLC and solid phases were analyzed by XRPD. Cocrystal stoichiometric solubility was determined from the measured eutectic concentrations of the components using previously developed method[18].

Dissolution experiments

The constant surface area dissolution rates of cocrystals and CBZD were determined using a rotating disk apparatus. Cocrystal or CBZD powder (~150 mg) was compressed in a stainless steel rotating disk die with a tablet radius of 0.50 cm at 85 MPa for 2 minutes using a Carver hydraulic press. The die containing the compact was mounted onto a stainless steel shaft attached to an overhead, variable speed motor. The disk was exposed to 150 mL of the dissolution medium in a water jacketed beaker with temperature controlled at 25°C and a rotation speed of 200 rpm was used. Dissolution medium was prepared on the day of the experiment by dissolving SLS in water and solution pH was adjusted using HCl or NaOH. Sink conditions were maintained throughout the experiments by ensuring the concentrations at the last time point of dissolution were less than 10% of the cocrystal solubility. Solution concentrations were measured using HPLC and solid phases after dissolutions were analyzed by XRPD.

HPLC

Waters HPLC equipped with a photodiode array detector was used for all analysis. The mobile phase was composed of 55% methanol and 45% water with 0.1% trifluoroacetic acid and the flow rate was 1 mL/min was used. Separation was achieved using Waters, Atlantis, T3 column

(5.0 µm, 100 Å) with dimensions of 4.6 x 250 mm. The sample injection volume was 20 µL. The wavelengths for the analytes were as follows: 284 nm for CBZ, 250 nm for SAC and 303 nm for SLC.

XRPD

XRPD diffractograms of solid phases were collected with a benchtop Rigaku Miniflex X-ray diffractometer using Cu-Kα radiation (λ = 1.54 Å), a tube voltage of 30 kV, and a tube current of 15 mA. Data was collected from 5 to 40° at a continuous scan rate of 2.5°/min.

DSC

Crystalline samples were analyzed by DSC using a TA instrument 2910 MDSC system equipped with a refrigerated cooling unit. All experiments were performed by heating the samples at a rate of 10 °C/min under a dry nitrogen atmosphere. Temperature and enthalpy of the instrument were calibrated using high purity indium standard.

Theoretical

The solubility of non-ionizable drug in surfactant solution can be described as:

$$S_{drug} = S_0(1 + K_s^R[m]) \quad (3.1)$$

where S_0 is the intrinsic solubility of the drug, K_s^R is the solubilization constant of the drug in surfactant solution and [m] is the concentration of the micelle[10].

The solubility of a 1:1 cocrystal with non-ionizable drug and acidic coformer in surfactant solution can be described as:

$$S_{cc} = \sqrt{K_{sp}(1 + K_s^R[m])(1 + K_s^{HA}[m] + \frac{K_a}{H^+})} \quad (3.2)$$

where K_{sp} is the solubility product of the cocrystal, K_s^{HA} is the solubilization constant of the coformer in surfactant solution and K_a is the ionization constant of the coformer[10]. Here, the solubilization of the ionized form of the coformer in surfactant solution is assumed to be negligible.

For rotating disk dissolution, the flux of both drug and cocrystal in surfactant solution can be described as follows:

$$J_R = 0.62 D_{R_{eff,drug}}^{2/3} \omega^{1/2} v^{-1/6} S_0 (1 + K_s^R[m]) \tag{3.3}$$

$$J_{cc} = 0.62 D_{R_{eff,cc}}^{2/3} \omega^{1/2} v^{-1/6} \sqrt{K_{sp}(1 + K_s^R[m])(1 + \frac{K_a}{H_0^+} + K_s^{HA}[m])} \tag{3.4}$$

where $D_{R_{eff,drug}}$ and $D_{R_{eff,cc}}$ are the effective diffusivities of the drug determined from the dissolution of drug and cocrystal respectively, ω is the rotation speed during dissolution and v is the viscosity of the dissolution media[16, 19]. The effective diffusivity in surfactant solution can be described as:

$$D_{R_{eff}} = \frac{D_{aq} + K_S D_m [m]}{1 + K_S [m]} \tag{3.5}$$

where D_{aq} is the aqueous diffusivity and D_m is the micellar diffusivity[20].

The dissolution advantage of cocrystal, $\emptyset$, is defined as the ratio of the cocrystal flux over the drug flux, which is given by:

$$\emptyset = \frac{J_{cc}}{J_R} = \left(\frac{D_{R_{eff,cc}}}{D_{R_{eff,drug}}}\right)^{2/3} \frac{\sqrt{K_{sp}(1 + K_s^R[m])(1 + \frac{K_a}{H_0^+} + K_s^{HA}[m])}}{S_0(1 + K_s^R[m])} \tag{3.6}$$

A $\emptyset$ value greater than 1 indicates the cocrystal has higher dissolution rate than the drug; whereas the dissolution rate of cocrystal is less than the drug with $\emptyset$ value below 1. Equation 3.6 is specific

for determining the cocrystal dissolution advantage under surfactant conditions. However, a simplified equation can be derived to apply for dissolution under different solution conditions:

$$\emptyset = \left(\frac{D_{R,cc}}{D_{R,drug}}\right)^{2/3} \frac{S_{cc}}{S_{drug}} \quad (3.7)$$

where $\frac{D_{R,cc}}{D_{R,drug}}$ is the diffusivity advantage and $\frac{S_{cc}}{S_{drug}}$ is the solubility advantage of the cocrystal. By knowing the cocrystal diffusivity and solubility advantage, the dissolution advantage of cocrystal can be predicted under the different solution conditions. The dissolution advantage of cocrystal would only depend on the solubility advantage if the diffusion coefficients are the same for the drug and cocrystal. This is usually true under aqueous conditions with no surfactant. However, under surfactant conditions, the effective diffusion coefficient of the drug maybe different from the cocrystal due to the different solubility dependence on surfactant concentration. Therefore, besides the solubility advantage, the effective diffusion coefficients of both drug and cocrystal have to be taken into consideration as well for determining the dissolution advantage of cocrystal under surfactant conditions. Due to the differential diffusion coefficients, dissolution advantages can be imparted to cocrystals with lower solubility than the parent drugs, as long as the diffusion coefficients of the cocrystals are large enough to compensate for the disadvantages in solubility.

Results and discussion

Solubility study

The equilibrium solubility of both cocrystals as a function of surfactant concentration at pH 1 was determined using the eutectic point measurement. At the eutectic point, the solid phases of both the drug and cocrystal are in equilibrium with solution and the concentrations of both cocrystal components can be measured[18]. The relative solubility of the cocrystal to the parent drug

can be accessed by the eutectic constant, K_{eu}, which is a ratio of the coformer eutectic concentration over the drug eutectic concentration[18, 21]. Cocrystal is more soluble than the parent drug when $K_{eu} > 1$; but it is less soluble than the parent drug when $K_{eu} < 1$[18, 21]. The eutectic concentrations of the cocrystal components[16] and K_{eu} as a function of SLS at pH 1 are shown in Figure 3.1 and 3.2. The concentrations of both components increase with surfactant concentration increases, however, the drug concentrations are higher than the coformer concentrations at all surfactant concentrations. This is expected because all the solubility studies were performed at surfactant concentrations above the CSC, where the cocrystals are less soluble. The eutectic constants shown in Figure 3.1 and 3.2 further confirm the thermodynamic stability of the cocrystals under these conditions. K_{eu} values decrease as SLS concentration increases because the surfactant concentration is further away from the CSC.

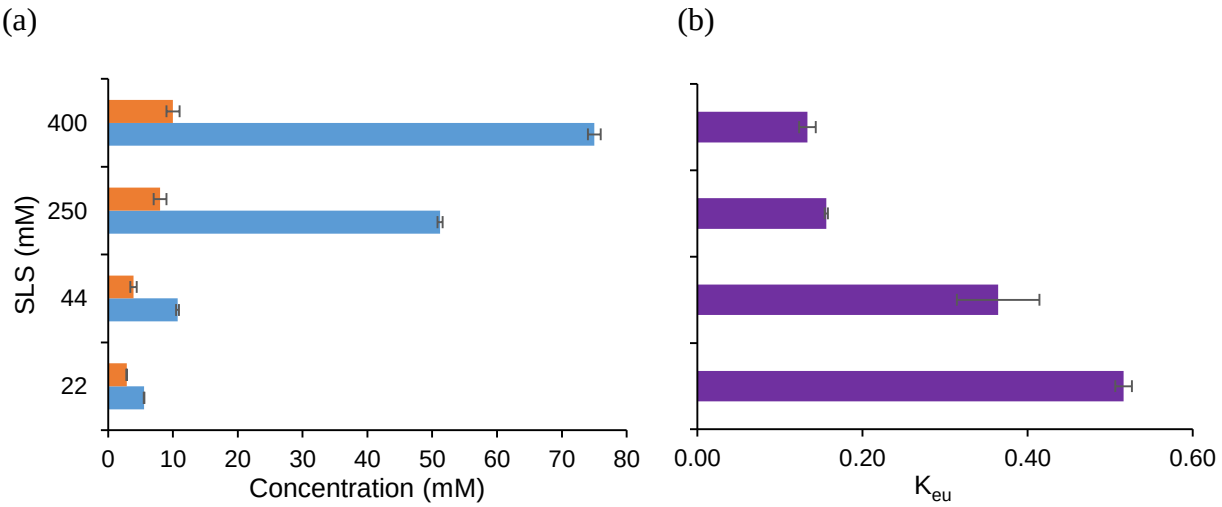

Figure 3.1. (a) Eutectic concentrations of CBZ (■) and SAC (■) measured at the eutectic point for CBZ-SAC at pH 1 as a function of SLS concentration[16]. (b) K_{eu} values calculated from the eutectic concentrations.

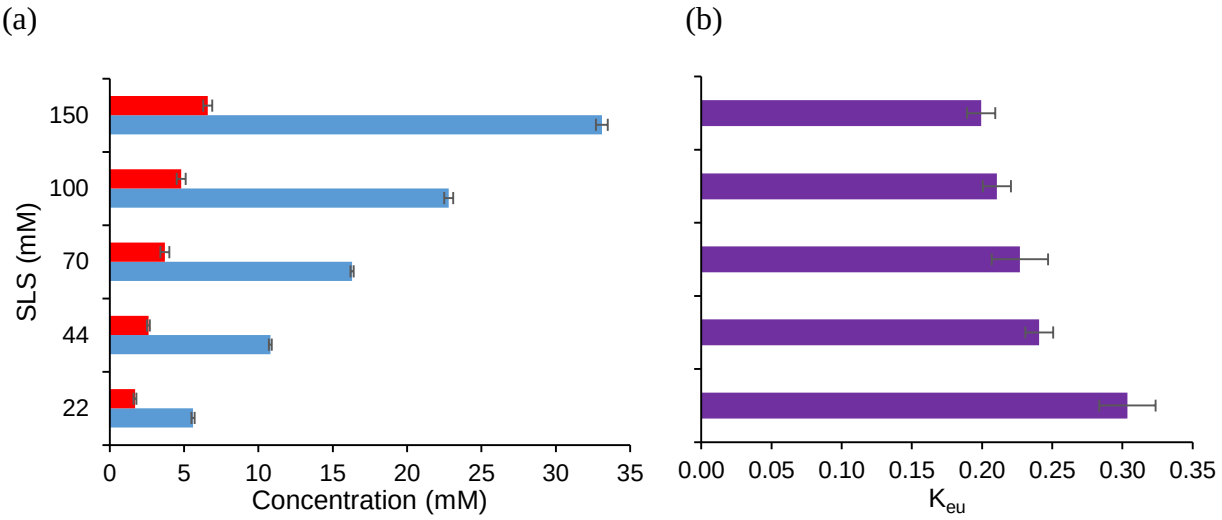

Figure 3.2. (a) Eutectic concentrations of CBZ (■) and SLC (■) measured at the eutectic point for CBZ-SLC at pH 1 as a function of SLS concentration[16]. (b) K_{eu} values calculated from the eutectic concentrations.

The equilibrium solubility of cocrystals can be calculated from the eutectic concentrations of the cocrystal components using the following equation[18]:

$$S_{cc} = \sqrt{[drug]_{eutectic}[coformer]_{eutectic}} \tag{3.8}$$

The solubility of CBZD is the same as the eutectic concentration because the solid phase of CBZD is in equilibrium with solution. Previous studies have shown that the solubilization of CBZD by SLS is not affected by the presence of coformer[10, 12, 13]. The solubility of CBZ-SAC and CBZ-SLC was determined and compared to CBZD in Figure 3.3 and 3.4, respectively. Solubility of both drug and cocrystals increases as surfactant concentration increases, however, the drug has a greater rate of increase compared to both of the cocrystals. As shown in equations 3.1 and 3.2, the solubility of drug has a linear dependence on surfactant concentration, while the cocrystal has a square root dependence. This explains why the drug has a higher increase in solubility as a function of surfactant concentration compared to the cocrystals. The square root dependence of cocrystal solubility on surfactant concentration is a result of the preferential solubilization of the

drug compared to the coformers by surfactant[10]. Since the solubility studies were performed above the CSC, both cocrystals exhibited no solubility advantage over the parent drug, as indicated in Figure 3.3 and 3.4 with the ratios of S_{cc}/S_{drug} less than 1. The S_{cc}/S_{drug} ratios of both cocrystals decrease as SLS concentration increases because the difference in solubility between the drug and cocrystals increases as the concentration of SLS moves further away from the CSC.

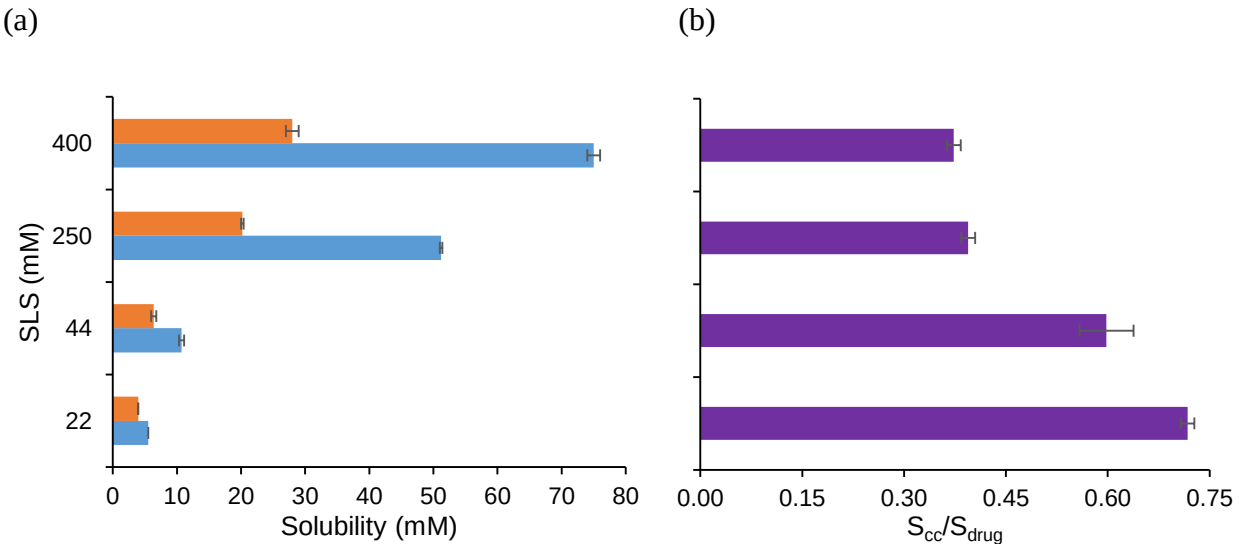

Figure 3.3. (a) Solubility of CBZD (■) and CBZ-SAC (■) at pH 1 as a function of SLS concentration[16]. (b) Solubility advantage of CBZ-SAC, S_{cc}/S_{drug}, calculated from the solubility data.

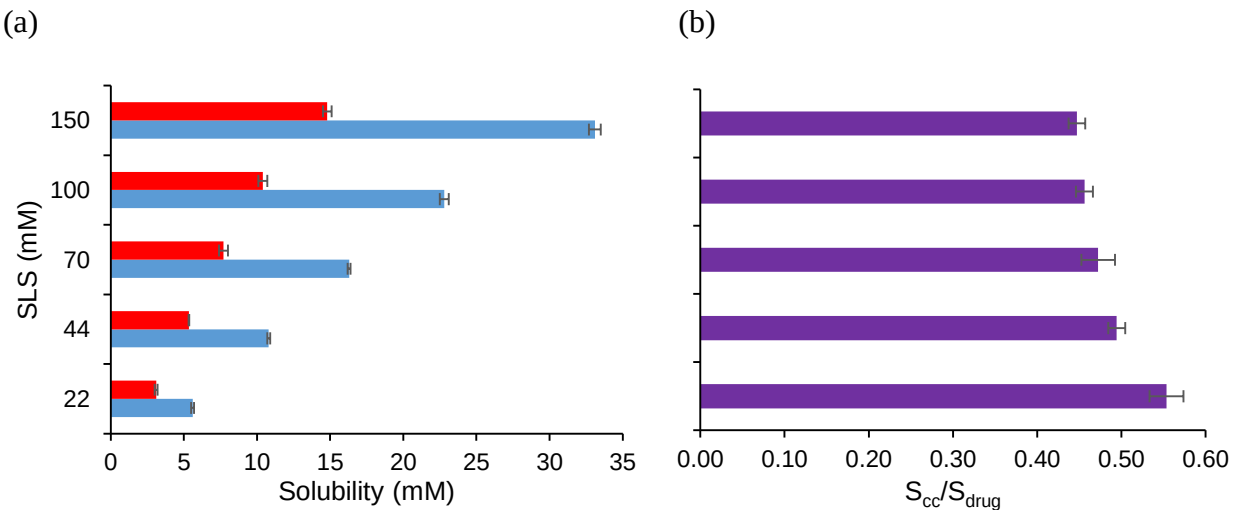

Figure 3.4. (a) Solubility of CBZD (■) and CBZ-SLC (■) at pH 1 as a function of SLS concentration[16]. (b) Solubility advantage of CBZ-SLC, S_{cc}/S_{drug}, calculated from the solubility data.

Effect of surfactant on dissolution of CBZD and CBZ cocrystals

Dissolution studies of CBZD, CBZ-SAC and CBZ-SLC were performed at pH 1 as a function of SLS concentration. The flux values of CBZD are compared to CBZ-SAC in Figure 3.5 and CBZ-SLC in Figure 3.6. Flux of both drug and cocrystals increases as SLS concentration increases, however, there is a greater increase for the drug compared to the two cocrystals because it has a greater solubility dependence on surfactant concentration. Dissolution advantages were determined by comparing the cocrystal flux to CBZD flux. Both cocrystals have no dissolution advantages over the parent drug under these dissolution conditions as indicated by $\emptyset < 1$ shown in Figure 3.5 and 3.6. Under these conditions, the solubility of the drug is higher than both of the cocrystals, so the flux of both CBZ-SAC and CBZ-SLC is smaller than CBZD. As shown in equation 3.7, $\emptyset$ is proportional to S_{cc}/S_{drug}, so it follows the same trend as the solubility advantage, in which the dissolution advantage decreases with increasing SLS concentration.

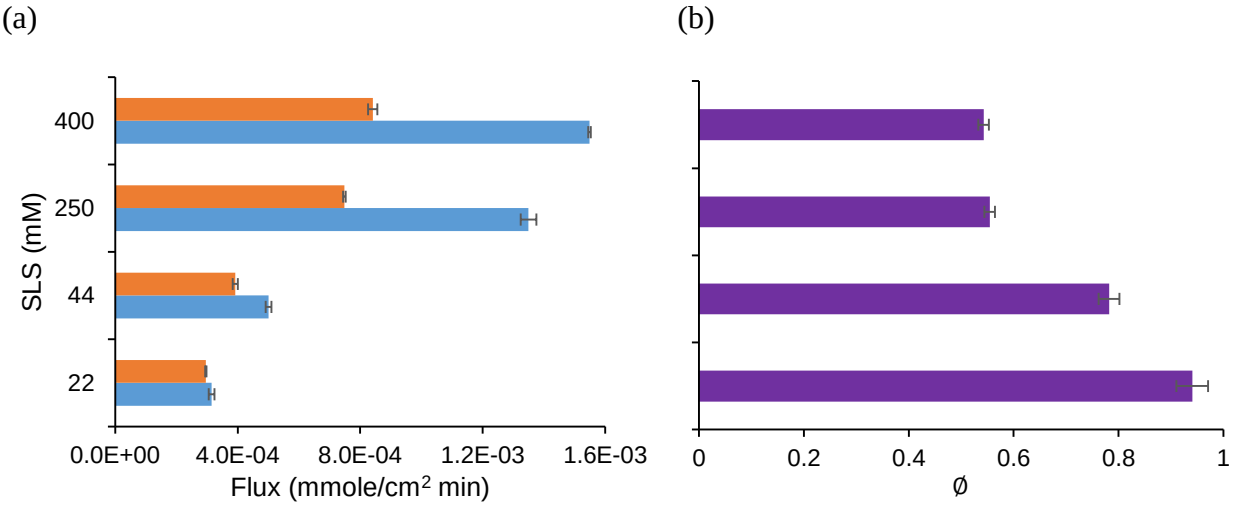

Figure 3.5. (a) Flux of CBZD (■) and CBZ-SAC[16] (■) at pH 1 as a function of SLS concentration. (b) Dissolution advantage ($\emptyset$) of CBZ-SAC calculated from the experimental flux.

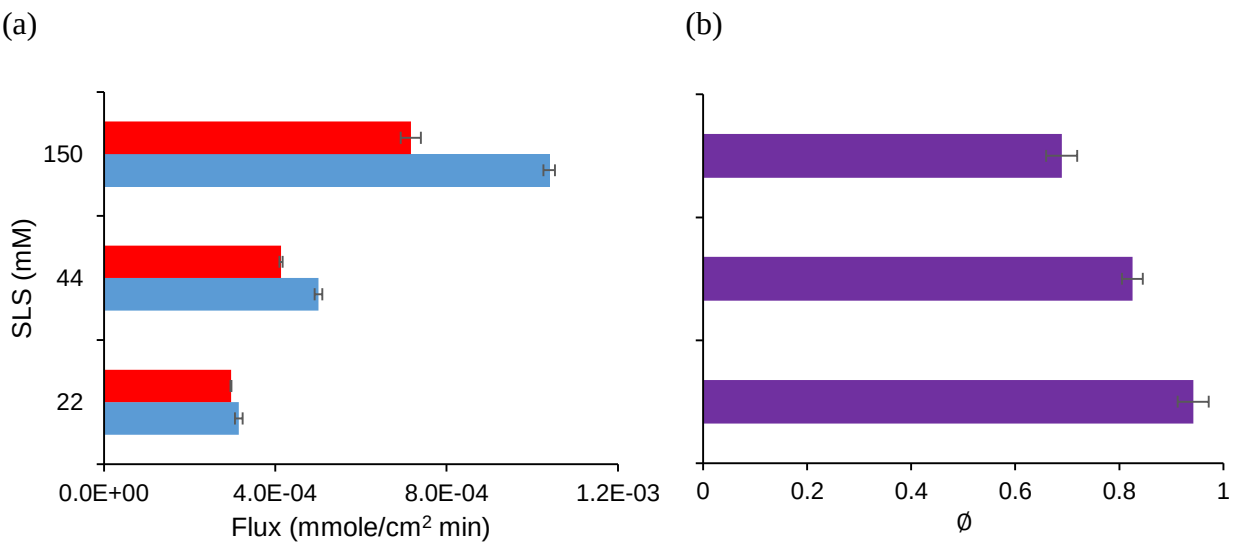

Figure 3.6. (a) Flux of CBZD (■) and CBZ-SLC[16] (■) at pH 1 as a function of SLS concentration. (b) Dissolution advantage (Ø) of CBZ-SLC calculated from the experimental flux.

Micellar diffusion coefficients

Micellar diffusion coefficients of CBZ as a function of SLS concentration have been determined from the dissolution of CBZ-SAC and CBZ-SLC in previous study[16]. Micellar diffusion coefficients determined from the two cocrystals are different from each other and this difference may be due to the different chemical environment surrounding the micelles during dissolution[16]. Using equations 3.3, 3.4 and 3.5, micellar diffusion coefficients of CBZ can be determined from the dissolution of CBZD as a function of SLS concentration at pH 1. These micellar diffusivities are compared to those determined from the dissolution of CBZ-SAC and CBZ-SLC in Figure 3.7. The micellar diffusivities of CBZ determined from the dissolution of CBZD follow the same trend as the ones determined from the cocrystals. As shown in Figure 3.7, micellar diffusivities of all three solid forms decrease with increasing surfactant concentration and these relationships can be fitted into power regressions. The decrease in micellar diffusivities is possibly due to the increase in micellar size and electric repulsion as SLS concentration increases, and detailed explanation was provided elsewhere[16]. Among the three sets of micellar diffusion

coefficients, the ones determined from the dissolution of CBZD are the lowest. Detailed analysis of this is beyond the scope of this study. However, the difference in solubility dependence on surfactant concentration between the drug and cocrystal could be the potential reason for the difference in micellar diffusion coefficients. The solubility of CBZD has a stronger dependence on surfactant concentration compared to the cocrystals as indicated by the linear dependence shown in equation 3.1. It is possible that more drug molecules are solubilized into the micelles during the dissolution of CBZD compared to the dissolution of the cocrystals and thus results in slower micellar diffusion compared to the cocrystals.

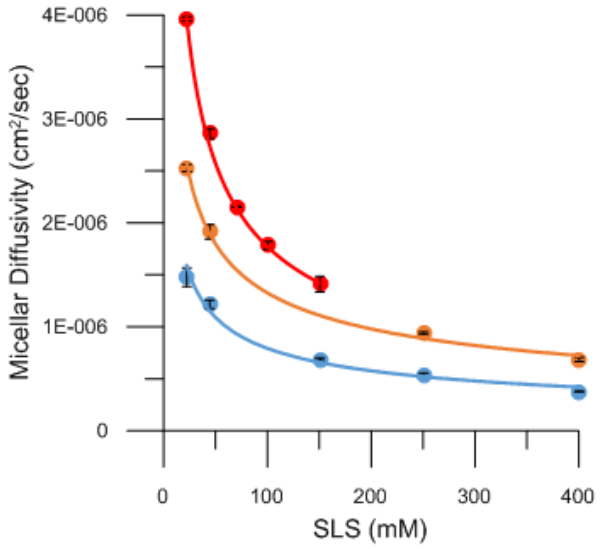

Figure 3.7. Micellar diffusivities of CBZ determined from the dissolution of CBZD (——), CBZ-SAC[16] (——) and CBZ-SLC[16] (——) at pH 1 as a function of SLS. The circles are the experimental data and the solid lines are the power regressions.

Solubility and dissolution enhancements by SLS

Due to micellar solubilization, the solubility and dissolution of CBZD and the two cocrystals can be enhanced in the presence of surfactant. The solubility and dissolution enhancements by SLS for CBZD, CBZ-SAC and CBZ-SLC were determined by normalizing the solubility and dissolution data at all surfactant concentrations to those at 22 mM SLS. As shown

in Figure 3.8, both solubility and dissolution enhancements increase as surfactant concentration increases, however, the enhancement for solubility is greater than that for dissolution and this difference increases as surfactant concentration increases. According to equations 3.3 and 3.4, the flux of the drug and cocrystal is proportional to solubility, so the dissolution enhancement should theoretically be proportional to the solubility enhancement. However, the presence of surfactant increases the solubility of a compound by solubilizing it into the micelles, but at the same time, it decreases the diffusivity of the solubilized compound. The counter effect of surfactant on solubility and micellar diffusivity results in lower dissolution enhancement compared to the solubility enhancement. This counter effect increases as surfactant concentration increases and results in greater difference between the solubility and dissolution enhancements. As expected, both solubility and dissolution enhancements of CBZD are higher than those of CBZ-SAC and CBZ-SLC because of the higher solubility dependence on surfactant.

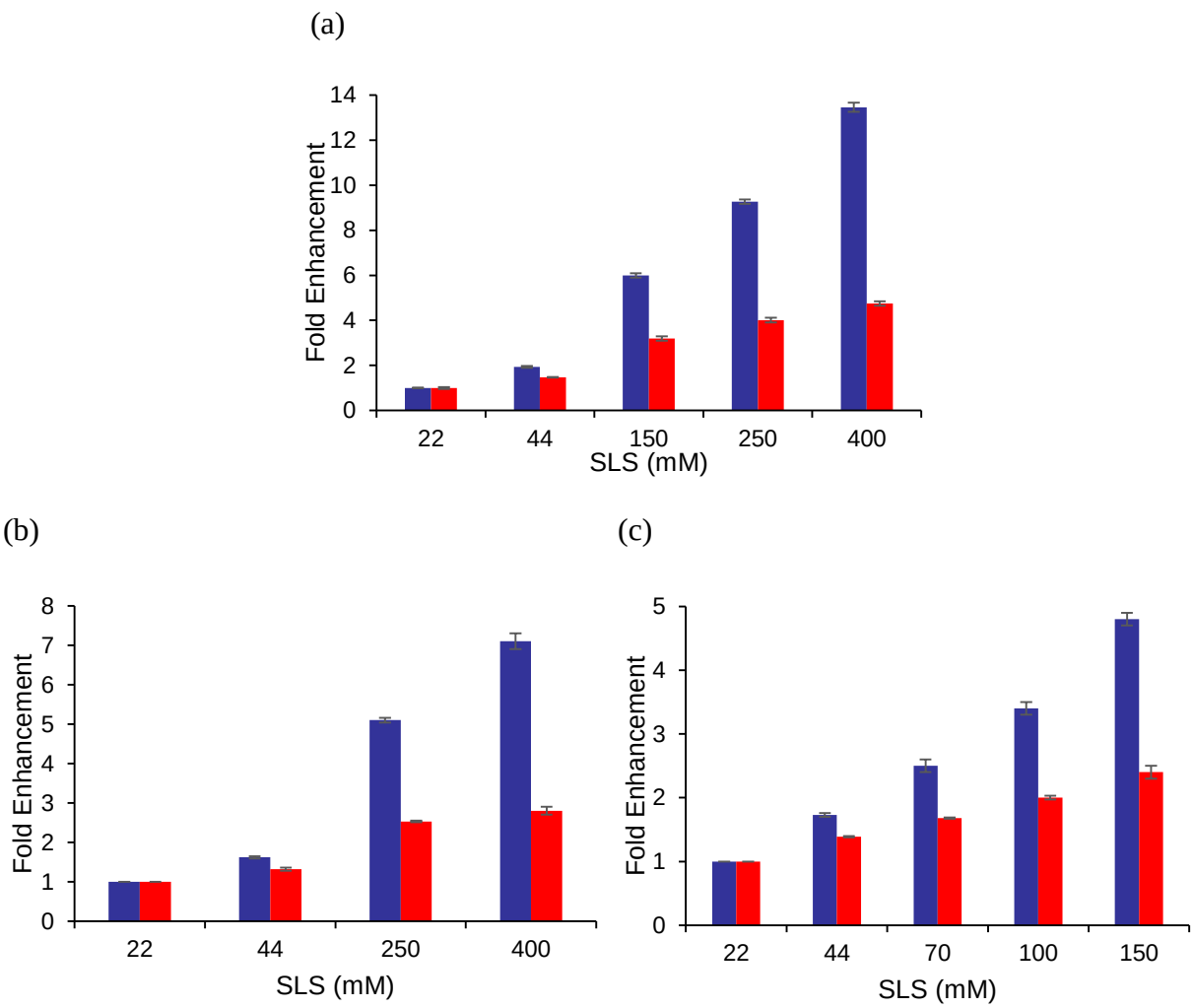

Figure 3.8. Solubility (■) and dissolution (■) enhancements of CBZD (a), CBZ-SAC (b) and CBZ-SLC (c) at pH 1 as a function of SLS. Both solubility and dissolution enhancements were determined by normalizing the data to 22 mM SLS.

Cocrystal solubility and dissolution advantage comparison

The solubility and dissolution advantages of both cocrystals at pH 1 as a function of SLS concentration were compared and shown in Figure 3.9. Both solubility and dissolution advantages decrease with increasing SLS concentration because the surfactant concentration is moving away from the CSC. However, the dissolution advantages of both cocrystals are higher than the solubility advantages at all surfactant concentrations. According to equation 3.6, dissolution

advantage depends on both the solubility and diffusivity advantages. As discussed earlier, the micellar diffusivities of CBZ determined from the dissolution of CBZD are smaller than those determined from both of the cocrystals. Therefore, the dissolution advantages of both cocrystals are enhanced by the higher micellar diffusions compared to the parent drug. The enhancement in dissolution advantage of CBZ-SLC is greater than CBZ-SAC because there is larger difference in micellar diffusivity between CBZD and CBZ-SLC.

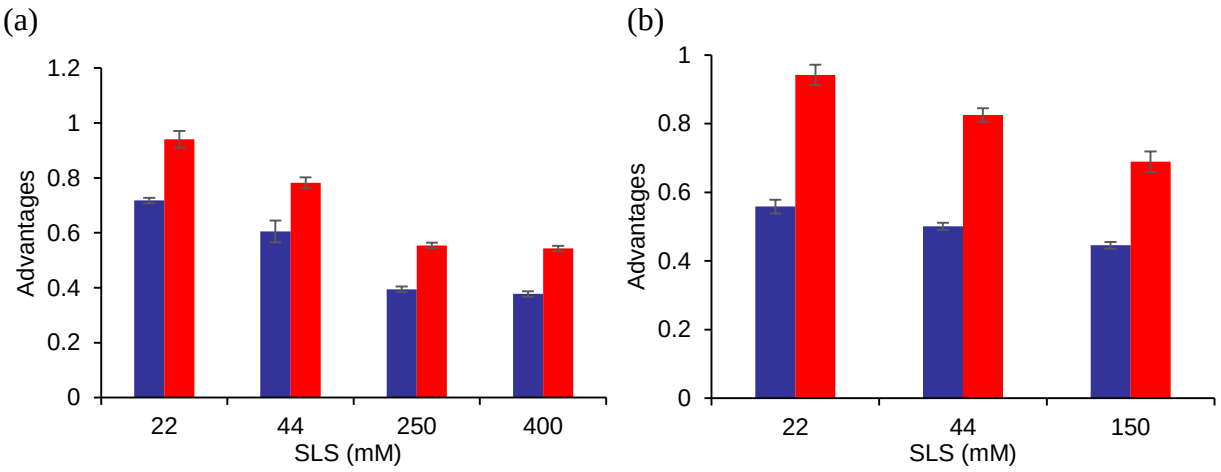

Figure 3.9. Solubility (■) and dissolution (■) advantages of CBZ-SAC (a) and CBZ-SLC (b) at pH 1 as a function of SLS.

Effect of pH on dissolution of CBZD and CBZ cocrystals

By cocrystallizing with acidic coformers, SAC and SLC, the nonionizable drug, CBZD, is able to possess pH dependent dissolution. The effect of pH on the dissolution of CBZ-SAC and CBZ-SLC was evaluated at constant surfactant concentration as a function of bulk pH and compared to the parent drug in Figure 3.10 and 3.11, respectively. The flux of CBZD is predicted to be constant as a function of bulk pH due to its nonionizable property. Since pH has no effect on the dissolution of CBZD, dissolution experiments were conducted in SLS solutions with no pH adjustment. The flux of both CBZ-SAC and CBZ-SLC increases as bulk pH increases because of

the acidity of the coformers. However, both flux plateau at bulk pH ranges from 4 to 8, where the coformers are self-buffering the pH microenvironment at the dissolving surface. Interfacial pH is relatively constant in this region, so no significant change in flux is observed in this region. The dissolution advantages, Ø, of both cocrystals were determined by comparing the experimental cocrystal flux to CBZD flux, and these values are shown in Figure 3.10 for CBZ-SAC and Figure 3.11 for CBZ-SLC. As shown in these figures, there exists a transition pH where the flux of the drug is the same as the cocrystal flux. Below this transition pH, the drug flux is higher, however, above it, the cocrystal flux becomes higher. Theoretically, both cocrystals should not display any dissolution advantages under these conditions since the dissolution studies were performed above the CSC to prevent the solid phase transformation of the cocrystals back to the stable drug form. Under these dissolution conditions, both cocrystals have no solubility advantage over the parent drug as indicated by the ratios of S_{cc}/S_{drug} less than 1 shown in Table 3.1 and 3.2. Despite the lower solubility, CBZ-SAC and CBZ-SLC can still display higher dissolution rates compared to CBZD above the transition pH. According to equation 3.6, the cocrystal dissolution advantage is dependent on not only the solubility advantage, but also the diffusivity advantage. As shown in Figure 3.7 above, the effective diffusivities of CBZ determined from the dissolution of CBZ-SAC and CBZ-SLC are higher than those of CBZD. The effective diffusion coefficient of CBZ-SAC at 400 mM SLS and CBZ-SLC at 150 mM SLS is about 1.7x and 2.1x higher than that of CBZD, respectively. These differences in effective diffusion coefficients are not large enough to impart dissolution advantages to both cocrystals below the transition pH because the solubility advantages are too low under these conditions as shown in Table 3.1 and 3.2. As the solubility advantages of both cocrystals become higher above the transition pH, the higher effective diffusivities of both

cocrystals is able to compensate for the disadvantages in solubility and impart dissolution advantages.

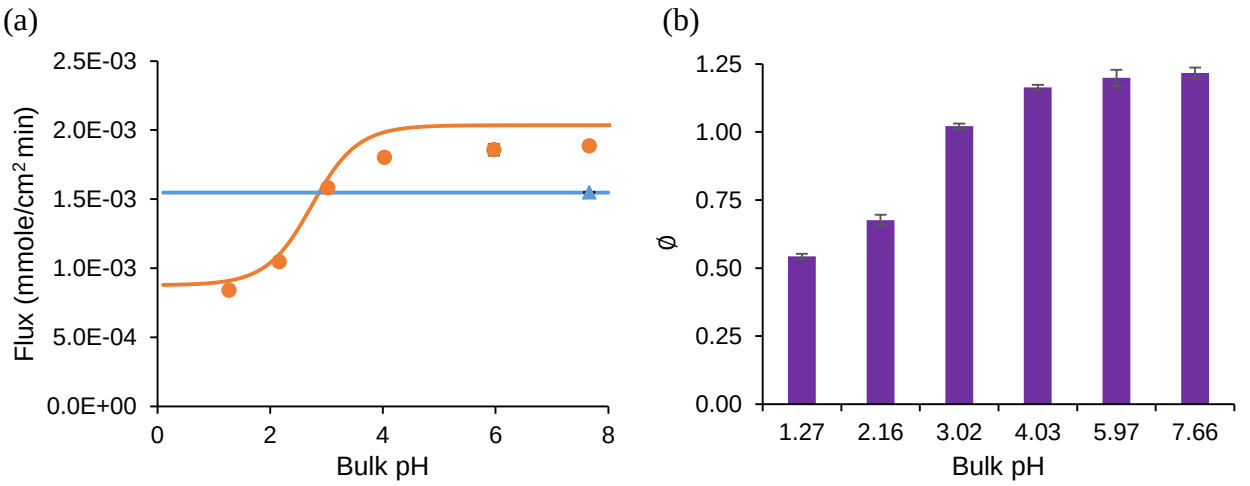

Figure 3.10. (a) Flux of CBZD and CBZ-SAC at 400 mM SLS as a function of bulk pH. (b) Dissolution advantages, Ø, of CBZ-SAC calculated from the experimental flux. The flux of CBZD (——) are predicted using equation 3.3 and the flux of CBZ-SAC (——) are predicted using equation 3.4. CBZD experimental flux: ▲; CBZ-SAC experimental flux: ●.

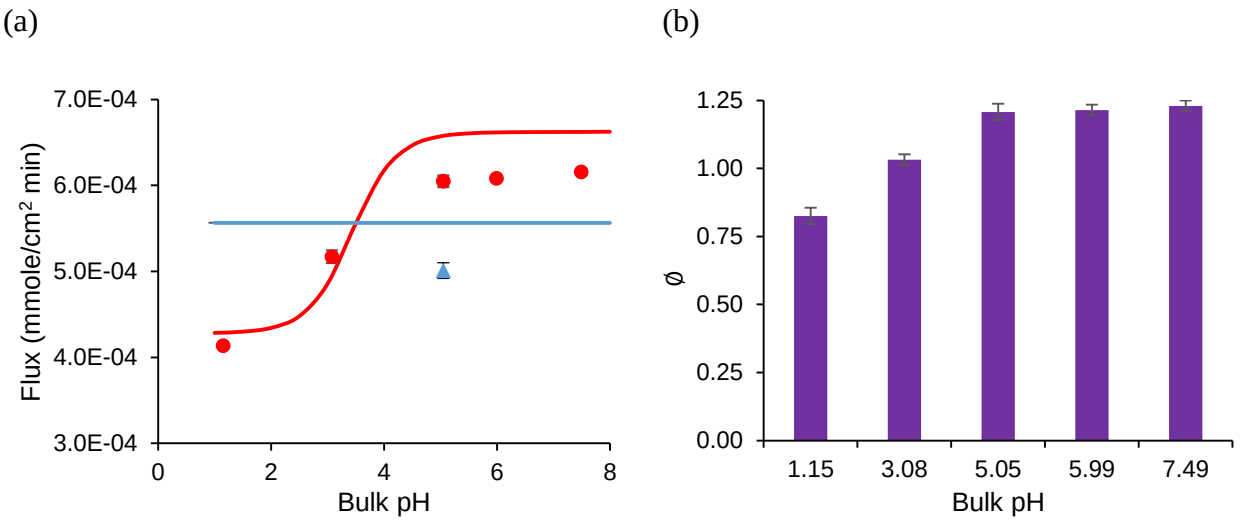

Figure 3.11. (a) Flux of CBZD and CBZ-SLC at 44 mM SLS as a function of bulk pH. (b) Dissolution advantages, Ø, of CBZ-SLC calculated from the experimental flux. The flux of CBZD (——) are predicted using equation 3.3 and the flux of CBZ-SLC (——) are predicted using equation 3.4. CBZD experimental flux: ▲; CBZ-SAC experimental flux: ●.

By knowing the solubility and diffusivity advantages, the dissolution advantages of cocrystals can be predicted using equation 3.6. The predicted dissolution advantages of CBZ-SAC and CBZ-SLC are shown in Table 3.1 and 3.2, respectively. These predicted values agree well with the experimental values shown in Figure 3.10 and 3.11. The higher effective diffusivity of the cocrystals is able to compensate for the disadvantage in solubility and results in dissolution advantage for both cocrystals without having to deal with the solid phase transformation of the cocrystals during dissolution.

Table 3.1. Theoretical predictions of dissolution advantages for CBZ-SAC at 400 mM SLS as a function of pH.

pH		**Solubility[b] (mM)**		**S_{cc}/S_{drug}**	**$D_{eff,R}$ (x 10^{-7} cm^2/sec)**		**Predicted**
Bulk	**Interfacial[a]**	**CBZD**	**CBZ-SAC**		**CBZD**	**CBZ-SAC[c]**	**ø[d]**
1.27	1.27	74.2	30.4	0.41	4.16±0.02	7.2±0.3	0.59
2.16	2.15		36.8	0.50			0.72
3.02	2.78		54.6	0.74			1.07
4.03	3.00		66.2	0.89			1.28
5.97	3.03		68.0	0.92			1.33
7.66	3.03		68.0	0.92			1.33

a) From reference [16].
b) Predicted from equation 3.1 for CBZD and equation 3.2 for CBZ-SAC.
c) From reference [16].
d) Predicted from equation 3.6.

Table 3.2. Theoretical predictions of dissolution advantages for CBZ-SLC at 44 mM SLS as a function of pH.

pH		**Solubility[b] (mM)**		**S_{cc}/S_{drug}**	**$D_{eff,R}$ (x 10^{-6} cm^2/sec)**		**Predicted**
Bulk	**Interfacial[a]**	**CBZD**	**CBZ-SLC**		**CBZD**	**CBZ-SLC[c]**	**ø[d]**
1.15	1.15	12.2	6.53	0.54	1.41±0.04	2.98±0.04	0.88
3.08	2.97		6.27	0.51			0.84
5.05	3.65		8.49	0.70			1.15
5.99	3.66		8.55	0.70			1.15
7.49	3.66		8.55	0.70			1.15

a) From reference [16].
b) Predicted from equation 3.1 for CBZD and equation 3.2 for CBZ-SAC.
c) From reference [16].
d) Predicted from equation 3.6.

Dissolution conditions for maintaining cocrystal dissolution advantage

Solid phase transformation is one of the challenges for developing cocrystals because it can lead to minimal or no dissolution advantage compared to the parent drug. The enhanced dissolution rate through cocrystallization can potentially increase the bioavailability of the parent drug. Therefore, it would be beneficial to formulate a cocrystal that can display higher dissolution rate than the parent drug without having to deal with solid phase transformation during dissolution. It is possible to develop such formulations because the effective diffusivity of the cocrystal in the presence of surfactant is found to be larger than the drug and this allows the cocrystal to achieve dissolution advantage even it has lower solubility than the parent drug. Knowledge of the dissolution behavior of cocrystals would help to develop feasible formulations. To evaluate the dissolution conditions in which the cocrystals can maintain both dissolution advantage and thermodynamic stability for formulation development, the combination effect of pH and surfactant concentration on the dissolution of CBZD is compared to CBZ-SAC and CB-SLC in Figure 3.12. Because of the nonionizable property, the dissolution rate of CBZD is only affected by the surfactant concentration, whereas the cocrystals are affected by both surfactant and pH because of the acidity of the coformers. As shown in Figure 3.12, CBZ-SAC is able to achieve dissolution advantages from bulk pH 3 to 8 at SLS concentrations range from 22 to 400 mM. However, this does not mean that the cocrystal is thermodynamically stable under all these conditions. The CSC for CBZ-SAC at bulk pH 3 is 161 mM SLS and from bulk pH 4 to 8 is 306 mM. This suggests that CBZ-SAC would be able to maintain dissolution advantage without solid phase transformation at bulk pH 3 with SLS concentration of 161 mM and above; and from bulk pH 4 to 8 with SLS concentration of 306 mM and above. These surfactant concentrations maybe too high for oral formulation. However, the CSC for CBZ-SLC at bulk pH up to 8 is only 21 mM SLS. This means

that the cocrystal is thermodynamically stable and less soluble than the parent drug under all the dissolution conditions shown in Figure 3.12. Although it is less soluble than CBZD, CBZ-SLC is able to maintain dissolution advantages at SLS concentrations range from 22 to 70 mM and bulk pH ranges from 4 to 8 because of the higher effective diffusivities.

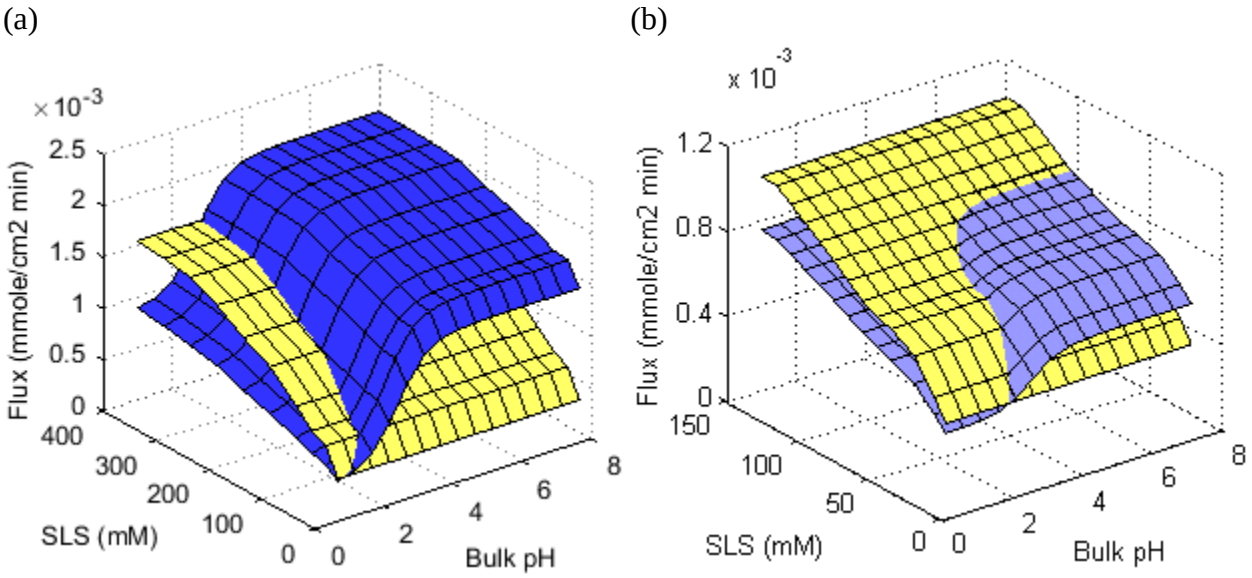

Figure 3.12. (a) Theoretical flux comparison of CBZD (yellow) to CBZ-SAC (blue), and (b) CBZD (yellow) to CBZ-SLC (purple) as a function of pH and SLS concentration. Flux predictions of CBZD were determined using equation 3.3 and cocrystals were from reference[16].

Conclusions

This work has compared the effect of pH and surfactant on the dissolution of CBZD to its two cocrystals, CBZ-SAC and CBZ-SLC. Solubility and dissolution pH dependence are imparted to CBZ through the cocrystallization with acidic coformers. Because of the preferential solubilization of the drug over the coformers by surfactant, the solubility dependence on surfactant of the drug is different from the cocrystals. There is a linear dependence for the solubility of the drug, whereas cocrystal solubility has a square root dependence. Because of this different dependence, the enhancements in solubility and dissolution by surfactant for the drug are higher

than for both of the cocrystals. Cocrystal dissolution advantage can be determined by comparing the cocrystal flux to the drug flux. Based on the mass transport analyses, cocrystal dissolution advantage is proportional to both the solubility and diffusivity advantages. In this study, the micellar diffusivity of CBZ determined from the dissolution of CBZD is found to be smaller than those of the cocrystals because the drug has a higher solubility dependence on surfactant. Because of the higher diffusivities, cocrystals with lower solubility than the parent drug do not necessarily have slower dissolution rates. The diffusivity advantages allow cocrystals to compensate for their lower solubility above the CSC and result in higher dissolution rates compared to the parent drug. Dissolution conditions where the cocrystal can obtain both thermodynamic stability and dissolution advantage are useful information for cocrystal formulation development and these conditions can be evaluated through the simple mass transport models provided in this work.

References

1. Alhalaweh, A.; Roy, L.; Rodriguez-Hornedo, N.; Velaga, S. P. pH-Dependent Solubility of Indomethacin-Saccharin and Carbamazepine-Saccharin Cocrystals in Aqueous Media. *Molecular Pharmaceutics* **2012,** *9*, 2605-2612.
2. Bethune, S. J.; Huang, N.; Jayasankar, A.; Rodriguez-Hornedo, N. Understanding and Predicting the Effect of Cocrystal Components and pH on Cocrystal Solubility. *Crystal Growth and Design* **2009,** *9*, (9), 3976-3988.
3. McNamara, D. P.; Childs, S. L.; Giordano, J.; Iarriccio, A.; Cassidy, J.; Shet, M. S.; Mannion, R.; O'Donnell, E.; Park, A. Use of a glutaric acid cocrystal to improve oral bioavailability of a low solubility API. *Pharmaceutical Research* **2006,** *23*, (8), 1888-1897.
4. Childs, S. L.; Kandi, P.; Lingireddy, S. R. Formulation of a Danazol Cocrystal with Controlled Supersaturation Plays an Essential Role in Improving Bioavailability. *Molecular Pharmaceutics* **2013,** *10*, (8), 3112-3127.

5. Cheney, M. L.; Weyna, D. R.; Shan, N.; Hanna, M.; Wojtas, L.; Zaworotko, M. J. Supramolecular Architectures of Meloxicam Carboxylic Acid Cocrystals, a Crystal Engineering Case Study. *Crystal Growth & Design* **2010,** *10*, 4401-4413.

6. Kuminek, G.; Cao, F.; Rocha, A. B. d. O. d.; Cardoso, S. G.; Rodriguez-Hornedo, N. Cocrystals to Facilitate Delivery of Poorly Soluble Compounds Beyond-Rule-of-5. *Advanced Drug Delivery Reviews* **2016,** *Manuscript under review.*

7. Rodriguez-Hornedo, N.; Nehm, S. J.; Jayasankar, A., Cocrystals: Design, Properties, and Formation Mechanisms. In *Encyclopedia of PHarmaceutical Technology*, Francis and Taylor: London, United Kingdom, 2007; pp 615-635.

8. Vishweshwar, P.; McMahon, J. A.; Bis, J. A.; Zaworotko, M. J. Pharmaceutical Co-Crystals. *Journal of Pharmaceutical Sciences* **2006,** *95*, (3), 499-516.

9. Amidon, G. L.; Lennernas, H.; Shah, V. P.; Crison, J. R. A Theoretical Basis for a Biopharmaceutic Drug Classification: The Correlation of *in Vitro* Drug Product Dissolution and *in Vivo* Bioavailability. *Pharmaceutical Research* **1995,** *12*, (3), 413-420.

10. Huang, N.; Rodriguez-Hornedo, N. Engineering Cocrystal Solubility, Stability, and pHmax by Micellar Solubilization. *Journal of Pharmaceutical Sciences* **2011,** *100*, (12), 5219-5234.

11. Kuminek, G.; Rodriguez-Hornedo, N.; Siedler, S.; Rocha, H. V. A.; Cuffini, S. L.; Cardoso, S. G. How Cocrystals of Weakly Basic Drugs and Acidic Coformers Might Modulate Solubilty and Stability. *CHem. Commun.* **2016,** *52*, (34), 5832-5.

12. Huang, N.; Rodriguez-Hornedo, N. Engineering Cocrystal Thermodynamic Stability and Eutectic Points by Micellar Solubilization and Ionization. *CrystEngComm* **2011,** *13*, 5409-5422.

13. Huang, N.; Rodriguez-Hornedo, N. Effect of Micellar Solubilization on Cocrystal Solubility and Stability. *Crystal Growth & Design* **2010,** *10*, 2050-2053.

14. Lipert, M. P.; Rodriguez-Hornedo, N. Cocrystal Transition Points: Role of Cocrystal Solubility, Drug Solubility, and Solubilizing Agents. *Molecular Pharmaceutics* **2015,** *12*, (10), 3535-3546.

15. Maheshwari, C.; Andre, V.; Reddy, S.; Roy, L.; Duarte, T.; Rodrigez-Hornedo, N. Tailoring aqueous solubility of a highly soluble compound via cocrystallization: effect of coformer ionization, pH(max) and solute-solvent interactions. *Crystengcomm* **2012,** *14*, (14), 4801-4811.

16. Cao, F.; Amidon, G.; Rodriguez-Hornedo, N.; Amidon, G. Mechanistic Analysis of Cocrystal Dissolution as a Function of pH and Micellar Solubilization. *Molecular Pharmaceutics* **2015,** *13*, (3), 1030-1046.

17. Rodríguez-Hornedo, N.; Nehm, S. J.; Seefeldt, K. F.; Pagán-Torres, Y.; Falkiewicz, C. J. Reaction Crystallization of Pharmaceutical Molecular Complexes. *Molecular Pharmaceutics* **2006,** *3*, (3), 362-367.

18. Good, D. J. a. R.-H., N. Solubility Advantage of pHarmaceutical Cocrystals. *Crystal Growth & Design* **2009,** *9*, (5), 2252-2264.

19. Crison, J. R.; Shah, V. P.; Skelly, J. P.; Amidon, G. L. Drug Dissoluiton into Micellar Solutions: Development of a Convective Diffusion Model and Comparison to the Film Equilibrium Model with Application to Surfactant-Facilitated Dissolution of Carbamazepine. *Journal of Pharmaceutical Sciences* **1996,** *85*, (9), 1005-1011.

20. Amidon, G. E.; Higuchi, W. I.; Ho, N. F. H. Theoretical and Experimental Studies of Transport of Micelle-Solubilized Solutes. *Journal of Pharmaceutical Sciences* **1982,** *71*, (1), 77-84.

21. Good, D. J.; Rodriguez-Hornedo, N. Cocrystal Eutectic Constants and Prediction of Solubility Behavior. *Crystal Growth & Design* **2010,** *10*, (3), 1028-1032.

CHAPTER 4

COMMON COFORMER EFFECT ON THE DISSOLUTION RATE OF COCRYSTAL

Abstract

The presence of excess coformer in solution is known to decrease the solubility of cocrystals because of the solubility product behavior. However, its effect on dissolution rates has not been addressed. The purpose of this work is to develop mass transport models to evaluate the common coformer effect on the dissolution rates of cocrystals. These mass transport analyses not only provide useful insights for the oral absorption of cocrystals with drug membrane permeation higher than the coformer, but also validate the surface saturation model that was developed previously to describe the dissolution process of cocrystals. Rotating disk dissolution experiments of the model cocrystal, carbamazepine salicylic acid (CBZ-SLC) show that the dissolution rates decrease with increasing coformer concentration. The common coformer effect decreases the ability of CBZ-SLC in lowering the pH at the dissolving surface due to the lower degree of coformer ionization and results in higher interfacial pH. The higher interfacial pH subsequently reduces the common coformer effect on the dissolution rate of CBZ-SLC because of the acidity of salicylic acid.

Introduction

Cocrystals have gained tremendous interest in pharmaceutical industry in recent years due to their potential of increasing bioavailability of poorly water soluble drugs[1-5]. The solubility and dissolution behavior of cocrystals have been widely studied[1, 3, 4, 6-8] in order to gain a better understanding on the oral absorption of these cocrystalline materials. The solubility mechanism of cocrystals have been well studied by Rodriguez, et al.[9-12] and the dissolution mechanism has been proposed by a recent study[13]. Detailed mass transport models have been developed to predict the pH at the dissolving surface (i.e. interfacial pH) and the flux of cocrystals[13]. These mass transport analyses emphasize the importance of physicochemical properties of the cocrystal components on the rate of dissolution.

Cocrystals usually contain components with different physicochemical properties, such as hydrophobicity, micellar solubilization, diffusion coefficient and permeability. The more lipophilic drug usually has a faster membrane permeation compared to the less lipophilic coformer. The faster permeation of the drug through the intestinal membrane can result in excess coformer concentration in the intestinal lumen. This excess coformer concentration can impact the dissolution rate of the cocrystal if it is not fully dissolved.

Cocrystals behave similarly to pharmaceutical salts in a way that the solubility is also described by the solubility product of the components. The presence of excess counter ion can suppress the degree of salt dissociation because of the solubility product behavior and this phenomenon is known as the common ion effect[14-17]. The solubility of hydrochloride salts have been shown to decrease in dilute hydrochloric solutions and similar behavior was also observed for other pharmaceutical salts in solutions containing their counter ions[14-17]. Because of the common ion effect, the dissolution rates of pharmaceutical salts are also suppressed by the

presence of counter ions[14-17]. With similar solubility product behavior, the solubility of cocrystals also decrease in solutions containing excess coformer[9, 18]. The solubility of carbamazepine-nicotinamide cocrystal has been shown to decrease with increasing nicotinamide concentration in solution[18]. While the effect of excess coformer on the solubility of cocrystals has been addressed, its effect on the dissolution rates has not been explored. Using pharmaceutical salts as an analogy, the effect of excess coformer on the solubility and dissolution of cocrystals is defined as the common coformer effect. Herein, mechanism based models were developed to evaluate the common coformer effect on the dissolution behavior of cocrystals.

Surface saturation model has been proposed previously to describe the dissolution mechanism of cocrystals[13]. It is difficult to validate this model experimentally because it would require the measurements of surface concentrations of the cocrystal components. Another purpose of this work is to validate the surface saturation model by varying the coformer concentration at the dissolving surface by the addition of coformer in the bulk solution. To evaluate the common coformer effect and validate the surface saturation model, rotating disk dissolution experiments of carbamazepine salicylic acid (CBZ-SLC) cocrystal were performed in dissolution media containing different salicylic acid concentrations.

Materials and methods

Materials

Anhydrous carbamazepine (CBZ), salicylic acid (SLC) and sodium lauryl sulfate (SLS) were purchased from Sigma Chemical Company (St. Louis, MO) and used as received. Acetonitrile, methanol and hydrochloric acid were purchased from Fisher Scientific (Pittsburgh, PA). Sodium hydroxide pellets were purchased from J.T. Baker (Philipsburg, NJ). Water used in

this study was filtered through a double deionized purification system (Milli Q Plus Water System) from Millipore Co. (Bedford, MA).

Cocrystal synthesis

Cocrystals were prepared by reaction crystallization method[19] at room temperature. CBZ-SLC was prepared by adding 1:1 molar ratio of CBZ and SLC in acetonitrile solution containing 0.1 M SLC. Solid phases were characterized by X-ray powder diffraction (XRPD) and differential scanning calorimetry (DSC).

Dissolution experiments

Constant surface area dissolution rates of CBZ-SLC were determined using a rotating disk apparatus. Cocrystal powder (~150 mg) was compressed in a stainless steel rotating disk die with a tablet radius of 0.50 cm at approximately 85 MPa for 2 minutes using a hydraulic press. The die containing the compact was mounted onto a stainless steel shaft attached to an overhead, variable speed motor. The disk was exposed to 150 mL of dissolution medium in a water jacketed beaker with temperature controlled at 25°C and a rotation speed of 200 rpm was used. Dissolution medium was prepared on the day of the experiment by dissolving SLC in 150 mM SLS solution and solution pH was adjusted using HCl or NaOH. Sink conditions were maintained throughout the experiments by ensuring the concentrations at the last time point of the dissolution were less than 10% of the cocrystal solubility. Bulk solution pH was maintained at constant throughout the dissolution using HCl or NaOH. Solution concentrations were measured using HPLC and solid phases after dissolution were analyzed by XRPD.

HPLC

Waters HPLC equipped with a photodiode array detector was used for all analysis. The mobile phase was composed of 55% methanol and 45% water with 0.1% trifluoroacetic acid and the flow rate was 1 mL/min was used. Separation was achieved using Waters, Atlantis, T3 column (5.0 µm, 100 Å) with dimensions of 4.6 x 250 mm. The sample injection volume was 20 µL. The wavelengths for the analytes were as follows: 284 nm for CBZ and 303 nm for SLC.

XRPD

XRPD diffractograms of solid phases were collected with a benchtop Rigaku Miniflex X-ray diffractometer using Cu-Kα radiation (λ = 1.54 Å), a tube voltage of 30 kV, and a tube current of 15 mA. Data was collected from 5 to 40° at a continuous scan rate of 2.5°/min.

DSC

Crystalline samples were analyzed by DSC using a TA instrument 2910 MDSC system equipped with a refrigerated cooling unit. All experiments were performed by heating the samples at a rate of 10 °C/min under a dry nitrogen atmosphere. Temperature and enthalpy of the instrument were calibrated using high purity indium standard.

Theoretical

Surface saturation model was previously developed to describe the dissolution mechanism of cocrystals[13]. Because of the different diffusivities between the drug and coformer, the concentrations of the cocrystal components are different at the dissolving surface in order to maintain stoichiometric dissolution[13]. Due to faster diffusion, the coformer concentration is lower than that of the drug at the dissolving surface, whereas the drug is able to maintain the same

concentration as the solubility of the cocrystal[13]. The depletion in concentration of the faster diffusing component at the dissolving surface is not easy to demonstrate experimentally because of the difficulty in measuring the surface concentrations. Alternative approaches to validate this model are to vary the coformer concentrations at the dissolving surface by the addition of coformer in the bulk solution. Approach 1 is to achieve a coformer concentration that is the same as the drug at the dissolving surface by adding equivalent amount of coformer that would be depleted due to rapid diffusion in the dissolution medium. Approach 2 is to achieve a coformer concentration that is higher than the drug at the dissolving surface by adding larger amount of coformer than the depleted amount in the dissolution medium. By adding coformer in the dissolution medium, the depleted coformer concentration at the dissolving surface due to faster diffusion can be replenished to the same or even higher concentration than the drug. Knowing the solubility product behavior of cocrystals, the presence of excess coformer in the dissolution medium can influence the solubility and consequently, the dissolution of cocrystals. Therefore, besides validation, these approaches can also be used to demonstrate the common coformer effect on the dissolution of cocrystals.

Approach 1: $[R]_{aq,0} = [A]_{aq,0}$

A schematic representation of approach 1 for a 1:1 cocrystal with nonionizable components, RA is illustrated in Figure 4.1. At time = 0, the cocrystal would first dissociate into its components to give equal molar concentrations of R and A at the dissolving surface according to its solubility. However, with the excess coformer added in the bulk solution, the coformer concentration would be higher than the drug concentration at the dissolving surface before any diffusion happens. As both drug and coformer diffuse away from the dissolving surface, the coformer concentration would be depleted due to faster diffusion. However, the coformer

concentration added in the bulk solution is the same as the depleted concentration, so the coformer would be able to maintain the same surface concentration as the drug at steady state.

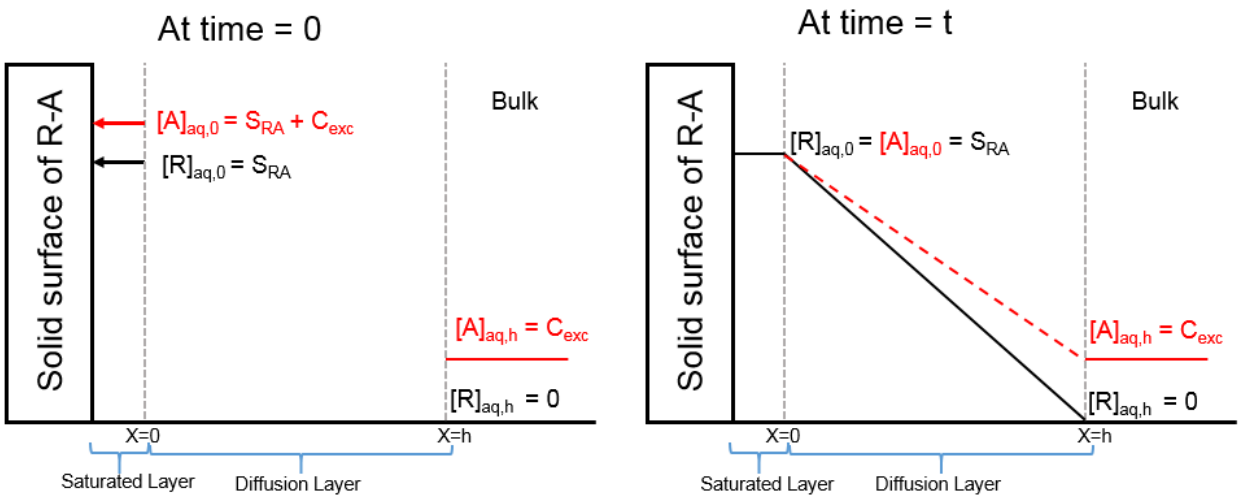

Figure 4.1. Schematic representation of approach 1 for the dissolution of RA with R and A as the nonionizable components. The concentration of coformer added in the bulk solution is the same as the depleted coformer concentration due to faster diffusion. $[R]_{aq,0}$ and $[A]_{aq,0}$ represent the concentrations of R and A at the surface; $[R]_{aq,h}$ and $[A]_{aq,h}$ represent the concentrations of R and A in the bulk solution; S_{RA} is the solubility of the cocrystal and C_{exc} is the concentration of coformer added in the dissolution medium.

Approach 2: $[R]_{aq,0} < [A]_{aq,0}$

The schematic representation of approach 2 is shown in Figure 4.2. Similar to approach 1, the coformer concentration at the dissolving surface is higher than that of the drug before any diffusion happens. However, for this approach, the coformer would be able to maintain a surface concentration that is higher than the drug concentration at steady state because the coformer concentration added in the dissolution medium is higher than the depleted concentration due to faster diffusion.

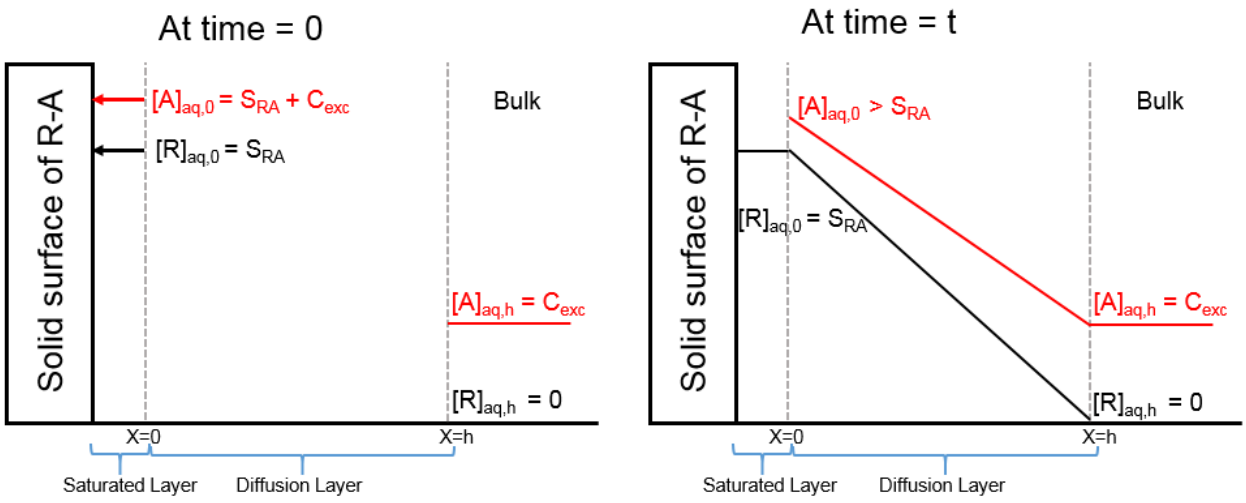

Figure 4.2. Schematic representation of approach 2 for the dissolution of RA with R and A as the nonionizable components. The concentration of coformer added in the bulk solution is higher than the depleted coformer concentration. $[R]_{aq,0}$ and $[A]_{aq,0}$ represent the concentrations of R and A at the surface; $[R]_{aq,h}$ and $[A]_{aq,h}$ represent the concentrations of R and A in the bulk; S_{RA} is the solubility of the cocrystal and C_{exc} is the concentration of coformer added in the dissolution medium.

Chemical equilibria within diffusion layer

Carbamazepine salicylic acid (CBZ-SLC) is chosen as the model cocrystal because it has a low solubility product, so it does not require much coformer to achieve the two approaches. CBZ-SLC has higher solubility than the parent drug, so solid phase transformation can happen during dissolution. Previous studies have shown that the cocrystal can be stabilized during dissolution in 150 mM SLS at bulk pH up to 7.5[13]. To avoid the complication of conversion, all dissolution studies were performed in 150 mM SLS. Chemical equilibria involved for the dissolution of CBZ-SLC in the presence of SLS can be written as follows with R representing the non-ionizable drug, CBZ and HA as the acidy coformer, SLC:

$$(RHA)_{solid} \leftrightharpoons R_{aq} + HA_{aq} \tag{4.1}$$

$$K_{sp} = [R]_{aq}[HA]_{aq} \tag{4.2}$$

$$H_2O + HA_{aq} \leftrightharpoons H_3O^+ + A^-_{aq} \quad (4.3)$$

$$K_a = \frac{[H_3O^+][A^-]_{aq}}{[HA]_{aq}} \quad (4.4)$$

$$H_3O^+ + OH^- \leftrightharpoons 2H_2O \quad (4.5)$$

$$K_w = [H_3O^+][OH^-] \quad (4.6)$$

$$HA_{aq} + OH^- \leftrightharpoons H_2O + A^-_{aq} \quad (4.7)$$

$$K_1 = \frac{[A^-]_{aq}}{[HA]_{aq}[OH^-]} \quad (4.8)$$

$$R_{aq} + m \leftrightharpoons R_m \quad (4.9)$$

$$K_S^R = \frac{[R]_m}{[R]_{aq}[m]} \quad (4.10)$$

$$HA_{aq} + m \leftrightharpoons HA_m \quad (4.11)$$

$$K_S^{HA} = \frac{[HA]_m}{[HA]_{aq}[m]} \quad (4.12)$$

where K_{sp} is the solubility product of the cocrystal, K_a is the ionization constant of HA, K_w is the dissociation constant of water, K_1 is the ratio of K_a / K_w, K_S^R is the solubilization constant of R and K_S^{HA} is the solubilization constant of HA, m is the micellar concentration in solution and it is equal to the total surfactant concentration minus the critical micellar concentration (CMC). Subscript aq denotes the aqueous phase and m denotes the micellar phase.

Common coformer effect on solubility

As shown in equation 4.2, the solubility product, K_{sp}, is a chemical equilibrium constant describing the solubility of the cocrystal. In the presence of excess coformer, the solubility of

cocrystal would decrease in order to maintain a constant K_{sp} value. This behavior is very similar to the common ion effect of pharmaceutical salts and it is defined as the common coformer effect. In the presence of excess coformer, the solubility of CBZ-SLC in surfactant solution can be described as follow[18]:

$$S_{cc} = \frac{-C_{exc} + \sqrt{{C_{exc}}^2 + 4K_{sp}(1 + K_S^R[m])(1 + \frac{K_a}{H^+} + K_S^{HA}[m])}}{2} \quad (4.13)$$

where C_{exc} is the concentration of excess coformer in the dissolution medium.

According to the surface saturation model, the total concentrations of the cocrystal components at the dissolving surface can be written as follows[13]:

$$[R]_T = [R]_{aq} + [R]_m = S_{cc} \quad (4.14)$$

$$[HA]_T = [HA]_{aq} + [HA]_m + [A^-]_{aq} = (\frac{D_{R_{eff}}}{D_{HA_{eff}}})^{2/3} S_{cc} \quad (4.15)$$

where $D_{R_{eff}}$ and $D_{HA_{eff}}$ are the effective diffusion coefficients of R and HA, S_{cc} is the solubility of cocrystal and subscript T denotes the total concentration. For approach 1, excess coformer would be added to the dissolution medium so that the coformer concentration at the dissolving surface would be the same as the drug concertation and this can be described by the following:

$$[R]_T = [HA]_T + C_{exc} \quad (4.16)$$

Substituting equations 4.13, 4.14 and 4.15 into 4.16, the concentration of coformer required to achieve approach 1 can be described as follow:

$$C_{exc} = \sqrt{\frac{4K_{sp}(1+K_S^R[m])(1+\frac{K_a}{H^+}+K_S^{HA}[m])}{[\frac{2}{1-\left(\frac{D_{R_{eff}}}{D_{HA_{eff}}}\right)^{\frac{2}{3}}}+1]^2-1}} \quad (4.17)$$

By knowing the equilibrium constants and the effective diffusion coefficients, the concentration of coformer required in the bulk solution to achieve equivalent concentrations of cocrystal components at the surface can be calculated as a function of pH and surfactant concentration.

Detailed mass transport analyses for the two approaches are shown in Appendix 4A. These analyses allow the validation of the surface saturation model and the evaluation of the common coformer effect on interfacial pH and flux of the cocrystals. Both approaches are based on the following assumptions: all chemical reactions and solute solubilization within the diffusion layer occur instantaneously, free solute and micelle are in equilibrium throughout the diffusion layer, the ionized form of the coformer is not solubilized by surfactant, aqueous diffusivity of the ionized and non-ionized forms are the same. For simplification of the interfacial pH prediction, the effective diffusivity of the coformer is assumed to be the same as the aqueous diffusivity because it is not significantly solubilized by the surfactant. In this study, the effect of surfactant concentration on the viscosity of dissolution medium was not accounted for the mass transport analyses. Although the viscosity of the dissolution medium may approximately double at high surfactant concentration (eg: 300 mM)[20], its impact on the hydrodynamic boundary layer is small. The viscosity of dissolution medium is not expected to significantly affect the diffusion of free species as they are assumed to be diffusing through the aqueous phase where the surfactant concentration is equal to the critical micellar concentration (CMC) and the viscosity is not substantially different from water[21]. The effect of viscosity on the diffusion coefficient of the micelles incorporates the effect of viscosity changes.

Results and discussion

Physicochemical properties of CBZ-SLC and its components such as solubility product, ionization constant, micellar solubilization constant and diffusion coefficient are required to perform the mass transport analyses for the dissolution of cocrystal in the presence of excess coformer in the dissolution medium. These properties can be obtained from the literature and they are summarized in Table 4.1. All dissolution experiments in this study were performed in 150 mM SLS to prevent solid phase transformation of the cocrystal back to the stable drug form. Therefore, the solubilization constants of CBZ and SLC and effective diffusion coefficient of CBZ in Table 4.1 are obtained from 150 mM SLS. The effective diffusivity of SLC is not listed in Table 4.1 because it has a pH dependence due to the ionization properties of SLC. By knowing the micellar diffusivity (D_m), the effective diffusivity of SLC at a given pH can be estimated using the following equation:

$$D_{HA_{eff}} = \frac{D_{aq}(1+\frac{K_a}{H^+})+K_S^{HA}D_m[m]}{1+\frac{K_a}{H^+}+K_S^{HA}[m]} \tag{4.18}$$

Table 4.1. Physicochemical properties of CBZ-SLC and its components.

Cocrystal	K_{sp} (mM^2)[a]	pKa of SLC[a]	K_s in 150 mM SLS (mM^{-1})[a]		Diffusion coefficient (x 10^{-6} cm^2/sec)[a]		
			CBZ	SLC	$D_{R_{aq}}$	$D_{R_{eff}}$	$D_{HA_{aq}}$
CBZ-SLC	0.40	3.0	0.43	0.060	5.7	1.5	7.7

a) From Reference [13].

Evaluation of approach 1

The concentrations of coformer required to establish approach 1 were calculated using equation 4.17 as a function of bulk pH, and these are summarized in Table 4.2. As pH increases, the solubility of CBZ-SLC increases due to the acidity of SLC, consequently, it requires higher

SLC concentration in the dissolution medium to compensate for the depletion of SLC at the dissolving surface due to faster diffusion. The concentrations of SLC are the same at the self-buffering region of CBZ-SLC because there is only minimal change in interfacial pH at bulk pH from 5.0 to 7.5.

Table 4.2. Concentrations of SLC required to establish approach 1 as a function of bulk pH.

pH		**SLC (mM)[b]**
Bulk	**Interfacial[a]**	
1.0	1.0	2.87
2.0	2.0	3.05
3.0	3.0	4.45
5.0	3.8	8.50
6.0	3.8	8.56
7.5	3.8	8.57

a) Calculated using equation 4A.27 from Appendix 4A;
b) Calculated using equation 4.17.

The solubility of cocrystal decreases in the presence of coformer in excess to the stoichiometric concentration because of the solubility product behavior. The decrease in cocrystal solubility lowers the degree of coformer ionization at the dissolving surface and thus influences the pH at the interface. The common coformer effect on interfacial pH and solubility of CBZ-SLC as a function of bulk pH for approach 1 is summarized in Table 4.3. Interfacial pH is not affected by the common coformer effect at bulk pH $\leq pK_a$ of SLC (3.0) because the pH microenvironment is dominated by the bulk pH. As bulk pH increases above the pK_a value, the ability in lowering interfacial pH is smaller in the presence of excess coformer. The common coformer effect decreases the solubility of CBZ-SLC and lowers the degree of SLC ionization at the interface, and thus results in slightly higher interfacial pH. As shown in Table 4.3, solubility of CBZ-SLC decreases in the presence of SLC at all pH. As the SLC concentrations required to achieve approach 1 are very small at pH 1 and 2, there is no significant decrease in solubility of CBZ-SLC

under these conditions. The common coformer effect on the dissolution rates of CBZ-SLC under these conditions may not be very significant. Therefore, dissolution studies of CBZ-SLC at bulk pH 3, 5 and 7.5 were performed to evaluate the mass transport model for approach 1.

Table 4.3. Common coformer effect on interfacial pH and solubility of CBZ-SLC as a function of bulk pH.

pH		SLC (mM)[b]	S_{cc} (mM)[c]
Bulk	**Interfacial[a]**		
1.0	1.0	0	15.6
	1.0	2.87	14.2
2.0	2.0	0	15.7
	2.0	3.05	14.2
3.0	3.0	0	16.4
	3.0	4.45	14.3
5.0	3.7	0	19.3
	3.8	8.50	16.3
6.0	3.7	0	19.4
	3.8	8.56	16.4
7.5	3.7	0	19.4
	3.8	8.57	16.4

a) Absence of SLC is from reference [13] and presence of SLC is from Table 4.1;
b) From Table 4.2;
c) Calculated using equation 4.13.

Dissolution studies of CBZ-SLC at bulk pH 3, 5 and 7.5 were performed in 150 mM SLS containing SLC concentrations shown in Table 4.2 to maintain equal component concentrations at the dissolving surface. The rotating disk dissolution concentration profiles are shown in Figure 4.3. The linear dissolution behavior indicated that no solid phase transformation happened during dissolution under these conditions.

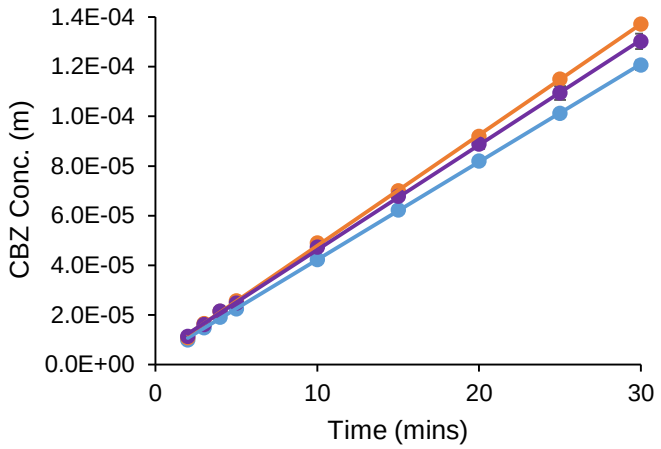

Figure 4.3. Dissolution concentration profiles of CBZ-SLC in 150 mM SLS at pH 3.06, 4.5 mM SLC (—); pH 5.03, 8.2 mM SLC (—) and pH 7.50, 8.3 mM SLC (—).

To evaluate the predictive power of the mass transport model for approach 1, the experimental flux of CBZ-SLC were calculated from the dissolution concentration profiles shown in Figure 4.3 and compared to the theoretical predictions. Table 4.4 summarizes the interfacial pH, concentrations of the cocrystal components at the surface, the theoretical and experimental flux of CBZ-SLC in the absence and presence of excess SLC. With no excess SLC in the dissolution medium, the concentration of SLC at the dissolving surface is smaller than that of CBZ because it is depleted due to faster diffusion. By adding the depleted amount of SLC in the dissolution medium, the SLC concentration at the dissolving surface is able to maintain the same concentration as that of the drug. The presence of excess SLC decreases the solubility of CBZ-SLC due to the common coformer effect and thus lowers the concentration of CBZ at the dissolving surface compared to that without excess coformer. The common coformer effect is also reflected in the dissolution of CBZ-SLC by the lower flux in the presence of excess SLC compared to those in the absence of excess SLC. As shown in Table 4.4, the theoretical flux predictions have excellent agreement with the experimental values. The developed mass transport model with consideration of interfacial pH for approach 1 is able to accurately predict the flux of CBZ-SLC.

Table 4.4. Interfacial pH, concentrations of CBZ and SLC at the dissolving surface, predicted and experimental flux of CBZ-SLC in the absence and presence of excess SLC.

pH		SLC (mM)	Conc. at the surface (mM)		Flux ($\times 10^{-4}$ mmole/cm^2 min)		% difference
Bulk	Interfacial		CBZ[a]	SLC[b]	Predicted	Experimental	
3.11 ± 0.02	3.0	0	16.4	5.5	8.0[c]	7.9 ± 0.2[c]	2.1
3.06 ± 0.01	3.0	4.47 ± 0.01	14.4	14.4	7.0[d]	7.5 ± 0.1	7.0
4.96 ± 0.03	3.7	0	19.3	6.5	9.4[c]	9.8 ± 0.4[c]	4.4
5.03 ± 0.03	3.8	8.2 ± 0.5	16.3	16.3	7.9[d]	8.5 ± 0.1	7.2
7.5 ± 0.1	3.7	0	19.4	6.5	9.4[c]	9.69 ± 0.01[c]	2.9
7.5 ± 0.1	3.8	8.3 ± 0.5	16.4	16.4	8.0[d]	8.1 ± 0.2	1.1

a) Calculated using equation 4.14;
b) Calculated using equation 4.15;
c) From reference [13];
d) Calculated using equation 4A.33 from Appendix 4A.

Evaluation of approach 2

Approach 2 is to establish a higher coformer concentration than the drug concentration at the dissolving surface by adding coformer in the dissolution medium that is higher than the required concentration for approach 1. The interfacial pH and surface concentrations of the cocrystal components at bulk pH 3 as a function of SLC are summarized in Table 4.5. Because the bulk pH is at the pK_a value of SLC, there is not much deviation in interfacial pH from the bulk pH as a function of SLC. With no SLC in the dissolution medium, surface concentration of SLC is less than CBZ due to its rapid diffusion. In 4.47 mM SLC solution, the concentrations of the cocrystal components at the dissolving surface are the same because this SLC concentration is the required concentration for approach 1 (Table 4.2). By further increasing the SLC concentration in the dissolution medium, the SLC concentration at the dissolving surface becomes higher than that of CBZ. By varying the SLC concentration in the dissolution medium, the surface concentration of SLC can be the same as or higher than the drug concentration.

Table 4.5. Interfacial pH and surface concentrations of CBZ and SLC at bulk pH 3 in 150 mM SLS as a function of SLC.

pH		SLC (mM)	Surface concentration (mM)	
Bulk	**Interfacial[a]**		**CBZ[b]**	**SLC[c]**
3.11 ± 0.02	3.0	0	16.4	5.5
3.06 ± 0.01	3.0	4.47 ± 0.01	14.4	14.4
3.04 ± 0.02	3.0	6.64 ± 0.01	13.4	15.8
3.03 ± 0.01	3.0	25.01 ± 0.01	8.1	30.5
2.98 ± 0.02	3.0	45.02 ± 0.01	5.3	48.6

a) Calculated using equation 4A.28 from Appendix 4A;
b) Calculated using equation 4.14;
c) Calculated using equation 4.15.

The common coformer effect on the interfacial pH of CBZ-SLC at bulk pH 5 is shown in Figure 4.4. This bulk pH value is above the pK_a of SLC, so the cocrystal has the ability to lower the interfacial pH due to the ionization of the coformer. However, this ability decreases as the concentration of SLC increases in the bulk solution. As shown in Figure 4.4, interfacial pH increases with increasing SLC concentration in the dissolution medium. The presence of SLC in the bulk solution decreases the solubility of the cocrystal and thus lowers the ionization of the coformer at the interface. The higher interfacial pH can have implications in reducing the common coformer effect on dissolution rates of cocrystals.

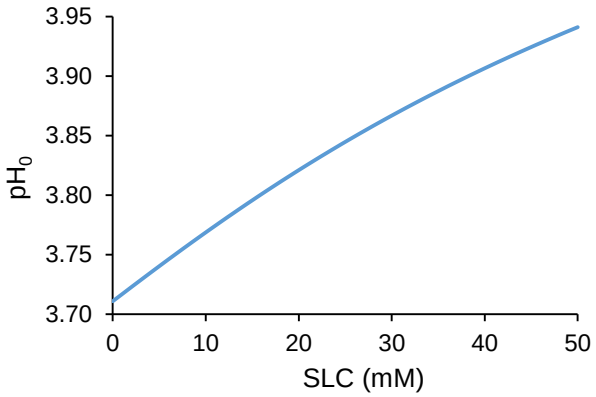

Figure 4.4. Interfacial pH of CBZ-SLC in 150 mM SLS at bulk pH 5 as a function of SLC. Interfacial pH was predicted using equation 4A.28 from Appendix 4A with physicochemical parameters shown in Table 4.1.

Approach 2 was evaluated by performing dissolution experiments for CBZ-SLC at bulk pH 3 and 5 as a function of excess SLC in 150 mM SLS dissolution media. The dissolution concentration profiles of CBZ-SLC at bulk pH 3 and 5 as a function of SLC are shown in Figure 4.5. Solid phase transformation did not occur during dissolution as indicated by the linear dissolution behavior. Dissolution rates of CBZ-SLC decrease with increasing SLC concentration due to the common coformer effect. The impact of common coformer effect on the dissolution of CBZ-SLC at bulk pH 3 is greater than at bulk pH 5 as indicated by the larger decrease in dissolution rates at bulk pH 3 as a function of SLC concentration.

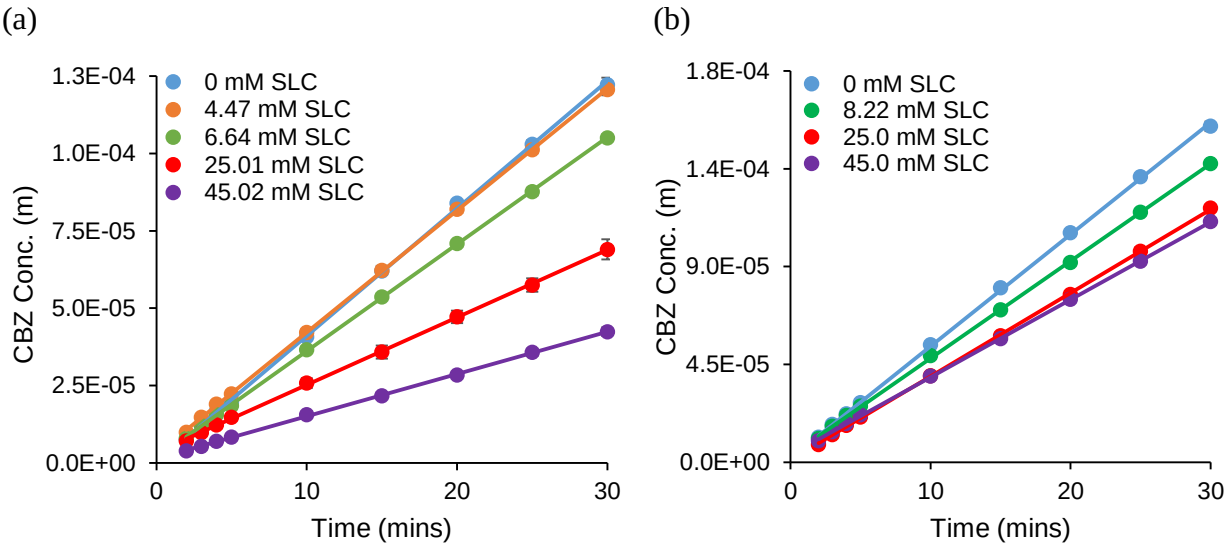

Figure 4.5. Dissolution concentration profiles of CBZ-SLC in 150 mM SLS at bulk pH 3.0 (a) and bulk pH 5 (b) as a function of SLC concentration.

Flux of CBZ-SLC at bulk pH 3 and 5 as a function of SLC was calculated from the dissolution rates and compared to the theoretical predictions as shown in Figure 4.6. The flux of CBZ-SLC at both pH decreases as SLC concentration increases. The common coformer effect on the flux of CBZ-SLC is greater at bulk pH 3 than pH 5 as indicated by the steeper curve shown in Figure 4.6 for pH 3. The common coformer effect is dampened at bulk pH 5 because of the

increase in interfacial pH as a function of SLC concentration shown in Figure 4.4. The increased interfacial pH can help to reduce the common coformer effect on the solubility and dissolution of CBZ-SLC because of the acidity of SLC. The mass transport model is able to capture the common coformer effect on the dissolution of CBZ-SLC as indicated by the excellent agreement between the theoretical and experimental flux as a function of SLC concentration. However, there are some deviations in the flux predictions at bulk pH 5 from the experimental values. The largest deviation is at 45 mM SLC, but the flux prediction is still within a factor of two compared to the experimental value. These deviations may be due to the pH sensitivity of CBZ-SLC flux because the interfacial pH at bulk pH 5 is predicted to be above the pK_a value of SLC. A 0.5 unit pH change in interfacial pH at 45 mM SLC can lead to a roughly 70% change in flux prediction of CBZ-SLC. Obviously, accurate interfacial pH prediction is essential for predicting the flux of cocrystal with ionizable components.

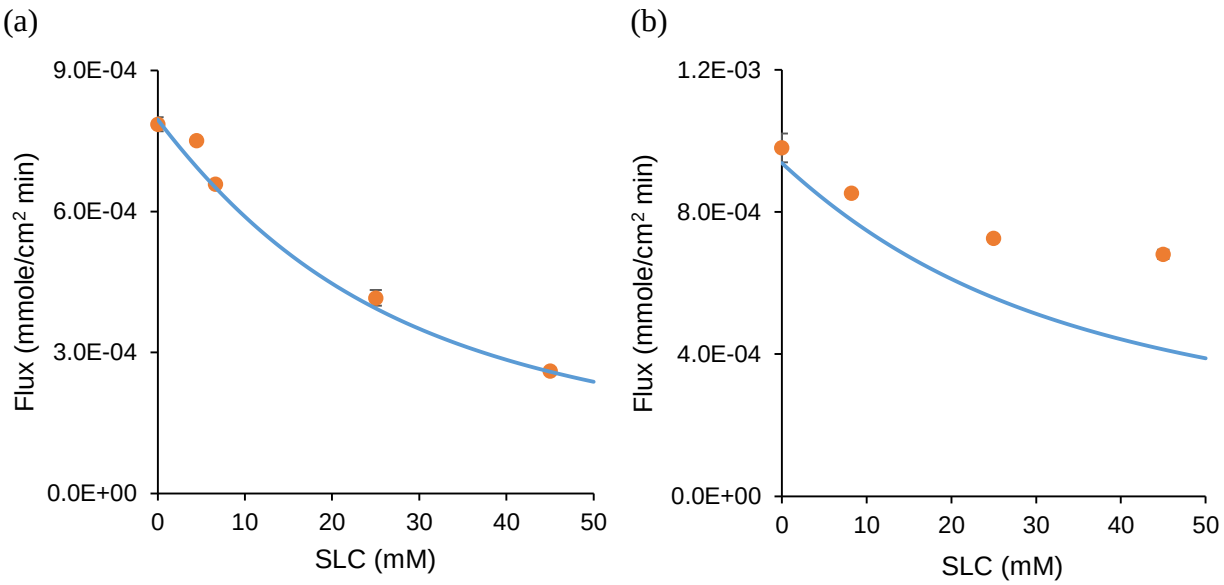

Figure 4.6. The experimental (orange circle) and theoretical (blue line) flux comparison of CBZ-SLC in 150 mM SLS at bulk pH 3 (a) and 5 (b) as a function of SLC. Flux predictions were calculated using equation 4A.33 from Appendix 4A with physicochemical properties shown in Table 4.1.

Conclusions

This chapter has demonstrated the influence of common coformer effect on the interfacial pH and flux of cocrystals. The establishment of the two approaches in this study adds another level of confidence to the surface saturation model developed previously for the dissolution of cocrystals. The mass transport analyses based on the surface saturation model for the two approaches are able to evaluate the impact of coformer in the bulk solution on interfacial pH and flux of cocrystals. The presence of excess coformer can decrease the cocrystal solubility and lower the degree of coformer ionization at the dissolving surface, and consequently, the interfacial pH would be higher compared to the absence of excess coformer. It is essential to understand the influence of common coformer effect on interfacial pH because it is required for accurate flux predictions. The flux of cocrystal is predicted to decrease with increasing coformer concentration because of the solubility product behavior of cocrystal. In the case of oral absorption, the lower membrane permeation of the coformer can potentially result in excess coformer in the intestinal lumen that can influence the dissolution of the continually dissolving cocrystal due to the common coformer effect. These mass transport models can provide useful insights on how the differential permeability between the cocrystal components can influence the oral absorption of the drug from the cocrystalline materials.

References

1. Weyna, D. R.; Cheney, M. L.; Shan, N.; Hanna, M.; Zaworotko, M. J.; Sava, V.; Song, S.; Sanchez-Ramos, J. R. Improving Solubility and Pharmacokinetics of Meloxicam via Multiple-Component Crystal Formation. *Molecular Pharmaceutics* **2012,** *9*, 2094-2102.

2. Childs, S. L.; Kandi, P.; Lingireddy, S. R. Formulation of a Danazol Cocrystal with Controlled Supersaturation Plays an Essential Role in Improving Bioavailability. *Molecular Pharmaceutics* **2013,** *10*, (8), 3112-3127.

3. McNamara, D. P.; Childs, S. L.; Giordano, J.; Iarriccio, A.; Cassidy, J.; Shet, M. S.; Mannion, R.; O'Donnell, E.; Park, A. Use of a glutaric acid cocrystal to improve oral bioavailability of a low solubility API. *Pharmaceutical Research* **2006,** *23*, (8), 1888-1897.

4. Smith, A. J.; Kavuru, P.; Wojtas, L.; Zaworotko, M. J.; Shytle, R. D. Cocrystals of Quercetin with Improved Solubility and Oral Bioavailability. *Molecular Pharmaceutics* **2011,** *8*, (5), 1867-1876.

5. Bak, A.; Gore, A.; Yanez, E.; Stanton, M.; Tufekcic, S.; Syed, R.; Akrami, A.; Rose, M.; Surapaneni, S.; Bostick, T.; King, A.; Neervannan, S.; Ostovic, D.; Koparkar, A. The Co-crystal Approach to Improve the Exposure of a Water-insoluble Compound: AMG 517 Sorbic Acid Co-crystal Characterization and Pharmacokinetics. *Journal of Pharmaceutical Sciences* **2008,** *97*, (9), 3942-3956.

6. Thakuria, R.; Delori, A.; Jones, W.; Lipert, M. P.; Roy, L.; Rodriguez-Hornedo, N. Pharmaceutical Cocrystals and Poorly Soluble Drugs. *International Journal of Pharmaceutics* **2013,** *453*, (1), 101-125.

7. Jung, M.; Kim, J.; Kim, M.; Alhalaweh, A.; Cho, W.; Hwang, S.; Velaga, S. P. Bioavailability of Indomethacin-Saccharin Cocrystals. *Journal of Pharmacy and Pharmacology* **2010,** *62*, 1560-1568.

8. Cheney, M. L.; Shan, N.; Healey, E. R.; Hanna, M.; Wojtas, L.; Zaworotko, M. J.; Sava, V.; Song, S.; Sanchez-Ramos, J. R. Effects of Crystal Form on Solubility and Pharmacokinetics: A Crystal Enginneering Case Study of Lamotrigine. *Crystal Growth & Design* **2010,** *10*, 394-405.

9. Good, D. J. a. R.-H., N. Solubility Advantage of pHarmaceutical Cocrystals. *Crystal Growth & Design* **2009,** *9*, (5), 2252-2264.

10. Bethune, S. J.; Huang, N.; Jayasankar, A.; Rodriguez-Hornedo, N. Understanding and Predicting the Effect of Cocrystal Components and pH on Cocrystal Solubility. *Crystal Growth and Design* **2009,** *9*, (9), 3976-3988.

11. Huang, N.; Rodriguez-Hornedo, N. Engineering Cocrystal Solubility, Stability, and pHmax by Micellar Solubilization. *Journal of Pharmaceutical Sciences* **2011,** *100*, (12), 5219-5234.

12. Roy, L.; Lipert, M. P.; Rodriguez-Hornedo, N., Co-crystal Solubility and Thermodynamic Stability. In *Rsc Drug Discov*, Royal Society of Chemistry: 2012; pp 247-279.

13. Cao, F.; Amidon, G.; Rodriguez-Hornedo, N.; Amidon, G. Mechanistic Analysis of Cocrystal Dissolution as a Function of pH and Micellar Solubilization. *Molecular Pharmaceutics* **2015,** *13*, (3), 1030-1046.

14. Serajuddin, A. T. M.; Sheen, P.-C.; Augustine, M. A. Common Ion Effect on Solubility and Dissolution Rate of the Sodium Salt of an Organic Acid. *journal of Pharmacy and Pharmacology* **1987,** *39*, (8), 587-591.

15. Shozo, M.; Midori, O.; Tanekazu, N. Unusual Solubility and Dissoluton Behavior of Pharmaceutical Hydrochloride Salts in Chloride-Containing Media. *International Journal of Pharmaceutics* **1980,** *6*, (1), 77-85.

16. Serajuddin, A. T. M.; Jarowski, C. I. Effect of Diffusion Layer pH and Solubility on the Dissolution Rate of Pharmaceutical Bases and Their Hydrochloride Salts I: Phenazopyridine. *journal of Pharmaceutical Sciences* **1985,** *74*, (2), 142-147.

17. Li, S.; Doyle, P.; Metz, S.; Royce, A. E.; Serajuddin, A. T. Effect of Chloride Ion on Dissolution of Different Salt Forms of Haloperidol, A Model Basic Drug. *journal of Pharmaceutical Sciences* **2005,** *94*, (10), 2224-31.

18. Nehm, S. J.; Rodríguez-Spong, B.; Rodríguez-Hornedo, N. Phase Solubility Diagrams of Cocrystals Are Explained by Solubility Product and Solution Complexation. *Crystal Growth & Design* **2005,** *6*, (2), 592-600.

19. Rodríguez-Hornedo, N.; Nehm, S. J.; Seefeldt, K. F.; Pagán-Torres, Y.; Falkiewicz, C. J. Reaction Crystallization of Pharmaceutical Molecular Complexes. *Molecular Pharmaceutics* **2006,** *3*, (3), 362-367.

20. Kabir-ud-Din; David, S. L.; Kumar, S. Viscosities of Sodium Dodecyl Sulfate Solutions in Aqueous Ammonium Salts. *Journal of Chemical & Engineering Data* **1997,** *42*, (6), 1224-1226.

21. Poskanzer, A. M.; Goodrich, F. C. Surface Viscosity of Sodium Dodecyl Sulfate Solutions with and without Added Dodecanol. *The Journal of Physical Chemistry* **1975,** *79*, (20), 2122-2126.

22. Levich, V. G., *Physico-chemical Hydrodynamics*. Prentice-Hall: Englewood Cliffs, N.J., 1962.

APPENDIX 4A

The flux of all the species across the diffusion layer include both the diffusion and chemical reactions happening during dissolution. At steady state, the diffusion and simultaneous chemical reactions of the individual species within the diffusion layer can be written using Fick's law as follows:

$$\frac{\partial [R]_{aq}}{\partial t} = D_{R_{aq}} \frac{\partial^2 [R]_{aq}}{\partial x^2} + \phi_1 = 0 \quad (4A.1)$$

$$\frac{\partial [R]_m}{\partial t} = D_{R_m} \frac{\partial^2 [R]_m}{\partial x^2} + \phi_2 = 0 \quad (4A.2)$$

$$\frac{\partial [HA]_{aq}}{\partial t} = D_{HA_{aq}} \frac{\partial^2 [HA]_{aq}}{\partial x^2} + \phi_3 = 0 \quad (4A.3)$$

$$\frac{\partial [A^-]_{aq}}{\partial t} = D_{A^-_{aq}} \frac{\partial^2 [A^-]_{aq}}{\partial x^2} + \phi_4 = 0 \quad (4A.4)$$

$$\frac{\partial [HA]_m}{\partial t} = D_{HA_m} \frac{\partial^2 [HA]_m}{\partial x^2} + \phi_5 = 0 \quad (4A.5)$$

$$\frac{\partial [OH^-]}{\partial t} = D_{OH^-} \frac{\partial^2 [OH^-]}{\partial x^2} + \phi_6 = 0 \quad (4A.6)$$

$$\frac{\partial [H^+]}{\partial t} = D_{H^+} \frac{\partial^2 [H^+]}{\partial x^2} + \phi_7 = 0 \quad (4A.7)$$

where $\phi_{1\text{-}7}$ are the reaction rate functions. At equilibrium, the reaction rate of the reactant should be the opposite of the product. Based on the chemical equilibria, the following can be written:

$$\phi_1 = -\phi_2 \quad (4A.8)$$

$$\phi_3 = -\phi_4 - \phi_5 \quad (4A.9)$$

The reaction rate of A^- can be reflected by the reaction rate of H^+ and OH^-, therefore,

$$\phi_4 = \phi_7 - \phi_6 \tag{4A.10}$$

Based on equation 4A.10, equation 4A.9 can be written as:

$$\phi_3 = \phi_6 - \phi_5 - \phi_7 \tag{4A.11}$$

Based on the equations 4A.8, 4A.9 and 4A.11, the following mass balance equations can be written:

$$D_{R_{aq}} \frac{d^2\,[R]_{aq}}{dx^2} = -D_{R_m} \frac{d^2\,[R]_m}{dx^2} \tag{4A.12}$$

$$D_{HA_{aq}} \frac{d^2\,[HA]_{aq}}{dx^2} = -D_{A^-_{aq}} \frac{d^2[A^-]_{aq}}{dx^2} - D_{HA_m} \frac{d^2\,[HA]_m}{dx^2} \tag{4A.13}$$

$$D_{HA_{aq}} \frac{d^2\,[HA]_{aq}}{dx^2} = D_{OH^-} \frac{d^2\,[OH^-]}{dx^2} - D_{H^+} \frac{d^2[H^+]}{dx^2} - D_{HA_m} \frac{d^2\,[HA]_m}{dx^2} \tag{4A.14}$$

Integrating equations 4A.12 to 4A.14 once gives:

$$D_{R_{aq}} \frac{d[R]_{aq}}{dx} = -D_{R_m} \frac{d\,[R]_m}{dx} + C_1 \tag{4A.15}$$

$$D_{HA_{aq}} \frac{d\,[HA]_{aq}}{dx} = -D_{A^-_{aq}} \frac{d[A^-]_{aq}}{dx} - D_{HA_m} \frac{d\,[HA]_m}{dx} + C_2 \tag{4A.16}$$

$$D_{HA_{aq}} \frac{d\,[HA]_{aq}}{dx} = D_{OH^-} \frac{d\,[OH^-]}{dx} - D_{H^+} \frac{d[H^+]}{dx} - D_{HA_m} \frac{d\,[HA]_m}{dx} + C_3 \tag{4A.17}$$

Since A^-_{aq} is the product of the reaction between HA and OH^-, so its flux can be reflected by both OH^- and H^+:

$$-D_{A^-_{aq}} \frac{d[A^-]_{aq}}{dx} = D_{OH^-} \frac{d\,[OH^-]}{dx} - D_{H^+} \frac{d[H^+]}{dx} \tag{4A.18}$$

With this mass balance relationship, it can be seen that

$$C_2 = C_3 \tag{4A.19}$$

Integrating equations 4A.15 to 4A.17 gives:

$$D_{R_{aq}}[R]_{aq} = -D_{R_m}[R]_m + C_1 x + C_4 \tag{4A.20}$$

$$D_{HA_{aq}}[HA]_{aq} = -D_{HA_m}[HA]_m - D_{A^-_{aq}}[A^-]_{aq} + C_2 x + C_5 \tag{4A.21}$$

$$D_{HA_{aq}}[HA]_{aq} = D_{OH^-}[OH^-] - D_{H^+}[H^+] - D_{HA_m}[HA]_m + C_3 x + C_6 \tag{4A.22}$$

Interfacial pH and flux of the species can be evaluated by solving these mass balance equations with the following boundary conditions.

Boundary conditions:

At $x = 0$:	at $x = h$:
$[R]_{aq,0} = \frac{-C_{exc} + \sqrt{{C_{exc}}^2 + 4K_{sp}(1+K_S^R[m])(1+\frac{K_a}{H^+}+K_S^{HA}[m])}}{2(1+K_S^R[m])}$	$[R]_{aq,h} = 0$ (sink conditions)
$[HA]_{aq,0} = (\frac{D_{R_{eff}}}{D_{HA_{eff}}})^{2/3} \frac{-C_{exc} + \sqrt{{C_{exc}}^2 + 4K_{sp}(1+K_S^R[m])(1+\frac{K_a}{H^+}+K_S^{HA}[m])}}{2(1+\frac{K_a}{H_0^+}+K_S^{HA}[m])} + [HA]_{aq,h}$	$[HA]_{aq,h} = [HA]_{aq,h}$
$[R]_{m,0} = unknown$	$[R]_{m,h} = 0$ (sink conditions)
$[HA]_{m,0} = unknown$	$[HA]_m = [HA]_{m,h}$
$[A^-]_{aq,0} = unknown$	$[A^-]_{aq} = [A^-]_{aq,h}$
$[H^+] = [H^+]_0$	$[H^+] = [H^+]_h$
$[OH^-] = [OH^-]_0$	$[OH^-] = [OH^-]_h$

Evaluation of pH at the interface

Applying the above boundary conditions to equations 4A.21 and 4A.22, at $x = 0$:

$$D_{HA_{aq}}\left(\frac{D_{R_{eff}}}{D_{HA_{eff}}}\right)^{2/3}\frac{-C_{exc}+\sqrt{{C_{exc}}^2+4K_{sp}\left(1+K_s^R[m]\right)\left(1+\frac{K_a}{H^+}+K_s^{HA}[m]\right)}}{2\left(1+\frac{K_a}{H_0^+}+K_s^{HA}[m]\right)}+[HA]_{aq,h}=$$

$$-D_{HA_m}[HA]_{m,0}-D_{A_{aq}^-}[A^-]_{aq,0}+C_5 \quad (4A.23)$$

$$D_{HA_{aq}}\left(\frac{D_{R_{eff}}}{D_{HA_{eff}}}\right)^{2/3}\frac{-C_{exc}+\sqrt{{C_{exc}}^2+4K_{sp}\left(1+K_s^R[m]\right)\left(1+\frac{K_a}{H^+}+K_s^{HA}[m]\right)}}{2\left(1+\frac{K_a}{H_0^+}+K_s^{HA}[m]\right)}+[HA]_{aq,h}=D_{OH^-}[OH^-]_0-$$

$$D_{H^+}[H^+]_0-D_{HA_m}[HA]_{m,0}+C_6 \quad (4A.24)$$

and at $x = h$:

$$D_{HA_{aq}}[HA]_{aq,h}=-D_{HA_m}[HA]_{m,h}-D_{A_{aq}^-}[A^-]_{aq,h}+C_2h+C_5 \quad (4A.25)$$

$$D_{HA_{aq}}[HA]_{aq,h}=D_{OH^-}[OH^-]_h-D_{H^+}[H^+]_h-D_{HA_m}[HA]_{m,h}+C_3h+C_6 \quad (4A.26)$$

For approach 1, a fifth order equation can be obtained by combining equations 4A.23 to 4A.26 and substitute equation 4.17 for C_{exc} to calculate the interfacial pH:

$$A{[H^+]_0}^5+B{[H^+]_0}^4+C{[H^+]_0}^3+D{[H^+]_0}^2+E[H^+]_0+F=0 \quad (4A.27)$$

where,

$A=D_{H^+}^2(1+K_s^{HA}[m]);$

$B=-2D_{H^+}(D_{H^+}[H^+]_h-D_{OH^-}[OH^-]_h)(1+K_s^{HA}[m])+D_{H^+}^2K_a;$

$C=-2D_{H^+}D_{OH^-}K_w(1+K_s^{HA}[m])+(1+K_s^{HA}[m])(D_{H^+}[H^+]_h-D_{OH^-}[OH^-]_h)^2-2D_{H^+}(D_{H^+}[H^+]_h-D_{OH^-}[OH^-]_h)K_a;$

$D=2D_{OH^-}K_w(D_{H^+}[H^+]_h-D_{OH^-}[OH^-]_h)(1+K_s^{HA}[m])-2D_{H^+}D_{OH^-}K_wK_a+(D_{H^+}[H^+]_h-D_{OH^-}[OH^-]_h)^2K_a;$

$E = (D_{OH^-}K_w)^2(1 + K_s^{HA}[m]) + 2D_{OH^-}K_w(D_{H^+}[H^+]_h - D_{OH^-}[OH^-]_h)K_a -$
$(D_{A_{aq}^-}^{\frac{1}{3}} D_{R_{eff}}^{\frac{2}{3}} \mathrm{K_a}\sqrt{K_{sp}(1 + K_s^R[m])}(\sqrt{\frac{1}{g} + 1} - \frac{1}{\sqrt{g}}))^2;$

$F = K_a(D_{OH^-}K_w)^2;$

and $g = [\frac{2}{1-\left(\frac{D_{R_{eff}}}{D_{HA_{eff}}}\right)^{\frac{2}{3}}} + 1]^2 - 1.$

For approach 2, a sixth order equation is obtained by combining equations 4A.23 to 4A.26 for calculating the interfacial pH:

$$A[H^+]_0{}^6 + B[H^+]_0{}^5 + C[H^+]_0{}^4 + D[H^+]_0{}^3 + E[H^+]_0{}^2 + F[H^+]_0 + G = 0 \qquad (4A.28)$$

where,

$A = D_{H^+}^2(1 + K_s^{HA}[m])^2;$

$B = -2D_{H^+}(D_{H^+}[H^+]_h - D_{OH^-}[OH^-]_h)(1 + K_s^{HA}[m])^2 + 2D_{H^+}^2K_a(1 + K_s^{HA}[m]);$

$C = -2D_{H^+}D_{OH^-}K_w(1 + K_s^{HA}[m])^2 + (1 + K_s^{HA}[m])^2(D_{H^+}[H^+]_h - D_{OH^-}[OH^-]_h)^2 -$
$4D_{H^+}K_a(D_{H^+}[H^+]_h - D_{OH^-}[OH^-]_h)(1 + K_s^{HA}[m]) + (D_{H^+}K_a)^2 + D_{H^+}D_{A_{aq}^-}^{\frac{1}{3}} D_{R_{eff}}^{\frac{2}{3}} K_aC_{exc}(1 +$
$K_s^{HA}[m]);$

$D = 2D_{OH^-}K_w(D_{H^+}[H^+]_h - D_{OH^-}[OH^-]_h)(1 + K_s^{HA}[m])^2 - 4D_{H^+}D_{OH^-}K_wK_a(1 +$
$K_s^{HA}[m]) + 2 * (1 + K_s^{HA}[m])(D_{H^+}[H^+]_h - D_{OH^-}[OH^-]_h)^2K_a - 2D_{H^+}(D_{H^+}[H^+]_h -$
$D_{OH^-}[OH^-]_h){K_a}^2 - D_{A_{aq}^-}^{\frac{1}{3}} D_{R_{eff}}^{\frac{2}{3}} K_aC_{exc}(D_{H^+}[H^+]_h - D_{OH^-}[OH^-]_h)(1 + K_s^{HA}[m]) +$
$D_{A_{aq}^-}^{\frac{1}{3}} D_{R_{eff}}^{\frac{2}{3}} D_{H^+}{K_a}^2C_{exc};$

$E = (D_{OH^-}K_w)^2(1 + K_s^{HA}[m])^2 + 4D_{OH^-}K_wK_a(D_{H^+}[H^+]_h - D_{OH^-}[OH^-]_h)(1 + K_s^{HA}[m]) -$
$2D_{H^+}D_{OH^-}K_w{K_a}^2 + {K_a}^2(D_{H^+}[H^+]_h - D_{OH^-}[OH^-]_h)^2 - D_{A_{aq}^-}^{\frac{1}{3}} D_{R_{eff}}^{\frac{2}{3}} D_{OH^-}K_wK_aC_{exc}(1 +$
$K_s^{HA}[m]) - D_{A_{aq}^-}^{\frac{1}{3}} D_{R_{eff}}^{\frac{2}{3}} {K_a}^2C_{exc}(D_{H^+}[H^+]_h - D_{OH^-}[OH^-]_h) - K_{sp}(D_{A_{aq}^-}^{\frac{1}{3}} D_{R_{eff}}^{\frac{2}{3}} K_a)^2(1 +$
$K_s^R[m])(1 + K_s^{HA}[m]);$

$$F = 2K_a(1 + K_s^{HA}[m])(D_{OH^-}K_w)^2 + 2D_{OH^-}K_wK_a{}^2(D_{H^+}[H^+]_h - D_{OH^-}[OH^-]_h) - D_{A_{aq}^-}^{\frac{1}{3}} D_{R_{eff}}^{\frac{2}{3}} D_{OH^-}K_wK_a{}^2C_{exc} - K_{sp}K_a(D_{A_{aq}^-}^{\frac{1}{3}} D_{R_{eff}}^{\frac{2}{3}} K_a)^2(1 + K_s^R[m]);$$

$$G = (K_aD_{OH^-}K_w)^2.$$

Evaluation of flux of the cocrystal components

Applying the boundary conditions to equation 4A.20, at *x = 0*:

$$D_{R_{aq}} \frac{-C_{exc} + \sqrt{C_{exc}{}^2 + 4K_{sp}(1+K_s^R[m])(1+\frac{K_a}{H^+}+K_s^{HA}[m])}}{2(1+K_s^R[m])} =$$

$$-D_{R_m}K_s^R[m] \frac{-C_{exc} + \sqrt{C_{exc}{}^2 + 4K_{sp}(1+K_s^R[m])(1+\frac{K_a}{H^+}+K_s^{HA}[m])}}{2(1+K_s^R[m])} + C_4 \quad (4A.29)$$

and at *x = h*:

$$0 = C_1h + C_4 \quad (4A.30)$$

Combining equations 4A.29 and 4A.30 and solve for $-C_1$ for the flux of the cocrystal in terms of drug:

$$J_R = \frac{D_{R_{eff}}}{h} * \frac{1}{2}[-C_{exc} + \sqrt{C_{exc}{}^2 + 4K_{sp}(1 + K_s^R[m])\left(1 + \frac{K_a}{H^+} + K_s^{HA}[m]\right)}] \quad (4A.31)$$

For rotating disk, the thickness of the hydrodynamic boundary layer can be defined according to Levich[22]:

$$h = 1.612D^{\frac{1}{3}}v^{\frac{1}{6}}\omega^{-\frac{1}{2}} \quad (4A.32)$$

where v is the kinematic viscosity and ω is the angular velocity in radians per unit time.

Substituting equation 4A.32 into 4A.31, the flux of cocrystal in terms of drug can be written as:

$$J_R = 0.62 D_{R_{eff}}^{2/3} \omega^{1/2} v^{-1/6} \frac{-C_{exc} + \sqrt{{C_{exc}}^2 + 4K_{sp}(1 + K_S^R[m])(1 + \frac{K_a}{H^+} + K_S^{HA}[m])}}{2} \quad (4A.33)$$

This equation is applicable for both approaches to calculate the flux of the cocrystal in terms of drug concentration. Since the coformer concentration is not measuring, so the flux of the cocrystal in terms of coformer is not derived.

CHAPTER 5

MECHANISTIC ANALYSIS OF COCRYSTAL DISSOLUTION AS A GUIDE FOR RATIONAL SELECTION

Abstract

The dissolution behavior of a dibasic drug, ketoconazole (KTZ) under the influence of pH has been evaluated and compared to its three 1:1 cocrystals with diacidic coformers, fumaric acid (FUM), succinic acid (SUC), and adipic acid (ADP). Mass transport models were developed by applying Fick's Law of diffusion to dissolution with simultaneous chemical reactions in the hydrodynamic boundary layer adjacent to the dissolving surface to predict the interfacial pH and flux of the parent drug and cocrystals. All three cocrystals have the ability to modulate the interfacial pH to different extents compared to the parent drug due to the acidity of the coformers. The pH effect on the dissolution of KTZ is significantly reduced by the cocrystallization with acidic coformers. Due to the different dissolution pH dependence, there exists a transition pH where the flux of the cocrystal is the same as the parent drug. Below this transition pH, the KTZ flux would be higher, but above it, the cocrystal flux would be higher. The development of mass transport models not only provides a mechanistic understanding of the dissolution behavior, but also helps to rationalize the selection process of cocrystals.

Introduction

Cocrystals are multicomponent solids containing two or more different molecular components in the same crystal lattice with well-defined stoichiometry and they have emerged as a promising solid state modification strategy to enhance the solubility, dissolution and bioavailability of poorly water soluble compounds[1-5]. One of the advantages that cocrystals have to offer is the large diversity in formation, however, this can complicate the process of selecting the proper form for development since each cocrystal form can have very distinct physicochemical properties[6-8]. Among these properties, solubility and dissolution are important criteria for the selection process because they play significant roles in determining the oral absorption[9]. Consequently, mechanistic understanding of the solubility and dissolution processes would be beneficial for finding the cocrystal form with optimal physicochemical properties.

Unlike the well-established solubility mechanism, the dissolution mechanism of cocrystals is still under development. A recent study has presented the dissolution mechanism for 1:1 cocrystals with nonionizable drug and monoacidic coformers under the influence of both pH and surfactant[10]. Due to the different diffusion coefficients between the cocrystal components, the concentrations of the components at the dissolving surface have to be different in order to maintain stoichiometric dissolution[10]. Based on the solubility product behavior of cocrystals, two models have been developed to describe the dissolution process[10]. The interfacial equilibrium model is able to maintain constant solubility product at all time during dissolution, while the surface saturation model is only able to maintain the drug concentration at the stoichiometric solubility of the cocrystal[10]. The theoretical comparison between the two models has demonstrated the mass transport analysis based on the surface saturation model provides flux predictions that are more align with the experimental data[10]. In order to increase the applicability, the surface saturation

model is used in this study to perform mass transport analyses for cocrystals containing diverse ionization properties, specifically for cocrystals with dibasic drugs and diacidic coformers.

The model drug studied here is ketoconazole (KTZ), an antifungal drug used primarily for fungal infections[11-13]. It is a weakly dibasic drug with poor intrinsic solubility, pH dependent dissolution and variable oral absorption[11-13]. The dissolution of KTZ below pH 3 is rapid, but the rate is significantly reduced above pH 5[13, 14]. Many studies have demonstrated that the oral absorption of KTZ is impaired for patients with reduced gastric acid production[15-17]. Therefore, the prerequisite for adequate KTZ dissolution and oral absorption is the sufficient gastric acidity. There are studies showing the oral absorption of KTZ can be improved by co-administering with stomach acid stimulant or acidic beverage[11, 13, 17]. Knowing KTZ performs better under acidic conditions, it is interesting to figure out whether the cocrystallization with acidic coformers would help to improve its performance. The purpose of this study is to evaluate and compare the pH dependent dissolution of KTZ to its three cocrystals discovered by Martin, et al.[18], ketoconazole fumaric acid (KTZ-FUM), ketoconazole succinic acid (KTZ-SUC), and ketoconazole adipic acid (KTZ-ADP) cocrystals.

Materials and methods

Materials

Ketoconazole (KTZ) was purchased from Bosche Scientific (New Brunswick, NJ) and used as received. Adipic acid (ADP), succinic acid (SUC), fumaric acid (FUM), were purchased from Sigma-Aldrich (St. Louis, MO) and used as received. Methanol, 2-propanol and hydrochloric acid were purchased from Fisher Scientific (Pittsburgh, PA). Acetone was purchased from Acros Organics (NJ). Sodium hydroxide pellets were purchased from J.T. Baker (Philipsburg, NJ).

Trifluoroacetic acid was purchased from Aldrich Company (Milwaukee, WI). Water used in this study was filtered through a double deionized purification system (Milli Q Plus Water System) from Millipore Co. (Bedford, MA).

Cocrystal synthesis

Cocrystals were prepared by reaction crystallization method[19] at room temperature. KTZ-SUC and KTZ-FUM were prepared by adding 1:1 molar ratio of KTZ and coformers in acetone solution. KTZ-ADP was prepared by adding 1:1 molar ratio of KTZ and ADP in 2-propanol solution. Solid phases were characterized by X-ray powder diffraction (XRPD) and differential scanning calorimetry (DSC).

Cocrystal dissolution measurements

Constant surface area dissolution rates of KTZ and its cocrystals were determined using a rotating disk apparatus. Drug or cocrystal powder (~150 mg) was compressed in a stainless steel rotating disk die with a tablet radius of 0.50 cm at approximately 85 MPa for 2 minutes using a hydraulic press. The die containing the compact was mounted onto a stainless steel shaft attached to an overhead, variable speed motor. The disk was exposed to 150 mL of dissolution medium in a water jacketed beaker with temperature controlled at 25°C and a rotation speed of 200 rpm was used. All dissolution experiments were performed in water with pH adjusted using HCl or NaOH. The bulk pH during dissolution was maintained constant by adding HCl or NaOH as necessary. Sink conditions were maintained throughout the experiments by ensuring the concentrations at the last time point of the dissolution were less than 10% of the solubility. Solution concentrations were measured using HPLC and solid phases after dissolution were analyzed by XRPD.

HPLC

Waters HPLC equipped with a photodiode array detector was used for all analysis. The mobile phase was composed of 60% methanol and 40% water with 0.1% trifluoroacetic acid and the flow rate of 1 mL/min was used. Separation was achieved using Waters, Atlantis, T3 column (5.0 µm, 100 Å) with dimensions of 4.6 x 250 mm. The sample injection volume was 20 µL. However, it was increased to 100 µL for the dissolution of KTZ at pH 5 and 6 due to the low concentration. The wavelengths for the analytes were as follows: 230 nm for KTZ, 220 nm for FUM and 210 nm for both SUC and ADP.

XRPD

XRPD diffractograms of solid phases were collected with a benchtop Rigaku Miniflex X-ray diffractometer using Cu-Kα radiation (λ = 1.54 Å), a tube voltage of 30 kV, and a tube current of 15 mA. Data was collected from 5 to 40° at a continuous scan rate of 2.5°/min.

DSC

Crystalline samples were analyzed by DSC using a TA instrument 2910 MDSC system equipped with a refrigerated cooling unit. All experiments were performed by heating the samples at a rate of 10 °C/min under a dry nitrogen atmosphere. Temperature and enthalpy of the instrument were calibrated using high purity indium standard.

Theoretical

The mass transport models presented in this study describe the dissolution mechanisms of a dibasic drug and its three 1:1 cocrystals with diacidic coformers in solutions containing hydrogen ion, hydroxide ion and water as the reactive species. The mass transport analyses are based on the

classic film theory that postulates the existence of a diffusion boundary layer adjacent to the dissolving surface[20]. Due to the ionization properties, both drug and coformers can undergo chemical reactions with the reactive species from the bulk solution that can alter the pH at the dissolving surface. The dissolution process is determined by the concentration gradient across the diffusion boundary layer and influenced by the simultaneous diffusion and chemical reactions occurring at the dissolving surface and in the adjacent boundary layer[20, 21].

The chemical equilibria and equations for chemical equilibrium constants for the dissolution of the diabasic drug, B are as follows:

$$H_2O + BH_2^{2+} \leftrightharpoons H_3O^+ + BH^+ \tag{5.1}$$

$$K_{a1}^B = \frac{[H_3O^+][BH^+]}{[BH_2^{2+}]} \tag{5.2}$$

$$H_2O + BH^+ \leftrightharpoons H_3O^+ + B \tag{5.3}$$

$$K_{a2}^B = \frac{[H_3O^+][B]}{[BH^+]} \tag{5.4}$$

$$H_3O^+ + OH^- \leftrightharpoons 2H_2O \tag{5.5}$$

$$K_w = [H_3O^+][OH^-] \tag{5.6}$$

$$OH^- + BH_2^{2+} \leftrightharpoons H_2O + BH^+ \tag{5.7}$$

$$K_1 = \frac{[BH^+]}{[BH_2^{2+}][OH^-]} \tag{5.8}$$

$$OH^- + BH^+ \leftrightharpoons H_2O + B \tag{5.9}$$

$$K_2 = \frac{[B]}{[BH^+][OH^-]} \tag{5.10}$$

where K_{a1}^{B} and K_{a2}^{B} are the ionization constants for the dibasic drug. Under aqueous conditions, the solubility of the dibasic drug as a function of pH can be described as follow:

$$S_B = [B]_0(1 + \frac{H^+}{K_{a2}^B} + \frac{(H^+)^2}{K_{a1}^B K_{a2}^B}) \quad (5.11)$$

where $[B]_0$ is the intrinsic solubility of the drug.

The chemical equilibria and equations for chemical equilibrium constants for the dissolution of a 1:1 cocrystal with dibasic drug, B and diacidic coformer, H_2A are as follows:

$$(BH_2A)_{solid} \leftrightharpoons B + H_2A \quad (5.12)$$

$$K_{sp} = [B][H_2A] \quad (5.13)$$

$$H_2O + BH_2^{2+} \leftrightharpoons H_3O^+ + BH^+ \quad (5.14)$$

$$K_{a1}^{B} = \frac{[H_3O^+][BH^+]}{[BH_2^{2+}]} \quad (5.15)$$

$$H_2O + BH^+ \leftrightharpoons H_3O^+ + B \quad (5.16)$$

$$K_{a2}^{B} = \frac{[H_3O^+][B]}{[BH^+]} \quad (5.17)$$

$$H_2O + H_2A \leftrightharpoons H_3O^+ + HA^- \quad (5.18)$$

$$K_{a1}^{H_2A} = \frac{[H_3O^+][HA^-]}{[H_2A]} \quad (5.19)$$

$$H_2O + HA^- \leftrightharpoons H_3O^+ + A^{2-} \quad (5.20)$$

$$K_{a2}^{H_2A} = \frac{[H_3O^+][A^{2-}]}{[HA^-]} \quad (5.21)$$

$$H_3O^+ + OH^- \leftrightharpoons 2H_2O \quad (5.22)$$

$$K_w = [H_3O^+][OH^-] \tag{5.23}$$

$$OH^- + BH_2^{2+} \leftrightharpoons H_2O + BH^+ \tag{5.24}$$

$$K_1 = \frac{[BH^+]}{[BH_2^{2+}][OH^-]} \tag{5.25}$$

$$OH^- + BH^+ \leftrightharpoons H_2O + B \tag{5.26}$$

$$K_2 = \frac{[B]}{[BH^+][OH^-]} \tag{5.27}$$

$$H_2A + OH^- \leftrightharpoons H_2O + HA^- \tag{5.28}$$

$$K_3 = \frac{[HA^-]}{[H_2A][OH^-]} \tag{5.29}$$

$$OH^- + HA^- \leftrightharpoons H_2O + A^{2-} \tag{5.30}$$

$$K_4 = \frac{[A^{2-}]}{[HA^-][OH^-]} \tag{5.31}$$

where K_{sp} is the solubility product of the cocrystal, $K_{a1}^{H_2A}$ and $K_{a2}^{H_2A}$ are the ionization constants of the coformer. Under aqueous conditions, the stoichiometric solubility of the cocrystal as a function of pH can be described as:

$$S_{cc} = \sqrt{K_{sp}\left(1 + \frac{K_{a1}^{H_2A}}{[H^+]} + \frac{K_{a1}^{H_2A}K_{a2}^{H_2A}}{[H^+]^2}\right)\left(1 + \frac{[H^+]}{K_{a2}^{B}} + \frac{[H^+]^2}{K_{a1}^{B}K_{a2}^{B}}\right)} \tag{5.32}$$

Previously developed mass transport models for cocrystal dissolution have demonstrated that the concentrations of the cocrystal components at the dissolving surface can be different if they have different diffusion coefficients[10]. The model drug, KTZ, is a bigger molecule compared to the carboxylic acid coformers, and thus has smaller diffusion coefficient compared to the

coformers. According to the surface saturation model, the concentration of the slower diffusing component at the dissolving surface is maintained at the solubility of the cocrystal, while the concentration of the faster diffusing component is lower[10]. For the dissolution of 1:1 cocrystals with dibasic drugs and diacidic coformers, the concentrations of the components at the dissolving surface can be written as:

$$[B]_{T,0} = [B] + [BH^+] + [BH_2^{2+}] = S_{cc} \tag{5.33}$$

$$[H_2A]_{T,0} = [H_2A] + [HA^-] + [A^{2-}] = (\frac{D_B}{D_{H_2A}})^{2/3} S_{cc} \tag{5.34}$$

where D_B and D_{H_2A} are the diffusion coefficients of the drug and coformer, respectively, and subscript T,0 denotes the total concentration of the ionized and nonionized forms at dissolving surface.

The mass transport analyses for both drug and cocrystals are based on the assumptions that all chemical reactions within the diffusion layer happen instantaneously and the aqueous diffusivities of the ionized and non-ionized forms are the same. Detailed derivations of the mass transport models for the drug and cocrystals using the surface saturation model are provided in Appendix 5A. The mass transport analyses for cocrystal dissolution using the interfacial equilibrium model are also provided in Appendix 5B. In this Appendix, a comparison in cocrystal flux predictions between the surface saturation and interfacial equilibrium models is also included.

Results

Physicochemical properties

Accurate flux predictions for cocrystals require knowledge about the physicochemical properties of the cocrystals and their components, such as solubility product, ionization constant,

and diffusion coefficient and these can be obtained independently from the dissolution studies. The physicochemical properties of the model cocrystals are summarized in Table 5.1. The diffusion coefficient of KTZ is about 2x times smaller compared to the three coformers because of the bigger molecular size. These differential diffusion coefficients would result in different concentrations for the cocrystal components at the dissolving surface as predicted by the surface saturation model[10]. Because of the diprotic property, the drug and the three coformers have two pK_a values. The pK_a values of the parent drug are basic, while those of the coformers are acidic. Due to its basicity, the solubility of the drug decreases with increasing pH and reaches constant value at the pH region where the drug is completely un-ionized. By cocrystallizing with acidic coformers, the solubility pH dependence of the cocrystals is different from that of the parent drug. At low pH, where the basicity of the drug is dominated, the solubility of the cocrystals decreases with increasing pH. However, the rate of decrease is much lower compared to the parent drug because of the acidity of the coformers. As pH increases above the pK_a values of the coformers, the solubility of the cocrystals starts to increase because the acidity of the coformers is dominating the solubility pH effect. The basicity of the drug and acidity of the coformers result in U shape solubility curves for the three cocrystals as a function of pH[22] as shown in Figure 5.1. Because of the different solubility pH dependence between the drug and cocrystal, there exists a transition point on the solubility phase diagram where the solubility of the drug is the same as the cocrystal[22-24]. The pH at this transition point is known as the pH_{max}. The model cocrystals are thermodynamically stable below pH_{max}, but thermodynamically unstable above it and they have the tendency to transform back to the stable drug form. This transition point allows the true intrinsic dissolution measurements for the cocrystals at pH below the pH_{max}. Among the three

cocrystals, KTZ-FUM has the highest pH_{max} value because it has the lowest K_{sp}, so it requires a higher pH to reach the same solubility as the parent drug[22].

Table 5.1. Physicochemical properties of model cocrystals and their components.

Cocrystal (B-H_2A)	K_{sp} (x 10^{-2} mM^2)[a]	pK_a values		Diffusion coefficient (x 10^{-6} cm^2/sec)[d]	
		B[b]	H_2A[c]	$D_{B_{aq}}$	$D_{HA_{aq}}$
KTZ-FUM	0.15	2.94, 6.51	3.03, 4.38	3.56	8.67
KTZ-SUC	2.4		4.2, 5.6		8.38
KTZ-ADP	3.4		4.44, 5.44		7.07

a) From reference [22];
b) From reference [12];
c) From reference [18];
d) Determined using Othmer Thaker's equation[25].

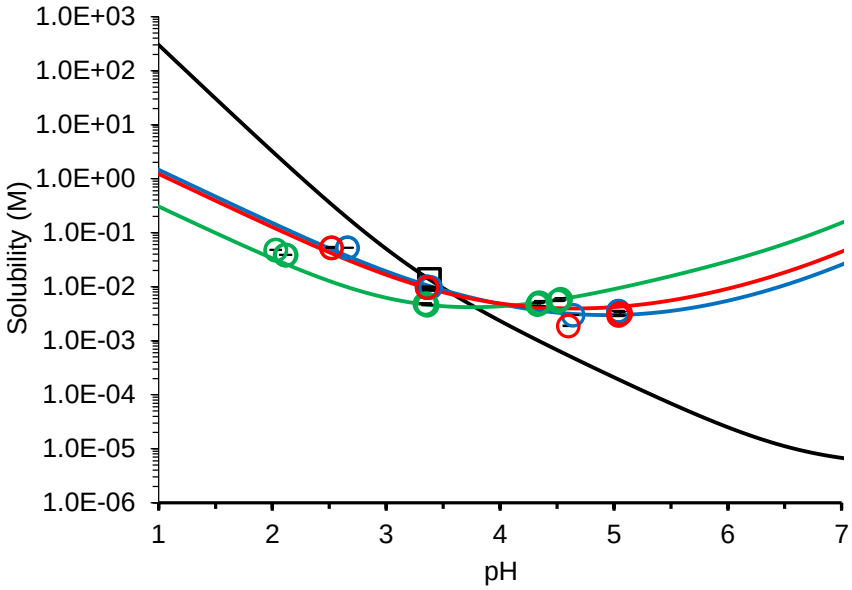

Figure 5.1. Solubility pH dependence of KTZ (—), KTZ-ADP (—), KTZ-SUC (—) and KTZ-FUM (—). pH_{max} value for KTZ-ADP is 3.6; KTZ-SUC is 3.6; and KTZ-FUM is 3.8. Solid lines represent the theoretical predictions and the symbols are the experimental data[22].

Interfacial pH predictions

With the knowledge of physicochemical properties, interfacial pH of KTZ and its three cocrystals can be predicted using equations 5A.20 and 5A.52 respectively from Appendix 5A. The

ability of KTZ in altering the pH microenvironment at the dissolving surface is compared to that of the three cocrystals in Figure 5.2. At low bulk pH, the interfacial pH of KTZ is higher than the bulk solution pH because KTZ is mostly ionized under these conditions and thus increases the pH at the dissolving surface. As bulk pH increases above the pK_a values, the ability of KTZ in increasing interfacial pH is limited by its lower degree of ionization at the dissolving surface. Therefore, interfacial pH is approximately the same as the bulk pH. By cocrystallizing with acidic coformers, all three cocrystals still have the ability to increase the interfacial pH at low bulk pH. However, the increase is much smaller compared to the drug because the ionization of KTZ is being suppressed by the acidic coformers. As bulk pH increases above the pK_a values of the coformers, interfacial pH of the cocrystals is dominated by the acidity of the coformers. The ionization of the coformers lowers the interfacial pH and results in a buffer effect at the dissolving surface, in which the interfacial pH does not change with bulk pH. The interfacial pH at the buffering region for KTZ-FUM is 4.1, KTZ-SUC is 4.7 and KTZ-ADP is 4.8. Even KTZ-FUM has the lowest K_{sp} among three cocrystals, it is still able to buffer the interfacial pH to the lowest because FUM is the most acidic among the three coformers. The interfacial pH at the buffering regions of the three cocrystals is above their pH_{max} values. This means that the cocrystals are thermodynamically unstable in these regions and have the tendency to transform back to the stable drug form during dissolution.

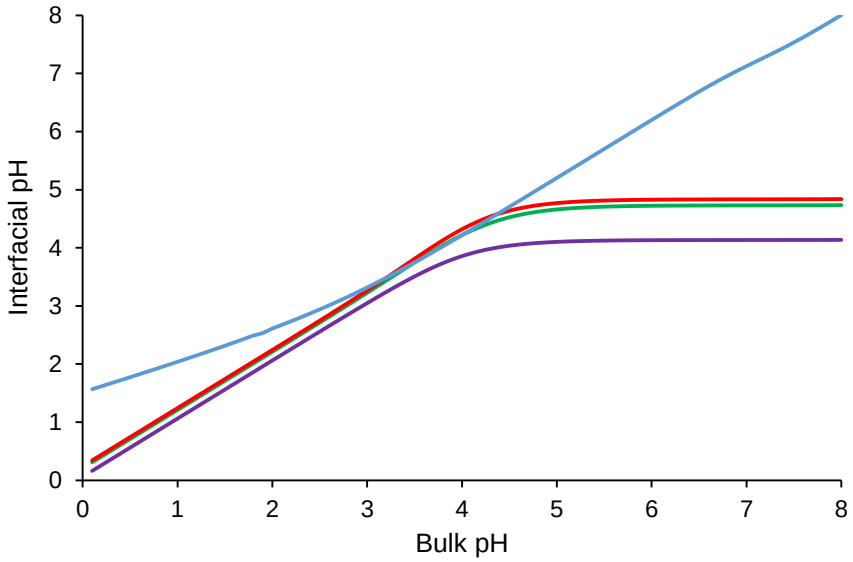

Figure 5.2. Interfacial pH of KTZ (—), KTZ-ADP (—), KTZ-SUC (—) and KTZ-FUM (—) as a function of bulk pH. Interfacial pH of both drug and cocrystals were calculated using equations 5A.20 and 5A.52 from Appendix 5A, respectively, with the physicochemical parameters shown in Table 5.1.

Drug crystallization may happen during the dissolution of highly soluble cocrystals and the crystallization process has a dependence on the degree of supersaturation generated in solution with respect to the parent drug. Knowing the interfacial pH, the degree of supersaturation at the dissolving cocrystal surface during dissolution can be determined from the solubility advantage of the cocrystal, which is a ratio of the cocrystal solubility over that of the drug. The solubility advantages of the three cocrystals as a function of bulk pH were calculated based on the interfacial pH predictions and these are shown in Figure 5.3. At bulk pH $\leq$ 3, all cocrystals do not exhibit solubility advantage as indicated by the ratios of S_{cc}/S_{drug} below 1. Under these bulk pH conditions, the interfacial pH of all cocrystals is below their pH_{max} values, so the drug is more soluble compared to the cocrystals. This means that the cocrystals are the stable forms and the precipitation of solid drug during dissolution should not occur at bulk pH $\leq$ 3. Above bulk pH 3, the S_{cc}/S_{drug} ratios of all three cocrystals are greater than 1, meaning that the cocrystals are more soluble than the parent drug because the interfacial pH is above their pH_{max} values. Under these

bulk pH conditions, all three cocrystals can generate supersaturation with respect to the parent drug in solution and provide the driving force for drug crystallization at the dissolving surface during dissolution. The rate of nucleation is inversely proportional to supersaturation[26], so the probability of drug precipitation during dissolution would increase as the degree of supersaturation increases. Among the three cocrystals, KTZ-ADP has the highest solubility advantage and this can translate into the highest tendency for drug precipitation during dissolution. Drug precipitation at the dissolving surface can impede the dissolution of cocrystal and this can lead to disagreement with the theoretical flux predictions since the mass transport models have not considered the transformation kinetic. The solubility advantage of KTZ-FUM is about 2 at the buffering region, so it may be able to sustain supersaturation during the 30 minute dissolution.

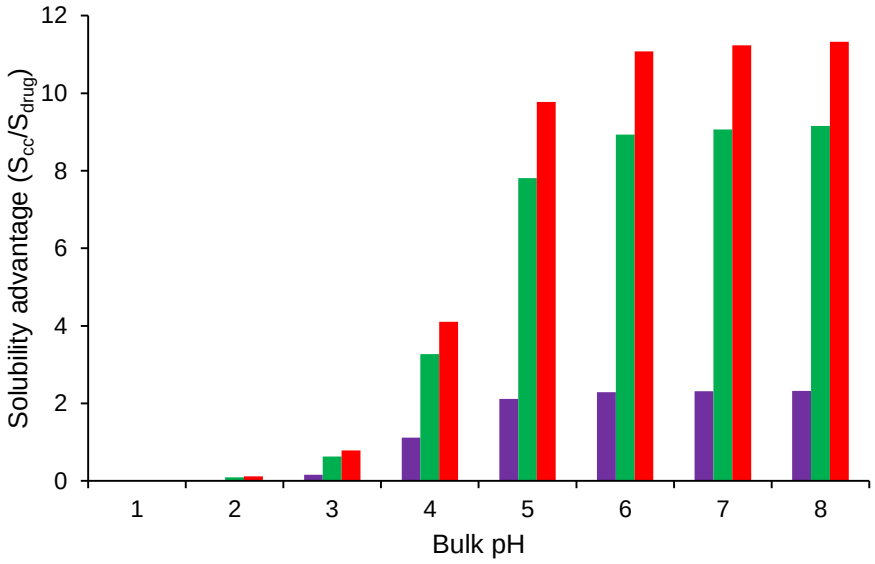

Figure 5.3. Solubility advantage for KTZ-FUM (■), KTZ-SUC (■) and KTZ-ADP (■) as a function of bulk pH. The solubility of the drug and cocrystals were calculated based on the interfacial pH predicted from Figure 5.2 using equation 5.11 and 5.32 respectively.

Effect of pH on KTZ dissolution

The effect of pH on the dissolution of KTZ was evaluated by performing rotating disk dissolution as a function of bulk pH. The dissolution concentration profiles of KTZ as a function of bulk pH are shown in Figure 5.4. Because of the basicity, the dissolution rates of KTZ decrease with increasing pH. KTZ is a poorly water soluble compound with an intrinsic solubility of 4.7 x 10^{-6} M[22], so the dissolution rate is very low when it is at minimal ionization. At bulk pH 4 and 5, the KTZ concentration was not detectable by HPLC until 5 and 10 minutes after dissolution started, respectively. At bulk pH 6, KTZ is almost completely unionized and its concentration could not be detected until 30 minutes after dissolution started. Therefore, the dissolution at bulk pH 6 had to extend to 60 minutes in order to get enough data points to determine the dissolution rate. The large error bars for the dissolution at bulk pH 6 is possibly associated with the low concentration of KTZ.

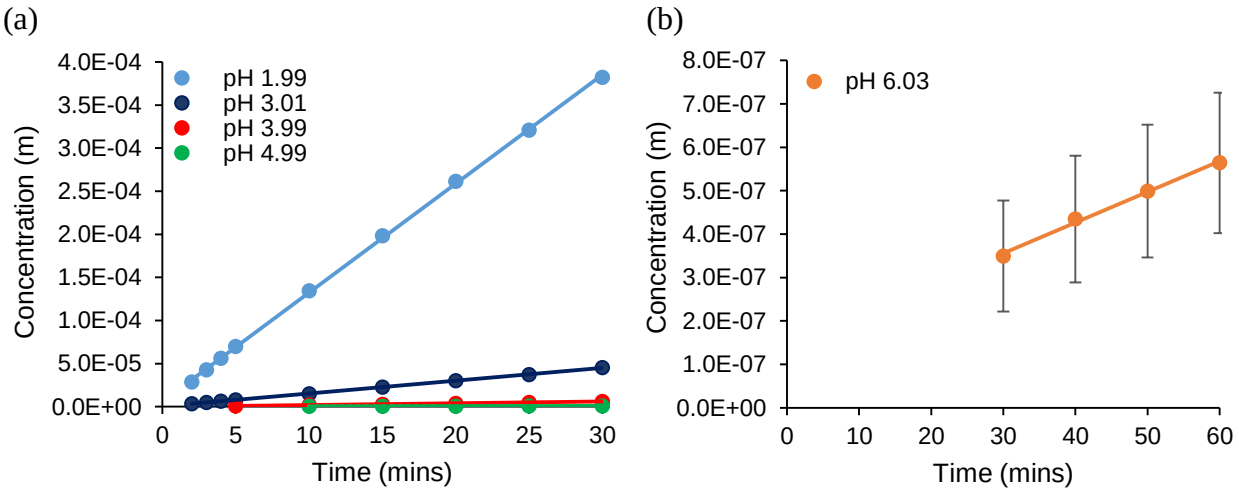

Figure 5.4. Dissolution concentration profiles of KTZ at bulk pH 2 to 5 (a) and bulk pH 6 (b).

The flux of KTZ as a function of bulk pH were calculated from the dissolution rates and compared to the theoretical predictions in Figure 5.5. KTZ is a weakly basic drug, so it does not

have much ability to self-buffer the pH at the dissolving surface. Consequently, the flux of KTZ can vary drastically as a function of bulk pH. There is almost 2000x difference between the flux of KTZ at pH 2 and 6. The large pH effect on the dissolution rate of KTZ may be responsible for its variability in oral absorption observed in patients.

Although there are some deviations in flux predictions for KTZ at low bulk pH, the theoretical values follow the same trend as the experimental data. The large deviations in flux predictions at low bulk pH could be possibly due to the assumption that the diffusion coefficients of the unionized and ionized forms are the same. In multicomponent electrolyte mass transport system, the diffusion of the charged species can be significantly different from the neutral species due to the electrostatic interactions between the diffusing species in order to maintain charge neutrality[27-29]. In general, the fast diffusing ion is coupled with a sluggish ion of opposite charge to counteract the charge separation between the ions[27-29]. In other words, the diffusion of the charged species can be accelerated or retarded by the electrostatic interactions[27-29]. At pH 2 and 3, KTZ is mostly in its ionized form. It is possible that the positively charged KTZ is coupled with the highly mobile hydroxide ion to maintain charge neutrality at the dissolving surface and thus results in faster diffusion compared to the neutral form of KTZ. The diffusion of KTZ under low bulk pH conditions may have been underestimated based on the assumption that the diffusion coefficient of the ionized form is the same as the nonionized form. The underestimation in diffusion coefficient of the ionized form of KTZ could result in deviations of flux predictions under low bulk pH conditions. Since the purpose of this paper is to provide a mechanistic understanding of the dissolution behavior of KTZ under the influence of pH, the diffusion coefficient of the ionized form was not evaluated for accurate flux predictions.

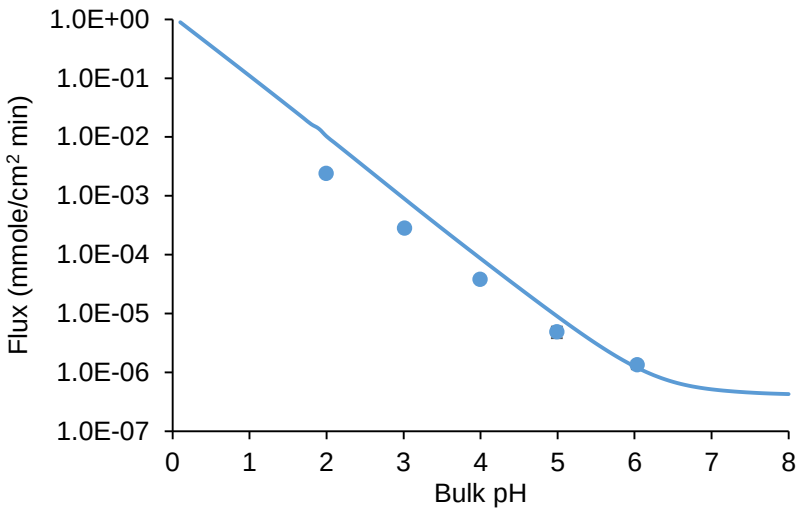

Figure 5.5. Theoretical (—) and experimental (•) flux comparison of KTZ as a function of bulk pH. The flux of KTZ were calculated using equation 5A.23 from Appendix 5A based on the interfacial pH predicted in Figure 5.2 and the physicochemical properties shown in Table 5.1.

Effect of pH on the dissolution of KTZ cocrystals

The pH effect on the dissolution of the three model KTZ cocrystals was also evaluated and the dissolution concentration profiles as a function of bulk pH are shown in Figure 5.6, 5.7 and 5.8 for KTZ-FUM, KTZ-SUC and KTZ-ADP, respectively. It is important to measure the concentration of the coformer during dissolution because it can serve as an indicator for solid phase transformation. If higher coformer concentration is observed for the dissolution of a 1:1 cocrystal, it is likely that the drug is precipitating at the dissolving surface because of its inability in sustaining supersaturation. Without knowing the coformer concentration, it could be difficult to confirm the stability of the cocrystal during dissolution when solid phase analysis, such as XRPD is not sensitive enough to detect the solid phase transformation. Among the three cocrystals, the measurements of both drug and coformer concentrations during dissolution were only possible for KTZ-FUM. For KTZ-SUC and KTZ-ADP, only the drug concentrations were determined because both coformer concentrations were below the detection limit. As shown in Figure 5.6, the coformer

concentrations match those of the drug at all bulk pH conditions studied here, which indicates no solid phase transformation occurred during the dissolution of KTZ-FUM. It seems like KTZ-SUC is also stable at all bulk pH conditions studied here as indicated by the linear dissolution behavior and the pure cocrystal structure from XRPD analysis after dissolution. KTZ-ADP was stable during dissolution at bulk pH 2 and 3 because the interfacial pH at these conditions was below the pH_{max}. Although the XRPD analyses after the dissolution of KTZ-ADP at bulk pH 4 to7 showed pure cocrystal phase, the nonlinear dissolution behavior under these conditions is a sign of solid phase transformation. An example of nonlinear dissolution behavior at bulk pH 6 for KTZ-ADP is demonstrated in Figure 5.7 (b).

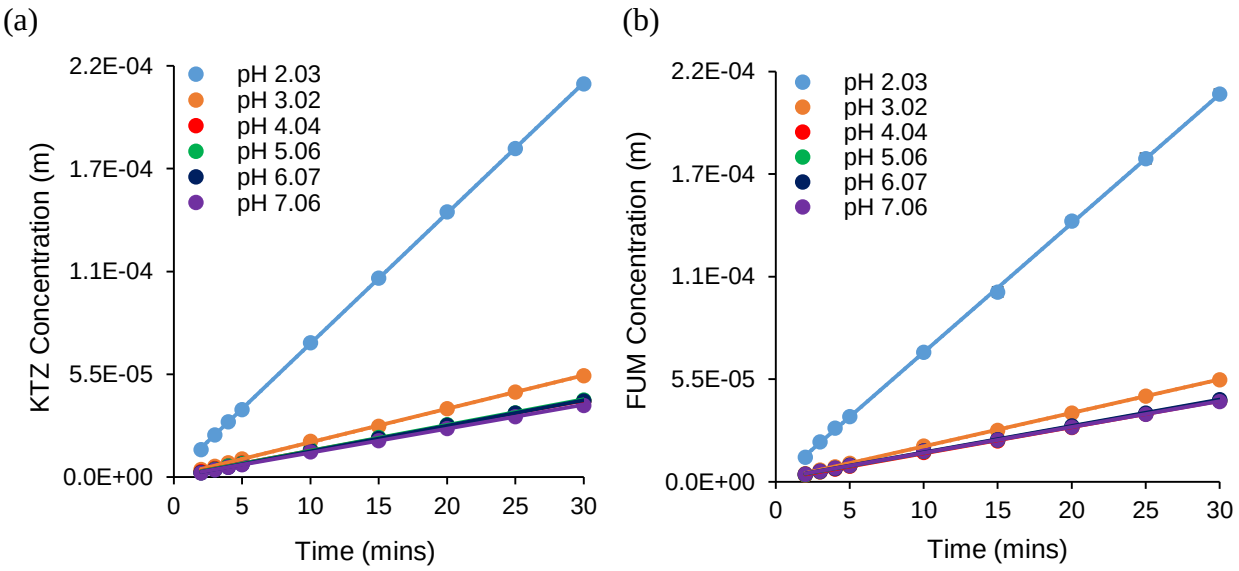

Figure 5.6. Dissolution concentration profiles of KTZ-FUM in terms of KTZ (a) and FUM (b) concentrations as a function of bulk pH.

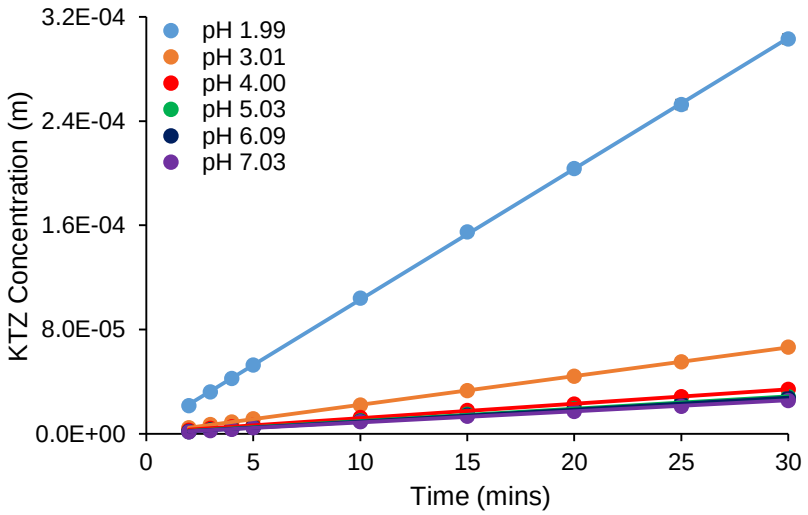

Figure 5.7. Dissolution concentration profiles of KTZ-SUC in terms of KTZ concentrations as a function of bulk pH.

(a) (b)

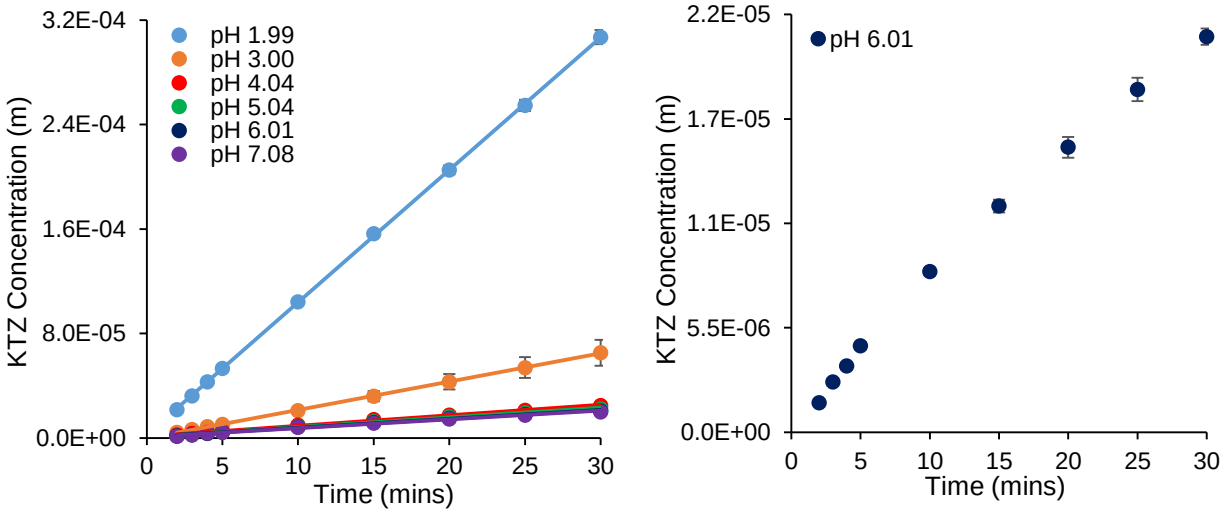

Figure 5.8. Dissolution concentration profiles of KTZ-ADP in terms of KTZ concentrations as a function of bulk pH (a) and the nonlinear dissolution behavior at bulk pH 6 (b).

To evaluate the predictive power of the mass transport model, the flux of the three cocrystals were calculated from the dissolution rates and compared to the theoretical predictions in Figure 5.9. The flux of all three cocrystals decreases with increasing bulk pH and reaches constant values at the buffering region since there is no significant change in interfacial pH. With

the acidic coformers, the flux of cocrystals still decreases with pH at low bulk pH because the pH effect on dissolution is dominated by the basic drug. The coformers take over the pH effect on the dissolution of cocrystals at bulk pH above the acidic pK_a values because the coformers start to ionize, while the drug ionization is suppressed. The acidity of the coformers dampens the pH effect on the dissolution of the cocrystals compared to the parent drug. There is about 5x difference in the flux of KTZ-FUM between pH 2 and 6, 11x for KTZ-SUC and 15x for KTZ-ADP. These differences are significantly smaller compared to the almost 2000x difference for KTZ. This significant reduction in flux variation due to pH can potentially mitigate the pH effect on oral absorption of KTZ.

By modeling interfacial pH, the mass transport model adequately describes the dissolution behavior of cocrystals under the influence of pH. There is an excellent agreement between the theoretical flux predictions and experimental data. As discussed earlier, the cocrystal flux can be over predicted if drug crystallization happened during dissolution. The driving force for solid phase transformation is the highest for KTZ-ADP (S_{cc}/S_{drug} = 11) as shown in Figure 5.3 and it was confirmed that drug precipitation occurred during dissolution at bulk pH 4 to 7. The solid phase transformation of the cocrystal results in deviations of theoretical flux predictions from the experimental data for KTZ-ADP.

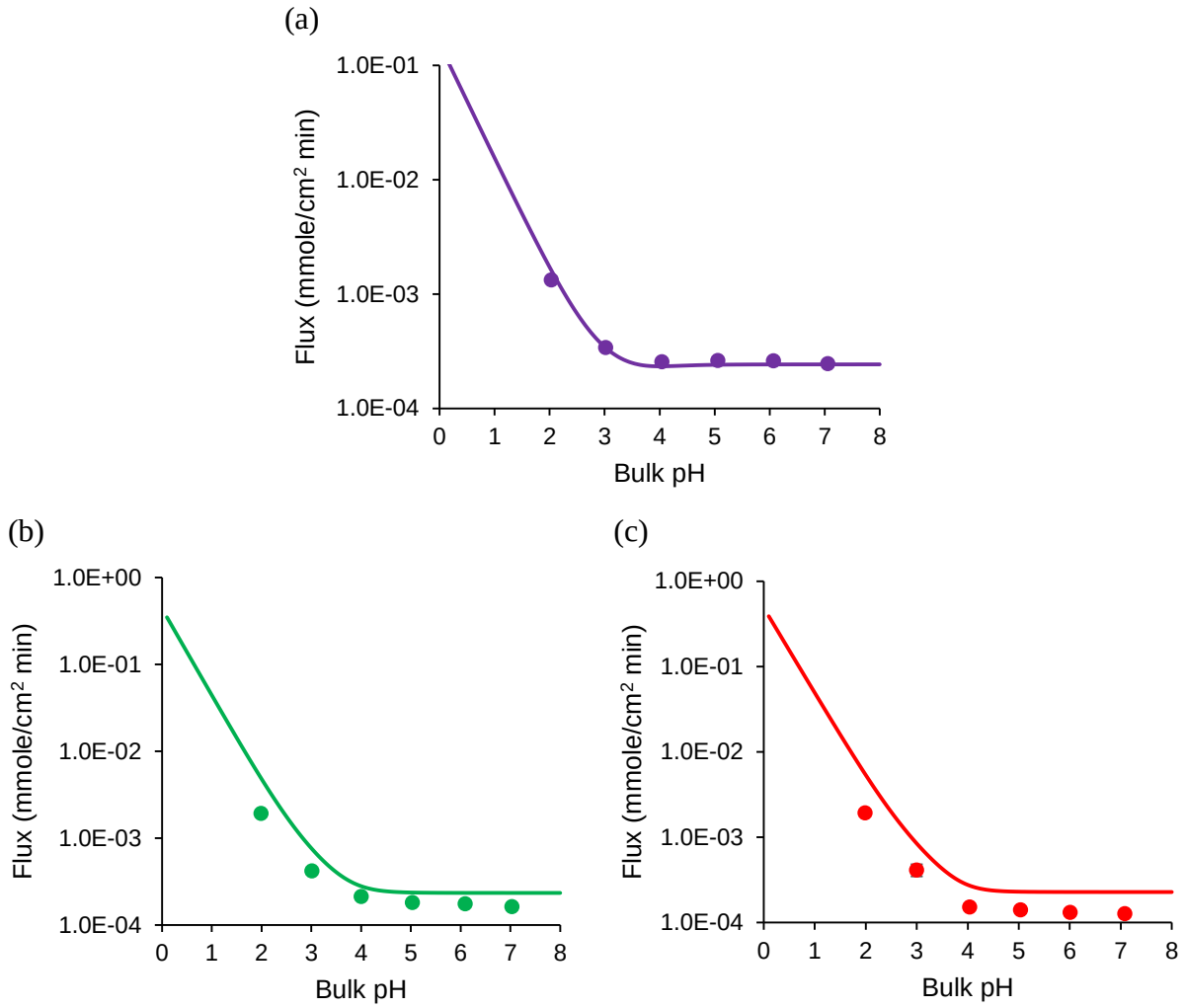

Figure 5.9. Theoretical (solid line) and experimental (solid circle) flux comparison of (a) KTZ-FUM, (b) KTZ-SUC and (c) KTZ-ADP. The theoretical flux of cocrystals were calculated using equation 5A.54 from Appendix 5A based on the interfacial pH predicted in Figure 5.2 and the physicochemical properties shown in Table 5.1.

Comparison of dissolution behavior

The pH effect on the flux of KTZ is compared with KTZ-FUM in Figure 5.10, KTZ-SUC in Figure 5.11 and KTZ-ADP in Figure 5.12. These Figures demonstrate that the dissolution pH dependence of KTZ is significantly reduced by cocrystallizing with acidic coformers. Due to the different pH dependence, there exists a transition pH where the flux of the drug is the same as the cocrystal for each of the three cocrystals. Below this transition pH, interfacial pH is below the

pH_{max}, so the KTZ flux is higher than those of the cocrystals. Above the transition pH, interfacial pH is above the pH_{max} and resulting in higher cocrystal flux compared to KTZ. This transition pH is different from the pH_{max} in a way that it is determined from the kinetic process. Consequently, it cannot be used to evaluate the thermodynamic stability of the cocrystals. However, it is still important because it provides the solution conditions at which the cocrystals would display dissolution advantages. The dissolution advantage of cocrystal is defined as the ratio of the cocrystal flux over that of the drug (J_{cc}/J_{drug}). Cocrystal has no dissolution advantage if $J_{cc}/J_{drug} \leq 1$, but it would display dissolution advantage if $J_{cc}/J_{drug} > 1$. The dissolution advantages of the three cocrystals were evaluated from the experimental data and shown in Figure 5.10 to 5.12 for the three cocrystals. At bulk pH 2, the dissolution advantages of all three cocrystals are below one because the pH is below the transition pH. At bulk pH 3, near the transition pH, all three cocrystals exhibit nearly the same flux as the drug. Above bulk pH 3, all cocrystals display dissolution advantages and these advantages increase with increasing pH because the flux of KTZ decrease with pH. Among the three cocrystals, KTZ-FUM has the highest dissolution advantage, follows by KTZ-SUC and KTZ-ADP.

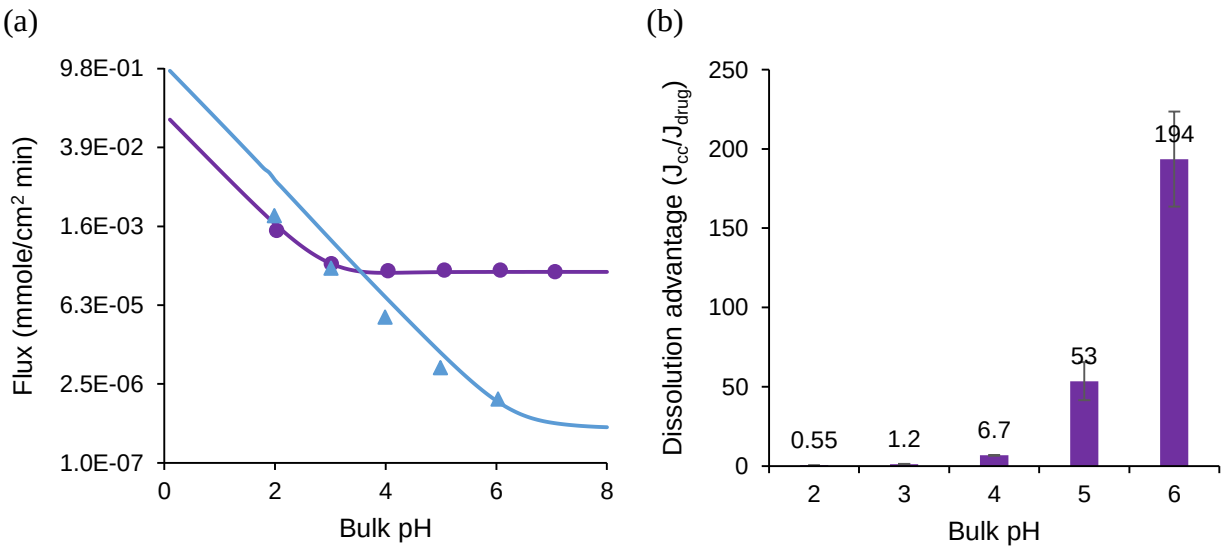

Figure 5.10. (a) Flux comparison between KTZ-FUM (—) and KTZ (—) as a function of bulk pH. (b) Dissolution advantages of KTZ-FUM determined from the experimental flux values. The solid lines represent the theoretical flux predictions and the symbols represent the experimental flux for KTZ-FUM (●) and KTZ (▲).

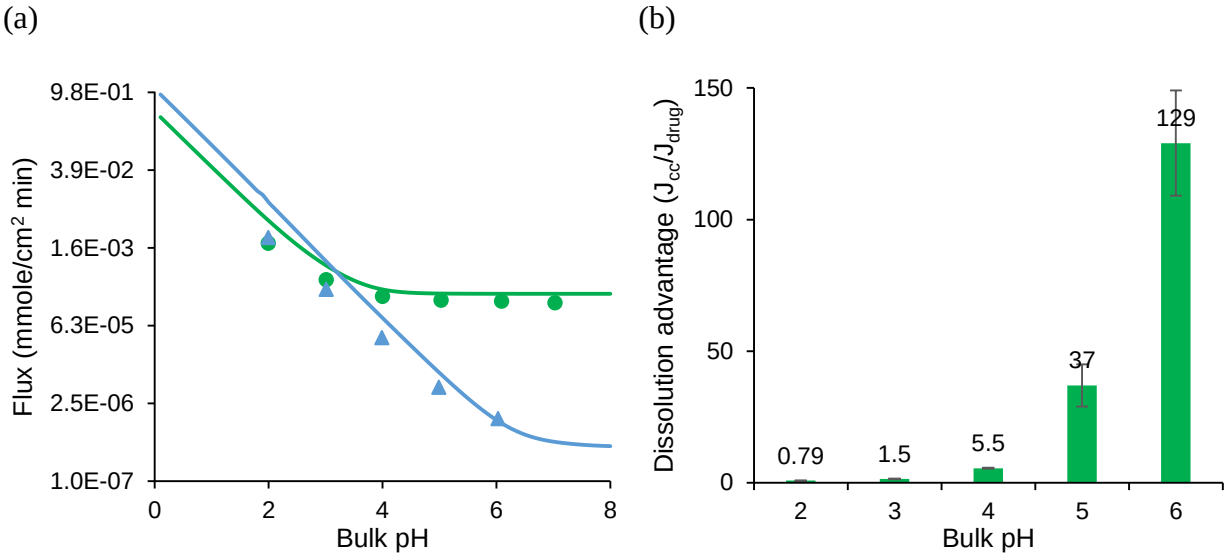

Figure 5.11. (a) Flux comparison between KTZ-SUC (—) and KTZ (—) as a function of bulk pH. (b) Dissolution advantages of KTZ-SUC determined from the experimental flux values. The solid lines represent the theoretical flux predictions and the symbols represent the experimental flux for KTZ-SUC (●) and KTZ (▲).

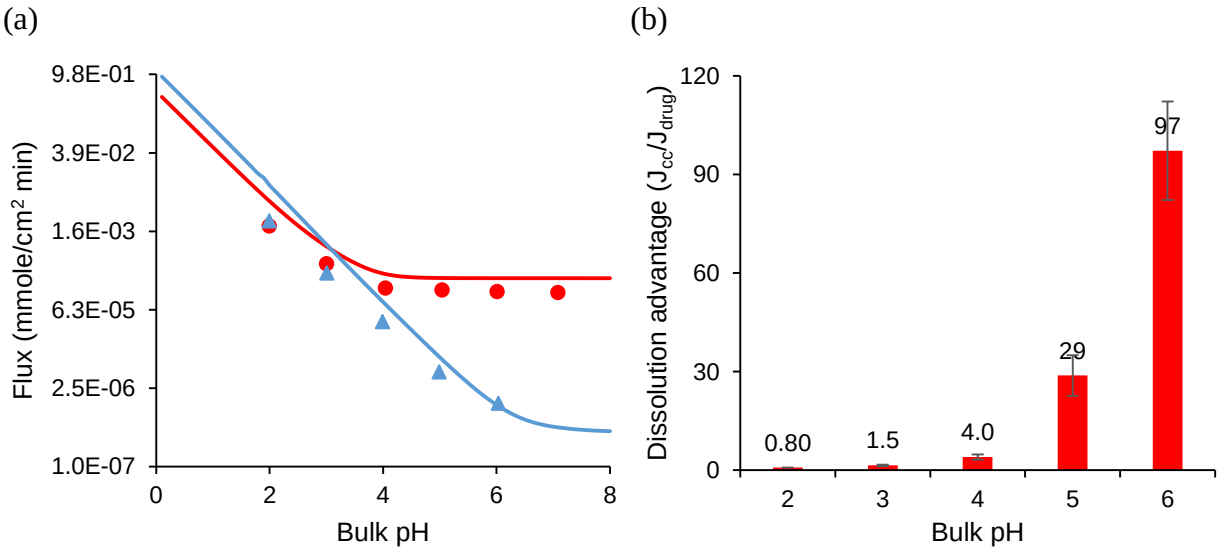

Figure 5.12. (a) Flux comparison between KTZ-ADP (—) and KTZ (—) as a function of bulk pH. (b) Dissolution advantage of KTZ-ADP determined from the experimental flux values. The

solid lines represent the theoretical flux predictions and the symbols represent the experimental flux for KTZ-ADP (●) and KTZ (▲).

Discussion

The selection of a solid form with optimal physicochemical properties that can lead to desired bioperformance is essential for successful oral drug product development. Solubility and dissolution are important parameters for determining the bioavailability of drugs that are given orally[9]. Hence, the solubility and dissolution advantages of cocrystals are important parameters to be considered during the cocrystal selection process. The advantage in diverse formation of cocrystals can become a challenge when it comes to the selection process. Depending on the properties of the coformers and solution conditions, cocrystals can behave very different in solution[30]. Cocrystals can generate solubility that are orders of magnitude different from that of the parent drug[30]. One of the important questions needs to be addressed during the selection process is what the most desired cocrystal solubility should be. Usually, higher cocrystal solubility would not necessarily lead to better performance because it is more prone for conversion during dissolution. The ideal candidate would be a cocrystal with a solubility advantage that allows supersaturation to be sustained in solution. Understanding the solution behavior of cocrystals would help to rationalize the selection process.

The three cocrystals studied in this work demonstrated different ability in modulating the dissolution behavior of the parent drug and this ability is dependent on the properties of the coformers and cocrystals. The ionization properties of the coformers allow the cocrystals to alter the interfacial pH to different extents compared to the parent drug. The ability of modeling interfacial pH allows the evaluation of cocrystal solubility advantage at the dissolving surface, which provides useful information regarding the thermodynamic stability of the cocrystals during

dissolution. Among the three cocrystals, KTZ-FUM is the most stable because the solubility advantage at the buffering region is 2, while KTZ-SUC is 9 and KTZ-ADP is 11. Although KTZ-FUM has the smallest solubility advantage, it is able to achieve the highest dissolution advantage. With high dissolution advantage and low risk of conversion, it is no doubt that KTZ-FUM is the favor cocrystal for further development at this stage. This work has mainly considered the pH effect on the dissolution of cocrystals, however, other factors, such as solubilizing agents should also be considered for the selection process.

Conclusions

The dissolution mechanism for 1:1 cocrystals with dibasic drug (KTZ) and diacidic coformers (FUM, SUC, ADP) under the influence of pH has been analyzed and compared to the parent drug through the development and evaluation of physically realistic mass transport models. The mass transport analyses for the dissolution of cocrystals are based on the previously developed surface saturation model. The mass transport models show that the pH at the dissolving cocrystal surface is different from that of the parent drug because of the ability of the coformers in lowering the interfacial pH. The dissolution behavior of both drug and cocrystals has been theoretically and experimentally demonstrated to be dependent on interfacial pH instead of bulk pH. This highlights the importance of modeling the almost experimentally inaccessible interfacial pH. The dissolution of KTZ has been shown to exhibit large pH effect, however, this pH effect is significantly reduced by cocrystallizing with acidic coformers. Because of the different pH dependence, there exists a transition pH that can serve as a turning point for the cocrystal dissolution advantage. Cocrystals can modulate the dissolution behavior of the parent drug by altering both interfacial pH and solubility. Having a thorough understanding on the thermodynamic and kinetic behavior of cocrystals can help to select the most suitable cocrystal for further development.

References

1. Weyna, D. R.; Cheney, M. L.; Shan, N.; Hanna, M.; Zaworotko, M. J.; Sava, V.; Song, S.; Sanchez-Ramos, J. R. Improving Solubility and Pharmacokinetics of Meloxicam via Multiple-Component Crystal Formation. *Molecular Pharmaceutics* **2012,** *9*, 2094-2102.

2. Childs, S. L.; Kandi, P.; Lingireddy, S. R. Formulation of a Danazol Cocrystal with Controlled Supersaturation Plays an Essential Role in Improving Bioavailability. *Molecular Pharmaceutics* **2013,** *10*, (8), 3112-3127.

3. McNamara, D. P.; Childs, S. L.; Giordano, J.; Iarriccio, A.; Cassidy, J.; Shet, M. S.; Mannion, R.; O'Donnell, E.; Park, A. Use of a glutaric acid cocrystal to improve oral bioavailability of a low solubility API. *Pharmaceutical Research* **2006,** *23*, (8), 1888-1897.

4. Smith, A. J.; Kavuru, P.; Wojtas, L.; Zaworotko, M. J.; Shytle, R. D. Cocrystals of Quercetin with Improved Solubility and Oral Bioavailability. *Molecular Pharmaceutics* **2011,** *8*, (5), 1867-1876.

5. Bak, A.; Gore, A.; Yanez, E.; Stanton, M.; Tufekcic, S.; Syed, R.; Akrami, A.; Rose, M.; Surapaneni, S.; Bostick, T.; King, A.; Neervannan, S.; Ostovic, D.; Koparkar, A. The Co-crystal Approach to Improve the Exposure of a Water-insoluble Compound: AMG 517 Sorbic Acid Co-crystal Characterization and Pharmacokinetics. *Journal of Pharmaceutical Sciences* **2008,** *97*, (9), 3942-3956.

6. Schultheiss, N.; Newman, A. Pharmaceutical Cocrystals and Their Physicochemical Properties. *Crystal Growth & Design* **2009,** *9*, (6), 2950-2967.

7. Thakuria, R.; Delori, A.; Jones, W.; Lipert, M. P.; Roy, L.; Rodriguez-Hornedo, N. Pharmaceutical Cocrystals and Poorly Soluble Drugs. *International Journal of Pharmaceutics* **2013,** *453*, (1), 101-125.

8. Williams, H. D.; Trevaskis, N. L.; Charman, S. A.; Shanker, R. M.; Charman, W. N.; Pouton, C. W.; Porter, C. J. H. Strategies to Address Low Drug Solubility in Discovery and Development. *Pharmacological Review* **2013,** *65*, 315-499.

9. Amidon, G. L.; Lennernas, H.; Shah, V. P.; Crison, J. R. A Theoretical Basis for a Biopharmaceutic Drug Classification: The Correlation of *in Vitro* Drug Product Dissolution and *in Vivo* Bioavailability. *Pharmaceutical Research* **1995,** *12*, (3), 413-420.

10. Cao, F.; Amidon, G.; Rodriguez-Hornedo, N.; Amidon, G. Mechanistic Analysis of Cocrystal Dissolution as a Function of pH and Micellar Solubilization. *Molecular Pharmaceutics* **2015,** *13*, (3), 1030-1046.

11. Chin, T. W. F.; Loeb, M.; Fong, I. W. Effects of an Acidic Beverage (Coca-Cola) on Absorption of Ketoconazole. *Antimicrobial Agents and Chemotherapy* **1995,** *39*, (8), 1671-1675.

12. Assessment Report Ketoconazole HRA. Agency, E. M., Ed. 2014.

13. Zhou, R.; Moench, P.; Heran, C.; Lu, X.; Mathias, N.; Faria, T. N.; Wall, D. A.; Hussain, M. A.; Smith, R. L.; Sun, D. pH-Dependent Dissolution *in Vitro* and Absorption *in Vivo* of Weakly Basic Drugs: Development of a Canine Model. *Pharmaceutical Research* **2005,** *22*, (2), 188-192.

14. Carlson, J. A.; Mann, H. J.; Canafax, D. M. Effect of pH on Disintegration and Dissolution of Ketoconazole Tablets. *American Journal of Health System Pharmacy* **1983,** *40*, (8), 1334-1336.

15. Piscitelli, S. C.; Goss, T. F.; Wilton, J. H.; D'Andrea, D. T.; Goldstein, H.; Schentag, J. J. Effects of Ranitidine and Sucralfate on Ketoconazole Bioavailability. *Antimicro Agents Chemother* **1991,** *35*, (9), 1765-1771.

16. Lelawongs, P.; Barone, J. A.; Colaizzi, J. L.; Hsuan, A. T.; Mechlinski, W.; Legendre, R.; Guarnieri, J. Effect of Food and Gastric Acidity on Absorption of Orally Administered Ketoconazole. *Clin Pharm* **1988,** *7*, (3), 228-35.

17. Blum, R. A.; D'Andrea, D. T.; Florentino, B. M.; Wilton, J. H.; Hilligoss, D. M.; Gardner, M. J.; Henry, E. B.; Goldstein, H.; Schentag, J. J. Increased Gastric pH and the Bioavailability of Fluconazole and Ketoconazole. *Annals of Internal Medicine* **1991,** *114*, (9), 755-757.

18. Martin, F. A.; Pop, M. M.; Borodi, G.; Filip, X.; Kacso, I. Ketoconazole Salt and Co-crystals with Enhanced Aqueous Solubility. *Crystal Growth & Design* **2013,** *13*, (10), 4295-4304.

19. Rodriguez-Hornedo, N.; Nehm, S. J.; Seefeldt, K. F.; Pagan-Torres, Y.; Falkiewicz, C. J. Reaction Crystallization of Pharmaceutical Molecular Complexes. *Molecular Pharmaceutics* **2006,** *3*, (3), 362-367.

20. Nernst, W. Theorie der Reaktionsgeschwindigkeit in heterogenen systemen. *Zeitschrift für Physikalische Chemie* **1904,** *47*, 52-55.

21. Mooney, K. G.; Mintun, M. A.; Himmelstein, K. J.; Stella, V. J. Dissolution Kinetics of Carboxylic Acids I: Effect of pH under Unbuffered Conditions. *American Pharmaceutical Association* **1981,** *70*, (1), 13-22.

22. Chen, Y.; Rodriguez-Hornedo, N., Solubility, pH_{max} and Dissolution of Ketoconazole Cocrystals in Aqueous Media. In *AAPS Poster Presentation (M1208)*, Orlando, Florida, 2015.

23. Bethune, S. J.; Huang, N.; Jayasankar, A.; Rodriguez-Hornedo, N. Understanding and Predicting the Effect of Cocrystal Components and pH on Cocrystal Solubility. *Crystal Growth and Design* **2009,** *9*, (9), 3976-3988.

24. Maheshwari, C.; Andre, V.; Reddy, S.; Roy, L.; Duarte, T.; Rodrigez-Hornedo, N. Tailoring aqueous solubility of a highly soluble compound via cocrystallization: effect of coformer ionization, pH(max) and solute-solvent interactions. *Crystengcomm* **2012,** *14*, (14), 4801-4811.

25. Othmer, D. F.; Thakar, M. S. Correlating Diffusion Coefficients in Liquids. *Industrial and Engineering Chemistry* **1953,** *45*, (3), 589-593.

26. Rodriguez-Hornedo, N.; Murphy, D. Significance of Controlling Crystallization Mechanisms and Kinetics in Pharmaceutical Systems. *Journal of Pharmaceutical Sciences* **1999,** *88*, (7), 651-660.

27. Avdeef, A.; Voloboy, D.; Foreman, A., 5.17 - Dissolution and Solubility. In *Comprehensive Medicinal Chemistry II*, Triggle, J. B. T. J., Ed. Elsevier: Oxford, 2007; pp 399-423.

28. Cussler, E. L., *Diffusion Mass Transfer in Fluid Systems*. 2nd ed.; Cambridge University Press: New York, 1997.

29. Rasouli, P.; Steefel, C. I.; Mayer, K. U.; Rolle, M. Benchmarks for Multicomponent Diffusion and Electrochemical Migration. *Computational Geosciences* **2015,** *19*, (3), 523-533.

30. Kuminek, G.; Cao, F.; Rocha, A. B. d. O. d.; Cardoso, S. G.; Rodriguez-Hornedo, N. Cocrystals to Facilitate Delivery of Poorly Soluble Compounds Beyond-Rule-of-5. *Advanced Drug Delivery Reviews* **2016,** *Manuscript under review.*

APPENDIX 5A

Mass transport analysis for drug

The flux of all the species across the diffusion layer include both the diffusion and chemical reactions happening during dissolution. At steady state, the diffusion and simultaneous chemical reactions of the individual species within the diffusion layer can be written using Fick's law as follows:

$$\frac{\partial[B]}{\partial t} = D_B \frac{\partial^2[B]}{\partial x^2} + \phi_1 = 0 \quad (5A.1)$$

$$\frac{\partial[BH^+]}{\partial t} = D_B \frac{\partial^2[BH^+]}{\partial x^2} + \phi_2 = 0 \quad (5A.2)$$

$$\frac{\partial[BH_2^{2+}]}{\partial t} = D_B \frac{\partial^2[BH_2^{2+}]}{\partial x^2} + \phi_3 = 0 \quad (5A.3)$$

$$\frac{\partial[OH^-]}{\partial t} = D_{OH^-} \frac{\partial^2[OH^-]}{\partial x^2} + \phi_4 = 0 \quad (5A.4)$$

$$\frac{\partial[H^+]}{\partial t} = D_{H^+} \frac{\partial^2[H^+]}{\partial x^2} + \phi_5 = 0 \quad (5A.5)$$

where $\phi_{1\text{-}5}$ are the reaction rate functions. At equilibrium, the reaction rate of the reactant should be the opposite of the product:

$$\phi_3 = -\phi_1 - \phi_2 \quad (5A.6)$$

The reaction rate of the acid and the base should be the same:

$$\phi_3 + \phi_5 = \phi_1 + \phi_4 \quad (5A.7)$$

Based on equations 5A.6 and 5A.7, the following mass balance equations can be written:

$$D_B \frac{d^2[B]}{dx^2} + D_B \frac{d^2[BH^+]}{dx^2} + D_B \frac{d^2[BH_2^{2+}]}{dx^2} = 0 \quad (5A.8)$$

$$D_{OH^-} \frac{d^2[OH^-]}{dx^2} + D_B \frac{d^2[B]}{dx^2} = D_{H^+} \frac{d^2[H^+]}{dx^2} + D_B \frac{d^2[BH_2^{2+}]}{dx^2} \quad (5A.9)$$

Integrating equations 5A.8 and 5A.9 once, gives:

$$D_B \frac{d[B]}{dx} + D_B \frac{d[BH^+]}{dx} + D_B \frac{d[BH_2^{2+}]}{dx} = C_1 \quad (5A.10)$$

$$D_{OH^-} \frac{d[OH^-]}{dx} + D_B \frac{d[B]}{dx} = D_{H^+} \frac{d[H^+]}{dx} + D_B \frac{d[BH_2^{2+}]}{dx} + C_2 \quad (5A.11)$$

By charge neutrality:

$$D_{OH^-} \frac{d[OH^-]}{dx} = D_{H^+} \frac{d[H^+]}{dx} + D_B \frac{d[BH^+]}{dx} + 2D_B \frac{d[BH_2^{2+}]}{dx} \quad (5A.12)$$

By combining equation 5A.10, 5A.11 and 5A.12, it can be shown that:

$$C_1 = -C_2 \quad (5A.13)$$

Integrating equations 5A.10 and 5A.11,

$$D_B[B] + D_B[BH^+] + D_B[\,BH_2^{2+}] = C_1 x + C_3 \quad (5A.14)$$

$$D_{OH^-}[OH^-] + D_B[B] = D_{H^+}[H^+] + D_B[\,BH_2^{2+}] + C_2 x + C_4 \quad (5A.15)$$

Boundary conditions:

At $x = 0$:

$[B] = [B]_0$ (intrinsic solubility of the drug)

$[BH^+] = unknown$

At $x = h$:

$[B] = 0$ (sink condition)

$[BH^+] = 0$ (sink condition)

$[\,BH_2^{2+}] = unknown$ $[\,BH_2^{2+}] = 0$ (sink condition)

$[H^+] = [H^+]_0$ $[H^+] = [H^+]_h$

$[OH^-] = [OH^-]_0$ $[OH^-] = [OH^-]_h$

Evaluation of interfacial pH

Applying the above boundary conditions to equations 5A.14 and 5A.15, at *x = 0*:

$$D_B[B]_0 + D_B[BH^+] + D_B[\,BH_2^{2+}] = C_3 \quad (5A.16)$$

$$D_{OH^-}[OH^-]_0 + D_B[B]_0 = D_{H^+}[H^+]_0 + D_B[\,BH_2^{2+}] + C_4 \quad (5A.17)$$

and at *x = h*, assuming sink conditions, equations 5A.14 and 5A.15 can be written as:

$$0 = C_1 h + C_3 \quad (5A.18)$$

$$D_{OH^-}[OH^-]_h = D_{H^+}[H^+]_h + C_2 h + C_4 \quad (5A.19)$$

Combining equations 5A.16 to 5A.19 and algebraically solving for interfacial pH, $[H^+]_0$, yields the following equation:

$$2D_B \frac{[B]_0}{K_{a1}^B K_{a2}^B}[H^+]_0{}^3 + \left(D_{H^+} + D_B \frac{[B]_0}{K_{a2}^B}\right)[H^+]_0{}^2 + (D_{OH^-}[OH^-]_h - D_{H^+}[H^+]_h)[H^+]_0 -$$

$$D_{OH^-}K_w = 0 \quad (5A.20)$$

Evaluation of flux

Combine equations 5A.16 and 5A.18, and solve for $-C_1$ for the total flux of the drug species across the diffusion layer:

$$J_B = \frac{D_B}{h}[B]_0 \left(1 + \frac{[H^+]_0}{K_{a2}^B} + \frac{[H^+]_0{}^2}{K_{a1}^B K_{a2}^B}\right) \quad (5A.21)$$

For rotating disk, the thickness of the hydrodynamic boundary layer can be defined according to Levich model[21]:

$$h = 1.612 D^{\frac{1}{3}} v^{\frac{1}{6}} \omega^{-\frac{1}{2}} \tag{5A.22}$$

where v is the kinematic viscosity and ω is the angular velocity in radians per unit time. Substitute equation 5A.22 into 5A.21, the flux of the drug becomes:

$$J_B = 0.62 D_B^{2/3} \omega^{1/2} v^{-1/6} [B]_0 \left(1 + \frac{[H^+]_0}{K_{a2}^B} + \frac{{[H^+]_0}^2}{K_{a1}^B K_{a2}^B}\right) \tag{5A.23}$$

Mass transport analysis for cocrystal

The flux of all the species across the diffusion layer include both the diffusion and chemical reactions happening during dissolution. At steady state, the diffusion and simultaneous chemical reactions of the individual species within the diffusion layer can be written using Fick's law as follows:

$$\frac{\partial [B]}{\partial t} = D_B \frac{\partial^2 [B]}{\partial x^2} + \phi_1 = 0 \tag{5A.24}$$

$$\frac{\partial [BH^+]}{\partial t} = D_B \frac{\partial^2 [BH^+]}{\partial x^2} + \phi_2 = 0 \tag{5A.25}$$

$$\frac{\partial [BH_2^{2+}]}{\partial t} = D_B \frac{\partial^2 [BH_2^{2+}]}{\partial x^2} + \phi_3 = 0 \tag{5A.26}$$

$$\frac{\partial [OH^-]}{\partial t} = D_{OH^-} \frac{\partial^2 [OH^-]}{\partial x^2} + \phi_4 = 0 \tag{5A.27}$$

$$\frac{\partial [H^+]}{\partial t} = D_{H^+} \frac{\partial^2 [H^+]}{\partial x^2} + \phi_5 = 0 \tag{5A.28}$$

$$\frac{\partial [H_2A]}{\partial t} = D_{H_2A} \frac{\partial^2 [H_2A]}{\partial x^2} + \phi_6 = 0 \tag{5A.29}$$

$$\frac{\partial[HA^-]}{\partial t} = D_{H_2A}\frac{\partial^2[HA^-]}{\partial x^2} + \phi_7 = 0 \quad (5A.30)$$

$$\frac{\partial[A^{2-}]}{\partial t} = D_{H_2A}\frac{\partial^2[A^{2-}]}{\partial x^2} + \phi_8 = 0 \quad (5A.31)$$

At equilibrium, the reaction rate of the reactant should be the opposite of the product. Based on the chemical equilibria, the followings can be written:

$$\phi_3 = -\phi_1 - \phi_2 \quad (5A.32)$$

$$\phi_6 = -\phi_7 - \phi_8 \quad (5A.33)$$

The reaction rate of the acid and the base should be the same:

$$\phi_3 + \phi_5 + \phi_6 = \phi_1 + \phi_4 + \phi_8 \quad (5A.34)$$

Based on equations 5A.32, 5A.33 and 5A.34, the following mass balance equations can be written:

$$D_B\frac{d^2[B]}{dx^2} + D_B\frac{d^2[BH^+]}{dx^2} + D_B\frac{d^2[BH_2^{2+}]}{dx^2} = 0 \quad (5A.35)$$

$$D_{H_2A}\frac{d^2[H_2A]}{dx^2} + D_{H_2A}\frac{d^2[HA^-]}{dx^2} + D_{H_2A}\frac{d^2[A^{2-}]}{dx^2} = 0 \quad (5A.36)$$

$$D_{OH^-}\frac{d^2[OH^-]}{dx^2} + D_B\frac{d^2[B]}{dx^2} + D_{H_2A}\frac{d^2[A^{2-}]}{dx^2} = D_{H^+}\frac{d^2[H^+]}{dx^2} + D_B\frac{d^2[BH_2^{2+}]}{dx^2}D_{H_2A}\frac{d^2[H_2A]}{dx^2} \quad (5A.37)$$

Integrate equations 5A.35 to 5A.37 once, gives:

$$D_B\frac{d[B]}{dx} + D_B\frac{d[BH^+]}{dx} + D_B\frac{d[BH_2^{2+}]}{dx} = C_1 \quad (5A.38)$$

$$D_{H_2A}\frac{d[H_2A]}{dx} + D_{H_2A}\frac{d[HA^-]}{dx} + D_{H_2A}\frac{d[A^{2-}]}{dx} = C_2 \quad (5A.39)$$

$$D_{OH^-}\frac{d[OH^-]}{dx} + D_B\frac{d[B]}{dx} + D_{H_2A}\frac{d[A^{2-}]}{dx} = D_{H^+}\frac{d[H^+]}{dx} + D_B\frac{d[BH_2^{2+}]}{dx} + D_{H_2A}\frac{d[H_2A]}{dx} + C_3 \quad (5A.40)$$

By charge neutrality:

$$D_{OH^-}\frac{d[OH^-]}{dx}+D_{H_2A}\frac{d[HA^-]}{dx}+2D_{H_2A}\frac{d[\,A^{2-}]}{dx}=D_{H^+}\frac{d[H^+]}{dx}+D_B\frac{d[BH^+]}{dx}+2D_B\frac{d[BH_2^{2+}]}{dx} \quad (5A.41)$$

By combining equations 5A.38 to 5A.41, it can be shown that:

$$C_3=C_2-C_1 \quad (5A.42)$$

Integrating equations 5A.38 to 5A.40, gives:

$$D_B[B]+D_B[BH^+]+D_B[\,BH_2^{2+}]=C_1x+C_4 \quad (5A.43)$$

$$D_{H_2A}[H_2A]+D_{H_2A}[HA^-]+D_{H_2A}[\,A^{2-}]=C_2x+C_5 \quad (5A.44)$$

$$D_{OH^-}[OH^-]+D_B[B]+D_{H_2A}[\,A^{2-}]=D_{H^+}[H^+]+D_B[\,BH_2^{2+}]+D_{H_2A}[H_2A]+C_3x+C_6 \quad (5A.45)$$

Based on equations 5.33 and 5.34, the concentrations of the nonionized drug and coformer at the dissolving surface can be written to include in the following boundary conditions:

At $x = 0$:	at $x = h$:
$[\mathrm{B}]=\frac{\sqrt{K_{sp}(1+\frac{K_{a1}^{H_2A}}{[H^+]_0}+\frac{K_{a1}^{H_2A}K_{a2}^{H_2A}}{[H^+]_0{}^2})(1+\frac{[H^+]_0}{K_{a2}^{B}}+\frac{[H^+]_0{}^2}{K_{a1}^{B}K_{a2}^{B}})}}{(1+\frac{[H^+]_0}{K_{a2}^{B}}+\frac{[H^+]_0{}^2}{K_{a1}^{B}K_{a2}^{B}})}$	$[\mathrm{B}]=0$ (sink condition)
$[H_2A]=(\frac{D_B}{D_{H_2A}})^{2/3}\frac{\sqrt{K_{sp}(1+\frac{K_{a1}^{H_2A}}{[H^+]_0}+\frac{K_{a1}^{H_2A}K_{a2}^{H_2A}}{[H^+]_0{}^2})(1+\frac{[H^+]_0}{K_{a2}^{B}}+\frac{[H^+]_0{}^2}{K_{a1}^{B}K_{a2}^{B}})}}{(1+\frac{K_{a1}^{H_2A}}{[H^+]_0}+\frac{K_{a1}^{H_2A}K_{a2}^{H_2A}}{[H^+]_0{}^2})}$	$[H_2A]=0$ (sink condition)
$[BH^+]=unknown$	$[BH^+]=0$ (sink condition)
$[BH_2{}^{2+}]=unknown$	$[BH_2{}^{2+}]=0$ (sink condition)
$[HA^-]=unknown$	$[HA^-]=0$ (sink condition)

$[A^{2-}] = unknown$ $[A^{2-}] = 0$ (sink condition)

$[H^+] = [H^+]_0$ $[H^+] = [H^+]_h$

$[OH^-] = [OH^-]_0$ $[OH^-] = [OH^-]_h$

Evaluation of interfacial pH

Applying the above boundary conditions to equations 5A.43 to 5A.45, at *x = 0*:

$$D_B \frac{\sqrt{K_{sp}(1+\frac{K_{a1}^{H_2A}}{[H^+]_0}+\frac{K_{a1}^{H_2A}K_{a2}^{H_2A}}{[H^+]_0^{\,2}})(1+\frac{[H^+]_0}{K_{a2}^B}+\frac{[H^+]_0^{\,2}}{K_{a1}^B K_{a2}^B})}}{(1+\frac{[H^+]_0}{K_{a2}^B}+\frac{[H^+]_0^{\,2}}{K_{a1}^B K_{a2}^B})} + D_B[BH^+] + D_B[\,BH_2^{2+}] = C_4 \quad (5A.46)$$

$$D_{H_2A}(\frac{D_B}{D_{H_2A}})^{2/3} \frac{\sqrt{K_{sp}(1+\frac{K_{a1}^{H_2A}}{[H^+]_0}+\frac{K_{a1}^{H_2A}K_{a2}^{H_2A}}{[H^+]_0^{\,2}})(1+\frac{[H^+]_0}{K_{a2}^B}+\frac{[H^+]_0^{\,2}}{K_{a1}^B K_{a2}^B})}}{(1+\frac{K_{a1}^{H_2A}}{[H^+]_0}+\frac{K_{a1}^{H_2A}K_{a2}^{H_2A}}{[H^+]_0^{\,2}})} + D_{H_2A}[HA^-] + D_{H_2A}[\,A^{2-}] = C_5 \quad (5A.47)$$

$$D_{OH^-}[OH^-]_0 + D_B \frac{\sqrt{K_{sp}(1+\frac{K_{a1}^{H_2A}}{[H^+]_0}+\frac{K_{a1}^{H_2A}K_{a2}^{H_2A}}{[H^+]_0^{\,2}})(1+\frac{[H^+]_0}{K_{a2}^B}+\frac{[H^+]_0^{\,2}}{K_{a1}^B K_{a2}^B})}}{(1+\frac{[H^+]_0}{K_{a2}^B}+\frac{[H^+]_0^{\,2}}{K_{a1}^B K_{a2}^B})} + D_{H_2A}[\,A^{2-}] = D_{H^+}[H^+]_0 +$$

$$D_B[\,BH_2^{2+}] + D_{H_2A}(\frac{D_B}{D_{H_2A}})^{2/3} \frac{\sqrt{K_{sp}(1+\frac{K_{a1}^{H_2A}}{[H^+]_0}+\frac{K_{a1}^{H_2A}K_{a2}^{H_2A}}{[H^+]_0^{\,2}})(1+\frac{[H^+]_0}{K_{a2}^B}+\frac{[H^+]_0^{\,2}}{K_{a1}^B K_{a2}^B})}}{(1+\frac{K_{a1}^{H_2A}}{[H^+]_0}+\frac{K_{a1}^{H_2A}K_{a2}^{H_2A}}{[H^+]_0^{\,2}})} + C_6 \quad (5A.48)$$

and at *x = h*, assuming sink conditions, equations 5A.43 to 5A.45 can be written as:

$$0 = C_1 h + C_4 \quad (5A.49)$$

$$0 = C_2 h + C_5 \quad (5A.50)$$

$$D_{OH^-}[OH^-]_h = D_{H^+}[H^+]_h + C_3 h + C_6 \quad (5A.51)$$

Combining equations 5A.46 to 5A.51 and algebraically solving for interfacial pH, $[H^+]_0$, yields the following equation:

$$Ax^8 + Bx^7 + Cx^6 + Dx^5 + Ex^4 + Fx^3 + Gx^2 + Hx + I = 0 \quad (5A.52)$$

where:

$A = 4{D_B}^2 K_{sp} - {D_{H^+}}^2 K_{a1}^B K_{a2}^B;$

$B = 4D_B K_{sp}\left(D_B K_{a1}^B + 2D_B K_{a1}^{H_2A} - {D_B}^{\frac{2}{3}} {D_{H_2A}}^{\frac{1}{3}} K_{a1}^{H_2A}\right) - {D_{H^+}}^2 K_{a1}^B K_{a2}^B\left(K_{a1}^{H_2A} + K_{a1}^B\right) - 2D_{H^+} K_{a1}^B K_{a2}^B (D_{OH^-}[OH^-]_h - D_{H^+}[H^+]_h);$

$C = {D_B}^2 K_{sp}\left({K_{a1}^B}^2 + 8K_{a1}^{H_2A} K_{a1}^B + 8K_{a1}^{H_2A} K_{a2}^{H_2A} + 4{K_{a1}^{H_2A}}^2\right) - 2{D_B}^{\frac{5}{3}} {D_{H_2A}}^{\frac{1}{3}} K_{sp}\left(2{K_{a1}^{H_2A}}^2 + 3K_{a1}^{H_2A} K_{a1}^B + 4K_{a1}^{H_2A} K_{a2}^{H_2A}\right) - 2D_{H^+} K_{a1}^B K_{a2}^B (D_{OH^-}[OH^-]_h - D_{H^+}[H^+]_h)\left(K_{a1}^{H_2A} + K_{a1}^B\right) - K_{a1}^B K_{a2}^B (D_{OH^-}[OH^-]_h - D_{H^+}[H^+]_h)^2 - {D_{H^+}}^2 K_{a1}^B K_{a2}^B\left(K_{a1}^{H_2A} K_{a2}^{H_2A} + K_{a1}^{H_2A} K_{a1}^B + K_{a1}^B K_{a2}^B\right) + 2D_{OH^-} D_{H^+} K_w K_{a1}^B K_{a2}^B + {D_B}^{\frac{4}{3}} {D_{H_2A}}^{\frac{2}{3}} K_{sp} {K_{a1}^{H_2A}}^2;$

$D = 2{D_B}^2 K_{sp} K_{a1}^{H_2A} K_{a1}^B\left(K_{a1}^B + 4K_{a2}^{H_2A} + 2K_{a1}^{H_2A}\right) - 2{D_B}^{\frac{5}{3}} {D_{H_2A}}^{\frac{1}{3}} K_{sp} K_{a1}^{H_2A}\left(2K_{a2}^{H_2A} + 2K_{a1}^{H_2A} K_{a1}^B + 2K_{a1}^B K_{a2}^B + K_{a1}^{H_2A} K_{a1}^B + {K_{a1}^B}^2 + 4K_{a1}^{H_2A} K_{a2}^{H_2A} + 6K_{a2}^{H_2A} K_{a1}^B\right) + 2{D_B}^{\frac{4}{3}} {D_{H_2A}}^{\frac{2}{3}} K_{sp} {K_{a1}^{H_2A}}^2\left(2K_{a2}^{H_2A} + K_{a1}^B\right) + 8{D_B}^2 K_{sp} {K_{a1}^{H_2A}}^2 K_{a2}^{H_2A} + 2D_{OH^-} D_{H^+} K_w K_{a1}^B K_{a2}^B\left(K_{a1}^{H_2A} + K_{a1}^B\right) - 2K_{a1}^B K_{a2}^B (D_{OH^-}[OH^-]_h - D_{H^+}[H^+]_h)\left(D_{H^+} K_{a1}^{H_2A} K_{a2}^{H_2A} + D_{H^+} K_{a1}^{H_2A} K_{a1}^B + D_{H^+} K_{a1}^B K_{a2}^B - D_{OH^-} K_w\right) - {D_{H^+}}^2 {K_{a1}^B}^2 K_{a2}^B\left(K_{a1}^{H_2A} K_{a1}^B + K_{a1}^{H_2A} K_{a2}^{H_2A}\right) - K_{a1}^B (D_{OH^-}[OH^-]_h - D_{H^+}[H^+]_h)^2 (K_{a1}^{H_2A} K_{a2}^B + K_{a1}^B K_{a2}^B);$

$E = {D_B}^2 K_{sp} {K_{a1}^B}^2\left(2K_{a1}^{H_2A} K_{a2}^{H_2A} + {K_{a1}^{H_2A}}^2\right) - 2{D_B}^{\frac{5}{3}} {D_{H_2A}}^{\frac{1}{3}} K_{sp} K_{a1}^{H_2A}\left(9K_{a1}^{H_2A} K_{a2}^{H_2A} K_{a1}^B + 2K_{a1}^{H_2A} K_{a1}^B K_{a2}^B + 2K_{a2}^{H_2A} {K_{a1}^B}^2 + 4K_{a1}^{H_2A} {K_{a2}^{H_2A}}^2 + 4K_{a2}^{H_2A} K_{a1}^B K_{a2}^B + K_{a1}^{H_2A} {K_{a1}^B}^2 + {K_{a1}^B}^2 K_{a2}^B\right) + {D_B}^{\frac{4}{3}} {D_{H_2A}}^{\frac{2}{3}} K_{sp} {K_{a1}^{H_2A}}^2\left({K_{a1}^B}^2 + 2K_{a1}^B K_{a2}^B + 4{K_{a2}^{H_2A}}^2 + 8K_{a2}^{H_2A} K_{a1}^B\right) - (D_{OH^-} K_w)^2 K_{a1}^B K_{a2}^B + 2K_{a1}^B K_{a2}^B (D_{OH^-}[OH^-]_h - D_{H^+}[H^+]_h)\left(D_{OH^-} K_w K_{a1}^{H_2A} + D_{OH^-} K_w K_{a1}^B - D_{H^+} K_{a1}^B K_{a1}^{H_2A} K_{a2}^{H_2A} - D_{H^+} K_{a1}^{H_2A} K_{a1}^B K_{a2}^B\right) + 2D_{OH^-} D_{H^+} K_w K_{a1}^B K_{a2}^B\left(K_{a1}^{H_2A} K_{a2}^{H_2A} + K_{a1}^{H_2A} K_{a1}^B + K_{a1}^B K_{a2}^B\right) - K_{a1}^B K_{a2}^B (D_{OH^-}[OH^-]_h - D_{H^+}[H^+]_h)^2\left(K_{a1}^{H_2A} K_{a2}^{H_2A} + K_{a1}^{H_2A} K_{a1}^B + K_{a1}^B K_{a2}^B\right) + 4{D_B}^2 K_{sp} {K_{a1}^{H_2A}}^2\left(2K_{a2}^{H_2A} K_{a1}^B + {K_{a2}^{H_2A}}^2\right) - {D_{H^+}}^2 (K_{a1}^B K_{a2}^B)^2 K_{a1}^{H_2A} K_{a2}^{H_2A};$

$F = 2{D_B}^{\frac{4}{3}} {D_{H_2A}}^{\frac{2}{3}} K_{sp} {K_{a1}^{H_2A}}^2 K_{a1}^B\left(2K_{a2}^{H_2A} K_{a1}^B + 4K_{a2}^{H_2A} K_{a2}^B + 4{K_{a2}^{H_2A}}^2 + K_{a1}^B K_{a2}^B\right) - 2{D_B}^{\frac{5}{3}} {D_{H_2A}}^{\frac{1}{3}} K_{sp} {K_{a1}^{H_2A}}^2 K_{a1}^B\left(6{K_{a2}^{H_2A}}^2 + 6K_{a2}^{H_2A} K_{a2}^B + K_{a1}^B K_{a2}^B + 3K_{a2}^{H_2A} K_{a1}^B + 2\frac{K_{a2}^{H_2A}}{K_{a1}^{H_2A}} K_{a1}^B K_{a2}^B\right) -$

$(D_{OH^-}K_w)^2K_{a1}^BK_{a2}^B\left(K_{a1}^{H_2A}+K_{a1}^B\right)+2D_{OH^-}K_wK_{a1}^BK_{a2}^B(D_{OH^-}[OH^-]_h-$
$D_{H^+}[H^+]_h)\left(K_{a1}^{H_2A}K_{a2}^{H_2A}+K_{a1}^{H_2A}K_{a1}^B+K_{a1}^BK_{a2}^B\right)+2D_{OH^-}D_{H^+}K_w{K_{a1}^B}^2K_{a1}^{H_2A}\left(K_{a2}^{H_2A}K_{a2}^B+{K_{a2}^B}^2\right)-$
${K_{a1}^B}^2K_{a1}^{H_2A}(D_{OH^-}[OH^-]_h-D_{H^+}[H^+]_h)^2\left(K_{a2}^{H_2A}K_{a2}^B+{K_{a2}^B}^2\right)-2D_{H^+}(D_{OH^-}[OH^-]_h-$
$D_{H^+}[H^+]_h)K_{a1}^{H_2A}K_{a2}^{H_2A}(K_{a1}^BK_{a2}^B)^2+2{D_B}^2K_{sp}{K_{a1}^{H_2A}}^2K_{a2}^{H_2A}K_{a1}^B(K_{a1}^B+2K_{a2}^{H_2A})$;

$G=D_B{}^{\frac{4}{3}}D_{H_2A}{}^{\frac{2}{3}}K_{sp}{K_{a1}^{H_2A}}^2K_{a1}^B\left(K_{a1}^B{K_{a2}^B}^2+8{K_{a2}^{H_2A}}^2K_{a2}^B+8K_{a2}^{H_2A}K_{a1}^BK_{a2}^B+4{K_{a2}^{H_2A}}^2K_{a1}^B\right)-$
$2D_B{}^{\frac{5}{3}}D_{H_2A}{}^{\frac{1}{3}}K_{sp}{K_{a1}^{H_2A}}^2K_{a2}^{H_2A}K_{a1}^B\left(4K_{a2}^{H_2A}K_{a2}^B+3K_{a1}^BK_{a2}^B+2K_{a2}^{H_2A}K_{a1}^B\right)-$
$(D_{OH^-}K_w)^2K_{a1}^BK_{a2}^B\left(K_{a1}^{H_2A}K_{a2}^{H_2A}+K_{a1}^{H_2A}K_{a1}^B+K_{a1}^BK_{a2}^B\right)+$
$2D_{OH^-}K_wK_{a1}^{H_2A}{K_{a1}^B}^2K_{a2}^B(D_{OH^-}[OH^-]_h-D_{H^+}[H^+]_h)\left(K_{a2}^{H_2A}+K_{a2}^B\right)+$
$2D_{OH^-}D_{H^+}K_wK_{a1}^{H_2A}K_{a2}^{H_2A}(K_{a1}^BK_{a2}^B)^2-(D_{OH^-}[OH^-]_h-D_{H^+}[H^+]_h)^2K_{a1}^{H_2A}K_{a2}^{H_2A}(K_{a1}^BK_{a2}^B)^2+$
${D_B}^2K_{sp}(K_{a1}^{H_2A}K_{a2}^{H_2A}K_{a1}^B)^2$;

$H=4D_B{}^{\frac{4}{3}}D_{H_2A}{}^{\frac{2}{3}}K_{sp}{K_{a1}^{H_2A}}^2K_{a2}^{H_2A}K_{a1}^BK_{a2}^B\left(K_{a1}^BK_{a2}^B+2K_{a2}^{H_2A}K_{a1}^B\right)-$
$(D_{OH^-}K_w)^2K_{a1}^{H_2A}{K_{a1}^B}^2K_{a2}^B\left(K_{a2}^{H_2A}+K_{a2}^B\right)+2D_{OH^-}K_wK_{a1}^{H_2A}K_{a2}^{H_2A}(K_{a1}^BK_{a2}^B)^2(D_{OH^-}[OH^-]_h-$
$D_{H^+}[H^+]_h)-4D_B{}^{\frac{5}{3}}D_{H_2A}{}^{\frac{1}{3}}K_{sp}(K_{a1}^{H_2A}K_{a2}^{H_2A}K_{a1}^B)^2K_{a2}^B$;

$I=4D_B{}^{\frac{4}{3}}D_{H_2A}{}^{\frac{2}{3}}K_{sp}(K_{a1}^{H_2A}K_{a2}^{H_2A}K_{a1}^BK_{a2}^B)^2-(D_{OH^-}K_w)^2K_{a1}^{H_2A}K_{a2}^{H_2A}(K_{a1}^BK_{a2}^B)^2$.

Evaluation of flux of the cocrystal components

Combine equations 5A.46 and 5A.49, and solve for $-C_1$ for the total flux of cocrystal in terms of drug species across the diffusion layer:

$$J_{cc}=\frac{D_B}{h}\sqrt{K_{sp}(1+\frac{K_{a1}^{H_2A}}{[H^+]_0}+\frac{K_{a1}^{H_2A}K_{a2}^{H_2A}}{{[H^+]_0}^2})(1+\frac{[H^+]_0}{K_{a2}^B}+\frac{{[H^+]_0}^2}{K_{a1}^BK_{a2}^B})} \tag{5A.53}$$

Substituting equation 5A.22 into equation 5A.53, the rotating flux of cocrystal can be written as:

$$J_{cc}=0.62D_B^{2/3}\omega^{1/2}\nu^{-1/6}\sqrt{K_{sp}(1+\frac{K_{a1}^{H_2A}}{[H^+]_0}+\frac{K_{a1}^{H_2A}K_{a2}^{H_2A}}{{[H^+]_0}^2})(1+\frac{[H^+]_0}{K_{a2}^B}+\frac{{[H^+]_0}^2}{K_{a1}^BK_{a2}^B})} \tag{5A.54}$$

APPENDIX 5B

This appendix provides the mass transport analysis for the dissolution of cocrystals based on the interfacial equilibrium model and as well as the comparison in interfacial pH and flux predictions between the surface saturation and interfacial equilibrium models.

Mass transport analysis based on interfacial equilibrium model

According to the interfacial equilibrium model, the concentrations of the cocrystal components have to increase in order to maintain constant solubility product at the dissolving surface at all time. For the dissolution of a 1:1 cocrystal with dibasic drug and diacidic coformer, the concentrations of the components at the dissolving surface can be written based on the interfacial equilibrium model as:

$$[B]_T = [B] + [BH^+] + [BH_2^{2+}] = (\frac{D_{H_2A}}{D_B})^{1/3} S_{cc} \quad (5B.1)$$

$$[H_2A]_T = [H_2A] + [HA^-] + [A^{2-}] = (\frac{D_B}{D_{H_2A}})^{1/3} S_{cc} \quad (5B.2)$$

Based on these two equations, the following boundary conditions can be written:

At $x = 0$: at $x = h$:

$$[B] = (\frac{D_{H_2A}}{D_B})^{1/3} \frac{\sqrt{K_{sp}(1+\frac{K_{a1}^{H_2A}}{[H^+]_0}+\frac{K_{a1}^{H_2A}K_{a2}^{H_2A}}{[H^+]_0^{\,2}})(1+\frac{[H^+]_0}{K_{a2}^B}+\frac{[H^+]_0^{\,2}}{K_{a1}^B K_{a2}^B})}}{(1+\frac{[H^+]_0}{K_{a2}^B}+\frac{[H^+]_0^{\,2}}{K_{a1}^B K_{a2}^B})} \qquad [B] = 0 \text{ (sink condition)}$$

$$[H_2A] = \left(\frac{D_B}{D_{H_2A}}\right)^{1/3} \frac{\sqrt{K_{sp}\left(1+\frac{K_{a1}^{H_2A}}{[H^+]_0}+\frac{K_{a1}^{H_2A}K_{a2}^{H_2A}}{[H^+]_0^{\,2}}\right)\left(1+\frac{[H^+]_0}{K_{a2}^{B}}+\frac{[H^+]_0^{\,2}}{K_{a1}^{B}K_{a2}^{B}}\right)}}{\left(1+\frac{K_{a1}^{H_2A}}{[H^+]_0}+\frac{K_{a1}^{H_2A}K_{a2}^{H_2A}}{[H^+]_0^{\,2}}\right)}$$ $[H_2A] = 0$ (sink condition)

$[BH^+] = unknown$ $[BH^+] = 0$ (sink condition)

$[BH_2^{\,2+}] = unknown$ $[BH_2^{\,2+}] = 0$ (sink condition)

$[HA^-] = unknown$ $[HA^-] = 0$ (sink condition)

$[A^{2-}] = unknown$ $[A^{2-}] = 0$ (sink condition)

$[H^+] = [H^+]_0$ $[H^+] = [H^+]_h$

$[OH^-] = [OH^-]_0$ $[OH^-] = [OH^-]_h$

Evaluation of interfacial pH

Applying the above boundary conditions to equations 5A.43 to 5A.45 and follow the steps shown in Appendix 5A, the following equation can be written to predict the interfacial pH:

$$Ax^8 + Bx^7 + Cx^6 + Dx^5 + Ex^4 + Fx^3 + Gx^2 + Hx + I = 0 \quad (5B.3)$$

where:

$A = 4D_B^{\frac{4}{3}} D_{H_2A}^{\frac{2}{3}} K_{sp} - D_{H^+}{}^2 K_{a1}^B K_{a2}^B;$

$B = 4D_B D_{H_2A}^{\frac{2}{3}} K_{sp}\left(D_B^{\frac{1}{3}} K_{a1}^B + 2D_B^{\frac{1}{3}} K_{a1}^{H_2A} - D_{H_2A}^{\frac{1}{3}} K_{a1}^{H_2A}\right) - D_{H^+}{}^2 K_{a1}^B K_{a2}^B\left(K_{a1}^{H_2A} + K_{a1}^B\right) - 2D_{H^+} K_{a1}^B K_{a2}^B (D_{OH^-}[OH^-]_h - D_{H^+}[H^+]_h);$

$C = D_B^{\frac{4}{3}} D_{H_2A}^{\frac{2}{3}} K_{sp}\left(K_{a1}^B{}^2 + 8K_{a1}^{H_2A} K_{a1}^B + 8K_{a1}^{H_2A} K_{a2}^{H_2A} + 4K_{a1}^{H_2A}{}^2\right) - 2D_B D_{H_2A} K_{sp}\left(2K_{a1}^{H_2A}{}^2 + 3K_{a1}^{H_2A} K_{a1}^B + 4K_{a1}^{H_2A} K_{a2}^{H_2A}\right) - 2D_{H^+} K_{a1}^B K_{a2}^B (D_{OH^-}[OH^-]_h - D_{H^+}[H^+]_h)\left(K_{a1}^{H_2A} + K_{a1}^B\right) -$

$K_{a1}^{B}K_{a2}^{B}(D_{OH^-}[OH^-]_h - D_{H^+}[H^+]_h)^2 - {D_{H^+}}^2K_{a1}^{B}K_{a2}^{B}\left(K_{a1}^{H_2A}K_{a2}^{H_2A} + K_{a1}^{H_2A}K_{a1}^{B} + K_{a1}^{B}K_{a2}^{B}\right) +$
$2D_{OH^-}D_{H^+}K_wK_{a1}^{B}K_{a2}^{B} + {D_{H_2A}}^{\frac{4}{3}}{D_B}^{\frac{2}{3}}K_{sp}{K_{a1}^{H_2A}}^2;$

$D = 2{D_B}^{\frac{4}{3}}{D_{H_2A}}^{\frac{2}{3}}K_{sp}K_{a1}^{H_2A}K_{a1}^{B}\left(K_{a1}^{B} + 4K_{a2}^{H_2A} + 2K_{a1}^{H_2A}\right) - 2D_BD_{H_2A}K_{sp}K_{a1}^{H_2A}\left(2K_{a2}^{H_2A} +$
$2K_{a1}^{H_2A}K_{a1}^{B} + 2K_{a1}^{B}K_{a2}^{B} + K_{a1}^{H_2A}K_{a1}^{B} + {K_{a1}^{B}}^2 + 4K_{a1}^{H_2A}K_{a2}^{H_2A} + 6K_{a2}^{H_2A}K_{a1}^{B}\right) +$
$2{D_{H_2A}}^{\frac{4}{3}}{D_B}^{\frac{2}{3}}K_{sp}{K_{a1}^{H_2A}}^2\left(2K_{a2}^{H_2A} + K_{a1}^{B}\right) + 8{D_B}^{\frac{4}{3}}{D_{H_2A}}^{\frac{2}{3}}K_{sp}{K_{a1}^{H_2A}}^2K_{a2}^{H_2A} +$
$2D_{OH^-}D_{H^+}K_wK_{a1}^{B}K_{a2}^{B}\left(K_{a1}^{H_2A} + K_{a1}^{B}\right) - 2K_{a1}^{B}K_{a2}^{B}(D_{OH^-}[OH^-]_h - D_{H^+}[H^+]_h)\left(D_{H^+}K_{a1}^{H_2A}K_{a2}^{H_2A} +\right.$
$\left.D_{H^+}K_{a1}^{H_2A}K_{a1}^{B} + D_{H^+}K_{a1}^{B}K_{a2}^{B} - D_{OH^-}K_w\right) - {D_{H^+}}^2{K_{a1}^{B}}^2K_{a2}^{B}\left(K_{a1}^{H_2A}K_{a1}^{B} + K_{a1}^{H_2A}K_{a2}^{H_2A}\right) -$
$K_{a1}^{B}(D_{OH^-}[OH^-]_h - D_{H^+}[H^+]_h)^2(K_{a1}^{H_2A}K_{a2}^{B} + K_{a1}^{B}K_{a2}^{B});$

$E = {D_B}^{\frac{4}{3}}{D_{H_2A}}^{\frac{2}{3}}K_{sp}{K_{a1}^{B}}^2\left(2K_{a1}^{H_2A}K_{a2}^{H_2A} + {K_{a1}^{H_2A}}^2\right) - 2D_BD_{H_2A}K_{sp}K_{a1}^{H_2A}\left(9K_{a1}^{H_2A}K_{a2}^{H_2A}K_{a1}^{B} +\right.$
$\left.2K_{a1}^{H_2A}K_{a1}^{B}K_{a2}^{B} + 2K_{a2}^{H_2A}{K_{a1}^{B}}^2 + 4K_{a1}^{H_2A}{K_{a2}^{H_2A}}^2 + 4K_{a2}^{H_2A}K_{a1}^{B}K_{a2}^{B} + K_{a1}^{H_2A}{K_{a1}^{B}}^2 + {K_{a1}^{B}}^2K_{a2}^{B}\right) +$
${D_{H_2A}}^{\frac{4}{3}}{D_B}^{\frac{2}{3}}K_{sp}{K_{a1}^{H_2A}}^2\left({K_{a1}^{B}}^2 + 2K_{a1}^{B}K_{a2}^{B} + 4{K_{a2}^{H_2A}}^2 + 8K_{a2}^{H_2A}K_{a1}^{B}\right) - (D_{OH^-}K_w)^2K_{a1}^{B}K_{a2}^{B} +$
$2K_{a1}^{B}K_{a2}^{B}(D_{OH^-}[OH^-]_h - D_{H^+}[H^+]_h)\left(D_{OH^-}K_wK_{a1}^{H_2A} + D_{OH^-}K_wK_{a1}^{B} - D_{H^+}K_{a1}^{B}K_{a1}^{H_2A}K_{a2}^{H_2A} -\right.$
$\left.D_{H^+}K_{a1}^{H_2A}K_{a1}^{B}K_{a2}^{B}\right) + 2D_{OH^-}D_{H^+}K_wK_{a1}^{B}K_{a2}^{B}\left(K_{a1}^{H_2A}K_{a2}^{H_2A} + K_{a1}^{H_2A}K_{a1}^{B} + K_{a1}^{B}K_{a2}^{B}\right) -$
$K_{a1}^{B}K_{a2}^{B}(D_{OH^-}[OH^-]_h - D_{H^+}[H^+]_h)^2\left(K_{a1}^{H_2A}K_{a2}^{H_2A} + K_{a1}^{H_2A}K_{a1}^{B} + K_{a1}^{B}K_{a2}^{B}\right) +$
$4{D_B}^{\frac{4}{3}}{D_{H_2A}}^{\frac{2}{3}}K_{sp}{K_{a1}^{H_2A}}^2\left(2K_{a2}^{H_2A}K_{a1}^{B} + {K_{a2}^{H_2A}}^2\right) - {D_{H^+}}^2(K_{a1}^{B}K_{a2}^{B})^2K_{a1}^{H_2A}K_{a2}^{H_2A};$

$F = 2{D_{H_2A}}^{\frac{4}{3}}{D_B}^{\frac{2}{3}}K_{sp}{K_{a1}^{H_2A}}^2K_{a1}^{B}\left(2K_{a2}^{H_2A}K_{a1}^{B} + 4K_{a2}^{H_2A}K_{a2}^{B} + 4{K_{a2}^{H_2A}}^2 + K_{a1}^{B}K_{a2}^{B}\right) -$
$2D_BD_{H_2A}K_{sp}{K_{a1}^{H_2A}}^2K_{a1}^{B}\left(6{K_{a2}^{H_2A}}^2 + 6K_{a2}^{H_2A}K_{a2}^{B} + K_{a1}^{B}K_{a2}^{B} + 3K_{a2}^{H_2A}K_{a1}^{B} + 2\frac{K_{a2}^{H_2A}}{K_{a1}^{H_2A}}K_{a1}^{B}K_{a2}^{B}\right) -$
$(D_{OH^-}K_w)^2K_{a1}^{B}K_{a2}^{B}\left(K_{a1}^{H_2A} + K_{a1}^{B}\right) + 2D_{OH^-}K_wK_{a1}^{B}K_{a2}^{B}(D_{OH^-}[OH^-]_h -$
$D_{H^+}[H^+]_h)\left(K_{a1}^{H_2A}K_{a2}^{H_2A} + K_{a1}^{H_2A}K_{a1}^{B} + K_{a1}^{B}K_{a2}^{B}\right) + 2D_{OH^-}D_{H^+}K_w{K_{a1}^{B}}^2K_{a1}^{H_2A}\left(K_{a2}^{H_2A}K_{a2}^{B} + {K_{a2}^{B}}^2\right) -$
${K_{a1}^{B}}^2K_{a1}^{H_2A}(D_{OH^-}[OH^-]_h - D_{H^+}[H^+]_h)^2\left(K_{a2}^{H_2A}K_{a2}^{B} + {K_{a2}^{B}}^2\right) - 2D_{H^+}(D_{OH^-}[OH^-]_h -$
$D_{H^+}[H^+]_h)K_{a1}^{H_2A}K_{a2}^{H_2A}(K_{a1}^{B}K_{a2}^{B})^2 + 2{D_B}^{\frac{4}{3}}{D_{H_2A}}^{\frac{2}{3}}K_{sp}{K_{a1}^{H_2A}}^2K_{a2}^{H_2A}K_{a1}^{B}(K_{a1}^{B} + 2K_{a2}^{H_2A});$

$G = {D_{H_2A}}^{\frac{4}{3}}{D_B}^{\frac{2}{3}}K_{sp}{K_{a1}^{H_2A}}^2K_{a1}^{B}\left(K_{a1}^{B}{K_{a2}^{B}}^2 + 8{K_{a2}^{H_2A}}^2K_{a2}^{B} + 8K_{a2}^{H_2A}K_{a1}^{B}K_{a2}^{B} + 4{K_{a2}^{H_2A}}^2K_{a1}^{B}\right) -$
$2D_BD_{H_2A}K_{sp}{K_{a1}^{H_2A}}^2K_{a2}^{H_2A}K_{a1}^{B}\left(4K_{a2}^{H_2A}K_{a2}^{B} + 3K_{a1}^{B}K_{a2}^{B} + 2K_{a2}^{H_2A}K_{a1}^{B}\right) -$
$(D_{OH^-}K_w)^2K_{a1}^{B}K_{a2}^{B}\left(K_{a1}^{H_2A}K_{a2}^{H_2A} + K_{a1}^{H_2A}K_{a1}^{B} + K_{a1}^{B}K_{a2}^{B}\right) +$
$2D_{OH^-}K_wK_{a1}^{H_2A}{K_{a1}^{B}}^2K_{a2}^{B}(D_{OH^-}[OH^-]_h - D_{H^+}[H^+]_h)\left(K_{a2}^{H_2A} + K_{a2}^{B}\right) +$
$2D_{OH^-}D_{H^+}K_wK_{a1}^{H_2A}K_{a2}^{H_2A}(K_{a1}^{B}K_{a2}^{B})^2 - (D_{OH^-}[OH^-]_h - D_{H^+}[H^+]_h)^2K_{a1}^{H_2A}K_{a2}^{H_2A}(K_{a1}^{B}K_{a2}^{B})^2 +$
${D_B}^{\frac{4}{3}}{D_{H_2A}}^{\frac{2}{3}}K_{sp}(K_{a1}^{H_2A}K_{a2}^{H_2A}K_{a1}^{B})^2;$

$$H = 4D_{H_2A}{}^{\frac{4}{3}} D_B{}^{\frac{2}{3}} K_{sp} K_{a1}^{H_2A\,2} K_{a2}^{H_2A} K_{a1}^{B} K_{a2}^{B} \left(K_{a1}^{B} K_{a2}^{B} + 2K_{a2}^{H_2A} K_{a1}^{B}\right) - (D_{OH^-} K_w)^2 K_{a1}^{H_2A} K_{a1}^{B\,2} K_{a2}^{B} \left(K_{a2}^{H_2A} + K_{a2}^{B}\right) + 2D_{OH^-} K_w K_{a1}^{H_2A} K_{a2}^{H_2A} (K_{a1}^{B} K_{a2}^{B})^2 (D_{OH^-}[OH^-]_h - D_{H^+}[H^+]_h) - 4D_B D_{H_2A} K_{sp} (K_{a1}^{H_2A} K_{a2}^{H_2A} K_{a1}^{B})^2 K_{a2}^{B};$$

$$I = 4D_{H_2A}{}^{\frac{4}{3}} D_B{}^{\frac{2}{3}} K_{sp} (K_{a1}^{H_2A} K_{a2}^{H_2A} K_{a1}^{B} K_{a2}^{B})^2 - (D_{OH^-} K_w)^2 K_{a1}^{H_2A} K_{a2}^{H_2A} (K_{a1}^{B} K_{a2}^{B})^2.$$

Evaluation of flux of the cocrystal components

Applying the above boundary conditions to equation 5A.43 from Appendix 5A and solve for $-C_1$ for the total flux of cocrystal in terms of drug species across the diffusion layer:

$$J_{cc} = \frac{D_{H_2A}{}^{\frac{1}{3}} D_B{}^{\frac{2}{3}}}{h} \sqrt{K_{sp}\left(1 + \frac{K_{a1}^{H_2A}}{[H^+]_0} + \frac{K_{a1}^{H_2A} K_{a2}^{H_2A}}{[H^+]_0{}^2}\right)\left(1 + \frac{[H^+]_0}{K_{a2}^{B}} + \frac{[H^+]_0{}^2}{K_{a1}^{B} K_{a2}^{B}}\right)} \quad (5B.4)$$

Substitute equation 5A.22 from Appendix 5A into equation 5B.4, the rotating flux of cocrystal can be written as:

$$J_{cc} = 0.62(D_B D_{H_2A})^{1/3} \omega^{1/2} \nu^{-1/6} \sqrt{K_{sp}\left(1 + \frac{K_{a1}^{H_2A}}{[H^+]_0} + \frac{K_{a1}^{H_2A} K_{a2}^{H_2A}}{[H^+]_0{}^2}\right)\left(1 + \frac{[H^+]_0}{K_{a2}^{B}} + \frac{[H^+]_0{}^2}{K_{a1}^{B} K_{a2}^{B}}\right)} \quad (5B.5)$$

Comparison between the surface saturation and interfacial equilibrium models

In order to evaluate the superiority between the surface saturation and interfacial equilibrium models, interfacial pH and flux of the cocrystals were predicted using both models and compared in Figure 5B.1 to 5B.3 for the three KTZ cocrystals. The surface concentration of the drug for the interfacial equilibrium model is greater than that for the surface saturation model because it has to raise above the stoichiometric solubility of the cocrystal in order to maintain constant K_{sp} at the surface at all times during dissolution. While the surface coformer concentration for the interfacial equilibrium model is lower than the drug concentration, it is still

higher than that for the surface saturation model. The different concentrations of the cocrystal components at the dissolving surface result in the slight difference in interfacial pH predictions between the two models. As shown in Figure 5B.1 to 5B.3, the predicted interfacial pH values at low bulk pH from the interfacial equilibrium model for all three cocrystals are slightly higher than those from the surface saturation model. This is due to the higher drug concentration at the dissolving surface predicted from the interfacial equilibrium model, which leads to greater basicity. On the other hand, the higher coformer concentration at the dissolving surface for the interfacial equilibrium model results in slightly lower interfacial pH predictions at high bulk pH compared to the surface saturation model. Although the theoretical flux predictions from both models follow the same trend as the experimental data, the predictions from the interfacial equilibrium model for all three cocrystals are greater than those from the surface saturation model as shown in Figure 5B.1 to 5B.3. The better agreement between the experimental data and theoretical flux predictions has again demonstrated the superiority of the surface saturation model over the interfacial equilibrium model.

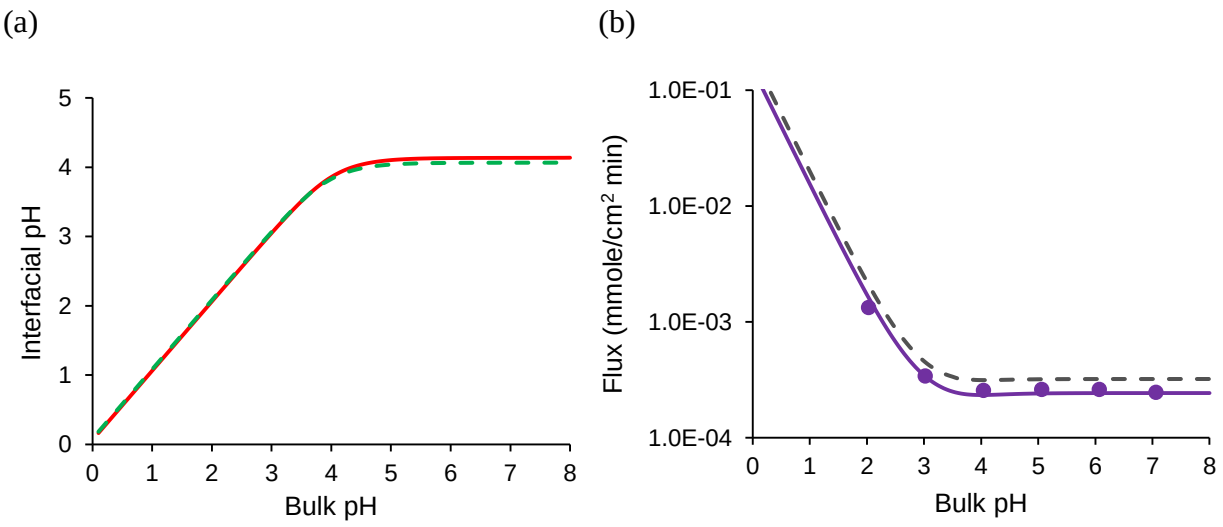

Figure 5B.1. Comparison of interfacial pH (a) and flux predictions (b) for KTZ-FUM between the interfacial equilibrium model (dotted line) and surface saturation model (solid line). The solid circles are the experimental flux values.

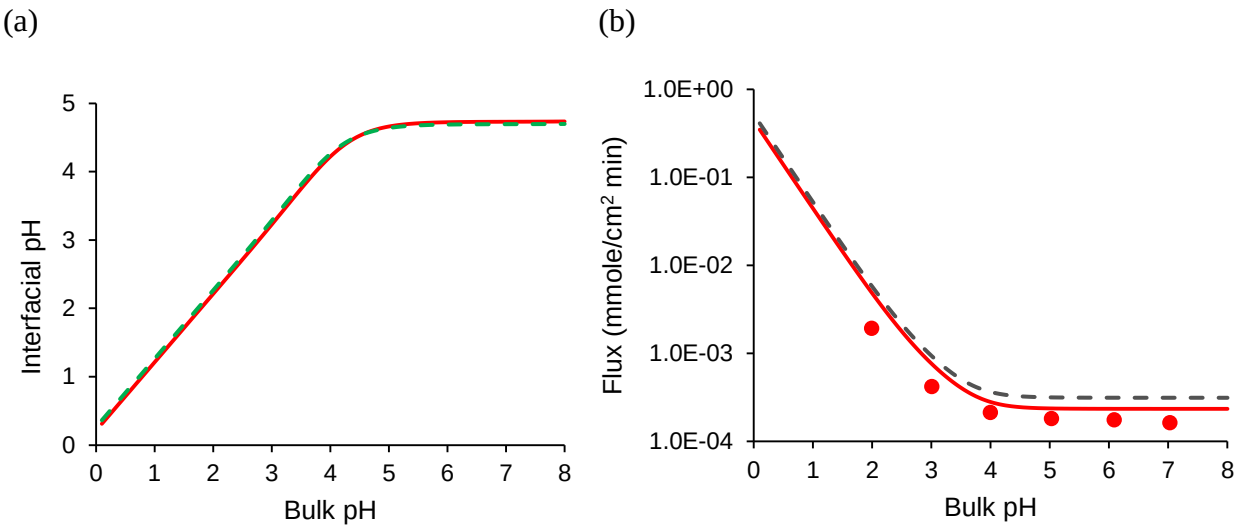

Figure 5B.2. Comparison of interfacial pH (a) and flux predictions (b) for KTZ-SUC between the interfacial equilibrium model (dotted line) and surface saturation model (solid line). The solid circles are the experimental flux values.

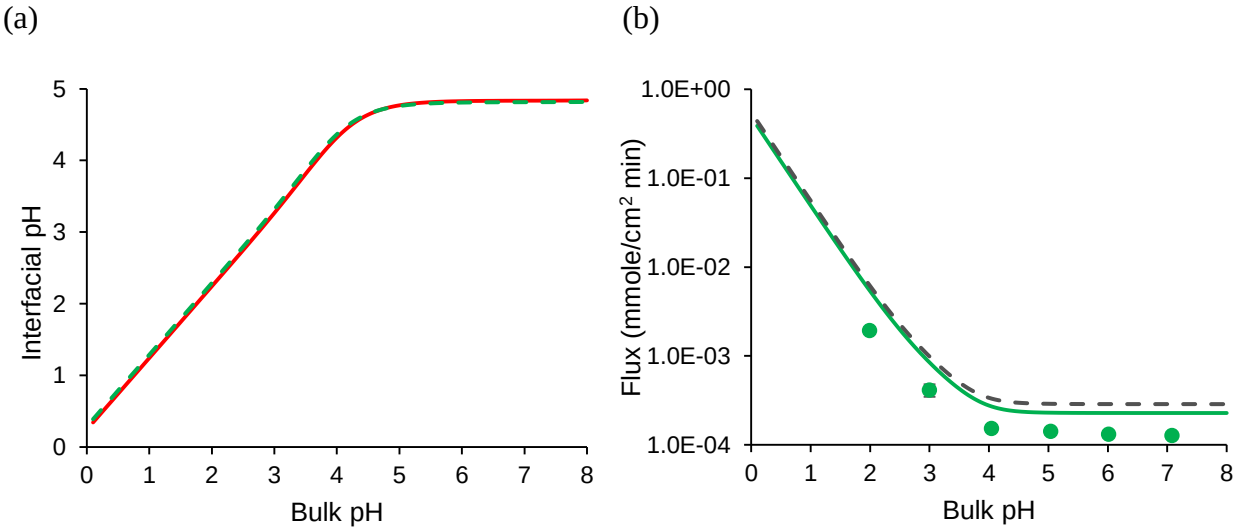

Figure 5B.3. Comparison of interfacial pH (a) and flux predictions (b) for KTZ-ADP between the interfacial equilibrium model (dotted line) and surface saturation model (solid line). The solid circles are the experimental flux values.

CHAPTER 6

EFFECT OF BUFFERING AGENTS ON THE DISSOLUTION OF COCRYSTALS

Abstract

Buffers are commonly encountered in drug development as they are frequently used in preparing dissolution media and sometimes even in drug formulations. The human GI tract also contains bicarbonate buffer to maintain the GI pH. It is well known that the properties and concentrations of buffers can have significant impact on the dissolution rates of ionizable drugs. Since cocrystals usually contain ionizable components, the influence of buffering agents on the dissolution rates of these cocrystalline materials should also be emphasized. The purpose of this study is to evaluate the effect of acetate and phosphate buffers on the dissolution of a 1:1 cocrystal with nonionizable drug and acidic coformer, carbamazepine-salicylic acid (CBZ-SLC). The mass transport model previously developed for this cocrystal has been extended to include the buffer properties for evaluating the buffer effect on interfacial pH and dissolution rates. The mass transport analyses have demonstrated the importance of pK_a value, diffusion coefficient and concentration of buffering agents in determining the interfacial pH. By modeling interfacial pH, the flux of cocrystal can be accurately predicted as a function of buffer concentration. In this study, the dissolution rate of CBZ-SLC increases with increasing buffer concentration and this increase is due to the elevation in interfacial pH by both acetate and phosphate buffers.

Introduction

The composition of dissolution media, such as pH and buffering agents can have significant impact on the dissolution rates of ionizable drugs[1-3]. For the dissolution of ionizable compounds, the pH at the dissolving surface is extremely important and this interfacial pH can be quite different from the pH of the bulk solution[1-3]. The presence of buffer species in the dissolution media can influence the interfacial pH and consequently alters the dissolution rates of ionizable drugs[2-6]. There has been studies in the literature demonstrating the influence of buffering agents on the dissolution rates of ionizable drugs[2-6]. In these studies, the dissolution rates of ionizable drugs increase as buffer concentration increases and the rate of increase is dependent on the properties and concentrations of the buffer in solutions[2-6]. The interfacial pH of naproxen has been shown to increase with increasing phosphate buffer concentration[4]. As the buffer capacity in the bulk solution exceeds the self-buffering capacity of naproxen, the interfacial pH becomes similar to the bulk pH[4]. Interfacial pH determines the dissolution behavior of naproxen in the presence of phosphate buffer and the dissolution rate of naproxen increases with increasing buffer concentration[4]. Both interfacial pH and dissolution behavior of ionizable drugs under the influence of buffer can be accurately predicted using mass transport analyses for dissolution with simultaneous chemical reactions in the hydrodynamic boundary layer adjacent to the dissolving surface[2-6].

The primary buffer species in human GI tract is bicarbonate and the buffer concentrations can vary depending on the location in the GI tract and other factors such as food and stress[7-9]. Physiological relevant dissolution media such as fasted state simulated intestinal fluid (FaSSIF) and fed state simulated intestinal fluid (FeSSIF) also contain phosphate buffer as the main buffering agent[10, 11]. Besides dissolution media, buffering agents have also been used in

formulations to prevent GI irritation and/or to promote dissolution of acidic drugs[12-14]. Buffering agents can be encountered both *in vivo* and *in vitro*, so it is essential to understand the mechanism of how they influence the dissolution rates of ionizable drugs.

The impact of pH on the dissolution rates of cocrystals under unbuffered conditions has been evaluated in previous chapters in this thesis. The purpose of this chapter is to evaluate the dissolution rates of cocrystals under the influence of buffering agents. The model cocrystal used in this study is carbamazepine-salicylic acid (CBZ-SLC) and the buffering agents are phosphate and acetate buffers. The mass transport analyses for this cocrystal based on the surface saturation model[15] were extended to include the chemical reactions of the coformer with the buffer species from the bulk solution. This new mass transport model can be used to predict the interfacial pH and flux of 1:1 cocrystals with non-ionizable drugs and acidic coformers as a function of pH and buffer concentration.

Materials and methods

Materials

Anhydrous carbamazepine (CBZ), salicylic acid (SLC), sodium lauryl sulfate (SLS), potassium phosphate monobasic, sodium acetate anhydrous and potassium phosphate dibasic anhydrous were purchased from Sigma Chemical Company (St. Louis, MO) and used as received. Acetonitrile, methanol and sodium phosphate monobasic were purchased from Fisher Scientific (Pittsburgh, PA). Sodium phosphate dibasic heptahydrate was purchased from Acros Organics (Pittsburgh, PA). Acetic acid was purchased from Mallinckrodt Baker (Phillipsburg, NJ). Water used in this study was filtered through a double deionized purification system (Milli Q Plus Water System) from Millipore Co. (Bedford, MA).

Cocrystal synthesis

Cocrystals were prepared by reaction crystallization method[16] at room temperature. CBZ-SLC was prepared by adding 1:1 molar ratio of CBZ and SLC in acetonitrile solution containing 0.1 M SLC. Solid phases were characterized by X-ray powder diffraction (XRPD) and differential scanning calorimetry (DSC).

Cocrystal dissolution measurements

Constant surface area dissolution rates of CBZ-SLC were determined using a rotating disk apparatus. Cocrystal powder (~150 mg) was compressed in a stainless steel rotating disk die with a tablet radius of 0.50 cm at approximately 85 MPa for 2 minutes using a hydraulic press. The die containing the compact was mounted onto a stainless steel shaft attached to an overhead, variable speed motor. The disk was exposed to 150 mL of the dissolution medium in a water jacketed beaker with temperature controlled at 25°C and a rotation speed of 200 rpm was used. Dissolution media containing different buffer concentrations in 150 mM SLS were prepared on the day of the experiment. The bulk solution pH did not change significantly throughout the experiment. Sink conditions were maintained throughout the experiments by ensuring the concentrations at the last time point of the dissolution were less than 10% of the cocrystal solubility. Solution concentrations were measured using HPLC and solid phases after dissolution were analyzed by XRPD.

HPLC

Waters HPLC equipped with a photodiode array detector was used for all analysis. The mobile phase was composed of 55% methanol and 45% water with 0.1% trifluoroacetic acid and the flow rate of 1 mL/min was used. Separation was achieved using Waters, Atlantis, T3 column

(5.0 µm, 100 Å) with dimensions of 4.6 x 250 mm. The sample injection volume was 20 µL. The wavelengths for the analytes were as follows: 284 nm for CBZ and 303 nm for SLC.

XRPD

XRPD diffractograms of solid phases were collected with a benchtop Rigaku Miniflex X-ray diffractometer using Cu-Kα radiation (λ = 1.54 Å), a tube voltage of 30 kV, and a tube current of 15 mA. Data was collected from 5 to 40° at a continuous scan rate of 2.5°/min.

DSC

Crystalline samples were analyzed by DSC using a TA instrument 2910 MDSC system equipped with a refrigerated cooling unit. All experiments were performed by heating the samples at a rate of 10 °C/min under a dry nitrogen atmosphere. Temperature and enthalpy of the instrument were calibrated using high purity indium standard.

Theoretical

The present model here describes the dissolution of 1:1 cocrystals with nonionizable drugs and monoacidic coformers in buffered media containing surfactant. This model is an extension from the previous model developed based on the surface saturation model with simultaneous chemical reactions in the hydrodynamic boundary layer adjacent to the dissolving surface[15]. Besides the chemical reactions with water and hydroxide ion, the acidic coformer also reacts with the basic components of the buffer in the dissolution medium. Although the mass transport model developed here is for the monoprotic buffer systems, it is also applicable to diprotic or even triprotic buffer systems as long as the pK_a value used is close to the bulk pH of the dissolution medium. This assumption has been tested for both diprotic and triprotic buffer systems[3]. By using relevant pK_a values, the flux predictions from the monoprotic model have been shown to be

identical to those from the diprotic and triprotic models [3]. These findings suggest that the transport mechanism of buffer is governed by the dissociation of the dominated buffer species in solution[3].

The chemical equilibria and the equations for equilibrium constants during the dissolution of 1:1 cocrystal, RHA with R as the nonionizable drug and HA as the weakly acidic coformer in buffered solution containing surfactant with B as the basic and BH^+ as the conjugate acidic buffer species, can be described as follows:

$$(RHA)_{solid} \leftrightharpoons R_{aq} + HA_{aq} \tag{6.1}$$

$$K_{sp} = [R]_{aq}[HA]_{aq} \tag{6.2}$$

$$R_{aq} + m \leftrightharpoons R_m \tag{6.3}$$

$$K_s^R = \frac{[R]_m}{[R]_{aq}[m]} \tag{6.4}$$

$$HA_{aq} + m \leftrightharpoons HA_m \tag{6.5}$$

$$K_s^{HA} = \frac{[HA]_m}{[HA]_{aq}[m]} \tag{6.6}$$

$$HA_{aq} \leftrightharpoons H_3O^+ + A_{aq}^- \tag{6.7}$$

$$K_a^{HA} = \frac{[H_3O^+][A^-]_{aq}}{[HA]_{aq}} \tag{6.8}$$

$$HA_{aq} + OH^- \leftrightharpoons H_2O + A_{aq}^- \tag{6.9}$$

$$K_1 = \frac{[A^-]_{aq}}{[HA]_{aq}[OH^-]} \tag{6.10}$$

$$BH_{aq}^+ \leftrightharpoons B_{aq} + H^+ \tag{6.11}$$

$$K_a^B = \frac{[H^+][B]_{aq}}{[BH^+]_{aq}} \tag{6.12}$$

$$BH_{aq}^+ + OH^- \leftrightharpoons B_{aq} + H_2O \tag{6.13}$$

$$K_2 = \frac{[B]_{aq}}{[BH^+]_{aq}[OH^-]} \tag{6.14}$$

$$HA_{aq} + B_{aq} \leftrightharpoons BH_{aq}^+ + A_{aq}^- \tag{6.15}$$

$$K_3 = \frac{[BH^+]_{aq}[A^-]_{aq}}{[B]_{aq}[HA]_{aq}} = \frac{K_s^{HA}}{K_a^B} \tag{6.16}$$

where K_{sp} is the solubility product of the cocrystal, K_s^R is the solubilization constant of R and K_s^{HA} is the solubilization constant of HA, m is the micellar concentration in solution and is equal to the total surfactant concentration minus the critical micellar concentration (CMC), K_a^{HA} and K_a^B are the ionization constants of HA and B. Subscript aq denotes the aqueous phase and m denotes the micellar phase. The underlying assumption in this analysis is that the buffer species and ionized form of coformer are not solubilized by surfactant.

In the presence of surfactant, the stoichiometric solubility of RHA can be predicted using the following equation:

$$S_{cc} = \sqrt{K_{sp}(1 + K_s^R[m])(1 + \frac{K_a}{H^+} + K_s^{HA}[m])} \tag{6.17}$$

Detailed derivations of the mass transport analyses based on the surface saturation model[15] developed previously to describe the dissolution of cocrystals are provided in Appendix 6A. The mass transport analyses are based on the following assumptions: chemical reactions and solute solubilization within the diffusion layer occur instantaneously, free solutes and micelles are in equilibrium throughout the diffusion layer, the ionized form of the coformer and buffer species are

not solubilized by surfactant, aqueous diffusivities of the ionized and non-ionized forms are the same. For simplification of the interfacial pH prediction, the effective diffusivity of the coformer is assumed to be the same as the aqueous diffusivity because it is not significantly solubilized by the surfactant. In this study, the effect of surfactant concentration on the viscosity of dissolution media was not accounted for the mass transport analyses. Although the viscosity of the dissolution media may approximately double at high surfactant concentration (eg: 300 mM)[17], its impact on the hydrodynamic boundary layer is small. The viscosity of dissolution media is not expected to significantly affect the diffusion of free species as they are assumed to be diffusing through the aqueous phase where the surfactant concentration is equal to the CMC and the viscosity is not substantially different from water[18]. The effect of viscosity on the diffusion coefficient of the micelles incorporates the effect of viscosity changes.

Results and discussion

Physicochemical properties

In this study, the effect of buffer on the dissolution of CBZ-SLC was evaluated using acetate and phosphate buffers in 150 mM SLS solutions. This surfactant concentration was maintained constant for all dissolution studies in order to rule out the surfactant effect on the dissolution rates of the cocrystal. In the absence of buffering agent, 150 mM SLS is sufficient to stabilize CBZ-SLC from the conversion back to the stable drug form during dissolution at bulk pH up to 8[15]. However, this concentration may not be sufficient for stabilizing the cocrystal in certain buffer concentrations due to the ability of buffer in elevating the interfacial pH. Consequently, solid phase transformation may be observed in some of the dissolution experiments. Physicochemical properties of CBZ-SLC and its components are required for the predictions of

interfacial pH and flux. The solubility product of CBZ-SLC was determined to be 0.40 mM^2, and the solubilization constant of CBZ is 0.43 mM^{-1} and SLC is 0.060 mM^{-1} in 150 mM SLS[15]. The pK_a values and diffusion coefficients for the cocrystal components and buffer species are summarized in Table 6.1. Although phosphoric acid has three pK_a values, only the second one was used in this study because the pH of the dissolution media were around this value. Therefore, the relevant buffer species in solutions are monobasic phosphate and dibasic phosphate.

Table 6.1. pK_a values and diffusion coefficients of cocrystal components and buffer species.

Compound	**pK_a**	**Diffusion Coefficient (x 10^{-6} cm^2/sec)**
Carbamazepine	-	1.48[a]
Salicylic Acid	3.0[a]	7.66[a]
Acetate	4.8[b]	10.9[d]
Phosphate	6.6[c]	8.1[c]

a) From reference [15];
b) From reference [2];
c) From reference [3];
d) From reference [4].

Influence of buffer on interfacial pH

The pH at the dissolving surface is important for determining the dissolution rates of cocrystals with ionizable components and this interfacial pH can be predicted using equation 6A.36 from Appendix 6A. The influence of buffering agents on the interfacial pH of CBZ-SLC as a function of bulk pH is shown in Figure 6.1. As shown in Figure 6.1, interfacial pH is influenced by both the properties and concentrations of the buffering agents. The buffer effect on interfacial pH is effective at bulk pH around the pK_a values of the buffers. The pK_a value of acetate buffer is 4.8, so the interfacial pH starts to deviate from the unbuffered system at bulk pH 4 and these deviations increase with increasing buffer concentration. The pK_a value of phosphate buffer is 6.6, so the deviations in interfacial pH from the unbuffered system do not start until at bulk pH

above 5. In both buffered systems, interfacial pH is elevated due to the chemical reactions between the acidic coformer and basic components of the buffers at the dissolving surface, which decrease the concentration of hydrogen ion and increase the interfacial pH. The relative acidity and basicity between the buffer and coformer can also play a role on influencing the interfacial pH[2]. The equilibrium constant from equation 6.16 for acetate and SLC is 63, while for phosphate and SLC is 3981. This means that the phosphate buffer is a lot more basic compared to SLC than acetate buffer to SLC. The lower basicity of acetate could not suppress the self-buffering ability of the coformer and allows it to self-buffer the interfacial pH similar to the unbuffered conditions for the buffer concentrations studied here. The self-buffering ability of the coformer vanishes in the more basic phosphate buffer system. Instead of plateauing, the interfacial pH in phosphate buffer solutions increases with bulk pH in an attempt to maintain a surface pH as close as to the bulk solution pH.

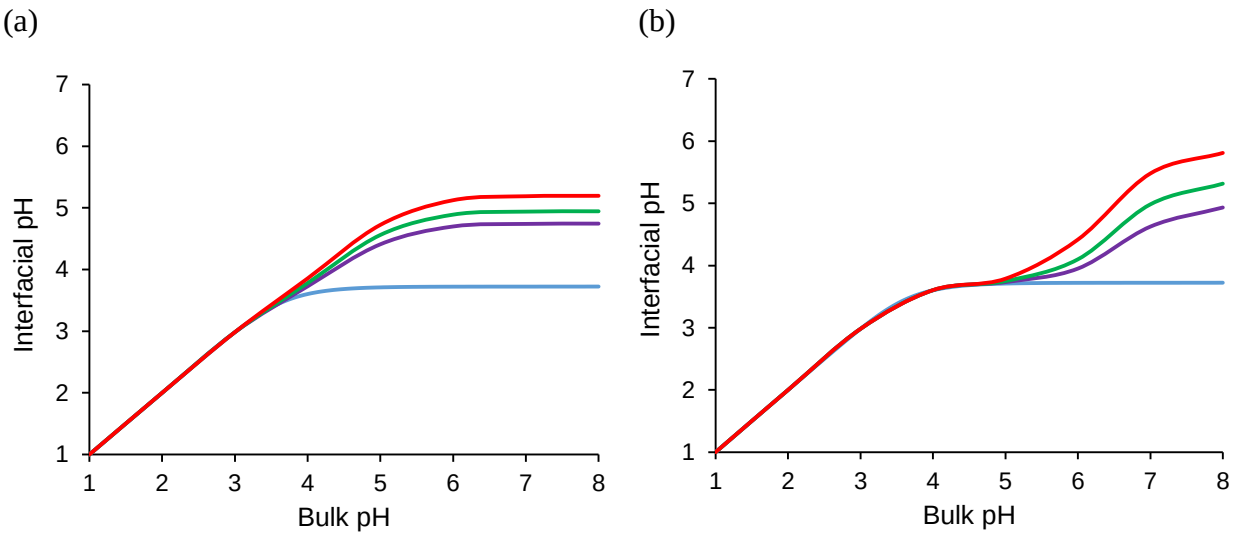

Figure 6.1. Theoretical predictions of interfacial pH for CBZ-SLC as a function of bulk pH in different acetate buffer (a) and phosphate buffer (b) concentrations at 150 mM SLS. No buffer: —; 15 mM: —; 25 mM: —; 50 mM: —. Interfacial pH were predicted using equation 6A.36 from Appendix 6A with the physicochemical properties shown in Table 6.1.

Evaluation of crital stabilization concentration (CSC)

Critical stabiliztion concentration (CSC) is defined as the surfactant concentration required to achieve equivalent solubility of the cocrystal and parent drug[19-21]. This concentration is pH dependent for cocrystals with ionizable components[19-21]. Due to the elevation in interfacial pH by buffer, the CSC values of CBZ-SLC should be evaluated at the bulk pH of dissolution experiments to determine if they are below the SLS concentration (150 mM) used in this study. The CSC values of CBZ-SLC for all the dissoluiton conditions studied in this work are summarized in Table 6.2. As shown in this table, the CSC values are below 150 mM SLS for most of the conditions, expect for 25 mM phosphate buffer at bulk pH 6.79, 50 mM phosphate buffer at bulk pH 6.78 and 50 mM acetate buffer at bulk pH 4.85. Since the CSC values in these conditions are above 150 mM SLS used in the dissolution experiments, solid phase transformation may occur during dissoltuion.

Table 6.2. Estimated CSC for CBZ-SLC in different bulk pH, phosphate and acetate buffer concentrations.

Buffer Conc. (mM)	**Phosphate buffer**			**Acetate buffer**		
	pH		**CSC[b] (mM)**	**pH**		**CSC[b] (mM)**
	Bulk	**Interfacial[a]**		**Bulk**	**Interfacial[a]**	
15	6.84	4.5	148	-	-	-
25	6.79	4.8	289	4.80	4.4	120
	6.03	4.1	63			
50	6.78	5.3	861	4.85	4.6	181
	6.03	4.5	127	3.97	3.8	36

a) Calculated using equation 6A.36 from Appendix 6A with the physicochemical properties shown in Table 6.1.
b) Calculated using previously developed equation[20].

Influence of buffer on dissolution

Effect of buffer on the dissolution rates of CBZ-SLC was evaluated by performing dissolution studies in 150 mM SLS at different buffer concentrations and bulk pH. For acetate

buffer, the dissolution profiles of CBZ-SLC in terms of components' concentrations are shown in Figure 6.2. Among the three dissolution conditions, only the 50 mM acetate buffer at bulk pH 4.85 was expected to have cocrystal conversion during dissolution as predicted by the CSC value shown in Table 6.2. This conversion was confirmed by the nonlinear dissolution behavior shown in Figure 6.2 and a mixed phase of CBZ-SLC and the dihydrated form of CBZ after dissolution by XRPD analysis. Theoretically, the dissolution of CBZ-SLC in 50 mM acetate buffer at bulk pH 4.85 should be faster than in 25 mM acetate buffer at bulk pH 4.80 due to the evaluation in interfacial pH. However, the dissolution rates of CBZ-SLC in these conditions are nearly the same as shown in Figure 6.2 due to the conversion of the cocrystal in 50 mM acetate buffer at bulk pH 4.85. The dissolution profiles of CBZ-SLC in terms of components' concentrations for phosphate buffer are shown in Figure 6.3 and 6.4. In Figure 6.3, the dissolution experiments were performed in 15, 25 and 50 mM phosphate buffer at bulk pH around 6.8. Among these conditions, CBZ-SLC is only stable in 15 mM phosphate buffer and these results are consistent with the CSC predictions shown in Table 6.2. The solid phase transformation of CBZ-SLC in both 25 and 50 mM phosphate buffer was demonstrated by the nonlinear dissolution behavior shown in Figure 6.3 and the XRPD analyses after dissolution. The dissolution rate of CBZ-SLC was only slightly higher in 50 mM phosphate buffer during the early dissolution time points and this did not last very long as the concentrations of both components became lower than those in 25 mM phosphate buffer by 10 minutes. These dissolution profiles suggest that the conversion rate of CBZ-SLC is much faster in 50 mM phosphate buffer than in 25 mM phosphate buffer. As shown in Table 6.2, the CSC for CBZ-SLC in 50 mM phosphate buffer is 5.7x larger than 150 mM SLS, while for 25 mM phosphate buffer is only 1.9x. The higher supersaturation generated with respect to the parent drug during the dissolution of CBZ-SLC in 50 mM phosphate buffer leads to faster conversion rate compared

to that in 25 mM phosphate buffer. In order to capture the true dissolution rates of CBZ-SLC, linear regressions were fitted using the first 4 data points for 25 mM phosphate buffer and first 3 data points for 50 mM phosphate buffer. The dissolution experiments of CBZ-SLC in 25 and 50 mM phosphate buffer at bulk pH 6 are shown in Figure 6.4. There was no solid phase transformation observed during dissolution for these two conditions, which is expected because the CSC values are below 150 mM SLS.

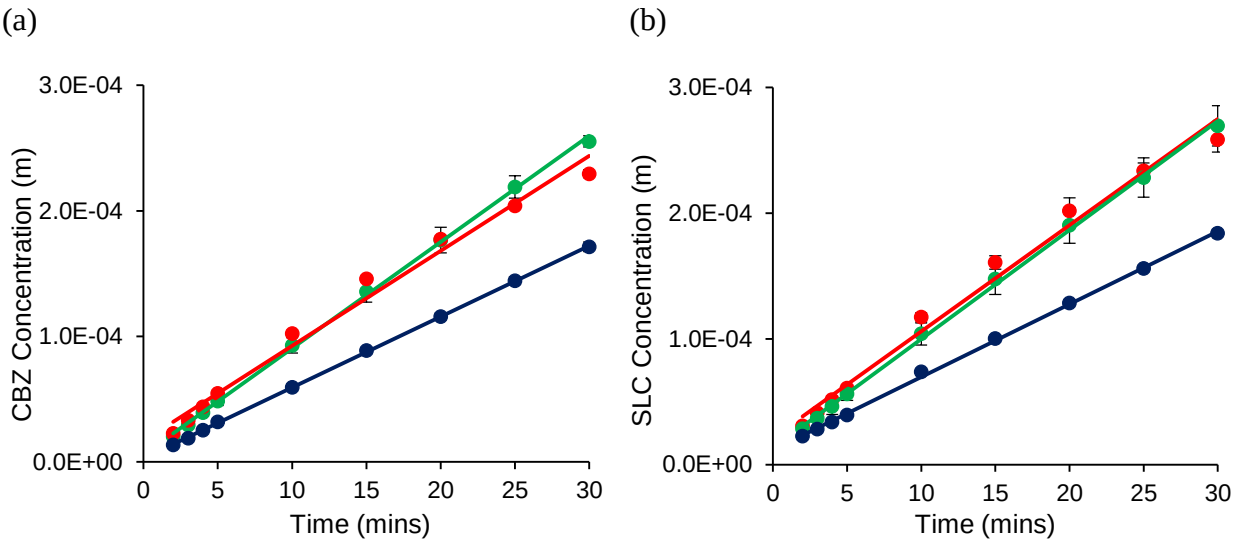

Figure 6.2. Dissolution profiles of CBZ-SLC in terms of CBZ concentrations (a) and SLC concentrations (b) in 150 mM SLS at different bulk pH and acetate buffer concentrations. 25 mM acetate buffer at pH 4.80: •; 50 mM acetate buffer at pH 4.85: •; 50 mM acetate buffer at pH 3.97: •. The solid circles are the experimental data and the lines are the fitted linear regressions.

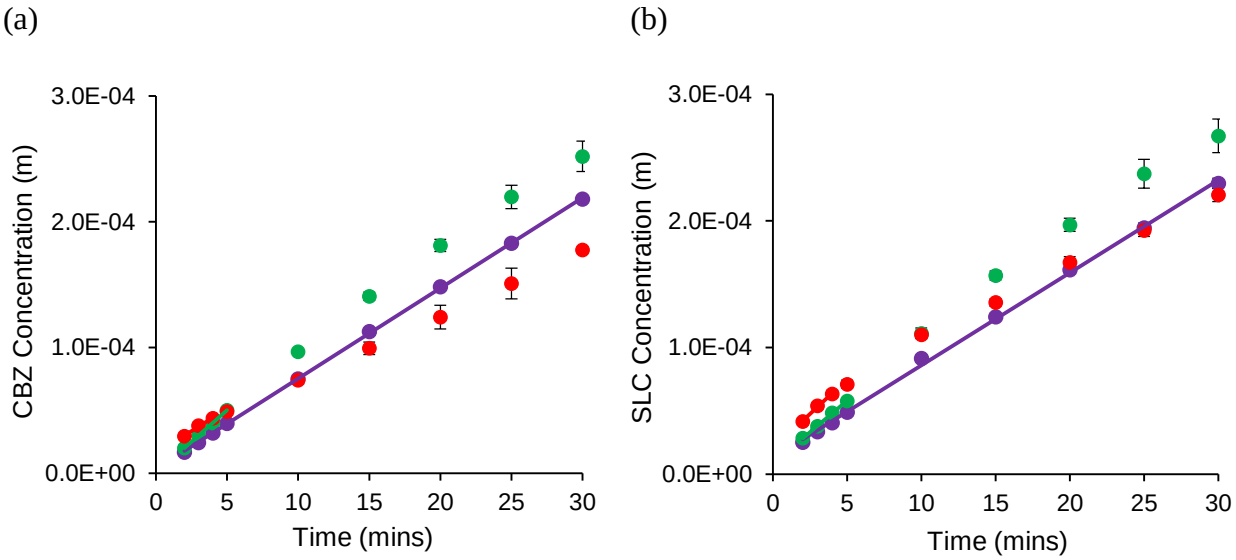

Figure 6.3. Dissolution profiles for CBZ-SLC in terms of CBZ concentrations (a) and SLC concentrations (b) in 150 mM SLS at different bulk pH and phosphate buffer concentrations. 15 mM phosphate buffer at pH 6.84: ●; 25 mM phosphate buffer at pH 6.79: ●; 50 mM phosphate buffer at pH 6.78: ●. The solid circles are the experimental data and the lines are the fitted linear regressions.

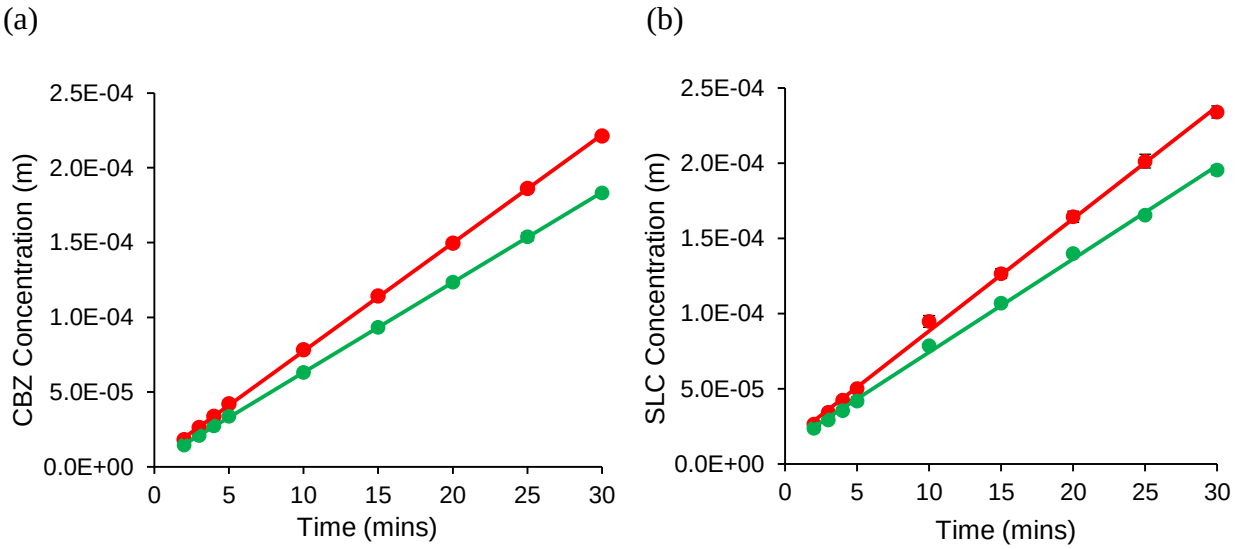

Figure 6.4. Dissolution profiles for CBZ-SLC in terms of CBZ concentrations (a) and SLC concentrations (b) in 150 mM SLS at different bulk pH and phosphate buffer concentrations. 25 mM phosphate buffer at pH 6.03: ●; 50 mM phosphate at pH 6.03: ●. The solid circles are the experimental points and the lines are the fitted linear regressions.

Evaluation of the mass transport model

To evaluate the predictive power of the mass transport model, the flux of CBZ-SLC in different buffer concentrations were calculated from the dissolution rates and compared to the theoretical predictions. The influence of pH and buffer concentration on the dissolution of CBZ-SLC is shown in Figure 6.5. The dissolution pH dependence of CBZ-SLC relies on the interfacial pH rather than bulk pH. Buffering agents have the ability to alter the interfacial pH and this ability is dependent on the properties and concentrations of the buffer. Therefore, the dissolution pH dependence of CBZ-SLC can vary depending on the types and concentrations of the buffer. As buffer concentration increases, interfacial pH increases due to the consumption of hydrogen ion at the dissolving surface and consequently, the flux of CBZ-SLC would increase because of the acidity of the coformer. Due to the rapid conversion of the cocrystal back to the parent drug, the concentration profile of CBZ-SLC in pH 6.78, 50 mM phosphate buffer shown in Figure 6.3 (a) represents the drug dissolution more than the cocrystal dissolution. Therefore, the flux of CBZ-SLC at this condition was calculated using the first 3 data points from the dissolution concentration profile in terms of SLC shown in Figure 6.3 (b) and compared to the theoretical flux in Figure 6.5. As shown in Figure 6.5, the theoretical predictions agree reasonably well with the experimental data. Some large deviations, such as at bulk pH 4.85, 50 mM acetate buffer and pH 6.78, 50 mM phosphate buffer, are due to the conversion of the cocrystal during dissolution. The precipitation of the dihydrated form of CBZ at the dissolving surface impeded the dissolution of CBZ-SLC and resulted in lower flux. The mass transport model in this study has not considered the cocrystal conversion, so the flux predictions would be overestimated when conversion happens during dissolution.

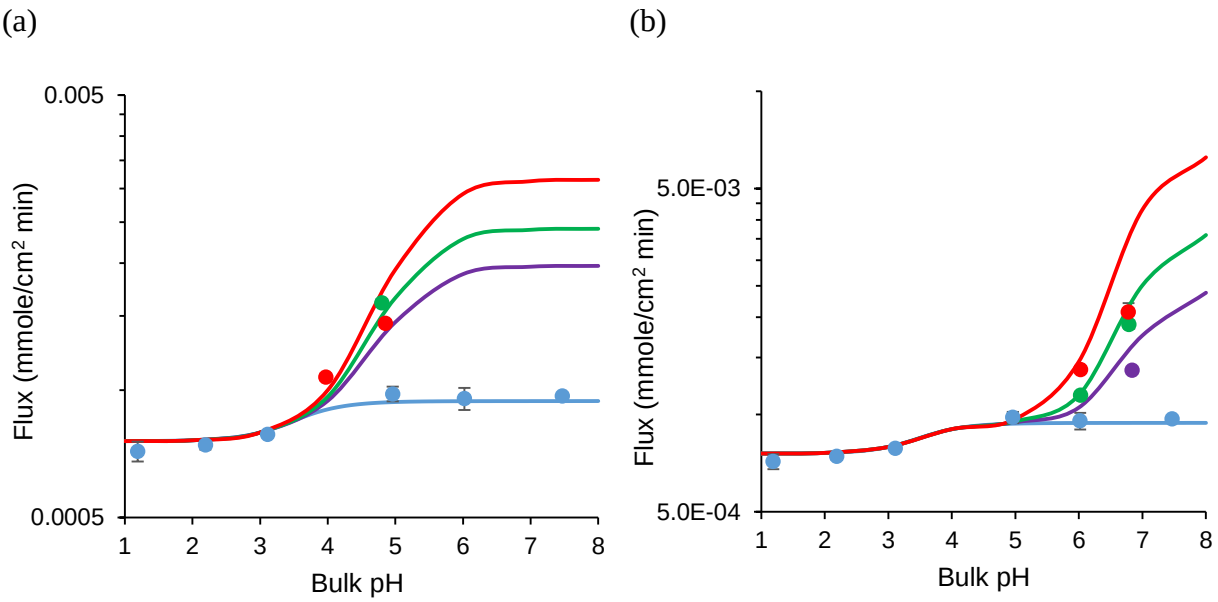

Figure 6.5. Flux of CBZ-SLC at 150 mM SLS as a function of bulk pH in acetate buffer (a) and phosphate buffer (b) solutions. 50 mM buffer: —; 25 mM buffer: —;15 mM buffer: —; and 0 mM buffer: —. Solid circles are experimental flux values of CBZ-SLC in terms of CBZ, except for pH 6.78, 50 mM phosphate buffer, which is in terms of SLC. Solid lines are theoretical flux predictions. The theoretical and experiment flux in 0 mM buffer are from reference [15]. The flux in the presence of buffer were calculated using equation 6A.40 from Appendix 6A based on the interfacial pH predicted in Figure 6.1.

Conclusions

The mass transport model for the dissolution of 1:1 cocrystals with nonionizable drugs and monoacidic coformers has been successfully extended to evaluate the effect of buffer on the dissolution rates of these cocrystals. The model was extended to include the simultaneous chemical reactions of the acidic coformer with the basic buffer species within the hydrodynamic boundary layer. The influence of buffer on interfacial pH can be accurately predicted using this mass transport model and the ability of buffer in altering this pH is dependent on the pK_a value, diffusion coefficient and concentration of the buffer. The two buffering agents used in this study, acetate and phosphate buffers, elevate the interfacial pH of CBZ-SLC in 150 mM SLS compared to that without buffer and this elevation increases with increasing buffer concentration. Based on

the interfacial pH predictions, the flux of CBZ-SLC can be adequately predicted as a function of buffer concentration. Due to the acidity of the coformer, the flux of CBZ-SLC increases as a function of buffer concentration because interfacial pH is evaluated by the presence of buffer. This study emphasizes the importance of including any parameters that can influence the pH at the dissolving surface in the mass transport analyses in order to obtain accurate flux predictions for ionizable compounds.

References

1. Mooney, K. G.; Mintun, M. A.; Himmelstein, K. J.; Stella, V. J. Dissolution Kinetics of Carboxylic Acids I: Effect of pH under Unbuffered Conditions. *American Pharmaceutical Association* **1981,** *70*, (1), 13-22.
2. Mooney, K. G.; Mintun, M. A.; Himmelstein, K. J.; Stella, V. J. Dissolution Kinetics of Carboxylic Acids II: Effect of Buffers. *American Pharmaceutical Association* **1981,** *70*, (1), 22-32.
3. Aunins, J. G.; Southard, M. Z.; Myers, R. A.; Himmelstein, k. J.; Stella, V. J. Dissolution of Carboxylic Acids III: The effect of Polyionizable Buffers. *Journal of Pharmaceutical Sciences* **1985,** *74*, (12), 1305-1316.
4. McNamara, D. P.; Amidon, G. L. Reaction Plane Approach for Estimating the Effects of Buffers on the Dissolution Rate of Acidic Drugs. *Journal of Pharmaceutical Sciences* **1988,** *77*, (6), 511-517.
5. Sheng, J. J.; McNamara, D. P.; Amidon, G. L. Toward an *In Vivo* Dissolution Methodology: a Comparison of Phosphate and Bicarbonate Buffers. *Molecular Pharmaceutics* **2009,** *6*, (1), 29-39.
6. Krieg, B. J. In Vivo Predictive Dissolution: Analyzing the Impact of Bicarbonate Buffer and Hydrodynamics on Dissolution. *University of Michigan* **2015,** *Dissertation*.
7. Rune, S. J. Acid-Base Parameters of Duodenal Contents in Man *Gastroenterology* **1972,** *62*, (4), 533-539.
8. Rees, W. D. W.; Botham, D.; Turnberg, L. A. A Demonstration of Bicarbonate Production by the Normal Human Stomach *In Vivo*. *Digestive Diseases and Sciences* **1982,** *27*, (11), 961-966.

9. Hogan, D. L.; Ainsworth, M. A.; Isenberg, J. I. Review Article: Gastroduodenal Bicarbonate Secretion. *Alimentary Pharmacology & Therapeutics* **1994,** *8,* (5), 475-88.

10. Vertzoni, M.; Fotaki, N.; Kostewicz, E.; Stippler, E.; Leuner, C.; Nicolaides, E.; Dressman, J.; Reppas, C. Dissolution Media Simulating the Intralumenal Composition of the Small Intestine: Physiological Issues and Practical Aspects. *Journal of Pharmacy and Pharmacology* **2004,** *56,* (4), 453-462.

11. Dressman, J. B.; Amidon, G. L.; Reppas, C.; Shah, V. P. Dissolution Testing as a Prognostic Tool for Oral Drug Absorption: Immediate Release Dosage Forms. *Pharmaceutical Research* **1998,** *15,* (1), 11-22.

12. Levy, G.; Hayes, B. A. Physicochemical Basis of the Buffered Acetylsalicylic Acid Controversy. *N. Engl. J. Med.* **1960,** *262,* 1053-1058.

13. Doherty, C.; York, P. Microenvironmental pH Control of Drug Dissolution. *International Journal of Pharmaceutices* **1988,** *50,* (3), 223-232.

14. Chakrabarti, S.; Southard, M. Z. Control of Poorly Soluble Drug Dissolution in Conditions Simulating the Gastrointestinal Tract Flow. 2. Cocompression of Drugs with Buffers. *American Chemical Society and American Pharmaceutical Association* **1996,** *86,* (4), 465-469.

15. Cao, F.; Amidon, G.; Rodriguez-Hornedo, N.; Amidon, G. Mechanistic Analysis of Cocrystal Dissolution as a Function of pH and Micellar Solubilization. *Molecular Pharmaceutics* **2015,** *13,* (3), 1030-1046.

16. Rodriguez-Hornedo, N.; Nehm, S. J.; Seefeldt, K. F.; Pagan-Torres, Y.; Falkiewicz, C. J. Reaction Crystallization of Pharmaceutical Molecular Complexes. *Molecular Pharmaceutics* **2006,** *3,* (3), 362-367.

17. Kabir-ud-Din; David, S. L.; Kumar, S. Viscosities of Sodium Dodecyl Sulfate Solutions in Aqueous Ammonium Salts. *Journal of Chemical & Engineering Data* **1997,** *42,* (6), 1224-1226.

18. Poskanzer, A. M.; Goodrich, F. C. Surface Viscosity of Sodium Dodecyl Sulfate Solutions with and without Added Dodecanol. *The Journal of Physical Chemistry* **1975,** *79,* (20), 2122-2126.

19. Huang, N.; Rodriguez-Hornedo, N. Effect of Micellar Solubilization on Cocrystal Solubility and Stability. *Crystal Growth & Design* **2010,** *10,* 2050-2053.

20. Huang, N.; Rodriguez-Hornedo, N. Engineering Cocrystal Solubility, Stability, and pHmax by Micellar Solubilization. *Journal of Pharmaceutical Sciences* **2011,** *100,* (12), 5219-5234.

21. Huang, N.; Rodriguez-Hornedo, N. Engineering Cocrystal Thermodynamic Stability and Eutectic Points by Micellar Solubilization and Ionization. *CrystEngComm* **2011,** *13*, 5409-5422.

APPENDIX 6A

The flux of all the species across the diffusion layer includes both the diffusion and chemical reactions happening during dissolution. At steady state, the diffusion and simultaneous chemical reactions of the individual species within the diffusion layer can be written using Fick's law as follows:

$$\frac{\partial [R]_{aq}}{\partial t} = D_{R_{aq}} \frac{\partial^2 [R]_{aq}}{\partial x^2} + \phi_1 = 0 \quad (6A.1)$$

$$\frac{\partial [R]_m}{\partial t} = D_{R_m} \frac{\partial^2 [R]_m}{\partial x^2} + \phi_2 = 0 \quad (6A.2)$$

$$\frac{\partial [HA]_{aq}}{\partial t} = D_{HA_{aq}} \frac{\partial^2 [HA]_{aq}}{\partial x^2} + \phi_3 = 0 \quad (6A.3)$$

$$\frac{\partial [A^-]_{aq}}{\partial t} = D_{A^-_{aq}} \frac{\partial^2 [A^-]_{aq}}{\partial x^2} + \phi_4 = 0 \quad (6A.4)$$

$$\frac{\partial [HA]_m}{\partial t} = D_{HA_m} \frac{\partial^2 [HA]_m}{\partial x^2} + \phi_5 = 0 \quad (6A.5)$$

$$\frac{\partial [OH^-]}{\partial t} = D_{OH^-} \frac{\partial^2 [OH^-]}{\partial x^2} + \phi_6 = 0 \quad (6A.6)$$

$$\frac{\partial [H^+]}{\partial t} = D_{H^+} \frac{\partial^2 [H^+]}{\partial x^2} + \phi_7 = 0 \quad (6A.7)$$

$$\frac{\partial [\mathrm{BH}^+]_{aq}}{\partial \mathrm{t}} = \mathrm{D}_{\mathrm{BH}^+} \frac{\partial^2 [\mathrm{BH}^+]_{aq}}{\partial \mathrm{x}^2} + \phi_8 = 0 \quad (6A.8)$$

$$\frac{\partial [B]_{aq}}{\partial \mathrm{t}} = \mathrm{D}_B \frac{\partial^2 [\mathrm{B}]_{aq}}{\partial \mathrm{x}^2} + \phi_9 = 0 \quad (6A.9)$$

where $\phi_{1\text{-}9}$ are the reaction rate functions. At equilibrium, the reaction rate of the reactant should be the opposite of the product. Based on the chemical equilibria, the followings can be written:

$$\phi_1 = -\phi_2 \tag{6A.10}$$

$$\phi_3 = -\phi_4 - \phi_5 \tag{6A.11}$$

$$\phi_8 = -\phi_9 \tag{6A.12}$$

Because of A^- is a product of the reactions between HA, B and BH^+, so reaction rate of A^- can be reflected by the reaction rate of B, H^+ and OH^-, therefore,

$$\phi_4 = \phi_7 - \phi_6 - \phi_9 \tag{6A.13}$$

Based on equation 6A.13, equation 6A.11 can be written as:

$$\phi_3 = \phi_6 + \phi_9 - \phi_5 - \phi_7 \tag{6A.14}$$

Based on the equations 6A.10, 6A.11, 6A.12 and 6A.14, the following mass balance equations can be written:

$$D_{R_{aq}} \frac{d^2\,[R]_{aq}}{dx^2} = -D_{R_m} \frac{d^2\,[R]_m}{dx^2} \tag{6A.15}$$

$$D_{HA_{aq}} \frac{d^2\,[HA]_{aq}}{dx^2} = -D_{A^-_{aq}} \frac{d^2[A^-]_{aq}}{dx^2} - D_{HA_m} \frac{d^2\,[HA]_m}{dx^2} \tag{6A.16}$$

$$D_{HA_{aq}} \frac{d^2\,[HA]_{aq}}{dx^2} = D_{OH^-} \frac{d^2\,[OH^-]}{dx^2} + D_{B_{aq}} \frac{d^2\,[B]_{aq}}{dx^2} - D_{H^+} \frac{d^2[H^+]}{dx^2} - D_{HA_m} \frac{d^2\,[HA]_m}{dx^2} \tag{6A.17}$$

$$D_{B_{aq}} \frac{d^2\,[B]_{aq}}{dx^2} = -D_{BH^+_{aq}} \frac{d^2\,[BH^+]_{aq}}{dx^2} \tag{6A.18}$$

Integrating equations 6A.15 to 6A.18 once gives:

$$D_{R_{aq}} \frac{d[R]_{aq}}{dx} = -D_{R_m} \frac{d\,[R]_m}{dx} + C_1 \quad (6A.19)$$

$$D_{HA_{aq}} \frac{d\,[HA]_{aq}}{dx} = -D_{A^-_{aq}} \frac{d[A^-]_{aq}}{dx} - D_{HA_m} \frac{d\,[HA]_m}{dx} + C_2 \quad (6A.20)$$

$$D_{HA_{aq}} \frac{d\,[HA]_{aq}}{dx} = D_{OH^-} \frac{d\,[OH^-]}{dx} + D_{B_{aq}} \frac{d\,[B]_{aq}}{dx} - D_{H^+} \frac{d[H^+]}{dx} - D_{HA_m} \frac{d\,[HA]_m}{dx} + C_3 \quad (6A.21)$$

$$D_{B_{aq}} \frac{d\,[B]_{aq}}{dx} = -D_{BH^+_{aq}} \frac{d\,[BH^+]_{aq}}{dx} + C_4 \quad (6A.22)$$

Since A^-_{aq} is the product of the reaction between HA, B and OH^-, so its flux can be reflected by B, OH^- and H^+:

$$-D_{A^-_{aq}} \frac{d[A^-]_{aq}}{dx} = D_{OH^-} \frac{d\,[OH^-]}{dx} + D_{B_{aq}} \frac{d\,[B]_{aq}}{dx} - D_{H^+} \frac{d[H^+]}{dx} \quad (6A.23)$$

With this mass balance relationship, it can be seen that

$$C_2 = C_3 \quad (6A.24)$$

Since the concentration of buffer is conserved, the total flux of buffer should be equal to zero, therefore,

$$C_4 = 0 \quad (6A.25)$$

Integrating equations 6A.19 to 6A.22 once gives:

$$D_{R_{aq}}[R]_{aq} = -D_{R_m}[R]_m + C_1 x + C_5 \quad (6A.26)$$

$$D_{HA_{aq}}[HA]_{aq} = -D_{HA_m}[HA]_m - D_{A^-_{aq}}[A^-]_{aq} + C_2 x + C_6 \quad (6A.27)$$

$$D_{HA_{aq}}[HA]_{aq} = D_{OH^-}[OH^-] + D_{B_{aq}}[B]_{aq} - D_{H^+}[H^+] - D_{HA_m}[HA]_m + C_3 x + C_7 \quad (6A.28)$$

$$D_{B_{aq}}[B]_{aq} + D_{BH^+_{aq}}[BH^+]_{aq} = C_8 \quad (6A.29)$$

Boundary conditions

Based on the surface saturation model and solubility of cocrystal under surfactant conditions, the following boundary conditions for each species can be written:

At $x = 0$:	at $x = h$:
$[R]_{aq,0} = \frac{\sqrt{K_{sp}(1+K_S^R[m])(1+\frac{K_a}{H_0^+}+K_S^{HA}[m])}}{1+K_S^R[m]}$	$[R]_{aq,h} = 0$ (under sink condition)
$[HA]_{aq,0} = (\frac{D_{R_{eff}}}{D_{HA_{eff}}})^{2/3} \frac{\sqrt{K_{sp}(1+K_S^R[m])(1+\frac{K_a}{H_0^+}+K_S^{HA}[m])}}{1+\frac{K_a}{H_0^+}+K_S^{HA}[m]}$	$[HA]_{aq,h} = 0$ (under sink condition)
$[R]_{m,0} = unknown$	$[R]_{m,h} = 0$ (under sink condition)
$[HA]_{m,0} = unknown$	$[HA]_{m,h} = 0$ (under sink condition)
$[A^-]_{aq,0} = unknown$	$[A^-]_{aq,h} = 0$ (under sink condition)
$[B]_{aq} = [B]_0$	$[B]_{aq} = [B]_h$
$[BH^+]_{aq} = [BH^+]_0$	$[BH^+]_{aq} = [BH^+]_h$
$[H^+] = [H^+]_0$	$[H^+] = [H^+]_h$
$[OH^-] = [OH^-]_0$	$[OH^-] = [OH^-]_h$

Evaluation of interfacial pH

Applying the above boundary conditions to equations 6A.27 to 6A.29, at $x = 0$:

$$D_{HA_{aq}}(\frac{D_{R_{eff}}}{D_{HA_{eff}}})^{2/3} \frac{\sqrt{K_{sp}(1+K_S^R[m])(1+\frac{K_a}{H_0^+}+K_S^{HA}[m])}}{1+\frac{K_a}{H_0^+}+K_S^{HA}[m]} = -D_{HA_m}[HA]_{m,0} - D_{A_{aq}^-}[A^-]_{aq,0} + C_6 \qquad (6A.30)$$

$$D_{HA_{aq}}\left(\frac{D_{R_{eff}}}{D_{HA_{eff}}}\right)^{2/3}\frac{\sqrt{K_{sp}\left(1+K_s^R[m]\right)\left(1+\frac{K_a}{H_0^+}+K_s^{HA}[m]\right)}}{1+\frac{K_a}{H_0^+}+K_s^{HA}[m]} = D_{OH^-}[OH^-]_0 + D_{B_{aq}}[B]_0 -$$

$$D_{H^+}[H^+]_0 - D_{HA_m}[HA]_{m,0} + C_7 \quad \text{(6A.31)}$$

$$D_{B_{aq}}[B]_0 + D_{BH^+_{aq}}[BH^+]_0 = C_8 \quad \text{(6A.32)}$$

and at $x = h$, since sink conditions are assumed, 6A.27 to 6A.29 can be written as:

$$C_2 h + C_6 = 0 \quad \text{(6A.33)}$$

$$0 = D_{OH^-}[OH^-]_h + D_{B_{aq}}[B]_h - D_{H^+}[H^+]_h + C_3 h + C_7 \quad \text{(6A.34)}$$

$$D_{B_{aq}}[B]_h + D_{BH^+_{aq}}[BH^+]_h = C_8 \quad \text{(6A.35)}$$

Combining equations 6A.30 to 6A.35 and algebraically solving for interfacial pH, $[H^+]_0$, yields the following equation:

$$A[H^+]_0{}^7 + B[H^+]_0{}^6 + C[H^+]_0{}^5 + D[H^+]_0{}^4 + E[H^+]_0{}^3 + F[H^+]_0{}^2 + G[H^+]_0 + H = 0 \quad \text{(6A.36)}$$

where

$$A = (D_{H^+}D_{BH^+_{aq}})^2(1 + K_s^{HA}[m]);$$

$$B = 2D_{H^+}D_{BH^+_{aq}}[D_{H^+}\mathrm{D_{B_{aq}}K_a^B} + D_{BH^+_{aq}}\left(\mathrm{D_{B_{aq}}[B]_h} - D_{H^+}[H^+]_h + D_{OH^-}[OH^-]_h\right)](1 + K_s^{HA}[m]);$$

$$C = 2D_{H^+}D_{BH^+_{aq}}\left[\mathrm{D_{B_{aq}}K_a^B}\left(D_{OH^-}[OH^-]_h - D_{BH^+_{aq}}[BH^+]_h - D_{H^+}[H^+]_h\right) - D_{OH^-}K_w D_{BH^+_{aq}}\right](1 + K_s^{HA}[m]) + (1 + K_s^{HA}[m])\left[D_{H^+}\mathrm{D_{B_{aq}}K_a^B} + D_{BH^+_{aq}}\left(\mathrm{D_{B_{aq}}[B]_h} - D_{H^+}[H^+]_h + D_{OH^-}[OH^-]_h\right)\right]^2 + 2\mathrm{K_a^{HA}}D_{H^+}D_{BH^+_{aq}}[D_{H^+}\mathrm{D_{B_{aq}}K_a^B} + D_{BH^+_{aq}}\left(\mathrm{D_{B_{aq}}[B]_h} - D_{H^+}[H^+]_h + D_{OH^-}[OH^-]_h\right)];$$

$$D = 2\left[D_{H^+}\mathrm{D_{B_{aq}}K_a^B} + D_{BH^+_{aq}}\left(\mathrm{D_{B_{aq}}[B]_h} - D_{H^+}[H^+]_h + D_{OH^-}[OH^-]_h\right)\right]\left[\mathrm{D_{B_{aq}}K_a^B}\left(D_{OH^-}[OH^-]_h - D_{BH^+_{aq}}[BH^+]_h - D_{H^+}[H^+]_h\right) - D_{OH^-}K_w D_{BH^+_{aq}}\right](1 +$$

$K_s^{HA}[m]) - 2D_{H^+}D_{BH_{aq}^+}D_{OH^-}K_w\mathrm{D_{B_{aq}}}\mathrm{K_a^B}(1 + K_s^{HA}[m]) +$
$2D_{H^+}D_{BH_{aq}^+}\mathrm{K_a^{HA}}\left[\mathrm{D_{B_{aq}}}\mathrm{K_a^B}\left(D_{OH^-}[OH^-]_h - D_{BH_{aq}^+}[BH^+]_h - D_{H^+}[H^+]_h\right) - D_{OH^-}K_wD_{BH_{aq}^+}\right] +$
$[D_{H^+}\mathrm{D_{B_{aq}}}\mathrm{K_a^B} + D_{BH_{aq}^+}\left(\mathrm{D_{B_{aq}}}[\mathrm{B}]_\mathrm{h} - D_{H^+}[H^+]_h + D_{OH^-}[OH^-]_h\right)]^2\mathrm{K_a^{HA}};$

$E = \left[\mathrm{D_{B_{aq}}}\mathrm{K_a^B}\left(D_{OH^-}[OH^-]_h - D_{BH_{aq}^+}[BH^+]_h - D_{H^+}[H^+]_h\right) - D_{OH^-}K_wD_{BH_{aq}^+}\right]^2(1 +$
$K_s^{HA}[m]) - 2D_{OH^-}K_w\mathrm{D_{B_{aq}}}\mathrm{K_a^B}\left[D_{H^+}\mathrm{D_{B_{aq}}}\mathrm{K_a^B} + D_{BH_{aq}^+}\left(\mathrm{D_{B_{aq}}}[\mathrm{B}]_\mathrm{h} - D_{H^+}[H^+]_h +\right.\right.$
$\left.\left.D_{OH^-}[OH^-]_h\right)\right](1 + K_s^{HA}[m]) - 2D_{H^+}D_{BH_{aq}^+}D_{OH^-}K_w\mathrm{D_{B_{aq}}}\mathrm{K_a^B}\mathrm{K_a^{HA}} + 2\left[D_{H^+}\mathrm{D_{B_{aq}}}\mathrm{K_a^B} +\right.$
$\left.D_{BH_{aq}^+}\left(\mathrm{D_{B_{aq}}}[\mathrm{B}]_\mathrm{h} - D_{H^+}[H^+]_h + D_{OH^-}[OH^-]_h\right)\right]\left[\mathrm{D_{B_{aq}}}\mathrm{K_a^B}\left(D_{OH^-}[OH^-]_h - D_{BH_{aq}^+}[BH^+]_h -\right.\right.$
$\left.\left.D_{H^+}[H^+]_h\right) - D_{OH^-}K_wD_{BH_{aq}^+}\right]\mathrm{K_a^{HA}} - (D_{A_{aq}^-}^{1/3}D_{R_{eff}}^{2/3}\mathrm{D_{B_{aq}}}\mathrm{K_a^{HA}}\sqrt{K_{sp}(1 + K_s^R[m])})^2;$

$F = \mathrm{K_a^{HA}}\left[\mathrm{D_{B_{aq}}}\mathrm{K_a^B}\left(D_{OH^-}[OH^-]_h - D_{BH_{aq}^+}[BH^+]_h - D_{H^+}[H^+]_h\right) - D_{OH^-}K_wD_{BH_{aq}^+}\right]^2 -$
$2D_{OH^-}K_w\mathrm{D_{B_{aq}}}\mathrm{K_a^B}\left[\mathrm{D_{B_{aq}}}\mathrm{K_a^B}\left(D_{OH^-}[OH^-]_h - D_{BH_{aq}^+}[BH^+]_h - D_{H^+}[H^+]_h\right) -\right.$
$\left.D_{OH^-}K_wD_{BH_{aq}^+}\right](1 + K_s^{HA}[m]) - 2D_{OH^-}K_w\mathrm{D_{B_{aq}}}\mathrm{K_a^B}\mathrm{K_a^{HA}}\left[D_{H^+}\mathrm{D_{B_{aq}}}\mathrm{K_a^B} + D_{BH_{aq}^+}\left(\mathrm{D_{B_{aq}}}[\mathrm{B}]_\mathrm{h} -\right.\right.$
$\left.\left.D_{H^+}[H^+]_h + D_{OH^-}[OH^-]_h\right)\right] - 2\mathrm{K_a^B}(D_{A_{aq}^-}^{1/3}D_{R_{eff}}^{2/3}\mathrm{D_{B_{aq}}}\mathrm{K_a^{HA}}\sqrt{K_{sp}(1 + K_s^R[m])})^2;$

$G = (D_{OH^-}K_w\mathrm{D_{B_{aq}}}\mathrm{K_a^B})^2(1 + K_s^{HA}[m]) - 2D_{OH^-}K_w\mathrm{D_{B_{aq}}}\mathrm{K_a^B}\mathrm{K_a^{HA}}\left[\mathrm{D_{B_{aq}}}\mathrm{K_a^B}\left(D_{OH^-}[OH^-]_h -\right.\right.$
$\left.\left.D_{BH_{aq}^+}[BH^+]_h - D_{H^+}[H^+]_h\right) - D_{OH^-}K_wD_{BH_{aq}^+}\right] - (D_{A_{aq}^-}^{1/3}D_{R_{eff}}^{2/3}\mathrm{D_{B_{aq}}}\mathrm{K_a^{HA}}\mathrm{K_a^B}\sqrt{K_{sp}(1 + K_s^R[m])})^2;$
$H = \mathrm{K_a^{HA}}(D_{OH^-}K_w\mathrm{D_{B_{aq}}}\mathrm{K_a^B})^2.$

Evaluation of flux of the cocrystal components:

Applying the boundary conditions to equation 6A.26, at *x = 0*:

$$D_{R_{aq}}\frac{\sqrt{K_{sp}(1+K_s^R[m])(1+\frac{K_a}{H_0^+}+K_s^{HA}[m])}}{1+K_s^R[m]} = -D_{R_m}K_s^R[m]\frac{\sqrt{K_{sp}(1+K_s^R[m])(1+\frac{K_a}{H_0^+}+K_s^{HA}[m])}}{1+K_s^R[m]} + C_5 \qquad (6A.37)$$

and at *x = h*, assuming sink conditions:

$$0 = C_1h + C_5 \qquad (6A.38)$$

Combining the above equations and solving for $-C_1$ for the flux of the cocrystal in terms of drug:

$$J_R = \frac{D_{R_{eff}}}{h_R}\sqrt{K_{sp}(1 + K_S^R[m])(1 + \frac{K_a}{H_0^+} + K_S^{HA}[m])} \quad (6A.39)$$

By substituting the thickness of the hydrodynamic boundary layer for rotating disk ($h = 1.612 D^{\frac{1}{3}} v^{\frac{1}{6}} \omega^{-\frac{1}{2}}$)[1], equation 6A.39 becomes:

$$J_R = 0.62 D_{R_{eff}}^{2/3} \omega^{1/2} v^{-1/6} \sqrt{K_{sp}(1 + K_S^R[m])(1 + \frac{K_a}{H_0^+} + K_S^{HA}[m])} \quad (6A.40)$$

The flux of the cocrystal in terms of coformer can be also solved in a similar manner by applying the boundary conditions to equation 6A.27:

$$J_{HA} = \frac{D_{HA_{eff}}^{\frac{1}{3}} D_{R_{eff}}^{\frac{2}{3}}}{h_{HA}}\sqrt{K_{sp}(1 + K_S^R[m])(1 + \frac{K_a}{H_0^+} + K_S^{HA}[m])} \quad (6A.41)$$

By substituting the boundary layer thickness into equation 6A.41, it can be shown to equal to equation 6A.40. This is expected since the flux of drug and coformer should be the same for a 1:1 cocrystal even though they have different diffusivities.

CHAPTER 7

CONCLUSIONS AND FUTURE DIRECTIONS

The fundamental frameworks have been built in this dissertation to understand the dissolution behavior of cocrystals under different solution conditions. Unlike the empirical approaches that are based on experimental observations, this thesis relies on the mass transport phenomenon to explain the dissolution behavior of cocrystals. The mechanism of cocrystal dissolution has been investigated through the development of mass transport models by applying Fick's law of diffusion to dissolution with simultaneous chemical reactions in the hydrodynamic boundary layer adjacent to the dissolving cocrystal solid surface. These mass transport models have emphasized the importance of physicochemical properties of the cocrystal components and solution conditions in determining the rates of cocrystal dissolution. Overall, this dissertation has provided the fundamental knowledge of cocrystal dissolution that is important for the cocrystal selection process and formulation development.

Based on the differential diffusion between the cocrystal components and the solubility product behavior of the cocrystals, two models, the surface saturation and interfacial equilibrium models have been developed to describe the dissolution process of cocrystals. The major differences between the two models are related to the boundary conditions of the cocrystal components at the dissolving solid-liquid interface due to the different ability of the models in maintaining the solubility product of the cocrystal. The different boundary conditions of the two models lead to different mass transport analyses that would result in different theoretical

predictions in interfacial pH and flux of the cocrystals. The better agreement between the experimental and theoretical flux makes the surface saturation model superior to the interfacial equilibrium model. Consequently, the surface saturation model was primarily used in this dissertation to perform mass transport analyses for evaluating the dissolution behavior of cocrystals in different solution conditions.

By validating the surface saturation model, the common coformer effect on the dissolution rates of cocrystals was also evaluated in this thesis. Similar to pharmaceutical salts, cocrystals also exhibit solubility product behavior. Therefore, the dissolution rates of cocrystals would decrease in the presence of excess coformer. These findings have provided useful insights for the effect of differential permeation between the cocrystal components on oral absorption. The higher drug permeation can potentially result in excess coformer in the intestine that can decrease the dissolution rate of the continually dissolving cocrystal and consequently, result in lower oral absorption.

One of the important findings of this thesis is that the interfacial pH is the significant factor that determines the dissolution rates of cocrystals with ionizable components. By cocrystallizing with different coformers, interfacial pH can be modulated to different extents compared to the parent drugs. For example, CBZ is nonionizable, so it has no ability to alter the pH at the dissolving surface and this means that the interfacial pH is the same as the bulk pH. However, when it cocrystallizes with acidic coformers, SAC and SLC, interfacial pH is significantly different from the bulk solution pH. For both cocrystals, interfacial pH decrease as coformers start to ionize and reach constant values at bulk pH ranges from 4 to 8 due to the self-buffering ability of the cocrystals. Similarly, KTZ cocrystals with acidic coformers also lower the interfacial pH compared to the basic KTZ. Besides the physicochemical properties of the cocrystals and their

components, solution composition, such as buffering agents can also affect the interfacial pH. The presence of acetate and phosphate buffers elevates the interfacial pH of CBZ-SLC due to the chemical reactions between the acidic coformer and basic buffer components at the dissolving surface. The mass transport models developed in this thesis are able to capture the interfacial pH behavior and allow accurate flux predictions for cocrystals under different solution conditions. Cocrystallization can not only modulate the interfacial pH, but also the dissolution pH dependence of the parent drugs.

Besides solubility advantage, cocrystals can also exhibit diffusivity advantage over the parent drug in the presence of surfactant. The effective diffusion coefficients of CBZ as a function of SLS were found to be smaller than those of the cocrystals. These differential diffusion coefficients could be potentially due to the different solubility dependence on SLS between the drug and cocrystals. Having higher diffusion coefficients, cocrystals would require lower or even no solubility advantages to maintain higher dissolution rates compared to the parent drugs. One of the challenges for current cocrystal development is the potential instability of the highly soluble cocrystals in solution. Therefore, the ability of identifying the conditions in which the cocrystals can exhibit both thermodynamic stability and dissolution advantage is important for formulation development.

The important physicochemical parameters have been established in this dissertation to predict the *in vitro* dissolution behavior of cocrystals. Moving forward with this project, *in vivo* predictive dissolution is the next logical direction. The dissolution conditions in this thesis did not accurately reflect the physiological environment of the human GI tract. Therefore, future dissolution studies should consider using biorelevant media, such as Fasted and Fed State Simulated Intestinal Fluids (FaSSIF and FeSSIF) at body temperature. Both FaSSIF and FeSSIF

contain physiologically relevant surfactants (such as bile salts and phospholipids) and buffer species that can influence the dissolution behavior of cocrystals. Although the mass transport models in this dissertation have considered both of these parameters, the power of these models in predicting the dissolution behavior of cocrystals in biorelevant media still remains to be explored. In order to be more physiologically relevant, future dissolution studies should also consider using powder dissolution instead of the current rotating disk dissolution. Although there are more parameters, such as particle sizes and surface areas that need to be considered for modeling the powder dissolution, the current mass transport analyses have provided the theoretical frameworks for the transition from rotating disk to powder dissolution.

The rates of dissolution and permeation are important for determining the bioavailability of oral drugs. The drug permeability can be different from the coformer permeability, and there is a lack of studies to evaluate the effect of this differential permeation on the oral absorption of cocrystals. Chapter 4 has shown that the presence of excess coformer can decrease the dissolution rate of cocrystal. Therefore, it is essential to investigate whether the slower permeation of the coformer would result in excess concentration that could alter the dissolution rate of the continually dissolving cocrystal. A dissolution/permeation system would be useful to simultaneously evaluate the dissolution and permeation of the cocrystal components to access the oral absorption mechanisms of cocrystals.

The mass transport models in this dissertation were developed with assumptions to keep the analyses simple. However, there are other factors that can influence the cocrystal dissolution rate have not been considered, such as ionic strength, viscosity, diffusion of the ionized components, solution mediated phase transformation, et al. Future mass transport analyses should consider all these factors to provide more rigorous mass transport models for cocrystal flux

predictions. There is also a lack of studies to demonstrate which model, surface saturation or interfacial equilibrium, is more physically realistic. Future studies should explore more in this area.